SC-4730 (RR)

D-1

SC-4730(RR)
TID-4500 (21st Ed.)
NUCLEAR EXPLOSIONS -
PEACEFUL APPLICATIONS

research report

THE EFFECT OF ROW CHARGE SPACING AND DEPTH ON CRATER DIMENSIONS

L. J. Vortman, 5412
L. N. Schofield, 5412

November 1963

Sandia Corporation
CONTRACTOR FOR U. S. ATOMIC ENERGY COMMISSION
ALBUQUERQUE, NEW MEXICO
LIVERMORE, CALIFORNIA

Issued by Sandia Corporation,
a prime contractor to the
United States Atomic Energy Commission

Printed in USA. Price $2.75. Available from the Office of
Technical Services, Department of Commerce,
Washington 25, D. C.

SC-4730(RR)
TID-4500 (21st Ed.)
NUCLEAR EXPLOSIONS -
PEACEFUL APPLICATIONS

SC-4730(RR)

THE EFFECT OF ROW CHARGE SPACING AND DEPTH ON CRATER DIMENSIONS

L. J. Vortman, 5412
L. N. Schofield, 5412

Sandia Laboratory, Albuquerque

November 1963

ABSTRACT

Forty row charges were fired in the Albuquerque fan-delta alluvium to define row-charge crater dimensions in terms of charge burial depth and the spacing between charges in the row. Sixty single charges were detonated at various burial depths for comparison. The factors limiting equivalence between row-charge craters and continuous line-charge craters are defined in terms of length of the row charge and also in terms of both burial depth and spacing. When the most efficient charge spacing was used, the optimum burial depth for row charges was 10 percent greater than the burial depth at which optimum crater dimensions were obtained from a single charge of the same weight. Channels were found to have a uniform width at a maximum charge spacing greater than the maximum spacing at which a uniform depth was obtained. The maximum spacing which produces a uniform channel width is a distance 30 percent greater than the crater radius of the same size charge detonated singly at that depth which produces an optimum single-crater radius. The maximum spacing for producing a uniform channel depth was found to be a distance 10 percent greater than the maximum single-charge crater radius in the same medium. The burst depth and spacing for the most efficient use of row charges is defined in this report, and the loss in cratering efficiency resulting from failure to work at optimum burst depth or optimum spacing can be evaluated from information obtained from this experiment. Throwout from the single charges and row charges was examined, but no scaling was derived.

PREFACE

Plowshare Program has contemplated the use of nuclear explosives for large scale excavations. The work described in this document is directed toward determining the optimum method of employing explosives to form a ditch, channel, or canal of certain desired dimensions. The field work was carried out during 1959-1961 by R. E. Fay and H. E. Waldorf under the direction of D. G. Palmer and funded by the Sandia Corporation Research Organization. The analysis and evaluation was done during 1962-1963 with the financial support of Plowshare Program through the San Francisco Operations Office and the Division of Peaceful Nuclear Explosives.

TABLE OF CONTENTS

LIST OF ILLUSTRATIONS

THE EFFECT OF ROW CHARGE SPACING AND DEPTH ON CRATER DIMENSIONS

CHAPTER 1. INTRODUCTION

Although ditching with chemical explosives is not a new art,[1] it differs from ditching with nuclear explosives in the following ways:

1. Chemical explosives ordinarily can compete with mechanical methods of excavation only on small or medium sized projects in soft, usually saturated, soils.[1,2,3] The cost of chemical explosives, other than their placement cost, is directly proportional to the amount of explosive used--cost is proportional to energy.

2. Nuclear explosives would be used only on large projects and without great regard for the medium being excavated. In the case of nuclear explosives, the cost is more nearly related to the number of exploding units, rather than to the amount of energy.

The empirical ditching formulae now in use for chemical explosives are difficult to apply to nuclear explosives, since high explosive charges are almost invariably cylinders made up of vertical stacks of dynamite sticks. Since a nuclear explosive is a point source of energy, it is best that empirical formulae for nuclear ditching be based on experiments with spherical charges of high explosive.

Because the use of a single row of spaced charges offers the simplest configuration for channel excavation with nuclear charges, it was appropriate that craters from a single row be explored before investigating craters from more complex configurations. Likewise, it was appropriate to explore the craters resulting from explosions in level ground before examining craters cut through varying terrain.

In the conventional employment of chemical explosives, it is sufficient to have only the required amount of explosive per unit volume excavated. Since it is easy to punch holes in soft soil, the spacing of charges is of little interest. On the other hand, since the objective in the employment of nuclear explosives is to keep the number of units as small as possible, it is necessary to determine the maximum spacing and the corresponding depth of burst which will give the desired crater dimensions while at the same time maximizing the amount of excavation per unit of explosive.

1.1 Objectives

The experiment described here was started in the fall of 1959 as a model study, using rows of spaced spherical charges in the local (Albuquerque) fan-delta alluvium, of the effects of spacing and depth of burst on crater parameters (depth, width, and volume).

The objectives were:

1. To determine the maximum spacing at which a uniform channel would result (as a function of the depth of burst of the charges in the row)--that is, to determine the maximum spacing at which the crater from a row of charges shows minimum variation in width and depth and is essentially the same as the crater which would result from the detonation of a continuous line charge.

2. To define, for spacings greater than that which would give a uniform channel crater, the ratios of minimum crater dimensions to maximum crater dimensions as a function of the depth of burst.

1.2 Background

In 1958 an exploratory series of shots was detonated in the same medium to explore crater parameters from single charges, continuous line charges, and a small number of rows of spaced charges.[4] With respect to spaced charges this earlier experiment consisted of two groups of shots. The first group was composed of shots consisting of two 2-pound cubes. These were detonated at scaled burst depths of 0.0ft/$lb^{1/3}$, and 0.50 ft/$lb^{1/3}$, and at scaled spacings from 0.25 ft/$lb^{1/3}$ to 2.5 ft/$lb^{1/3}$.

The second group consisted of thirteen shots with each shot containing five to ten 2-pound cubes. These were spaced at 0.5 ft/$lb^{1/3}$, 0.75 ft/$lb^{1/3}$, and 1.0 ft/$lb^{1/3}$, at scaled burst depths of 0.0, 0.5, 1.0, and 1.5 ft/$lb^{1/3}$.

While the earlier experiment established the relationship of crater dimensions with charge spacings and burst depths over the ranges of those parameters explored, it was clear that two charges in a row were insufficient to give craters which were two dimensional over any portion of their length, and that reactions between the two charges at certain spacings gave results which could not be reconciled with craters from rows of five or more charges. The 1958 experiments made it evident that it was possible to get a uniform channel crater at a given depth of burst by proper spacing of the charges. They also established that the maximum spacing at which a uniform channel resulted was a function of the depth of burst of the charge.

CHAPTER 2. EXPERIMENT DESIGN

2.1 Explosives

Because large scatter was observed in data from the 1958 series described in the last chapter, attempts were made to achieve more uniform test conditions in the series of tests described in this report. The 2-pound cubic TNT charges used in the 1958 series were replaced with 8- and 256-pound spheres having 1/2-ounce RDX and 6-pound 50-50 pentolite boosters, respectively. These were used with the expectation that the larger charges, relative to the nearly constant inhomogeneities in the soil, would reduce the scatter.

2.2 Medium

The Albuquerque fan-delta alluvium is composed of clayey sands, sandy clays, clayey silty sands, and has lenses of gravel, erratic cobbles, and boulders. The area picked for this series contains very little gravel, cobbles, or boulders; however, lenses of fine to coarse sand were encountered. Figure 2.1 contains a typical screen analysis of the alluvium as well as a graph of the dry density of this alluvium under conditions of artifical compaction and moisture control used in an earlier experiment. Figure 2.2 shows penetration resistance as a function of moisture content for in situ material, and represents the range of conditions over which shots were fired. These tests were all made with a 1/2-inch-diameter probe on a Proctor penetrometer, with which it is not possible to measure values greater than 2200 psi. In general measurements in undistributed material fall below those obtained from a compacted sample. Shear strength of the undisturbed material is greatly influenced by moisture content, and if the moisture content is increased only a few percent, the area is reduced to a quagmire.

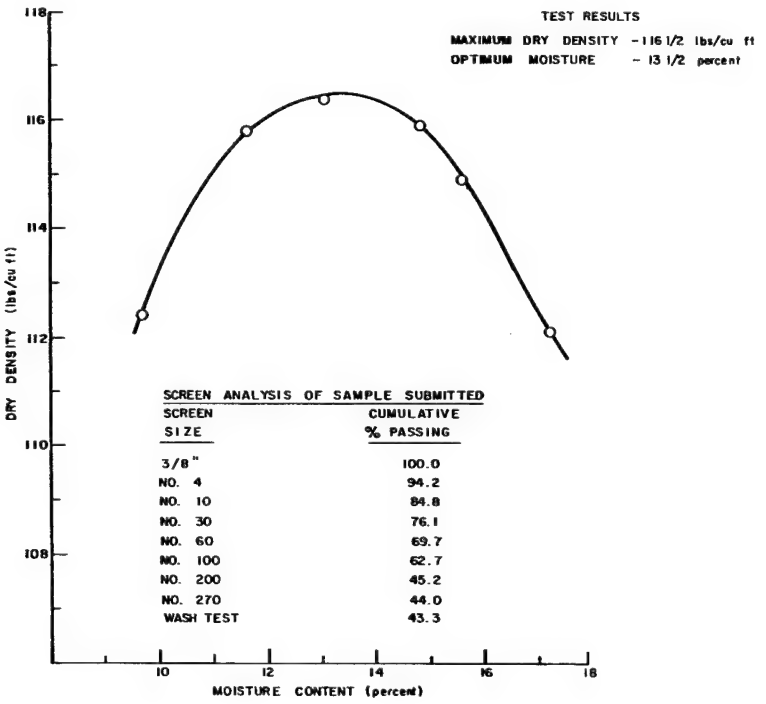

Figure 2.1 Typical screen analysis and dry density of alluvium under conditions of artificial compaction and moisture control

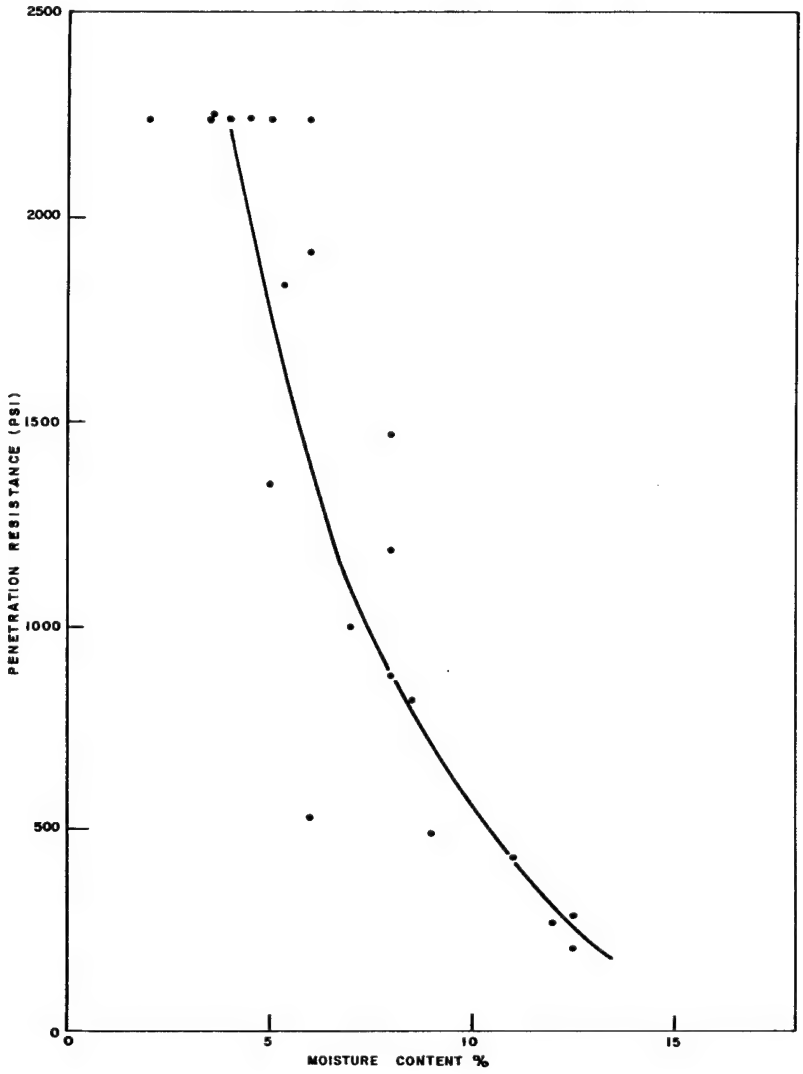

Figure 2.2 Penetration resistance versus moisture content for in situ alluvium

On the majority of shots the moisture content went from about 7 to 12 percent at 6 inches below the surface to 3 to 8 percent at a depth of 3 feet. It was found that, with the exception of keeping out rain, a canvas or plastic cover over the test area did not affect the moisture content of the medium below the first 3 to 4 inches.

Dry density varied greatly with moisture content. A trend of lower dry density with higher moisture content was noted.

2.3 Site Preparation

To prepare the site, loose surface dirt was graded off the selected area and each individual site was smoothed to form a plane with departures not larger than 1/4 inch. The area to be cratered was then covered with canvas to normalize the moisture near the surface. Surface moisture control was maintained for at least

5 days before shot time of the earlier shots in the hope of reducing scatter by stabilizing the moisture content. During the winter months areas to be cratered were kept warm enough to prevent freezing.

Before each shot, the area around the shot center was covered with plastic from the estimated extent of the true crater to about five times that distance (Figure 2.3). At the time the charges were placed, density measurements and soil water content samples were taken from the charge holes. A limited number of penetrometer readings were also obtained before each of the later shots in the series.

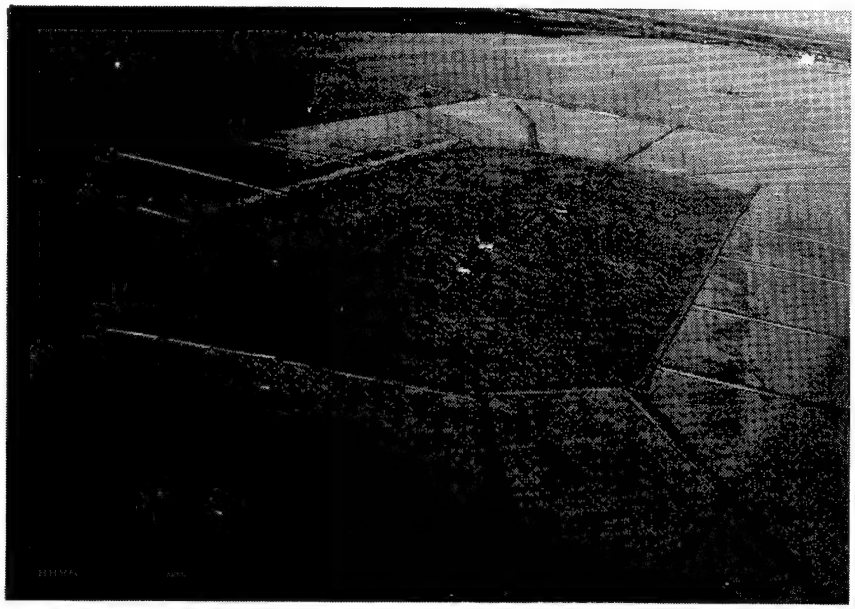

Figure 2.3 Typical preshot site preparation

2.4 Experiment Procedure

2.4.1 Craters

The charges were placed in augered holes in otherwise undisturbed earth. The holes were then back filled with the removed material and tamped in an attempt to match the *in situ* density of the soil. Just before shot time cameras were set up.

After the shot, measurements of the apparent crater were made by using the rig shown in Figure 2.4 on the 8-pound shots and by ground survey on the majority of the 256-pound shots. The rig consists of a row of uniform length rods held in a vertical position in a pipe beam. The pipe beam slides on calibrated tracks. To use the rig, the axis of the charges was re-established and the tracks set up parallel to the long axis of the crater. A trench was cleared on either side down to the plastic so that the end rods were at the original level. The pipe beam was then placed normal to the long axis of the crater and with the center vertical rod on the long axis. Each rod was then moved down until it just contacted the surface of the crater or lip and a picture of which Figure 2.4 is typical, taken of the resulting profile. The procedure was repeated at 6-inch intervals from crater centerline to beyond the end of the crater in both directions. The resulting photographs were enlarged to a scale made uniform by keeping the 10-foot black bar on the beam at the same size, and the crater profile taken directly off the photograph.

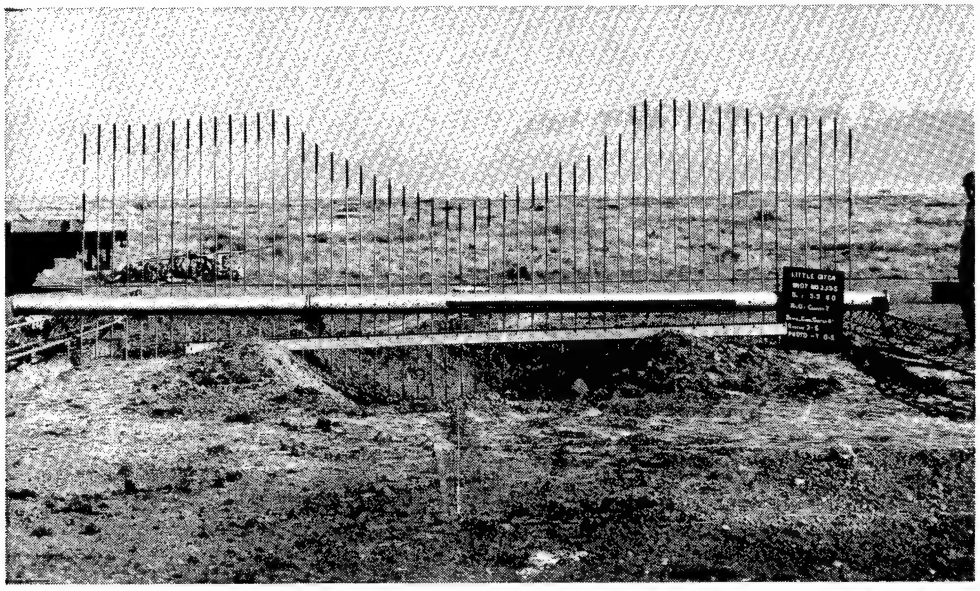

Figure 2.4 Jig for measuring crater dimensions

2.4.2 Throwout

Material thrown out of the crater was measured in two ways. Close to the crater 1-square-foot segments of the material were extracted down to the plastic surrounding the cratered region. At greater distances collection pans were placed around the area, and the material which fell within the pans was collected and weighed. On the earlier shots the 1-square-foot sections were obtained at the intersections of a 5-foot grid out to the limit of the plastic (Figure 2.5). Later the procedure was changed so that material was collected at stipulated points along each of eight radii through the center of the charge array. Throwout collection was made along each radius at distances of 30, 50, 75, 100, 200, and 300 feet. From the mass data collected at each station, throwout density contours were plotted, and integration of these areas gave the total amount of material ejected from the crater.

Figure 2.5 Collection of throwout samples

2.5 Summary of Shots

Information on each of the shots fired in this series is included in tables given in the following chapter. These tables also indicate the number of charges in each row. Table 2.1 summarizes the number of single charges fired at each burst depth and each scaled burst depth.* These charges were fired to provide the background for comparison with row charges. Figure 2.6 summarizes the row charge experiment showing the depth of burst and the spacing at which charges were fired together with the number of shots at each combination of burst depth and spacing. Two 256-pound charge shots were also fired.

TABLE 2.1

	Scaled depth of burst ($ft/lb^{1/3}$)	Actual depth of burst (ft)	Number of shots
8-pound charges	0.5	1	2
	0.75	1.5	11
	1.0	2.0	15
	1.25	2.5	11
	1.5	3	5
	2.0	4	5
	2.5	5	1
256-pound charges	0.5	3.17	1
	0.75	4.76	1
	1.00	6.35	1
	1.25	7.94	3
	1.50	9.52	2
	2.0	12.7	2

Shots in this experiment have been identified with a three-term code: a Roman Numeral, a Capital Letter, and an Arabic Number (e.g., IID5). The Roman Numeral indicates the phase of the experiment during which the shot was fired. The Letter indicates the depth of burst of the charge as shown in Figure 2.6. The Arabic Number indicates spacing between charges in the row. A repeat shot was indicated by a letter B following the code.

*Unless specifically stated otherwise, all scaled dimensions for single charges have been based on cube-root-of-yield scaling ($\ell \sim W^{1/3}$, where W is the charge weight in pounds unless specified otherwise).

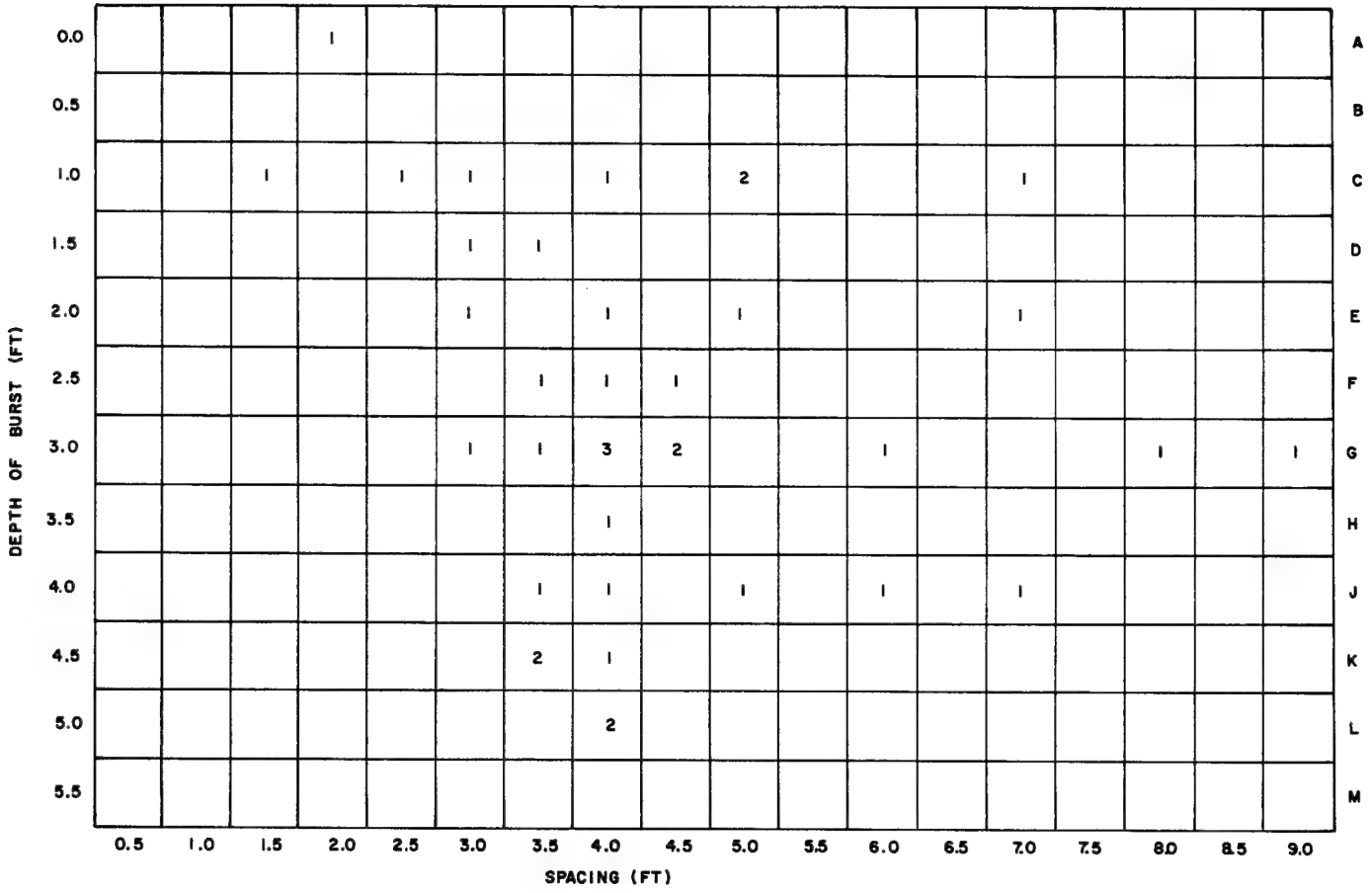

Figure 2.6 Summary of spacings and burst depths used in the row-charge experiment

CHAPTER 3. RESULTS

3.1 Craters from Single Charges

To obtain depth-of-burst curves from single charges which would be used as a standard of comparison for the rows of spaced charges, the series of 8-pound single spheres was detonated at varying depths. Because there was considerable scatter in crater dimensions and variation in the shape of the resulting craters, a series of eight 256-pound spheres was detonated so that the influence of the relatively constant inhomogeneities of the soil would be correspondingly less. At a later date two addition 256-pound spheres were detonated. Table 3.1 lists the single-charge shots fired.

In the 1958 series[4] using 2-pound cubes, the formation of mounds within the crater was observed on some shots at scaled depths of 1.5 $ft/lb^{1/3}$.

In order to obtain useful measurements from all craters, the craters were divided into three types:

Type I has no mound (Figure 3.1); Type II has a mound approximately in the center which may rise to any height from the bottom of the crater to above original grade (Figure 3.2); and Type III has a mound off the center (Figure 3.3).

Since none of the craters from the 256-pound charges (see Crater Topography, Appendix A) exhibits the type of mounding seen in the craters from 8-pound single charges, all Types II and III crater data have been omitted from the diameter and depth-of-burst curves (Figures 3.4, 3.5). They are included, however, in the volume depth-of-burst curve (Figure 3.6).

The depth-of-burst curves (Figures 3.4, 3.5, 3.6) have been weighted heavily in favor of the 256-pound charge craters.

The scaled diameters (Figure 3.4) of the 8-pound charge craters agree well with those of the 256-pound charges; in fact, they average about 4 percent larger. It is quite different with the scaled depth, however; the scaled depth (Figure 3.5) of the 8-pound charge craters is much less (an average of 25 percent less) than those of the 256-pound charges. Also, the scatter is much greater. With the scaled depth less, the scaled crater volumes are of course less for the 8-pound charge craters than for those of the 256-pound charges. The scaled volume plots (Figure 3.6) show the great variation in volume (as a result of variation in crater depth) which results from the different type craters. Those craters of Type I which show small volumes are actually transition craters from Type I to Type II, since all Type II craters show the least volume.

Something of the nature of the transition is evidenced by a comparison of Figure 3.6 with 3.7. Figure 3.7 shows right angle profiles of the craters, the data of which are plotted in Figure 3.6. All craters are made by 8-pound charges burst 2 feet (1.0 $ft/lb^{1/3}$) below the ground surface. The profiles are arranged in the vertical order in which the data appear in Figure 3.6. The uppermost crater is larger than predicted from scaling the 256-pound charge crater, and all others are smaller--the smallest having only one-quarter the scaled volume of the 256-pound charge crater. Only three craters (IV-3-2.0, 1E, IV-1-2.0) were identified as having mounds in the center (Type II). One (IV-4-2.0) was classed as having a mound at the side (Type III). There were others whose profiles show less pronounced indication of mounds (IV-10-20, IV-2-2.0, P 2-B, and IV-4.20). These profiles emphasize the great variation found in the dimensions of small charge craters even though burst depth, charge weight, and charge shape were the same.

Shot	Date	Charge weight lb	Dob ft	Dob w-1/3	Penetrometer lb (with 1/4" dia tip)	Water content percent	Wet density lb/ft^3	CRATER Av dia from area ft	Av dia from area ft w-1/3	Av max from charge center ft	Av max from charge center ft w-1/3	Av max dia of mound ft	Av max dia of mound ft w-1/3
1C	11-12-59	8	1.0	0.5	NR	7.5 at 1.0'	105 at 7.5"	5.6	2.8	NA	NA	NA	NA
1C8	6-29-59	8	1.0	0.5	NR	10.8 at 1.0'	NR	6.18	3.09	NA	NA	NA	NA
1D	11-10-59	8	1.5	0.75	NR	11.5 at 7"	102 at 7"	7.1	3.55	NA	NA	NA	NA
IV-1-1.5	4-11-60	8	1.5	0.75	63 at 0.32'	14 at 22"	114 at 0.32'	7.75	3.87	NA	NA	NA	NA
IV-2-1.5	4-14-60	8	1.5	0.75	93 at 0.16' 40 at 22"	7 at 12" 8.5 at 22"	93.5 at 0.16'	7.0	3.5	NA	NA	NA	NA
IV-3-1.5	4-18-60	8	1.5	0.75	40 at 0.19' 24 at 22"	4 at 0.19' 9 at 22"	85 at 0.19'	7.5	3.75	NA	NA	NA	NA
IV-4-1.5	4-19-60	8	1.5	0.75	108 at 0 75 at 0.13'	11 at 12" 9 at 22"	96 at 0.13'	6.9	3.45	7.1	3.55	1.34	0.67
IV-5-1.5	4-21-60	8	1.5	0.75	110 at 0 36 at 0.14'	11 at 12" 9 at 22"	93.3 at 0.14'	6.3	3.15	6.8	3.4	3.1	1.55
IV-6-1.5	4-25-60	8	1.5	0.75	82 at 0 75 at 0.16'	10 at 12" 4 at 0.16'	108 at 0.16'	6.9	3.45	NA	NA	NA	NA
IV-7-1.5	4-27-60	8	1.5	0.75	47 at 0 47 at 0.16'	8 at 12" 5 at 22"	104 at 0.16'	7.2	3.6	NA	NA	NA	NA
IV-8-1.5	4-28-60	8	1.5	0.75	105 at 0 63 at 0.16'	9 at 12" 7 at 22"	96 at 0.16'	6.5	3.25	NA	NA	0.9	0.45
IV-9-1.5	5-3-60	8	1.5	0.75	108 at 0 97 at 0.18'	10 at 12" 6 at 22"	107 at 0.18'	6.8	3.4	NA	NA	NA	NA
IV-10-1.5	5-13-60	8	1.5	0.75	89 at 0 82 at 0.19'	11 at 12" 7 at 22"	118 at 0.19'	7.2	3.6	NA	NA	NA	NA
1E	11-25-59	8	2.0	1.0	NR	9.5 at 12"	93 at 8"	7.5	3.75	7.70	3.85	2.0	1.0
P2A	10-21-59	8	2.0	1.0	NR	12	NR	7.3	3.65	NA	NA	NA	NA
P2B	11-23-59	8	2.0	1.0	NR	12 at 2'	102.5	7.1	3.55	NA	NA	NA	NA
P2C	4-5-60	8	2.0	1.0	NR	9 at 1' 4 at 2'	119	7.8	3.90	NA	NA	NA	NA
P8A	11-18-59	8	2.0	1.0	NR	10 at 2'	107.5	6.9	3.45	NA	NA	NA	NA
IV-1-2.0	4-11-60	8	2.0	1.0	57 at 0.31'	12.5 at 1.0' 5 at 2.0'	105	6.7	3.35	7.2	3.6	2.2	1.1
IV-2-2.0	4-15-60	8	2.0	1.0	52 at 0.21'	10 at 12" 6 at 28"	101 at 0.20'	7.7	3.85	NA	NA	NA	NA
IV-3-2.0	4-18-60	8	2.0	1.0	71 at 0.18' 49 at 2.3'	5 at 0.18' 7 at 2.3'	91.1 at 0.18'	7.6	3.8	7.90	3.95	2.2	1.1
IV-4-2.0	4-20-60	8	2.0	1.0	72 at 0.0 42 at 0.15'	11 at 12' 6 at 28"	89 at 0.15'	6.5	3.25	(315°) 7.6	3.8	3.0	1.5
IV-5-2.0	4-21-60	8	2.0	1.0	84 at 0.0 55 at 0.18'	12 at 12" 7 at 28'	114 at 0.18'	7.75	3.87	NA	NA	NA	NA
IV-6-2.0	4-26-60	8	2.0	1.0	66 at 0.0 34 at 0.19'	9 at 12" 4.5 at 28"	102 at 0.19'	7.4	3.7	NA	NA	NA	NA
IV-7-2.0	4-27-60	8	2.0	1.0	88 at 0.0 53 at 0.2'	10 at 12" 2 at 28"	87 at 0.2'	7.0	3.5	NA	NA	NA	NA
IV-8-2.0	5-2-60	8	2.0	1.0	110+ at 0.0 110+ at 0.14'	8 at 12" 3 at 28"	108 at 0.14'	6.9	3.45	NA	NA	NA	NA
IV-9-2.0	5-3-60	8	2.0	1.0	32 at 0 28 at 0.21'	8.5 at 12" 6.0 at 28"	101 at 0.21'	7.9	3.45	NA	NA	NA	NA
IV-10-2.0	5-12-60	8	2.0	1.0	76 at 0.0 71 at 0.15'	12 at 12" 9.5 at 28"	102 at 0.15'	7.6	3.8	NA	NA	NA	NA
1F	2-18-60	8	2.5	1.25	NR	4 at 2.5'	102 at 2.5'	8.1	4.05	NA	NA	NA	NA
IV-1-2.5	4-14-60	8	2.5	1.25	110 at 0.19' 72 at 0.24'	7.5 at 1' 10.5 at 2'	105 at 0.19'	6.9	3.45	(270°) 8.0	4.0	S	S
IV-2-2.5	4-15-60	8	2.5	1.25	110 at 12" 62 at 34"	12.5 at 12" 4 at 34"	107 at 0.15'	7.4	3.70	NA	NA	NA	NA

(1)

TABLE 3.1

CRATER

Wet density	Av dia from area		Av max from charge center		Av max dia of mound		Max depth		Depth at charge ℄		Height of mound		Volume		Lip height		Distance to max lip from ℄		Average lip height		r pe
lb/ft^3	ft	ft w-1/3	ft	ft w-1/3	ft	ft w-1/3	ft	ft w-1/3	ft	ft w-1/3	ft	ft w-1/3	ft^3	ft^3 w	ft	ft w-1/3	ft	ft w-1/3	ft	ft w-1/3	ft
105 at 7.5"	5.6	2.8	NA	NA	NA	NA	1.2	0.6	1.2	0.6	NA	NA	11.7	1.46	0.3	0.15	3.5	1.75			
NR	6.18	3.09	NA	NA	NA	NA	1.1	0.55	1.1	0.55	NA	NA	9.58	1.20	0.4	0.2	4.0	2.0			
102 at 7"	7.1	3.55	NA	NA	NA	NA	1.4	0.7	1.2	0.6	NA	NA	20.6	2.57	0.4	0.2	4.5	2.25			
114 at 0.32'	7.75	3.87	NA	NA	NA	NA	1.0	0.5	1.0	0.5	NA	NA	22.1	2.76	0.4	0.2	4.8	2.4			
93.5 at 0.16'	7.0	3.5	NA	NA	NA	NA	0.7	0.35	0.7	0.35	NA	NA	10.0	1.25	0.4	0.2	4.6	2.3			
85 at 0.19'	7.5	3.75	NA	NA	NA	NA	0.6	0.3	0.6	0.3	NA	NA	12.4	1.55	0.5	0.25	5.0	2.5			
96 at 0.13'	6.9	3.45	7.1	3.55	1.34	0.67	0.6	0.3	0.0	0.0	0.0	0.0	9.18	1.15	0.4	0.2	4.8	2.4			
93.3 at 0.14'	6.3	3.15	6.8	3.4	3.1	1.55	0.4	0.2	-0.4	-0.2	0.4	0.2	3.78	0.47	0.4	0.2	4.2	2.1			
108 at 0.16'	6.9	3.45	NA	NA	NA	NA	1.2	0.6	1.2	0.6	NA	NA	15.0	1.87	0.3	0.15	4.8	2.4			
104 at 0.16'	7.2	3.6	NA	NA	NA	NA	1.8	0.9	1.8	0.9	NA	NA	27.0	3.37	0.4	0.2	4.5	2.25			
96 at 0.16'	6.5	3.25	NA	NA	0.9	0.45	0.5	0.25	0.2	0.1	0.1	0.05	6.88	0.86	0.4	0.2	4.3	2.15			
107 at 0.18'	6.8	3.4	NA	NA	NA	NA	1.2	0.6	1.2	0.6	NA	NA	17.6	2.2	0.6	0.3	4.2	2.1			
118 at 0.19'	7.2	3.6	NA	NA	NA	NA	0.8	0.4	0.6	0.3	NA	NA	13.1	1.64	0.6	0.3	4.4	2.2			
93 at 8"	7.5	3.75	7.70	3.85	2.0	1.0	0.5	0.25	0.0	0.0	0.3	0.15	10.9	1.36	0.6	0.3	4.6	2.3			
NR	7.3	3.65	NA	NA	NA	NA	1.1	0.55	1.1	0.55	NA	NA	17.0	2.12	0.5	0.25	5.0	2.5			
102.5	7.1	3.55	NA	NA	NA	NA	0.7	0.35	0.4	0.2	NA	NA	12.1	1.51	0.6	0.3	4.5	2.25			
119	7.8	3.90	NA	NA	NA	NA	1.8	0.90	1.8	0.90	NA	NA	40.4	5.05	0.5	0.25	4.6	2.3			
107.5	6.9	3.45	NA	NA	NA	NA	1.4	0.70	1.4	0.70	NA	NA	19.0	2.37	0.4	0.20	4.4	2.2			
105	6.7	3.35	7.2	3.6	2.2	1.1	0.5	0.25	-0.4	-0.20	0.4	0.2	7.8	0.97	0.4	0.2	4.6	2.3			
101 at 0.20'	7.7	3.85	NA	NA	NA	NA	0.7	0.35	0.6	0.3	NA	NA	14.5	1.81	0.3	0.15	5.0	2.5			
1.1 at 0.18'	7.6	3.8	7.90	3.95	2.2	1.1	0.6	0.3	-0.2	-0.1	0.4	0.2	12.6	1.57	0.5	0.25	5.0	2.5			
89 at 0.15'	6.5	3.25	(315°) 7.6	3.8	3.0	1.5	0.6	0.3	-0.2	-0.1	0.4	0.2	9.6	1.2	0.4	0.2	4.6	2.3			
114 at 0.18'	7.75	3.87	NA	NA	NA	NA	0.8	0.4	0.8	0.4	NA	NA	18.1	2.26	0.5	0.25	5.2	2.6			
102 at 0.19'	7.4	3.7	NA	NA	NA	NA	1.6	0.8	1.6	0.8	NA	NA	28.7	3.59	0.4	0.2	4.8	2.4			
87 at 0.2'	7.0	3.5	NA	NA	NA	NA	1.4	0.7	1.4	0.7	NA	NA	23	2.87	0.6	0.3	5.0	2.5			
108 at 0.14'	6.9	3.45	NA	NA	NA	NA	1.2	0.6	1.2	0.6	NA	NA	20.2	2.52	0.4	0.2	4.6	2.3			
101 at 0.21'	7.9	3.45	NA	NA	NA	NA	1.4	0.7	1.4	0.7	NA	NA	29.3	3.66	0.6	0.3	5.4	2.7			
102 at 0.15'	7.6	3.8	NA	NA	NA	NA	1.0	0.5	1.0	0.5	NA	NA	19.7	2.46	0.8	0.4	5.0	2.5			
102 at 2.5'	8.1	4.05	NA	NA	NA	NA	1.7	0.85	1.7	0.85	NA	NA	35	4.37	0.7	0.35	4.8	2.4			
105 at 0.19'	6.9	3.45	(270°) 8.0	4.0	S	S	1.0	0.5	0.4	0.2	0.4	0.2	13.2	1.65	0.6	0.3	5.0	2.5			
107 at 0.15'	7.4	3.70	NA	NA	NA	NA	1.0	0.5	1.0	0.5	NA	NA	19.2	2.40	0.5	0.25	4.8	2.4			

(2)

Depth charge ℄		Height of mound		Volume		Lip height		Distance to max lip from ℄		Average lip height		Average radius to peak of lip		Mass of fallout		Remarks
	ft/w-1/3	ft	ft/w-1/3	ft³	ft³/w	ft	ft/w-1/3	ft	ft/w-1/3	ft	ft/w-1/3	ft	ft/w-1/3	kg	πr²d	
.2	0.6	NA	NA	11.7	1.46	0.3	0.15	3.5	1.75					682		Type I Crater
.1	0.55	NA	NA	9.58	1.20	0.4	0.2	4.0	2.0					-		Type I Crater
.2	0.6	NA	NA	20.6	2.57	0.4	0.2	4.5	2.25					1175		Type I Crater
.0	0.5	NA	NA	22.1	2.76	0.4	0.2	4.8	2.4					1473		Type I Crater
.7	0.35	NA	NA	10.0	1.25	0.4	0.2	4.6	2.3					NR		Type I Crater
.6	0.3	NA	NA	12.4	1.55	0.5	0.25	5.0	2.5					NR		Type I Crater
.0	0.0	0.0	0.0	9.18	1.15	0.4	0.2	4.8	2.4					1274		Type II Crater
4	-0.2	0.4	0.2	3.78	0.47	0.4	0.2	4.2	2.1					NR		Type II Crater
.2	0.6	NA	NA	15.0	1.87	0.3	0.15	4.8	2.4					NR		Type I Crater
8	0.9	NA	NA	27.0	3.37	0.4	0.2	4.5	2.25					807		Type I Crater
.2	0.1	0.1	0.05	6.88	0.86	0.4	0.2	4.3	2.15					NR		Type II Crater
2	0.6	NA	NA	17.6	2.2	0.6	0.3	4.2	2.1					NR		Type I Crater
6	0.3	NA	NA	13.1	1.64	0.6	0.3	4.4	2.2					NR		Type I Crater
0	0.0	0.3	0.15	10.9	1.36	0.6	0.3	4.6	2.3					1450		Type II Crater
1	0.55	NA	NA	17.0	2.12	0.5	0.25	5.0	2.5					NR		Type I Crater
4	0.2	NA	NA	12.1	1.51	0.6	0.3	4.5	2.25					NR		Type I Crater
8	0.90	NA	NA	40.4	5.05	0.5	0.25	4.6	2.3					1484		Type I Crater
4	0.70	NA	NA	19.0	2.37	0.4	0.20	4.4	2.2					NR		Type I Crater
4	-0.20	0.4	0.2	7.8	0.97	0.4	0.2	4.6	2.3					847		Type II Crater
6	0.3	NA	NA	14.5	1.81	0.3	0.15	5.0	2.5					NR		Type I Crater
2	-0.1	0.4	0.2	12.6	1.57	0.5	0.25	5.0	2.5					NR		Type II Crater
2	-0.1	0.4	0.2	9.6	1.2	0.4	0.2	4.6	2.3					1050		Type III Crater
8	0.4	NA	NA	18.1	2.26	0.5	0.25	5.2	2.6					NR		Type I Crater
6	0.8	NA	NA	28.7	3.59	0.4	0.2	4.8	2.4					NR		Type I Crater
4	0.7	NA	NA	23	2.87	0.6	0.3	5.0	2.5					1120		Type I Crater
2	0.6	NA	NA	20.2	2.52	0.4	0.2	4.6	2.3					NR		Type I Crater
4	0.7	NA	NA	29.3	3.66	0.6	0.3	5.4	2.7					NR		Type I Crater
0	0.5	NA	NA	19.7	2.46	0.8	0.4	5.0	2.5					NR		Type I Crater
7	0.85	NA	NA	35	4.37	0.7	0.35	4.8	2.4					NR		Type I Crater
4	0.2	0.4	0.2	13.2	1.65	0.6	0.3	5.0	2.5					934		Type III Crater
0	0.5	NA	NA	19.2	2.40	0.5	0.25	4.8	2.4					NR		Type I Crater

3

IV-3-2.5	4-19-60	8	2.5	1.25	50 at 0 35 at 0.18'	9.5 at 12" 3.0 at 34"	89 at 0.18'	7.7	3.85	7.8	3.9	0.9	0.45	0.6	0.3	
IV-4-2.5	4-20-60	8	2.5	1.25	58 at 0.0 31 at 0.19'	12 at 12" 6 at 34"	89 at 0.19'	7.96	3.98	NA	NA	NA	NA	0.9	0.45	
IV-5-2.5	4-25-60	8	2.5	1.25	72 at 0.0 60 at 0.14'	9 at 12" 3 at 34"	95 at 0.14'	7.8	3.9	NA	NA	NA	NA	2.0	1.0	
IV-6-2.5	4-26-60	8	2.5	1.25	110 at 0.0 110 at 0.16'	8 at 12" 3 at 34"	108 at 0.16'	7.2	3.6	NA	NA	NA	NA	1.2	0.6	
IV-7-2.5	4-28-60	8	2.5	1.25	100 at 0.0 55 at 0.15'	9 at 12" 4 at 34"	87 at 0.15'	7.5	3.75	NA	NA	NA	NA	1.6	0.8	
IV-8-2.5	5-2-60	8	2.5	1.25	82 at 0.0 82 at 0.15'	8 at 12" 3 at 34"	105 at 0.15'	7.5	3.75	NA	NA	NA	Na	2.0	1.0	
IV-9-2.5	5-12-60	8	2.5	1.25	101 at 0.0 78 at 0.19'	9 at 12" 7 at 34"	107 at 0.19'	8.1	4.05	NA	NA	NA	NA	1.0	0.5	
IV-10-2.5	5-13-60	8	2.5	1.25	101 at 0.0 83 at 0.14'	7 at 12" 3 at 34"	102 at 0.14'	7.2	3.6	NA	NA	NA	NA	1.4	0.7	
P3A	11-9-59	8	3.0	1.5	NR	8 at 3'	NR	5.5	2.75	(180°) 8.0	4.0	S	S	0.5	0.25	-
P3B	1-26-60	8	3.0	1.5	NR	10 at 10"	109 at 10"	7.92	3.96	NA	NA	NA	NA	2.2	1.1	
P4A	12-7-59	8	4.0	2.0	NR	11 at 1'	116 at 7.5"	7.1	3.55	(270) 9.0	4.5	5	2.5	0.4	0.2	-
P4B	1-27-60	8	4.0	2.0	NR	11 at 5.5"	118 at 5.5"	8.98	4.49	NA	NA	NA	NA	2.2	1.1	
P5A P5B	2-12-60	8	5.0	2.5	NR	7 at 0.23'	114 at 0.23'	NA	NA	NA	NA	NA	NA	NA	NA	-
III-0.5	6-8-60	256	3.17	0.5	35-110 at 0.0 34-108 at 0.15'	5-9 at 0.15'	111-114 at 0.15'	20.2	3.18	NA	NA	NA	NA	4.5	0.71	
III-0.75	6-17-60	256	4.76	0.75	67 at 0.0 62 at 0.15'	6-8 at 0.15'	94-105 at 0.14'	21.4	3.37	NA	NA	NA	NA	7.0	1.10	
III-1.00	6-13-60	256	6.35	1.0	53-108 at 0-0.15'	5.5-8 at 0.18'	98-100 at 0.18'	22.2	3.50	NA	NA	NA	NA	5.5	0.87	
III-1.25	7-19-60	256	7.94	1.25	45-110 at 0.0	3-6 at 0.15'	86-109 at 0.17'	23.4	3.68	NA	NA	NA	NA	5.7	0.90	
62-34	7-16-62*	256	7.94	1.25	NR	4.48 av	NR	23.4	3.68	NA	NA	NA	NA	5.1	0.80	
III-1.50	6-15-60	256	9.52	1.5	64-110 at 0.11'	4-5 at 0.11'	96-107 at 0.11'	25.3	3.98	NA	NA	NA	NA	3.5	0.55	
62-35	7-18-62*	256	9.53	1.5	NR	4.48 av	NR	23.8	3.75	NA	NA	NA	NA	4.9	0.77	
III-2.00a	7-26-60	256	12.7	2.0	70-110 at 0.18'	1.5 at 0.16' 9.5 at 0.34'	92-108 at 0.18'	23.2	3.65	NA	NA	NA	NA	2.8	0.44	
III-2.00b	8-22-60	256	12.7	2.0	48-106 at 0-0.2'	6-8 at .1'-.2'	88-91 at 0.2'	23.8	3.75	NA	NA	NA	NA	2.6	0.41	
III-1.25b	8-8-60	256	7.94	1.25	36-76 at 0-0.2"	2.5-5 at 0.2'	91-105 at 0.2'	22.8	3.59	NA	NA	NA	NA	5.2	0.82	
IV-4-3.0	7-28-60	8	3.0	1.5	60 at 0.17'	0.5 at 12" 2.0 at 40"	97-123 at 0.15'	8.1	4.05	NA	NA	NA	NA	0.8	0.4	(
IV-5-3.0	7-28-60	8	3.0	1.5	110 at 0-0.17'	1.5-3.0 at 0-12" 5 at 40"	at 0 to 0.5' 91.5-123.5	8.06	4.03	NA	NA	NA	NA	1.0	0.5	(
IV-6-3.0	7-29-60	8	3.0	1.5	110 at 0-0.13'	1.5 at 0.13'	108-118 at 0.1'	7.6	3.8	NA	NA	NA	NA	1.2	0.6	
IV-1-4.0	6-21-60	8	4.0	2.0	86 at 0.18'	7 at 12" 11 at 52"	95 at 0.18'	≈0	0	8.6	4.3	>8.6	-	0.2	0.1	-1
IV-2-4.0	6-22-60	8	4.0	2.0	110 at 0.0 110 at 0.18'	5 at 12" 5 at 52"	106 at 0.18'	6.6	3.3	9.4	4.7	NR	NR	0.4	0.2	-(
IV-3-4.0	6-23-60	8	4.0	2.0	90 at 0.0 84 at 0.15'	8.5 at 12" 5 at 52"	94 at 0.18'	0	0	NA	NA	NR	NR	0.0	0.0	-1

*These shots were fired as a part of a separate experiment.

DENOTATION:

NR = NOT RECORDED
NA = NOT APPLICABLE
S = ON SIDE OF CRATER

7.7	3.85	7.8	3.9	0.9	0.45	0.6	0.3	0.0	0.0	0.0	0.0	12.9	1.61	0.4	0.2	5.0	2.5					
7.96	3.98	NA	NA	NA	NA	0.9	0.45	0.6	0.3	NA	NA	20.6	2.57	0.5	0.25	5.2	2.6					
7.8	3.9	NA	NA	NA	NA	2.0	1.0	2.0	1.0	NA	NA	38.2	4.77	0.7	0.35	5.0	2.5					
7.2	3.6	NA	NA	NA	NA	1.2	0.6	1.2	0.6	NA	NA	20.2	2.52	0.6	0.3	5.0	2.5					
7.5	3.75	NA	NA	NA	NA	1.6	0.8	1.6	0.8	NA	NA	35.4	4.4	0.6	0.3	4.7	2.35					
7.5	3.75	NA	NA	NA	Na	2.0	1.0	2.0	1.0	NA	NA	38.4	4.8	0.6	0.3	5.0	2.5					
8.1	4.05	NA	NA	NA	NA	1.0	0.5	0.4	0.2	-0.2	0.1	22.9	2.86	0.6	0.3	5.0	2.5					
7.2	3.6	NA	NA	NA	NA	1.4	0.7	1.4	0.7	NA	NA	22.0	2.75	0.4	0.2	4.8	2.4					
5.5	2.75	(180°) 8.0	4.0	S	S	0.5	0.25	-0.6	-0.3	0.8	0.4	4.5	0.56	0.4	0.2	5.0	2.5					
7.92	3.96	NA	NA	NA	NA	2.2	1.1	2.2	1.1	NA	NA	53.0	6.62	0.8	0.4	4.6	2.3					
7.1	3.55	(270) 9.0	4.5	5	2.5	0.4	0.2	-0.8	-0.4	1.0	0.5	8.9	1.11	0.4	0.2	5.6	2.8					
8.98	4.49	NA	NA	NA	NA	2.2	1.1	2.2	1.1	NA	NA	66.3	8.29	1.0	0.5	5.8	2.9					
NA	NA	NA	NA	NA	NA	NA	NA	-1.4	-0.7	1.4	0.7	NA	NA	NA	NA	NA	NA					
20.2	3.18	NA	NA	NA	NA	4.5	0.71	4.5	0.71	NA	NA	643	2.51	1.0	0.16	12.0	1.89	0.8	0.13	12.0	1.89	
21.4	3.37	NA	NA	NA	NA	7.0	1.10	7.0	1.10	NA	NA	913	3.56	2.0	0.31	13.2	2.07	1.6	0.25	13.0	2.04	
22.2	3.50	NA	NA	NA	NA	5.5	0.87	5.5	0.87	NA	NA	983	3.84	2.0	0.31	13.5	2.12	1.6	0.25	13.5	2.12	
23.4	3.68	NA	NA	NA	NA	5.7	0.90	5.7	0.90	NA	NA	1210	4.73	1.8	0.28	13.8	2.17	1.5	0.24	13.6	2.14	
23.4	3.68	NA	NA	NA	NA	5.1	0.80	5.1	0.80	NA	NA	904	3.41	2.1	.33	13.5	2.12	NR	NR	NR	NR	
25.3	3.98	NA	NA	NA	NA	3.5	0.55	3.2	0.50	NA	NA	824	3.22	1.5	0.25	16.0	2.52	1.1	0.17	16.0	2.51	
23.8	3.75	NA	NA	NA	NA	4.9	0.77	5.1	0.77	NA	NA	1172	4.58	2.5	.39	15.8	2.49	NR	NR	NR	NR	
23.2	3.65	NA	NA	NA	NA	2.8	0.44	2.0	0.31	NA	NA	550	2.15	2.5	0.39	15.5	2.44	1.2	0.19	15.6	2.45	
23.8	3.75	NA	NA	NA	NA	2.6	0.41	1.0	0.16	NA	NA	438	1.71	2.5	0.39	16.5	2.60	1.1	0.17	16.4	2.57	
22.8	3.59	NA	NA	NA	NA	5.2	0.82	5.2	0.82	NA	NA	1139	4.45	2.5	0.39	13.5	2.12	1.6	0.25	13.8	2.17	
8.1	4.05	NA	NA	NA	NA	0.8	0.4	0.4	0.2	NA	NA	18.6	2.32	0.4	0.2	5.2	2.6					
8.06	4.03	NA	NA	NA	NA	1.0	0.5	0.4	0.2	NA	NA	25.9	3.24	0.6	0.3	5.2	2.6					
7.6	3.8	NA	NA	NA	NA	1.2	0.6	1.2	0.6	NA	NA	21.8	2.72	0.8	0.4	5.0	2.5					
≈0	0	8.6	4.3	>8.6	-	0.2	0.1	-1.4	-0.7	1.4	0.7	≈0	0	NA	NA	NA	NA					
6.6	3.3	9.4	4.7	NR	NR	0.4	0.2	-0.4	-0.2	0.8	0.4	6.2	0.78	NA	NA	NA	NA					
0	0	NA	NA	NR	NR	0.0	0.0	-1.6	-0.8	1.6	0.8	0	0	NA	NA	NA	NA					

2

0.0	0.0	0.0	0.0	12.9	1.61	0.4	0.2	5.0	2.5					NR		Type II Crater
0.6	0.3	NA	NA	20.6	2.57	0.5	0.25	5.2	2.6					1174		Type I Crater
2.0	1.0	NA	NA	38.2	4.77	0.7	0.35	5.0	2.5					NR		Type I Crater
1.2	0.6	NA	NA	20.2	2.52	0.6	0.3	5.0	2.5					NR		Type I Crater
1.6	0.8	NA	NA	35.4	4.4	0.6	0.3	4.7	2.35					1108		Type I Crater
2.0	1.0	NA	NA	38.4	4.8	0.6	0.3	5.0	2.5					NR		Type I Crater
0.4	0.2	-0.2	0.1	22.9	2.86	0.6	0.3	5.0	2.5					NR		Type III Crater
1.4	0.7	NA	NA	22.0	2.75	0.4	0.2	4.8	2.4					NR		Type I Crater
-0.6	-0.3	0.8	0.4	4.5	0.56	0.4	0.2	5.0	2.5					NR		Type III Crater
2.2	1.1	NA	NA	53.0	6.62	0.8	0.4	4.6	2.3					NR		Type I Crater
-0.8	-0.4	1.0	0.5	8.9	1.11	0.4	0.2	5.6	2.8					NR		Type III Crater
2.2	1.1	NA	NA	66.3	8.29	1.0	0.5	5.8	2.9					NR		Type I Crater
-1.4	-0.7	1.4	0.7	NA	NA	NA	NA	NA	NA					NR		Mound
4.5	0.71	NA	NA	643	2.51	1.0	0.16	12.0	1.89	0.8	0.13	12.0	1.89		2.24	Type I Crater
7.0	1.10	NA	NA	913	3.56	2.0	0.31	13.2	2.07	1.6	0.25	13.0	2.04	45,770	2.75	Type I Crater
5.5	0.87	NA	NA	983	3.84	2.0	0.31	13.5	2.12	1.6	0.25	13.5	2.12		2.17	Type I Crater
5.7	0.90	NA	NA	1210	4.73	1.8	0.28	13.8	2.17	1.5	0.24	13.6	2.14		2.03	Type I Crater
5.1	0.80	NA	NA	904	3.41	2.1	.33	13.5	2.12	NR	NR	NR	NR	NR	2.43	Type I Crater
3.2	0.50	NA	NA	824	3.22	1.5	0.25	16.0	2.52	1.1	0.17	16.0	2.51		2.14	Type I Crater
5.1	0.77	NA	NA	1172	4.58	2.5	.39	15.8	2.49	NR	NR	NR	NR	NR	1.86	Type I Crater
2.0	0.31	NA	NA	550	2.15	2.5	0.39	15.5	2.44	1.2	0.19	15.6	2.45		2.15	Type I Crater
1.0	0.16	NA	NA	438	1.71	2.5	0.39	16.5	2.60	1.1	0.17	16.4	2.57		2.64	Type I Crater
5.2	0.82	NA	NA	1139	4.45	2.5	0.39	13.5	2.12	1.6	0.25	13.8	2.17		1.86	Type I Crater
0.4	0.2	NA	NA	18.6	2.32	0.4	0.2	5.2	2.6							Type I Crater
0.4	0.2	NA	NA	25.9	3.24	0.6	0.3	5.2	2.6							Type I Crater
1.2	0.6	NA	NA	21.8	2.72	0.8	0.4	5.0	2.5							Type I Crater
-1.4	-0.7	1.4	0.7	≈0	0	NA	NA	NA	NA					960 KG		Mound
-0.4	-0.2	0.8	0.4	6.2	0.78	NA	NA	NA	NA					928 KG		Mound
-1.6	-0.8	1.6	0.8	0	0	NA	NA	NA	NA					901 KG		Mound

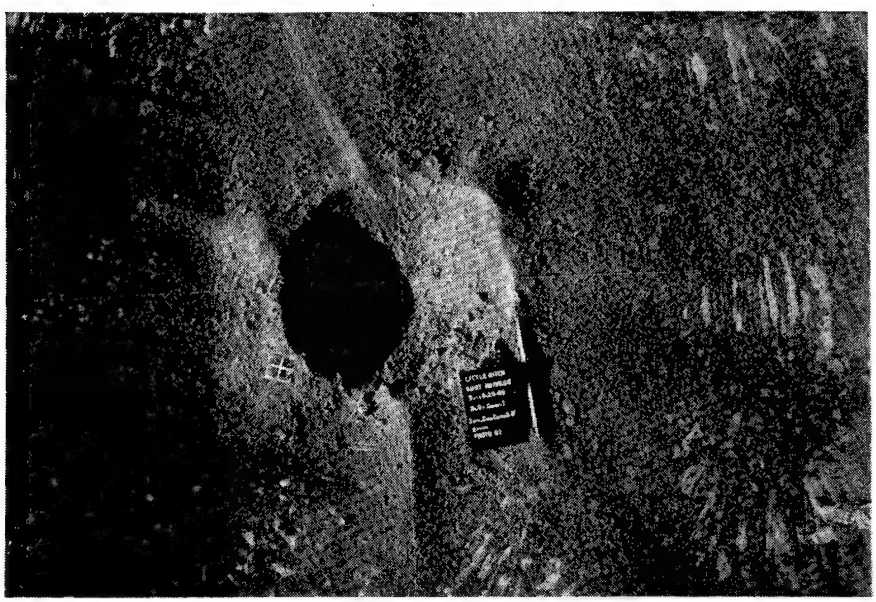

3.1a

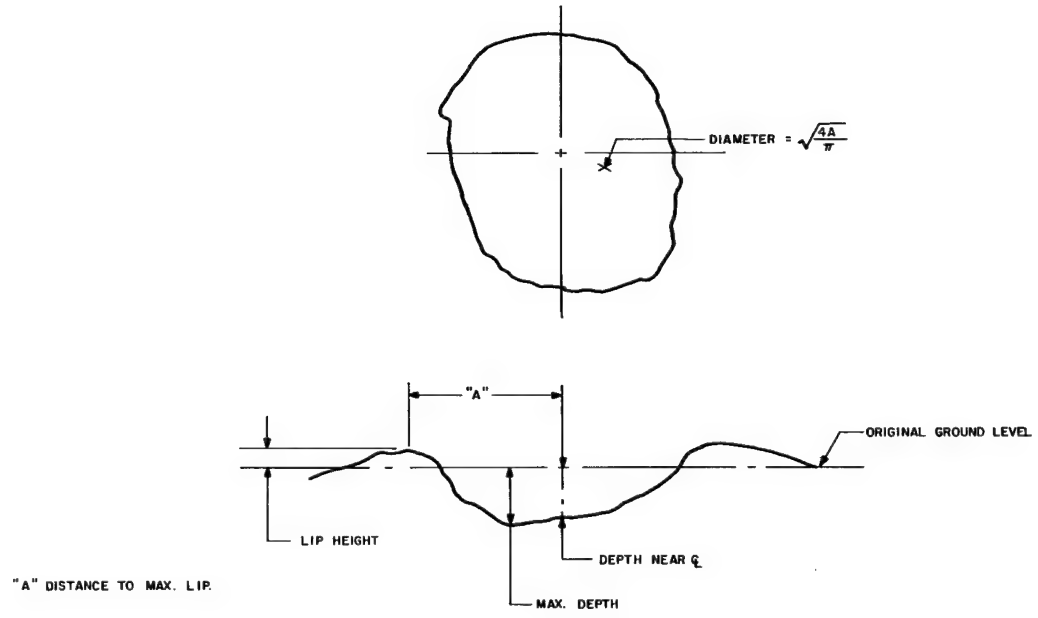

3.1b

Figure 3.1 Typical crater without a mound in the center

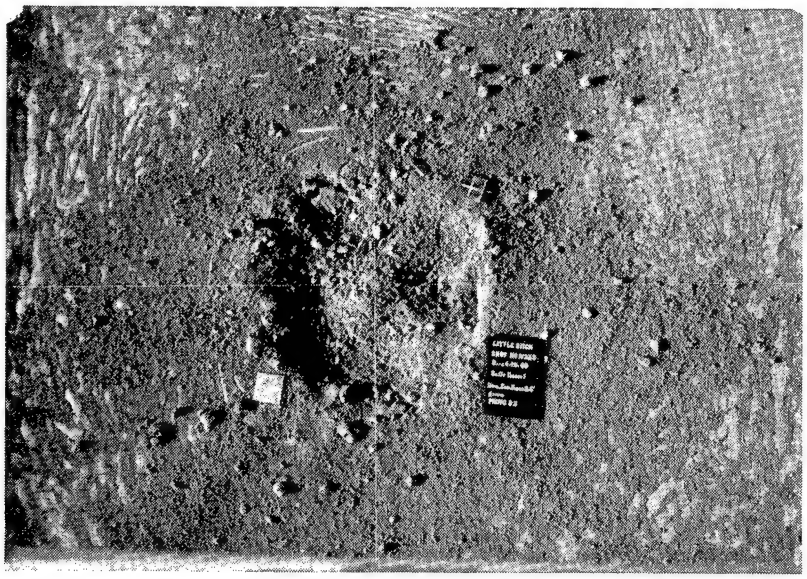

3.2a

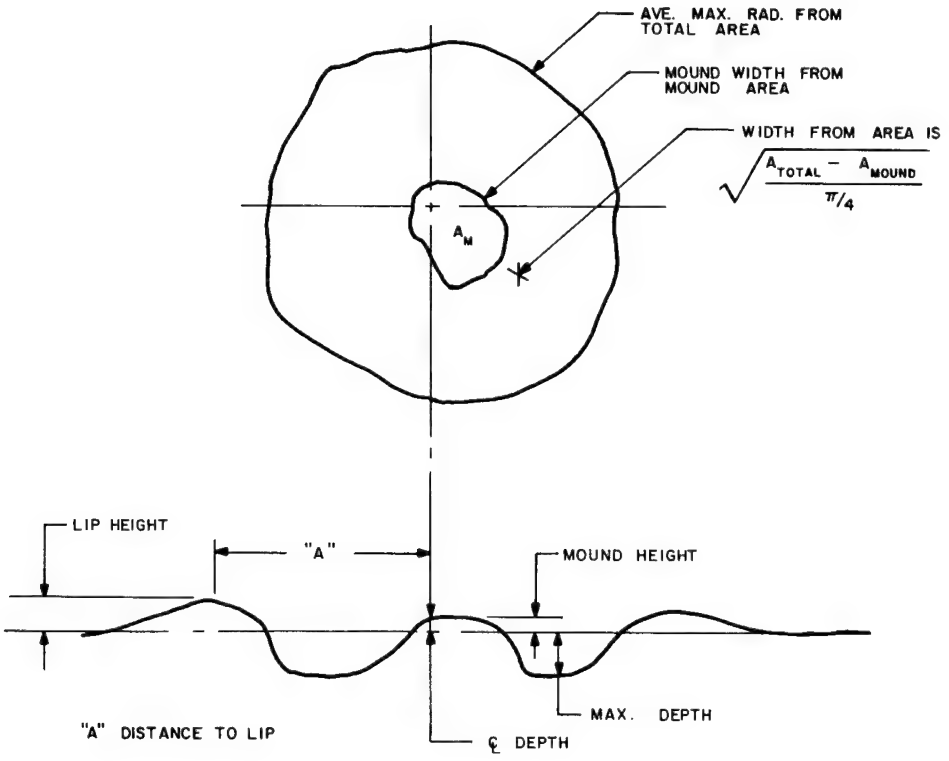

3.2b

Figure 3.2 Typical crater with a mound in the center

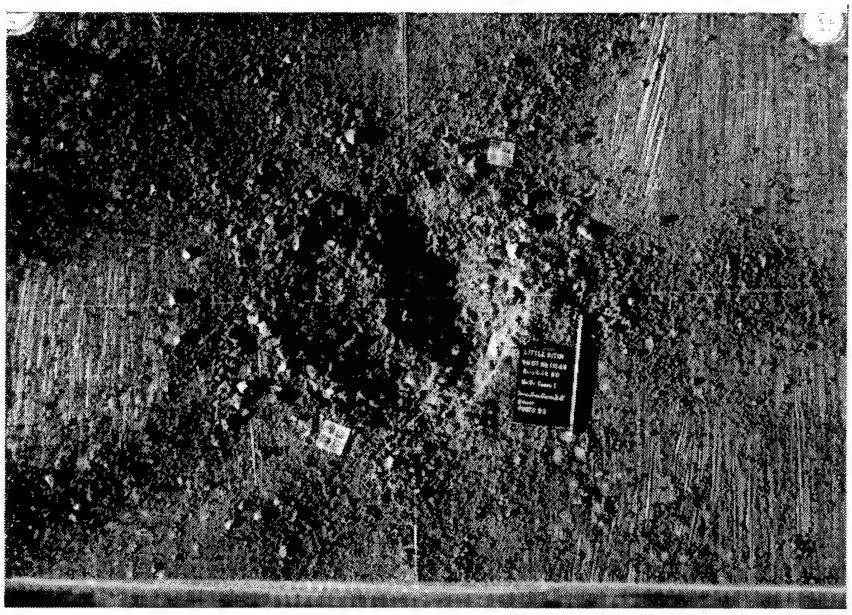

3.3a

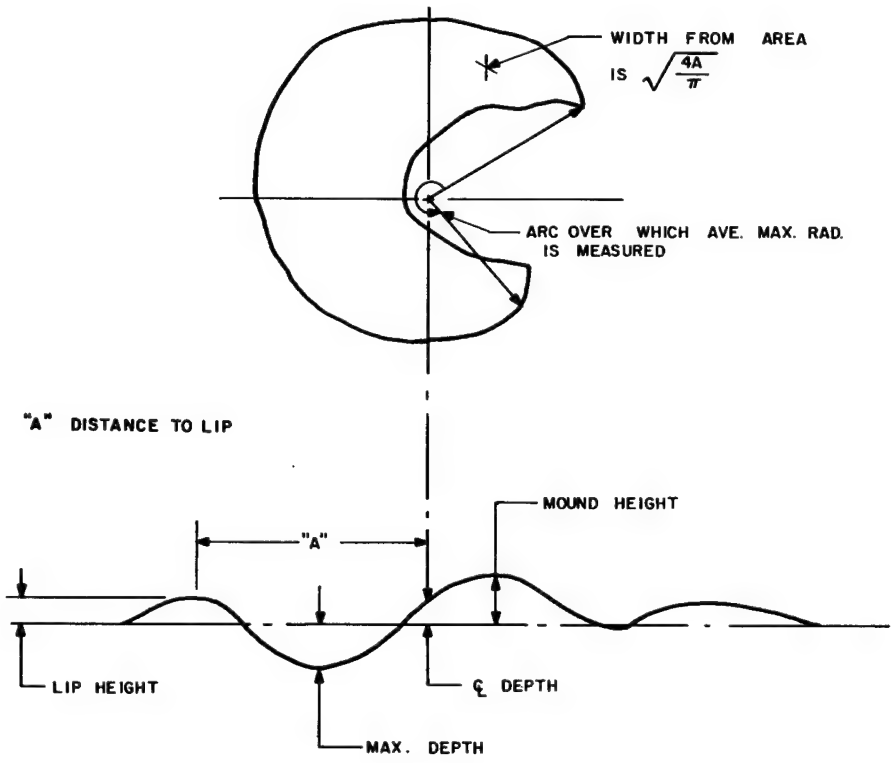

3.3b

Figure 3.3 Typical crater with a mound off-center

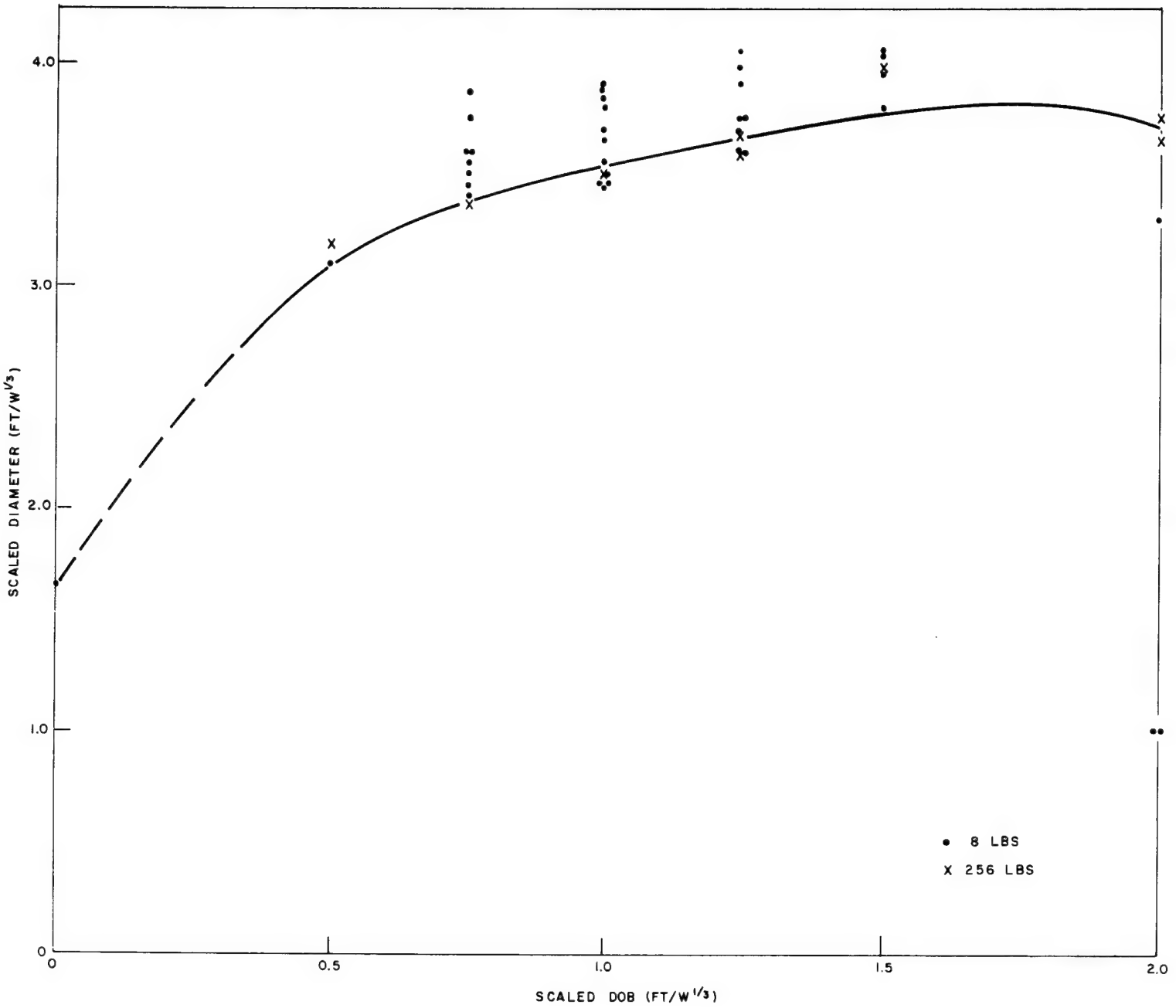

Figure 3.4 Single-charge scaled depth-of-burst curve for scaled crater diameter

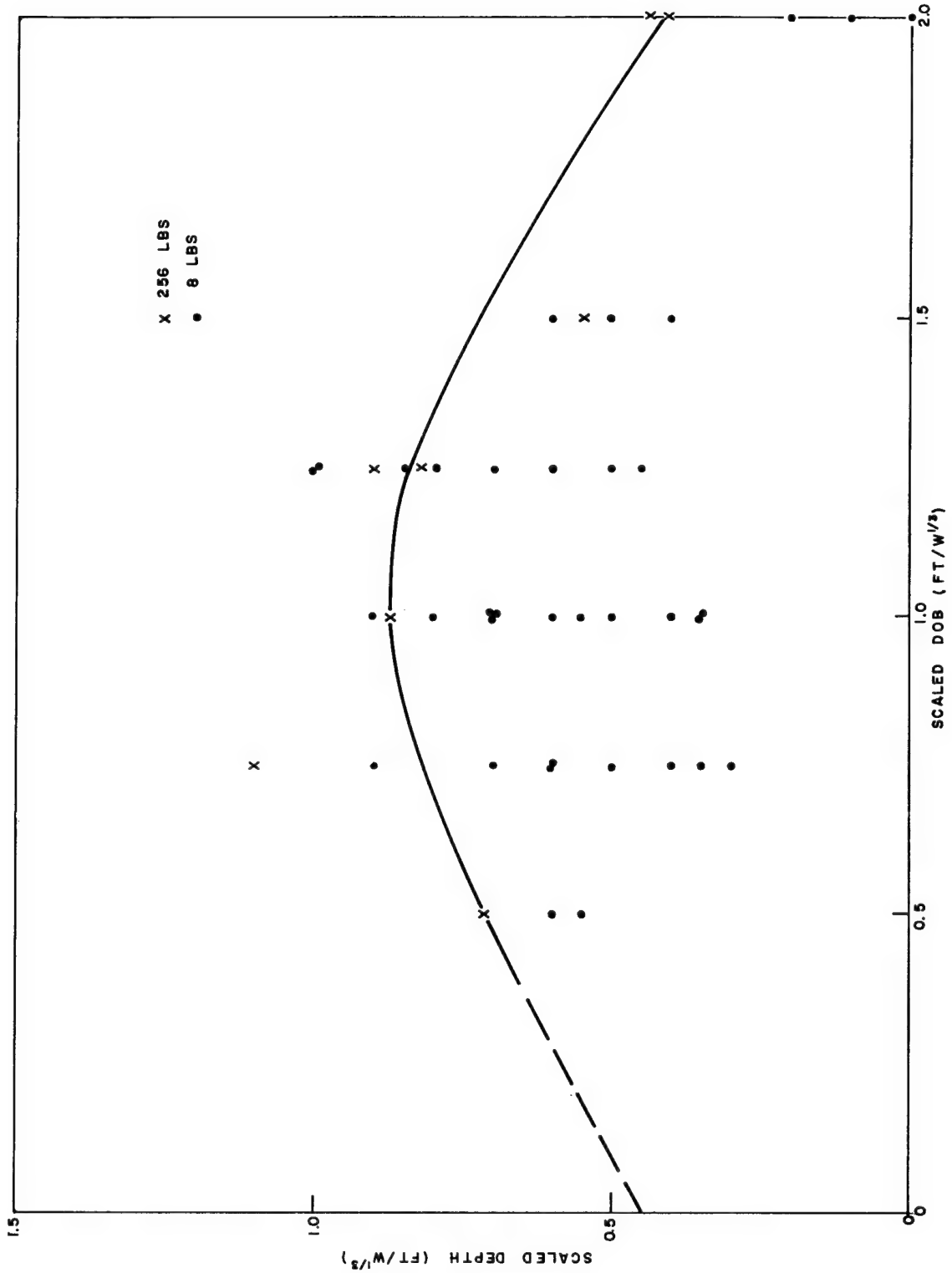

Figure 3.5 Single-charge scaled depth-of-burst curve for scaled crater depth

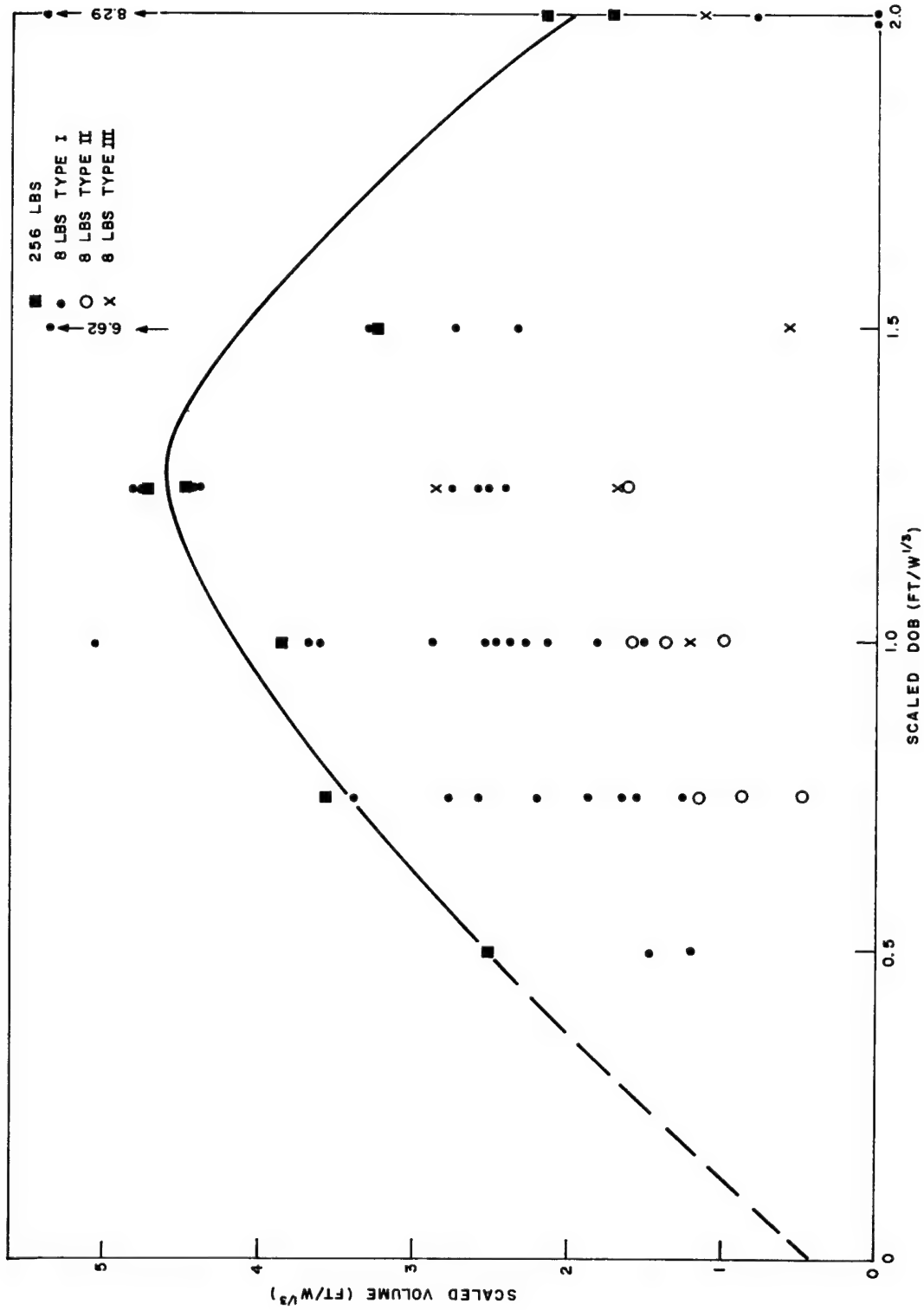

Figure 3.6 Single-charge scaled depth-of-burst curve for scaled crater volume

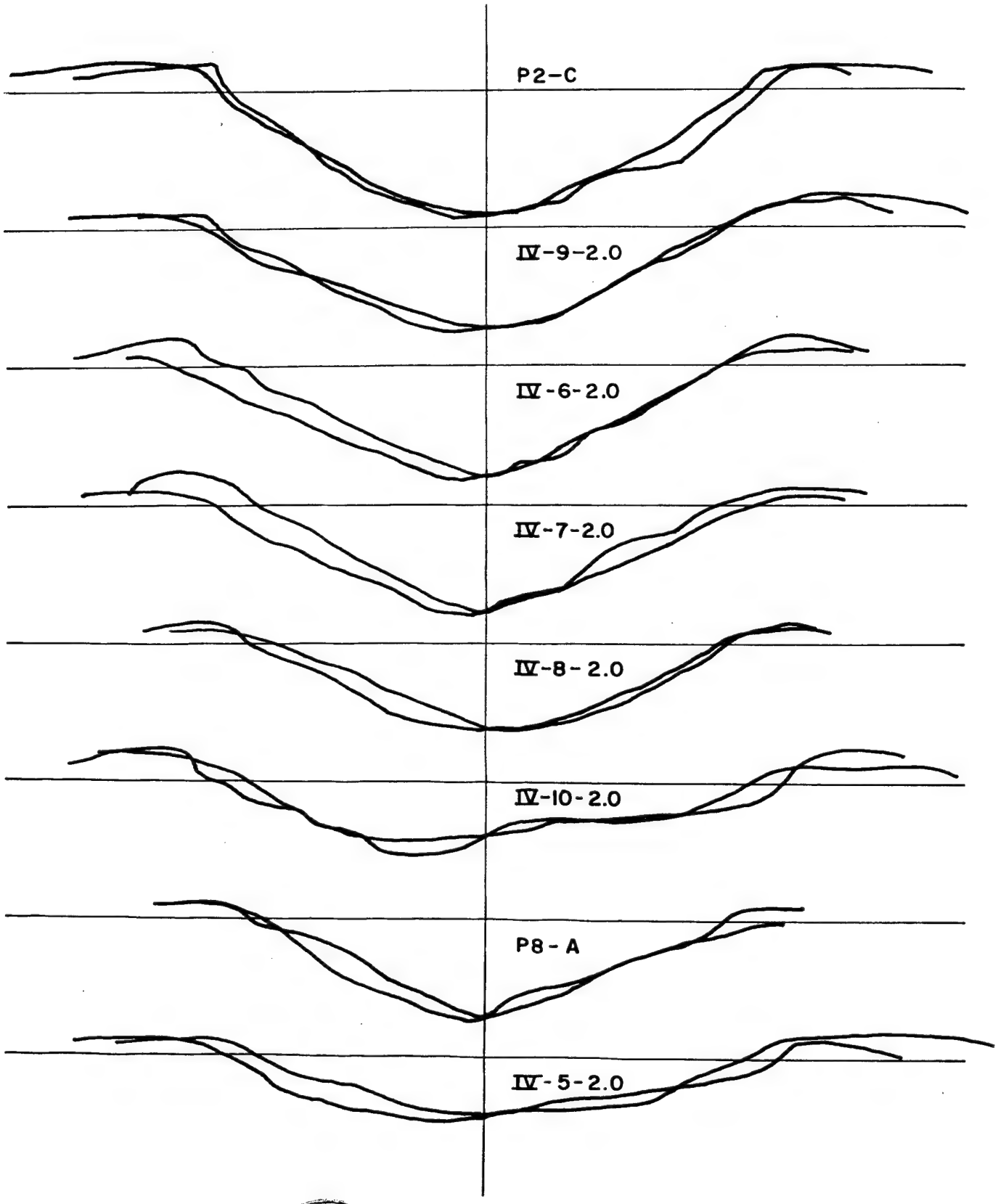

Figure 3.7 Right angle profiles of

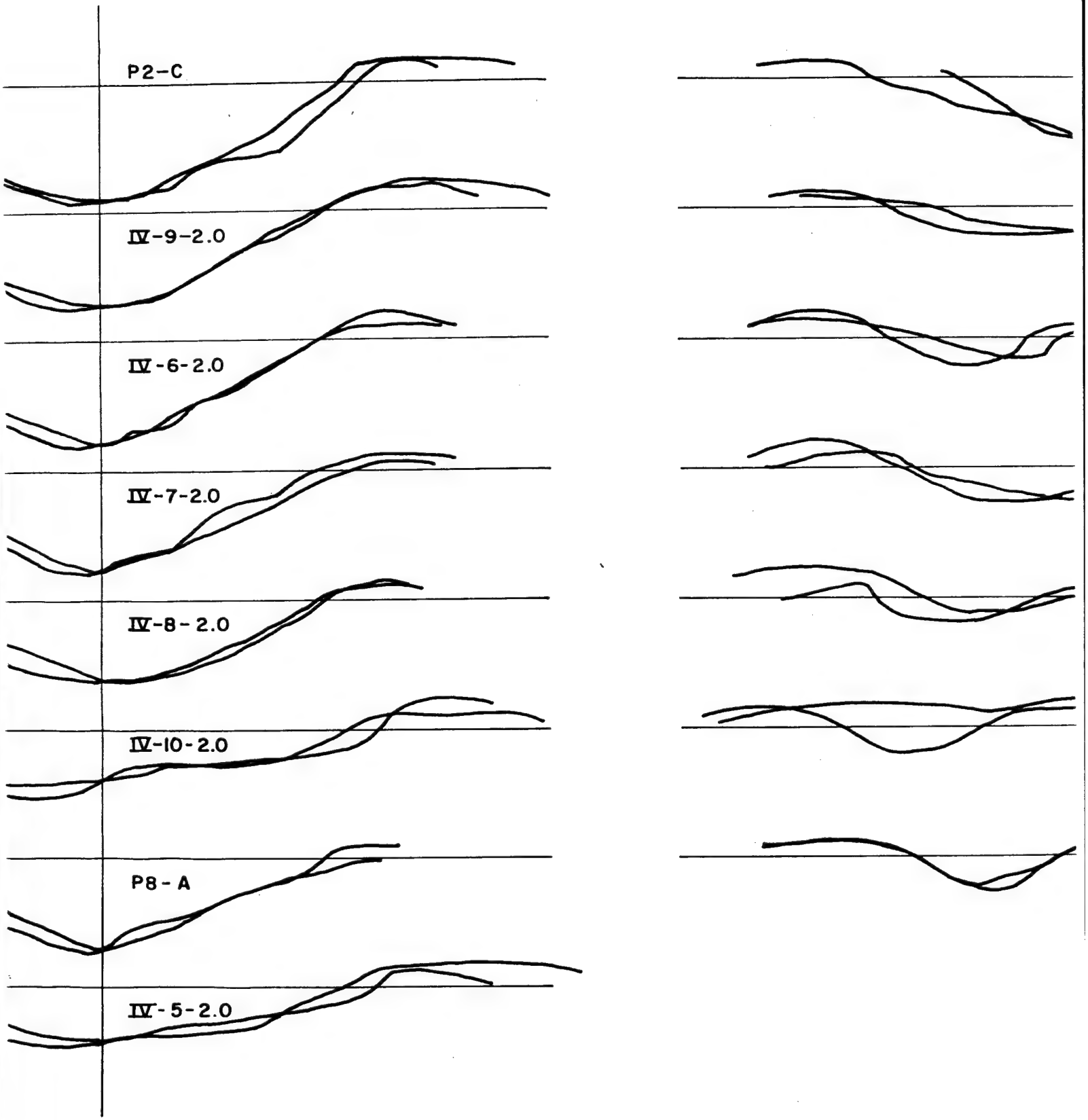

Figure 3.7 Right angle profiles of craters from single charges buried at 2

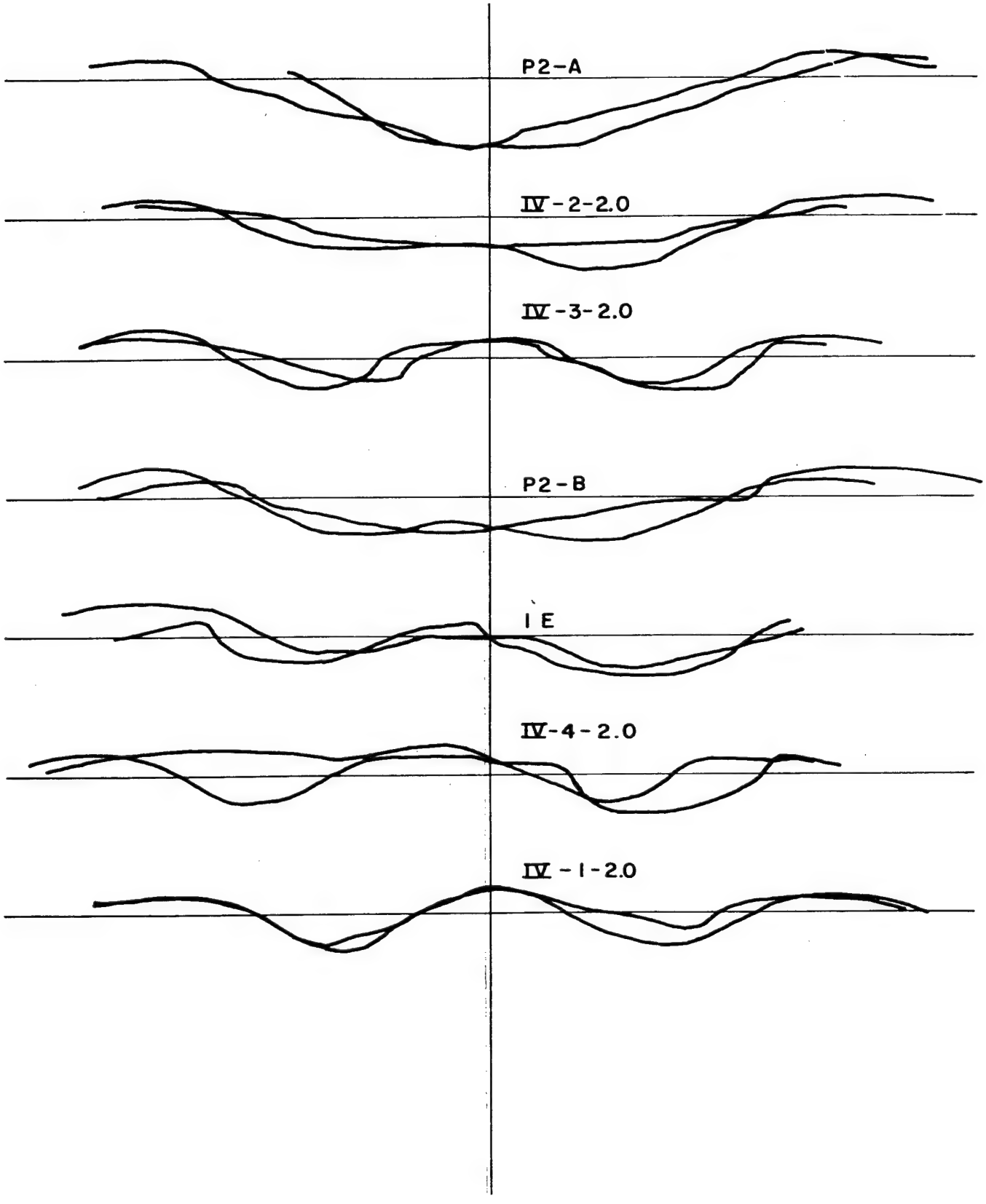

craters from single charges buried at 2 feet

3

3.2 Craters from Rows of Spaced Charges

The row-charge series consisted of 40 shots as listed in Table 3.2, and its purpose was to obtain crater parameters (width, depth, and volume) as a function of spacing and depth of burst. Topography of the row-charge craters is included in Appendix B. Profiles of the row charges together with those of the 256-pound single charges are included in Appendix C.

Figure 3.8 shows how crater dimensions have been defined for row-charge craters. A typical row-charge crater, where the spacing is large enough for line-charge equivalence to be exceeded, is widest and deepest at the charge location, and shallowest and narrowest at a saddle between charge locations. A uniform channel, one which is equivalent to a continuous line-charge crater, results when the charges are spaced close enough so that there is essentially no difference in the dimensions at and those between the charge locations. In the discussion which follows we have defined the uniform channel in terms of the ratios of the dimension at the saddle to the dimension at the charge, where, in each case, the dimensions used are the average of all dimensions except those about the end charges.

Because it is desirable for reasons given below to consider the row-charge craters in terms of their line-charge equivalents, the line-charge equivalent values of Table 3.2 are given in Table 3.3. The last two columns indicate the degree of line-charge equivalence with respect to crater width and depth.

Two regions may be delineated: (1) the region of line-charge equivalence, and (2) the region of line-charge disparity. They are separated by a boundary of line-charge equivalence. Where line-charge equivalence is maintained, the linear dimensions vary as $w^{1/2}$.

$$w^{1/2} = \left(\frac{W}{S}\right)^{1/2},$$

where w is the weight of a line charge in pounds per linear foot, W is the weight of a single charge in a row, and S is the spacing between charges in the row.*

There are two restrictions on the region of line-charge equivalence--that is the region throughout which the crater exhibits the uniform channel appearance of a line-charge crater, or in other words, where it shows no evidence of the separate contributions of the individual charges (Figure 3.9).

The first restriction is that for a given burst depth the row of charges must be long enough so that a significant portion of the crater is two dimensional, i.e., it must be free from the effects of the end of the crater. To maintain a linear crater, row charges must be lengthened with increasing burst depth. If the charge is too short, the yielded crater will approach that from a single charge. Figure 3.10 illustrates this, showing a line-charge crater from a charge of 10.9 lb/ft, 6.42-foot-long, at a burial depth of 3.3 feet. The crater has been filled with water to the original ground level so its surface contour is readily apparent. Carlson defines a relationship between charge length and burst depth such that the center one-third of the crater was two dimensional. His results are included in Figure 3.11 together with data from an earlier series of line-charge craters.[4] The shaded area in the figure represents the uncertainty between the area above where the craters are essentially two-dimensional and the area below where they are more nearly three-dimensional. In the latter case, the craters have a surface contour similar to that of Figure 3.10.

*See Reference 5 for additional information concerning scaling of line charges.

Shot no	Date	Charges: Weight lbs	Charges: No	Dob ft	Spacing ft	Av width ft	Av width at charge ft	Av width at saddle ft	Max depth ft	Av depth at charge (less outer charges) ft	Av depth at saddle (less outer saddles) ft	Total volume Ft^3/lb He
IIA-2	5-17-60	8 (41b/ft)	7	0.0	2.0	4.3	4.3	4.3	1.2	0.86	0.53	0.43
IIC-1.5	6-22-59	8	7	1.0	1.5	6.6	6.6	6.6	1.85	1.64	1.59	1.21
IIC-2.5	7-16-59	8	7	1.0	2.5	6.1	6.1	6.1	2.1	1.7	1.53	1.71
IIC-3	9-1-59	8	7	1.0	3.0	5.0	5.0	5.0	1.8	1.12	1.05	1.19
IIC-4	10-14-59	8	7	1.0	4.0	5.5	5.4	5.6	1.6	1.5	0.9	1.75
IIC-5	10-5-59	8	7	1.0	5.0	4.5	4.8	3.3	1.2	1.0	0.6	1.14
IIC-5B	9-24-59	8	7	1.0	5.0	4.2	5.0	2.4	1.2	1.0	0.4	1.06
IIC-7	10-16-59	8	7	1.0	7.0	-	5.6	0.4	1.4	1.2	0.04	1.61
IID-3	11-10-59	8	7	1.5	3.0	7.1	7.1	7.1	1.8	1.6	1.6	2.39
IID-3.5	3-9-60	8	7	1.5	3.5	6.1	6.3	6.0	2.0	1.8	1.7	2.45
IIE-3.0	12-9-59	8	7	2.0	3.0	8.3	8.3	8.3	2.0	1.8	1.7	3.43
IIE-4.0	3-10-60	8	7	2.0	4.0	7.7	7.8	7.6	2.8	2.5	2.3	4.8
IIE-5.0	5-24-60	8	7	2.0	5.0	6.0	6.6	5.1	2.0	1.8	1.4	3.3
IIE-7.0	5-27-60	8	7	2.0	7.0	5.3	6.6	2.8	1.5	1.3	0.4	2.3
IIF-3.5	11-13-59	8	7	2.5	3.5	8.01	8.01	8.01	2.0	1.9	1.8	3.64
IIF-4.0	3-11-60	8	7	2.5	4.0	8.05	8.05	8.05	2.4	2.1	2.1	4.66
IIF-4.5	3-30-60	8	7	2.5	4.5	8.02	8.02	8.02	2.4	2.3	2.3	5.91
IIG-3.0	1-29-60	8	7	3.0	3.0	9.32	9.32	9.32	3.0	2.4	2.4	4.28
IIG-3.5	11-10-59	8	7	3.0	3.5	8.9	8.9	8.9	2.4	1.8	1.8	4.00
IIG-4.0A	12-11-59	8	7	3.0	4.0	8.1	8.1	7.9	1.8	1.2	1.2	2.96
IIG-4.0C	2-16-60	8	7	3.0	4.0	9.03	9.03	9.03	2.9	2.6	2.6	5.98
IIG-4.0B	4-4-60	8	7	3.0	4.0	9.47	9.47	9.47	3.0	2.8	2.8	6.82
IIG-4.5	2-19-60	8	7	3.0	4.5	8.45	8.45	8.45	2.8	2.6	2.5	6.66
IIG-4.5	2-25-60	8	7	3.0	4.5	8.47	8.47	8.47	2.8	2.5	2.3	6.78
IIG-6.0	3-4-60	8	7	3.0	6.0	7.68	8.12	7.32	2.2	2.1	1.8	6.42
IIG-8.0	3-9-60	8	7	3.0	8.0	6.36	8.0	3.2	2.0	1.7	0.7	4.70
IIG-9.0	5-25-60	8	7	3.0	9.0	Same as II-J-7.0 with mounds between charges.						
IIH-4.0	3-28-60	8	7	3.5	4.0	9.59	9.6	9.6	2.6	2.0	2.2	5.11
IIJ-3.5	3-3-60	8	7	4.0	3.5	10.1	10.1	10.1	2.8	2.5	2.6	6.39
IIJ-4.0	4-6-60	8	7	4.0	4.0	9.93	9.55	9.77	2.0	1.24	1.5	4.37
IIJ-5.0	6-2-60	8	7	4.0	5.0	8.0	8.0	8.0	2.2	1.9	2.0	4.93
IIJ-6.0	3-14-61	8	9	4.0	6.0	5.11	5.23	4.25	1.2	0.47	0.52	1.87
IIJ-7.0	5-20-60	8	7	4.0	7.0	Fall back filled crater leaving an uneven surface at original ground level.						
IIL-4.0	6-1-60	8	7	5.0	4.0	9.4	9.1	9.0	2.2	1.7	1.8	4.86
IIL-4.0B	3-20-61	8	9	5.0	4.0	Mound with max height of 2.2'.						
V-14.3-9.52	8-17-60	256	8	9.52'	14.3'	28.8'	28.8'	28.8'	8.0'	6.5	6.5	6.42
V-15.87-9.52	12-30-60	256	8	9.52	15.87	24.5'	24.5'	24.5'	7.6'	6.0'	6.0'	5.14
II-K-3.5A	3-1-61	8	9	4.5	3.5	9.32	7.89	7.74	2.0	0.66	0.68	3.54
II-K-3.5B	3-6-61	8	9	4.5	3.5	9.72	9.58	8.02	1.8	0.3	0.33	3.01
II-K-4.0	3-9-61	8	9	4.5	4.0	8.51	8.61	8.33	1.8	1.03	1.05	3.60

TABLE 3.2

ing	Av width	Av width at charge	Av width at saddle	Max depth	Av depth at charge (less outer charges)	Av depth at saddle (less outer saddles)	Total volume	Volume of central section	Height of lip		Distance to max lip		Total Mass of Fallout	
									Side	End	Side From ℄	End From last chg		
t	ft	ft	ft	ft	ft	ft	Ft^3/lb He	Ft^3/lb He	ft	ft	ft	ft	KG	Av wid Area
.0	4.3	4.3	4.3	1.2	0.86	0.53	0.43	-	0.4	>0.2	3.6	-		-
.5	6.6	6.6	6.6	1.85	1.64	1.59	1.21	1.19	0.8	0.3	5.3	4.0	NR	1.6
.5	6.1	6.1	6.1	2.1	1.7	1.53	1.71	1.79	0.6	>0.2	4.1	4.0	2081	1.7
.0	5.0	5.0	5.0	1.8	1.12	1.05	1.19	1.08	0.8	0.2	4.5	5.5	2486	1.8
.0	5.5	5.4	5.6	1.6	1.5	0.9	1.75	1.85	0.6	0.4	4.4	4.2		1.7
.0	4.5	4.8	3.3	1.2	1.0	0.6	1.14	1.34	0.8	0.4	4.0	3.7		1.6
.0	4.2	5.0	2.4	1.2	1.0	0.4	1.06	0.94	0.6	>0.2	3.5	4.7		1.9
.0	-	5.6	0.4	1.4	1.2	0.04	1.61	1.94	0.8	0.2	0.0-3.0	3.0		-
.0	7.1	7.1	7.1	1.8	1.6	1.6	2.39	2.47	0.8	0.2	4.8	5.0		1.7
.5	6.1	6.3	6.0	2.0	1.8	1.7	2.45	2.60	0.8	>0.2	4.5	4.5		1.7
.0	8.3	8.3	8.3	2.0	1.8	1.7	3.43	3.80	0.8	>0.2	6.0	4.7	4790	1.4
.0	7.7	7.8	7.6	2.8	2.5	2.3	4.8	5.9	1.4	0.2	6.0	6.0	6462	1.6
.0	6.0	6.6	5.1	2.0	1.8	1.4	3.3	4.0	0.8	0.6	6.5	6.5		1.5
.0	5.3	6.6	2.8	1.5	1.3	0.4	2.3	2.4	1.0	0.2	2-5	4.5		1.6
.5	8.01	8.01	8.01	2.0	1.9	1.8	3.64	3.53	0.6	>0.2	5.6	5.0		1.8
.0	8.05	8.05	8.05	2.4	2.1	2.1	4.66	5.19	1.2	0.2	5.8	4.7	4960	1.6
.5	8.02	8.02	8.02	2.4	2.3	2.3	5.91	6.28	1.2	0.2	6.0	5.5	16,200	1.6
.0	9.32	9.32	9.32	3.0	2.4	2.4	4.28	5.43	1.2	0.4	6.5	5.5	5110	1.5
.5	8.9	8.9	8.9	2.4	1.8	1.8	4.00	4.21	0.8	0.2	6.0	5.0	NR	1.6
.0	8.1	8.1	7.9	1.8	1.2	1.2	2.96	3.12	0.8	0.2	6.0	4.8	5230	1.5
.0	9.03	9.03	9.03	2.9	2.6	2.6	5.98	6.96	1.0	0.2	6.2	5.0	6884	1.6
.0	9.47	9.47	9.47	3.0	2.8	2.8	6.82	8.22	1.0	0.4	6.7	5.0	19,207	1.6
.5	8.45	8.45	8.45	2.8	2.6	2.5	6.66	7.0	1.2	0.2	6.5	4.5		1.7
.5	8.47	8.47	8.47	2.8	2.5	2.3	6.78	5.95	1.2	0.8	6.0	5.5		1.9
.0	7.68	8.12	7.32	2.2	2.1	1.8	6.42	6.34	1.2	0.4	5.4	5.5	6219	1.7
.0	6.36	8.0	3.2	2.0	1.7	0.7	4.70	-	1.2	0.6	4.5	5.0		-
.0	Same as II-J-7.0 with mounds between charges.													
.0	9.59	9.6	9.6	2.6	2.0	2.2	5.11	6.72	1.2	0.2	6.6	5.4	5600	1.4
.5	10.1	10.1	10.1	2.8	2.5	2.6	6.39	7.25	1.5	0.2	7.0	5.5		1.5
.0	9.93	9.55	9.77	2.0	1.24	1.5	4.37	11.05	1.4	>0.2	7.3	-	15,485	.61
.0	8.0	8.0	8.0	2.2	1.9	2.0	4.93	5.24	1.6	0.2	7.0	5.0		1.8
.0	5.11	5.23	4.25	1.2	0.47	0.52	1.87	2.54	1.2	>0.2	5.7	5.0	NR	.74
.0	Fall back filled crater leaving an uneven surface at original ground level.													Original
.0	9.4	9.1	9.0	2.2	1.7	1.8	4.86	5.4	1.6	0.4	8.0	6.0		1.5
.0	Mound with max height of 2.2'.													-
.3'	28.8'	28.8'	28.8'	8.0'	6.5	6.5	6.42	6.42	3.0	1.0	20	7.5		1.6
.87	24.5'	24.5'	24.5'	7.6'	6.0'	6.0'	5.14	5.10	4.0	1.0	16	15		4.98
.5	9.32	7.89	7.74	2.0	0.66	0.68	3.54	1.83	1.8	0.2	7.5	-		1.4
.5	9.72	9.58	8.02	1.8	0.3	0.33	3.01	2.20	1.2	0.2	8.0	-		.6
.0	8.51	8.61	8.33	1.8	1.03	1.05	3.60	3.28	1.6	0.2	7.5	5.5		1.1

ABLE 3.2

me of tral tion lb He	Height of lip Side ft	Height of lip End ft	Distance to max lip Side From ℄ ft	Distance to max lip End From last chg ft	Total Mass of Fallout KG	Av width x av depth Area of profile	Penetrometer lbs (with 1/4" dia tip)	Water content percent	Density lbs/ft^3	Remarks
-	0.4	>0.2	3.6	-		-	18-60 at 0.0 26-51 at 0.19'	5-6 at .19'	96-103 at .19'	
.19	0.8	0.3	5.3	4.0	NR	1.68	NR	5.7	NR	
.79	0.6	>0.2	4.1	4.0	2081	1.72	NR	10.8	NR	
.08	0.8	0.2	4.5	5.5	2486	1.88	NR	8	0 to 6" 91	
.85	0.6	0.4	4.4	4.2		1.78	NR	NR	NR	
.34	0.8	0.4	4.0	3.7		1.68	NR	4.1	NR	
.94	0.6	>0.2	3.5	4.7		1.96	NR	3.8	NR	
.94	0.8	0.2	0.0-3.0	3.0		-	NR	NR	NR	
.47	0.8	>0.2	4.8	5.0		1.72	NR	7.0	81	
.60	0.8	>0.2	4.5	4.5		1.79	NR	7.0-8.0	110-117	
.80	0.8	>0.2	6.0	4.7	4790	1.43	NR	12.5	112.5	
.9	1.4	0.2	6.0	6.0	6462	1.62	NR	5.0-12.0	104-111	
.0	0.8	0.6	6.5	6.5		1.50	110 at 0' 95 at .15'	3.0-11.0	87-108	
.4	1.0	0.2	2-5	4.5		1.64	100 at 0' 90 at .16'	4.0-11.0	92-107	
.53	0.6	>0.2	5.6	5.0		1.83	NR	5.0-10.5	106	
.19	1.2	0.2	5.8	4.7	4960	1.63	NR	4.0-12.0	102-106	
.28	1.2	0.2	6.0	5.5	16,200	1.65	NR	3.0-10.0	92-115	
.43	1.2	0.4	6.5	5.5	5110	1.54	NR	11	111	
.21	0.8	0.2	6.0	5.0	NR	1.66	NR	7-12	99	
.12	0.8	0.2	6.0	4.8	5230	1.56	NR	7	101	
.96	1.0	0.2	6.2	5.0	6884	1.69	NR	12	112	
.22	1.0	0.4	6.7	5.0	19,207	1.61	NR	3-11	109-120	
.0	1.2	0.2	6.5	4.5		1.73	NR	7-9	107-113	
.95	1.2	0.8	6.0	5.5		1.92	NR	2-9	122-130	
.34	1.2	0.4	5.4	5.5	6219	1.78	NR	3-9	110.5	
-	1.2	0.6	4.5	5.0		-	NR	3-10.5	90-103	
							104 at 0.0 68 at 0.17'	5-12	102-112	
.72	1.2	0.2	6.6	5.4	5600	1.498	NR	3-11	110-115	
.25	1.5	0.2	7.0	5.5		1.55	NR	3-10	113-119	
.05	1.4	>0.2	7.3	-	15,485	.616	NR	5-8	107-115	Mound in channel
.24	1.6	0.2	7.0	5.0		1.86	88 at 0' 85 at .15'	3-12	100	
.54	1.2	>0.2	5.7	5.0	NR	.748	60-110	3-9	93.5-118.5	Mound in channel
						Original ground level	56 at 0.0' .67 at 0.18'	4-11	89-102	
.4	1.6	0.4	8.0	6.0		1.52 -	NR 62-110	3-3.5	113-115	
.42	3.0	1.0	20	7.5		1.63	0 to 110	2-6	94.5-112	
.10	4.0	1.0	16	15		4.98 1.79				
.83	1.8	>0.2	7.5	-		1.49	53-110	1-6	106.5-115	Mound in channel
.20	1.2	0.2	8.0	-		.608	65-110	1.5-5.5	118-125	Mound in channel
.28	1.6	0.2	7.5	5.5		1.18	74-110	2.5-6.0	99-100.6	

3

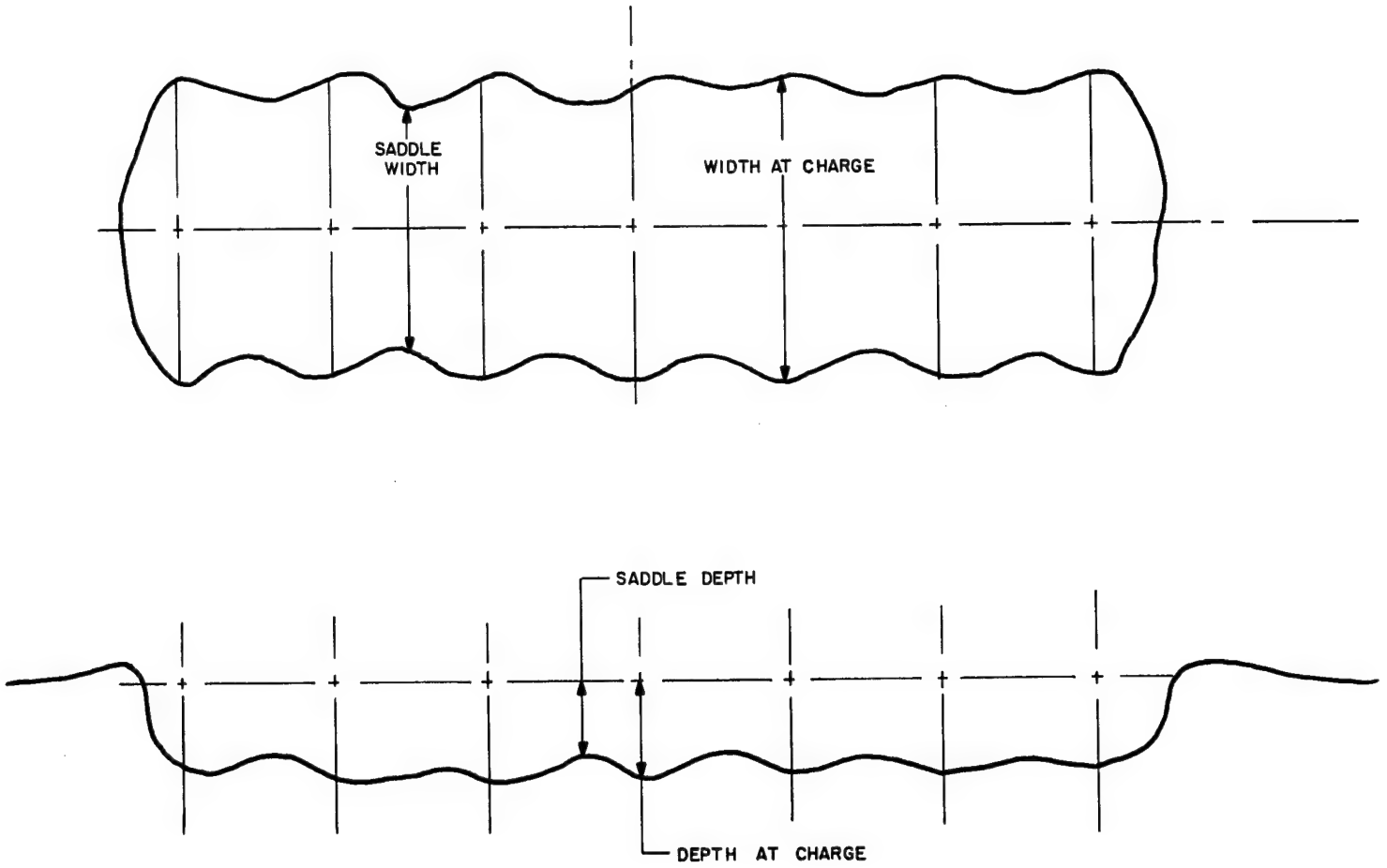

Figure 3.8 Definition of row charge crater dimensions

TABLE 3.3

Shot no.	Date	Charges: Weight lbs	Charges: no	Spacing ft	Line charge equivalent lbs/ft	Line charge equivalent lbs/ft w-1/2	Dob ft	Dob ft w-1/2	Av width ft w-1/2	Av width at charge ft w-1/2	Av width at saddle ft w-1/2	Max depth ft w-1/2	Av depth at charge (less outer charges) ft w-1/2	Av depth at saddle (less outer saddles) ft w-1/2	Saddle width width at charge	Saddle depth depth at charge
II-A2	5-17-60	8	7	2.0	4.0	2.0	0.0	0.0	2.15	2.15	2.15	0.60	0.43	0.26	1.00	0.60
II-C7	6-22-59	↑	↑	1.5	5.33	2.31	1.0	0.432	2.86	2.86	2.86	0.80	0.71	0.69	1.00	0.97
II-C2	7-16-59			2.5	3.20	1.79	1.0	0.558	3.41	3.41	3.41	1.17	0.95	0.86	1.00	0.91
II-C3	9-1-59			3.0	2.67	1.635	1.0	0.611	3.06	3.06	3.06	1.10	0.69	0.64	1.00	0.93
II-C4	10-14-59			4.0	2.00	1.414	1.0	0.707	3.89	3.82	3.96	1.13	1.06	0.64	1.04	0.60
II-C5	10-5-59			5.0	1.60	1.265	1.0	0.790	3.56	3.80	2.61	0.95	0.79	0.47	0.69	0.59
II-C5B	9-24-59			5.0	1.60	1.265	1.0	0.790	3.32	3.95	1.90	0.95	0.79	0.32	0.48	0.41
II-C6	10-16-59			7.0	1.14	1.068	1.0	0.936	-	5.24	0.37	1.31	1.12	0.04	0.07	0.04
II-D3	11-10-59			3.0	2.67	1.635	1.5	0.916	4.35	4.35	4.35	1.10	0.98	0.98	1.00	1.00
II-D3.5	3-9-60			3.5	2.29	1.515	1.5	0.990	4.03	4.16	3.96	1.32	1.19	1.12	0.95	0.94
II-E3.0	12-9-59			3.0	2.67	1.635	2.0	1.222	5.08	5.08	5.08	1.22	1.10	1.04	1.00	0.95
II-E4.0	3-10-60			4.0	2.00	1.414	2.0	1.414	5.44	5.51	5.37	1.98	1.77	1.63	0.97	0.92
II-E5.0	5-24-60			5.0	1.60	1.265	2.0	1.580	4.75	5.22	4.03	1.58	1.42	1.11	0.77	0.78
II-E7.0	5-27-60			7.0	1.14	1.068	2.0	1.872	4.96	6.18	2.62	1.40	1.22	0.37	0.42	0.30
II-F3.5	11-13-59			3.5	2.29	1.515	2.5	1.650	5.29	5.29	5.29	1.32	1.25	1.19	1.00	0.95
II-F4.0	3-11-60			4.0	2.00	1.414	2.5	1.767	5.69	5.69	5.69	1.70	1.48	1.48	1.00	1.00
II-F4.5	3-30-60			4.5	1.78	1.335	2.5	1.873	6.01	6.01	6.01	1.80	1.72	1.72	1.00	1.00
II-G3.0	1-29-60			3.0	2.67	1.635	3.0	1.833	5.70	5.70	5.70	1.84	1.47	1.47	1.00	1.00
II-G3.5	11-10-59			3.5	2.29	1.515	3.0	1.980	5.87	5.87	5.87	1.58	1.19	1.19	1.00	1.00
II-G4.0	12-11-59			4.0	2.00	1.414	3.0	2.121	5.73	5.73	5.59	1.27	0.85	0.85	0.98	1.00
II-G4.0	2-16-60			4.0	2.00	1.414	3.0	2.121	6.38	6.38	6.38	2.05	1.84	1.84	1.00	1.00
II-G4.0	4-4-60			4.0	2.00	1.414	3.0	2.121	6.70	6.70	6.70	2.12	1.98	1.98	1.00	1.00
II-G4.5	2-19-60			4.5	1.78	1.335	3.0	2.247	6.33	6.33	6.33	2.10	1.95	1.87	1.00	0.96
II-G4.5	2-25-60			4.5	1.78	1.335	3.0	2.247	6.34	6.34	6.34	2.10	1.87	1.72	1.00	0.92
II-G6.0	3-4-60			6.0	1.33	1.155	3.0	2.597	6.65	7.03	6.34	1.91	1.82	1.56	0.90	0.86
II-G8.0	3-9-60			8.0	1.00	1.00	3.0	3.000	6.36	8.00	3.20	2.00	1.70	0.70	0.40	0.41
II-G9.0	5-25-60			9.0	0.89	0.943	3.0	3.18	Mound						-	-
II-H4.0	3-28-60			4.0	2.00	1.414	3.5	2.474	6.78	6.79	6.79	1.84	1.41	1.56	1.00	1.11
II-J3.5	3-3-60			3.5	2.29	1.515	4.0	2.64	6.67	6.67	6.67	1.85	1.65	1.72	1.00	1.04
II-J4.0	4-6-60	↓	↓	4.0	2.00	1.414	4.0	2.828	7.02	6.75	6.91	1.41	0.88	1.06	1.02	1.20
II-J5.0	6-2-60	8	7	5.0	1.60	1.265	4.0	3.160	6.33	6.33	6.33	1.74	1.50	1.58	1.00	1.05
II-J6.0	3-14-61	8	9	6.0	1.33	1.155	4.0	3.463	4.42	4.53	3.68	1.04	0.41	0.45	0.81	1.10
II-J7.0	5-20-60	8	7	7.0	1.14	1.068	4.0	3.744	Mound	-	-	-	-	-	-	-
II-K3.5A	3-1-61	8	9	3.5	2.29	1.515	4.5	2.97	6.15	5.21	5.11	1.32	0.44	0.45	0.98	1.02
II-K3.5B	3-6-61	8	9	3.5	2.29	1.515	4.5	2.97	6.42	6.32	5.29	1.19	0.20	0.22	0.84	1.10
II-K4.0	3-9-61	8	9	4.0	2.00	1.414	4.5	3.181	6.02	6.09	5.89	1.27	0.73	0.74	0.97	1.01
II-L4.0	6-1-60	8	7	4.0	2.00	1.414	5.0	3.535	6.65	6.43	6.36	1.56	1.20	1.27	0.99	1.06
II-L4.0B	3-20-61	8	9	4.0	2.00	1.414	5.0	3.535	Mound with max height of 2.2'.						-	-
V-14.3-9.52	8-17-60	256	8	14.3	17.90	4.23	9.52	2.25	6.80	6.80	6.80	1.89	1.53	1.53	1.00	1.00
V-15.87-9.52	12-30-60	256	8	15.87	16.13	4.02	9.52	2.37	6.10	6.10	6.10	1.89	1.49	1.49	1.00	1.00

Figure 3.9 Typical row charge crater in the region of line charge equivalence--seven 8-pound charges, buried 3.5 feet, spaced 4 feet apart

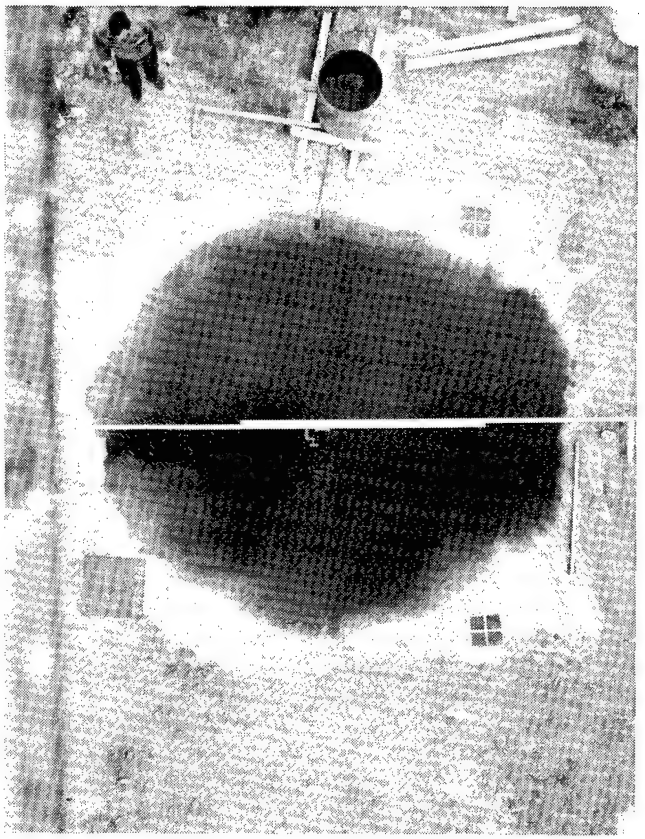

Figure 3.10 Surface contour of a row-charge crater wherein the row charge was too short for the crater to be linear

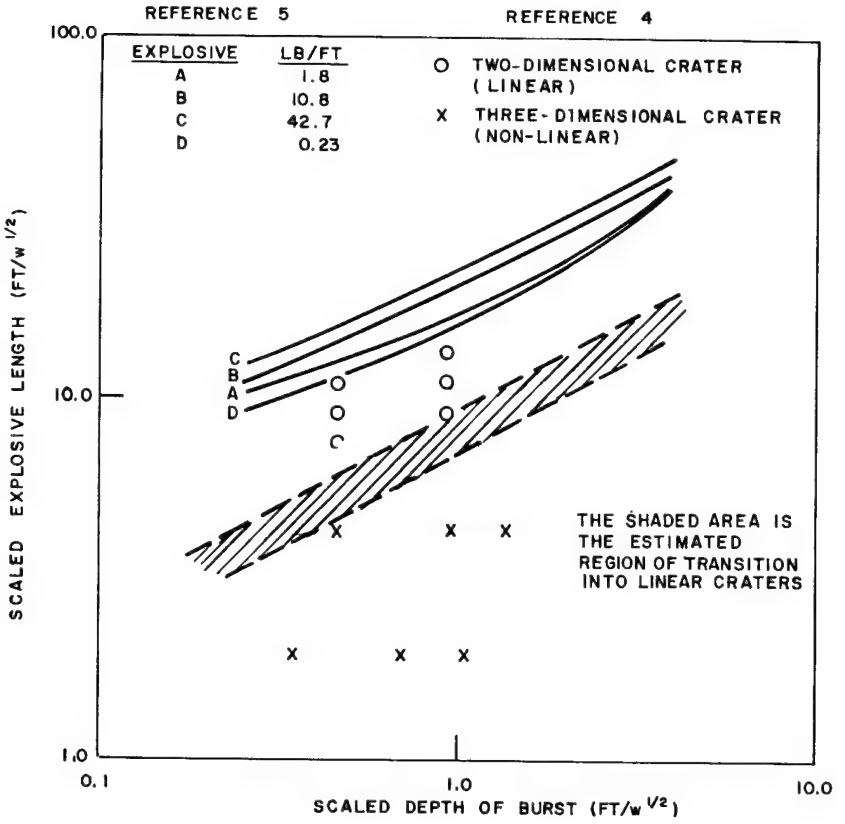

Figure 3.11 Scaled explosive length versus scaled burst depth for craters which are line-charge equivalent and those which are not

The three-dimensional limit is at:

$$\ell < 10 \ (dob/w^{1/2})^{1/2}$$

The two dimensional limit, if we use Carlson's criteria that at least the center third must be two dimensional, is:

$$\ell > 15 \ (dob/w^{1/2})^{1/2}$$

where $\ell = L/w^{1/2}$ is the scaled length of the charge in feet.

The second restriction is that the spacing between charges in the row must be small enough to prevent the separate contribution of each individual charge from being noticeable.

If the spacing is increased beyond the limitation of line-charge equivalence, the crater evidences ridges or saddles between the individual charges (Figure 3.12) and has crossed into the region of line-charge disparity. The definition of the boundary between these two regions as a function of burst depth was a minor objective of the experiment. As the spacing is increased further, mounds tend to form between the charges.

Figure 3.12 Typical row-charge crater in the region of line charge disparity--seven 8-pound charges buried 1 foot, spaced 7 feet apart

In many applications where linear craters are to be used as channels, it is not necessary to have an entirely uniform channel--some variation in channel dimensions is permissible. Take, for example, a ship channel through land whose elevation above water level is small. Under such conditions, a channel formed by explosive cratering will have more than the required depth when a satisfactory width has been achieved. Thus, it is the depth at the saddle that governs the spacing of the charges, and charge spacing which creates relatively high saddles is permissible. Throughout the region of line-charge disparity, we have defined later the following ratios of widths, where all measurements were made in planes perpendicular to the axis of the row:

$$\frac{\text{average width at midpoints between charges (saddles)}}{\text{average width at charge centers}} < 1.$$

A similar ratio has been defined for depth.

For the region of line-charge equivalence the spacing must be close enough that

$$\frac{\text{average depth at midpoints between charges}}{\text{average depth at charge centers}} \approx 1.$$

In the determination of the ratios, the dimensions about the end charges were neglected.

While linear charge scaling (dimensions proportional to $w^{1/2}$) can be used for row charges throughout the region of line-charge equivalence, it is not truly appreciable throughout the region of line-charge disparity; over this region it is preferable to scale linear dimensions as $W^{1/3}$, where W is the weight of an individual charge in the row, rather than by $(W/S)^{1/2}$. Merritt[6] has shown that the two types of scaling are mathematically equivalent for rows of spaced charges.

While the two types of scaling are equivalent, the application should be limited to the region of line-charge equivalence. Clearly, in the region of line-charge disparity, there is for the deeper burst depths, a spacing so large that, although the individual charges would crater, an equivalent line charge would be so small that it would be contained at that depth.

Fastax motion pictures of the ground-surface motion show that, in the region of line-charge disparity, the surface over each individual charge rises ahead of that between the charges. In the region of line-charge equivalence where S < dob, the effect of the individual charges is not evidenced, suggesting that the explosion cavities of the charges coalesce below ground raising the surface uniformly. Between S = dob and the boundary of line-charge equivalence as it is defined in Chapter 4, there is slight surficial evidence of the effect of individual charges evidencing a transition between the two cases. This suggests that a uniform crater may be obtained at a spacing slightly beyond that where the row charges behave as a line charge.

As the depth at which the explosion will be contained is approached, the mounds over individual charges are clearly definable in the region of line-charge disparity (Figure 3.13), but in the line-charge equivalent region the mound takes on a linear character comparable to that of containment of a true line charge (Figure 3.14).

Figure 3.13

Typical crater at a depth approaching containment in the region of line-charge disparity--seven 8-pound charges, buried 3 feet deep, spaced 9 feet apart (1/2 of crater shown)

Part I

Part II

Figure 3.14 Typical crater at a depth approaching containment in the region of line-charge equivalence--seven 8-pound charges, buried 4 feet deep, spaced 7 feet apart

3.3 Throwout

To achieve some degree of uniformity, the raw data obtained from the throwout collectors were plotted on semilog paper and a line faired through the data points from each radial line of collectors. By use of this procedure, values of constant density were obtained and plotted as constant density contours. (The plots are included as Appendix D). From these plots, plots of density as a function of area were obtained.

All of the shots were fired when there was little wind; however, the effect of wind is still evident on most shots at low density concentrations. The density patterns were also influenced in many cases by the tendency of the ejecta to form rays of throwout rather than a circumferentially uniform distribution as a function of distance.

Single Charges -- Figures 3.15 through 3.20 show the area-density plots for throwout for each depth of burst on the single charge shots. The values plotted are circumferential averages. The 256-pound data have been superimposed by scaling the density by $W^{1/3}$ and the area by $W^{2/3}$. The plots show that reproducibility was fairly good; however, the 256-pound data indicate, after scaling, that less throwout material was deposited at the greater scaled distances than on the 8-pound shots.

Row Charges -- One of the features of the crater formed from charges spaced close enough to yield line-charge-type craters was the small amount of material ejected off the ends (Figure 3.21). The full extent of this is illustrated by Shot C-7, where colored beads were buried at a depth of 1 foot (the charge depth) and located 1 foot from the end charge as shown in Figure 3.22. The majority of the beads were recovered closer to the charge center than they had been originally placed.

In an attempt to discover the cause of this inward movement of displaced material, pictures were taken of an end view and a side view of each shot. The view down the long axis (Figure 3.23) was very little different from that which would be taken of a single charge (Figure 3.24). However, the broadside view shows a nearly vertical path for the material on the ends (Figure 3.25).

This end effect was also noted on the line-charge series in Nevada (Toboggan).[5] The amount of throwout material off the crater ends seems to be related to depth of burst and spacing. Figure 3.26 shows a widely spaced line-charge series that exhibits an amount of throwout material off the ends more nearly comparable to that for single charges. It appears that, as a wide spacing is reached, the end charges begin to behave as single charges rather than as a part of the row. This may be considered as further evidence that the comparison of row-charge craters with line-charge craters should be restricted to row charges with close charge spacing--the region of line-charge equivalence.

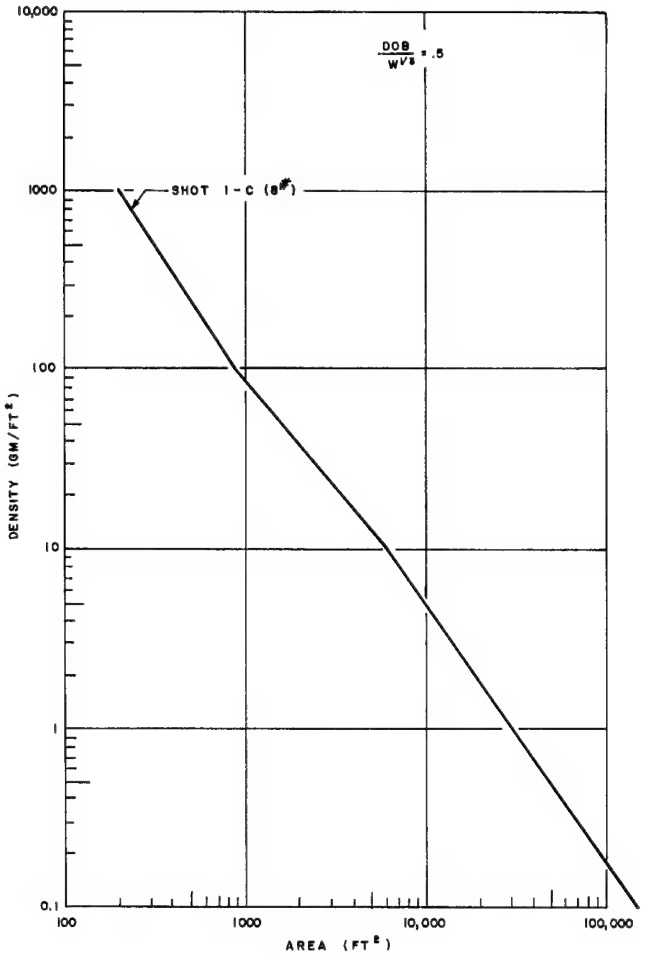

Figure 3.15 Throwout area-density curves for a single charge at a scaled burst depth of 0.5 ft/lb$^{1/3}$

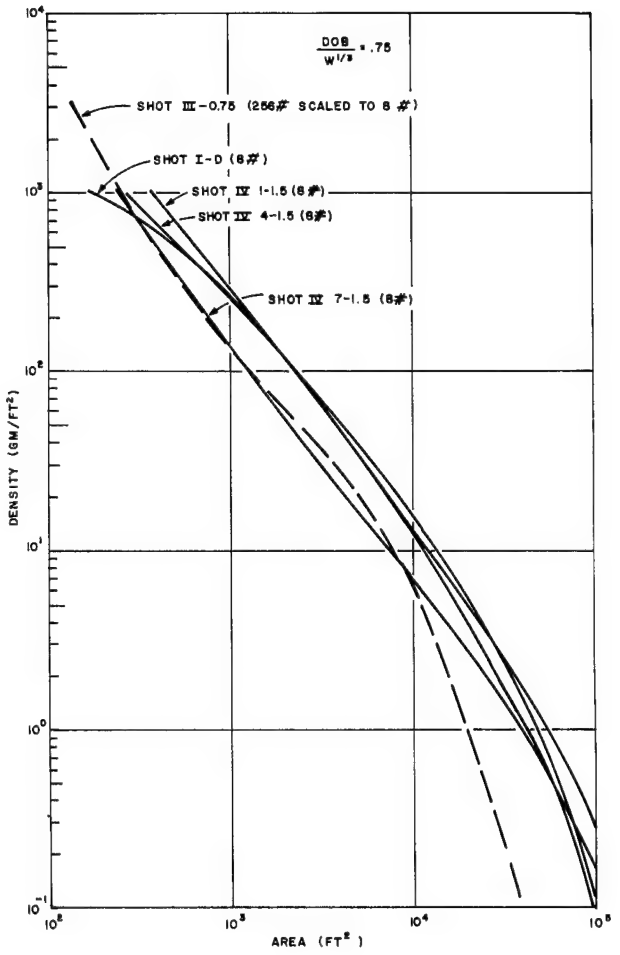

Figure 3.16 Throwout area-density curves for single charges at a scaled burst depth of 0.75 ft/lb$^{1/3}$

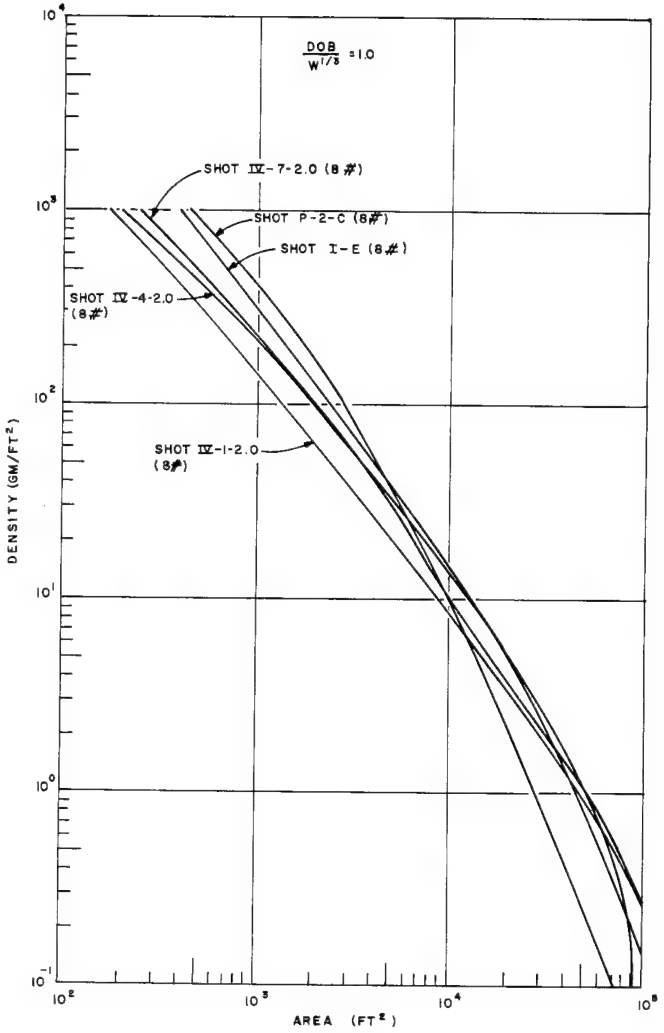

Figure 3.17 Throwout area-density curves for single charges at a scaled burst depth of 1.0 ft/lb$^{1/3}$

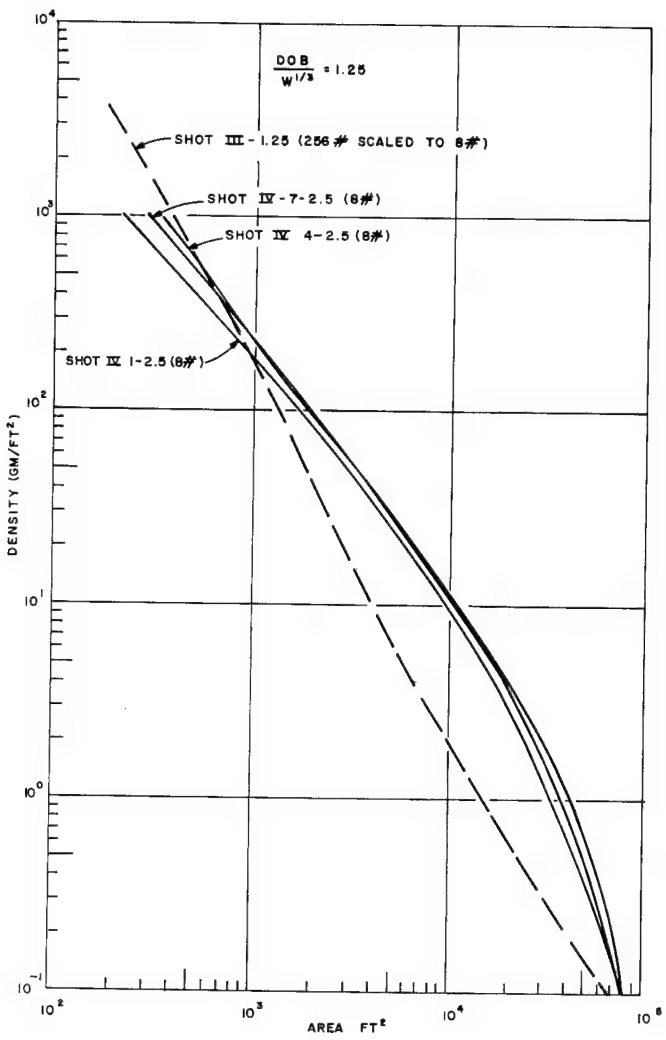

Figure 3.18 Throwout area-density curves for single charges at a scaled burst depth of 1.25 ft/lb$^{1/3}$

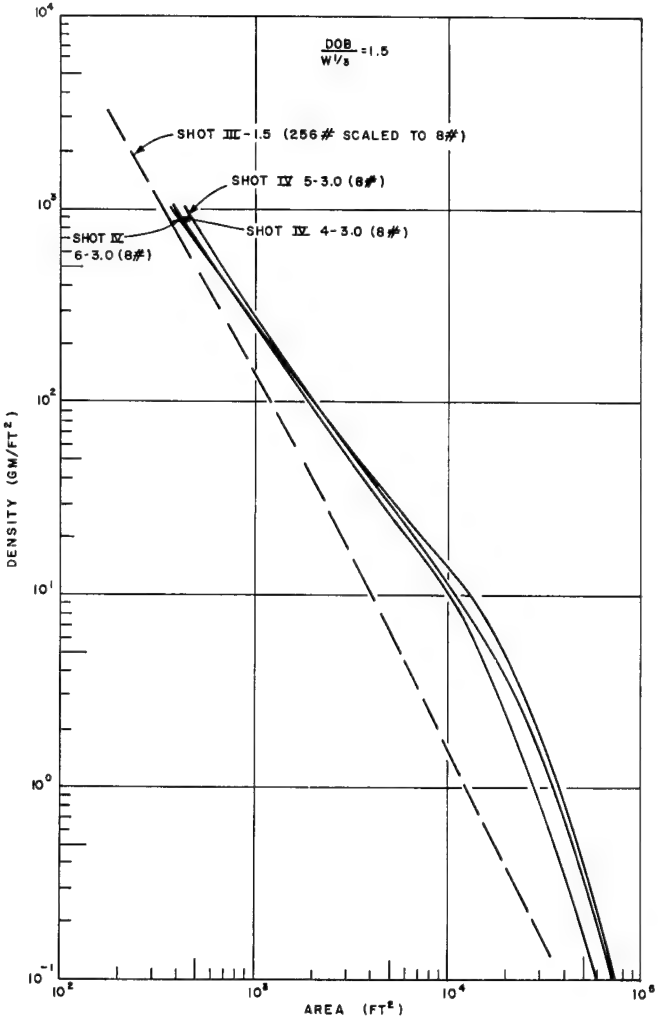

Figure 3.19 Throwout area-density curves for single charges at a scaled burst depth of 1.15 ft/lb$^{1/3}$

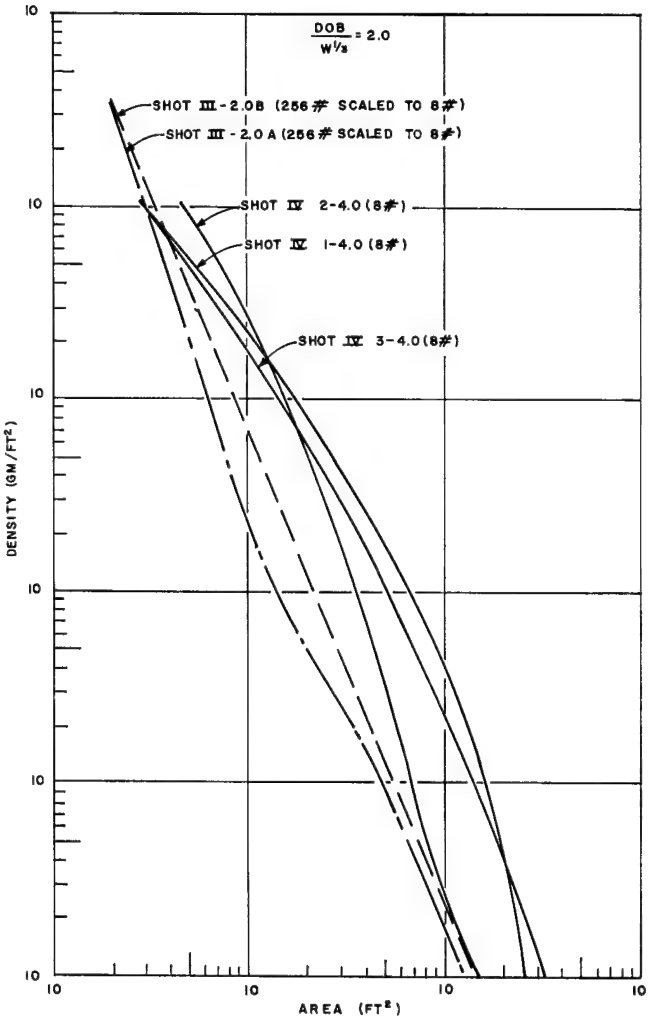

Figure 3.20 Throwout area-density curves for single charges at a scaled burst depth of 2.0 ft/lb$^{1/3}$

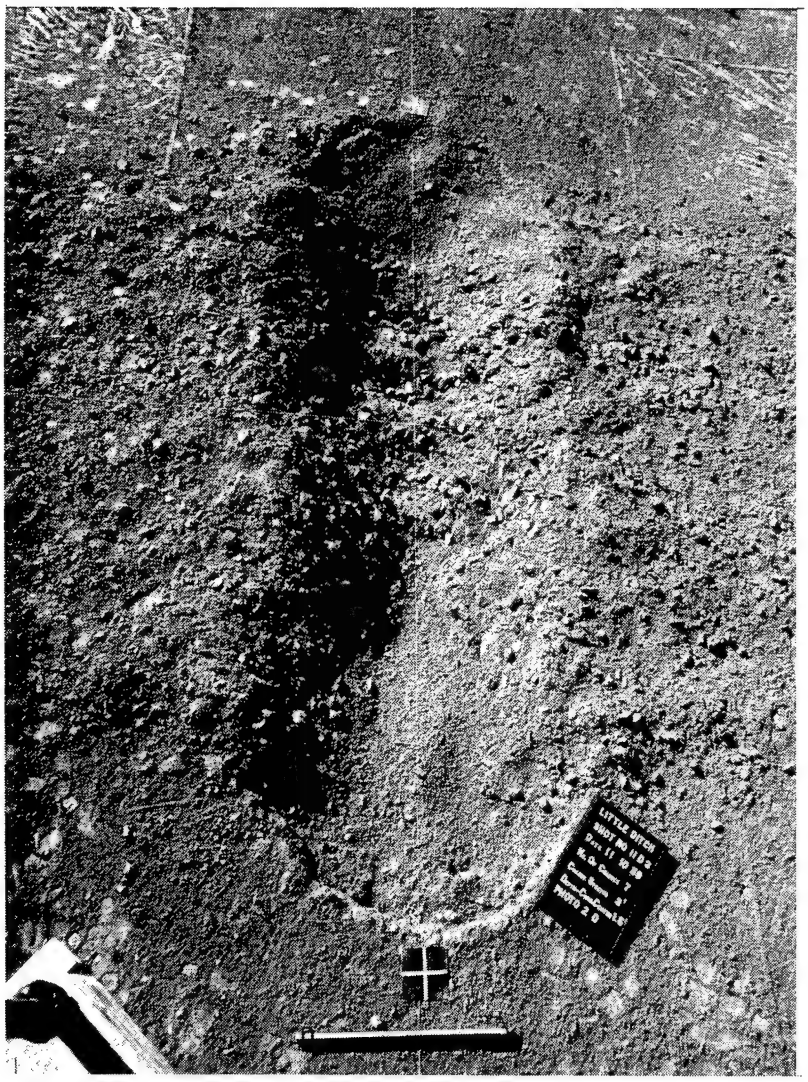

Figure 3.21 Typical row-charge crater showing absence of throwout off the end of the crater--seven 8-pound charges, buried 1.5 feet, spaced 3 feet apart

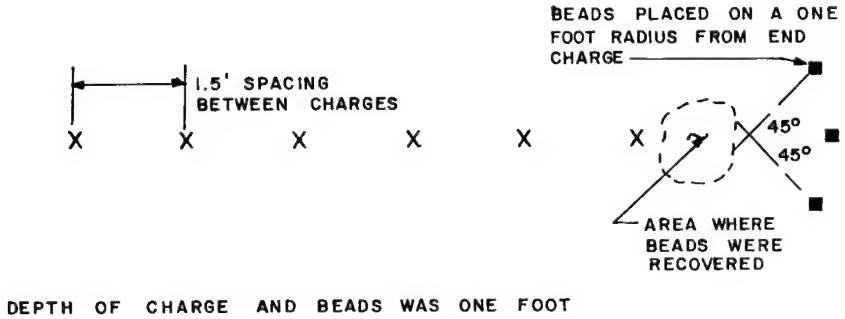

Figure 3.22 Passive evidence of inward motion of debris ejected from the end of the crater

Figure 3.23 Motion sequence, end-on view, 8-pound row charge, spaced 4 feet, buried 3 feet

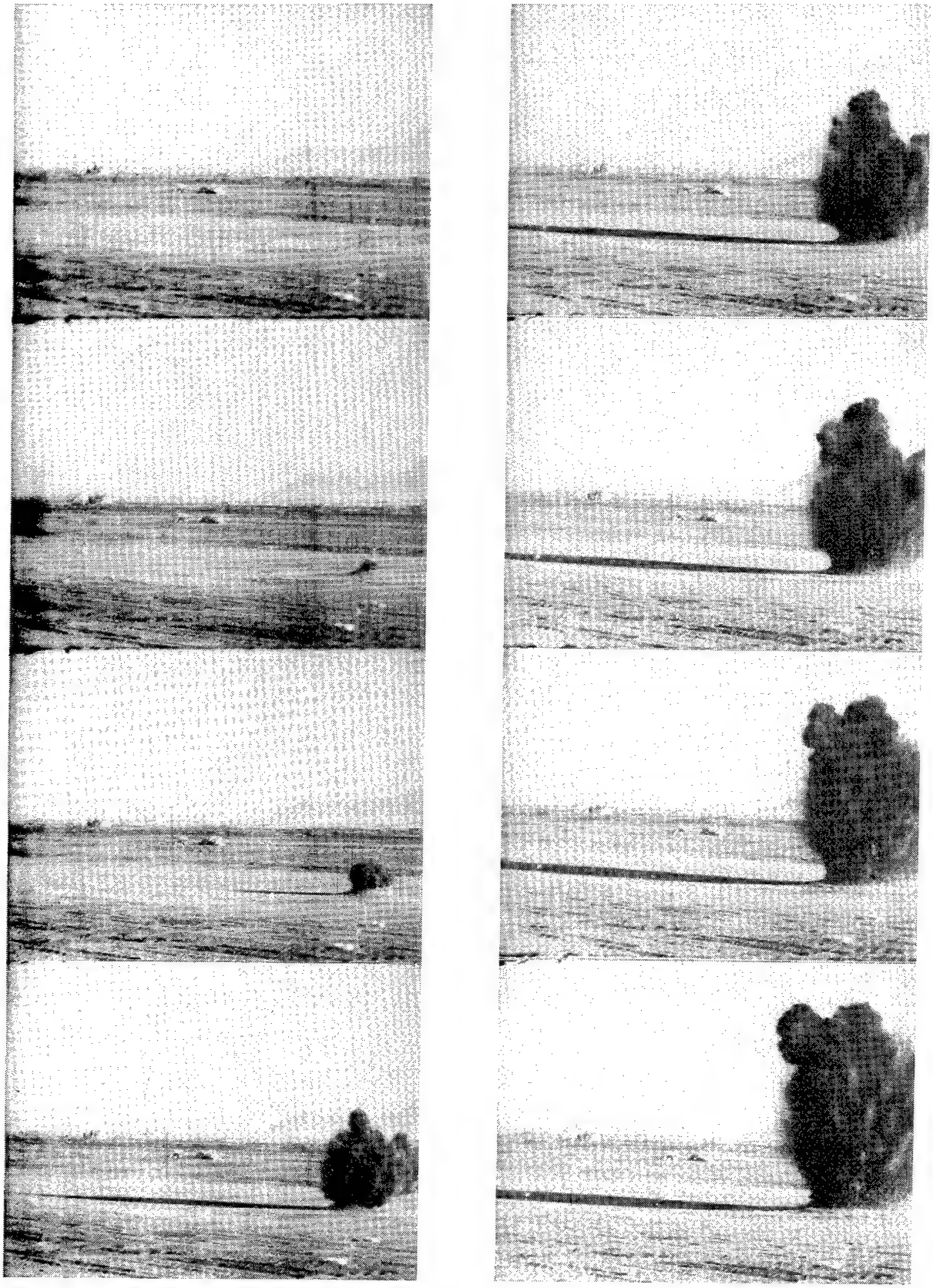

Figure 3.24 Motion sequence, 8-pound single charge, buried 3 feet

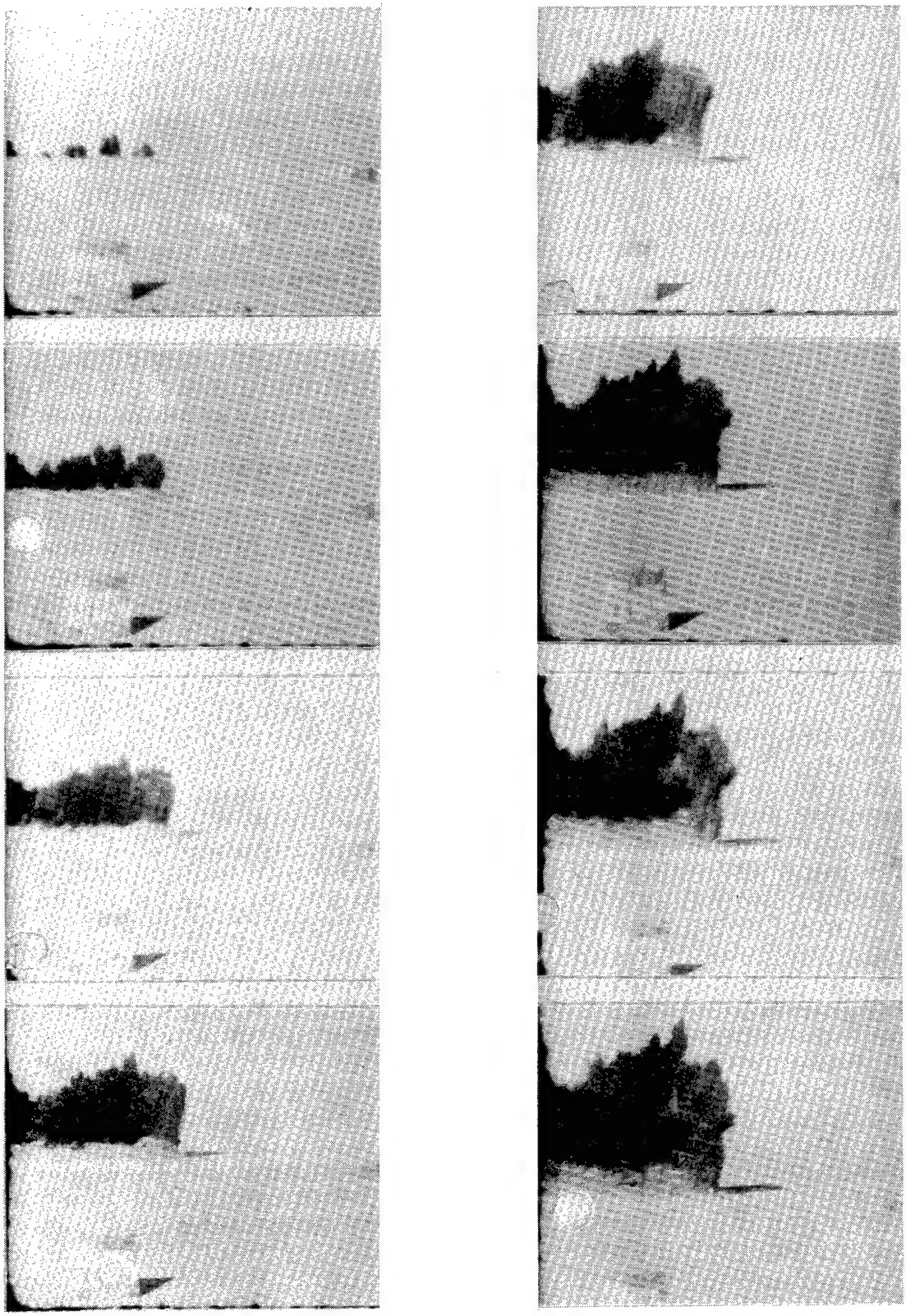

Figure 3.25 Motion sequence, broadside view, 8-pound row charge, spaced 4 feet, buried 3 feet

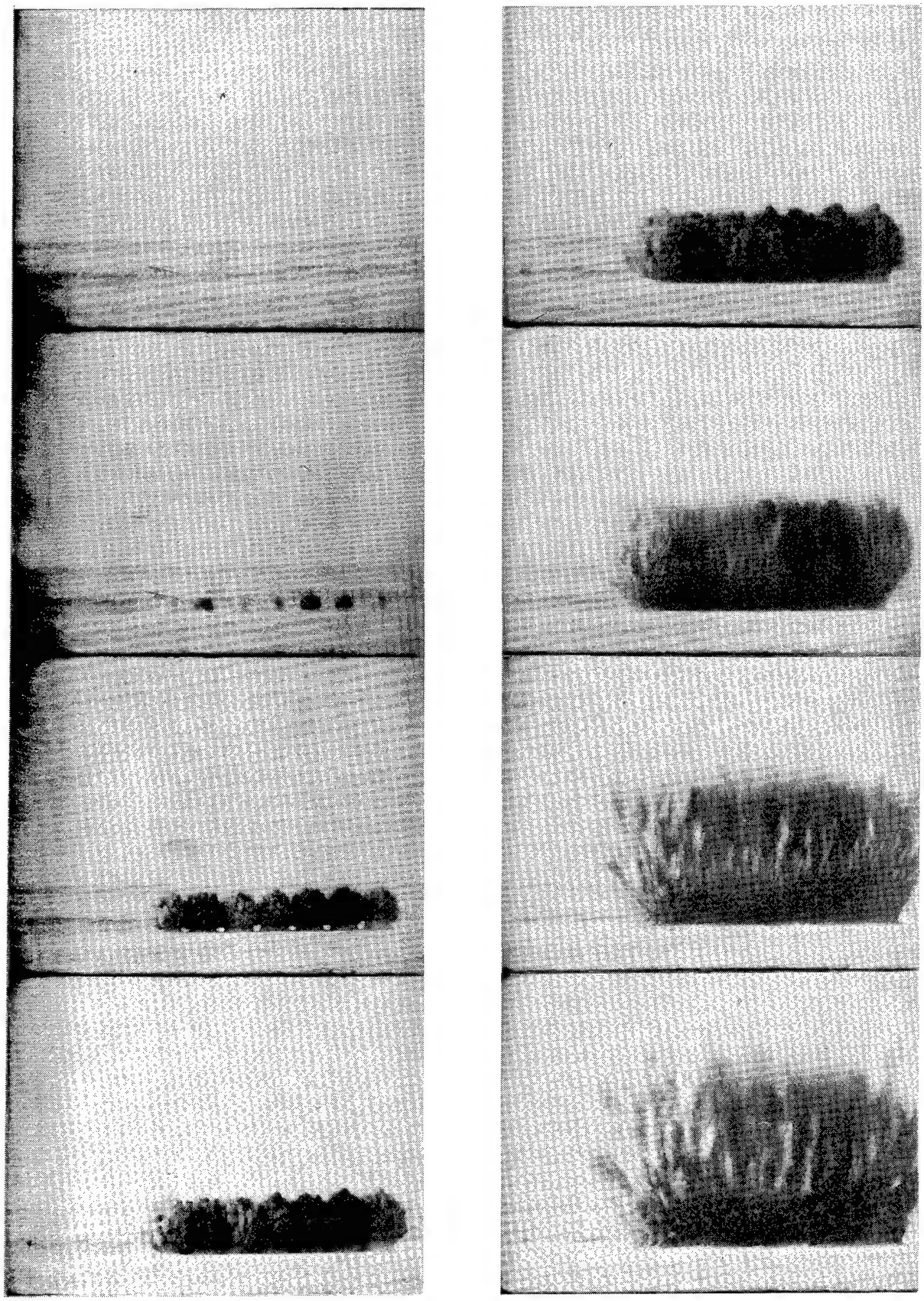

Figure 3.26 Motion sequence, broadside view, 8-pound row charge, spaced 8 feet, buried 3 feet

CHAPTER 4. DISCUSSION

4.1 Craters from Single Charges

Departures from cube root scaling of crater dimensions were found experimentally for the NTS alluvium.[7,8] If these departures are a manifestation of the effects of gravity on crater dimensions rather than the effects of the medium, then one would not be surprised to find similar departures for the Albuquerque soil. However, the range of charge weights used in this experiment was too small to permit detection of such departures, especially in view of the large scatter in crater dimensions of the 8-pound charges.

It is appropriate at this point to compare craters in the Albuquerque fan-delta alluvium with those in the most extensively cratered medium--the desert alluvium of Area 10 of the Atomic Energy Commission's Nevada Test Site. Figures 4.1, 4.2, and 4.3 show the radii depth and volume depth-of-burst curves for the 256-pound charge craters. The comparisons have been made using actual dimensions of 256-pound charge craters for both media to avoid confusion arising from uncertainties in scaling.

The depth and radius depth-of-burst curves for the Albuquerque soil reach maxima at shallower burst depths than those for the NTS soil, the difference between the depths of the peaks for the two soils being slightly greater in the case of crater depth.

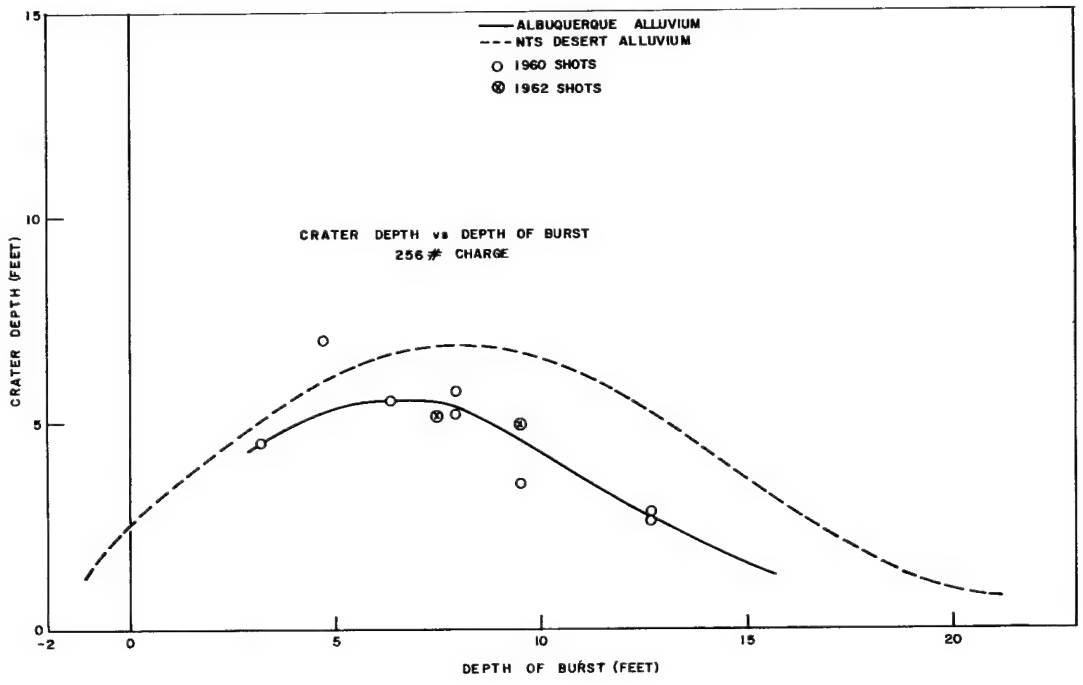

Figure 4.1 Crater depth depth-of-burst curve, 256-pound charges

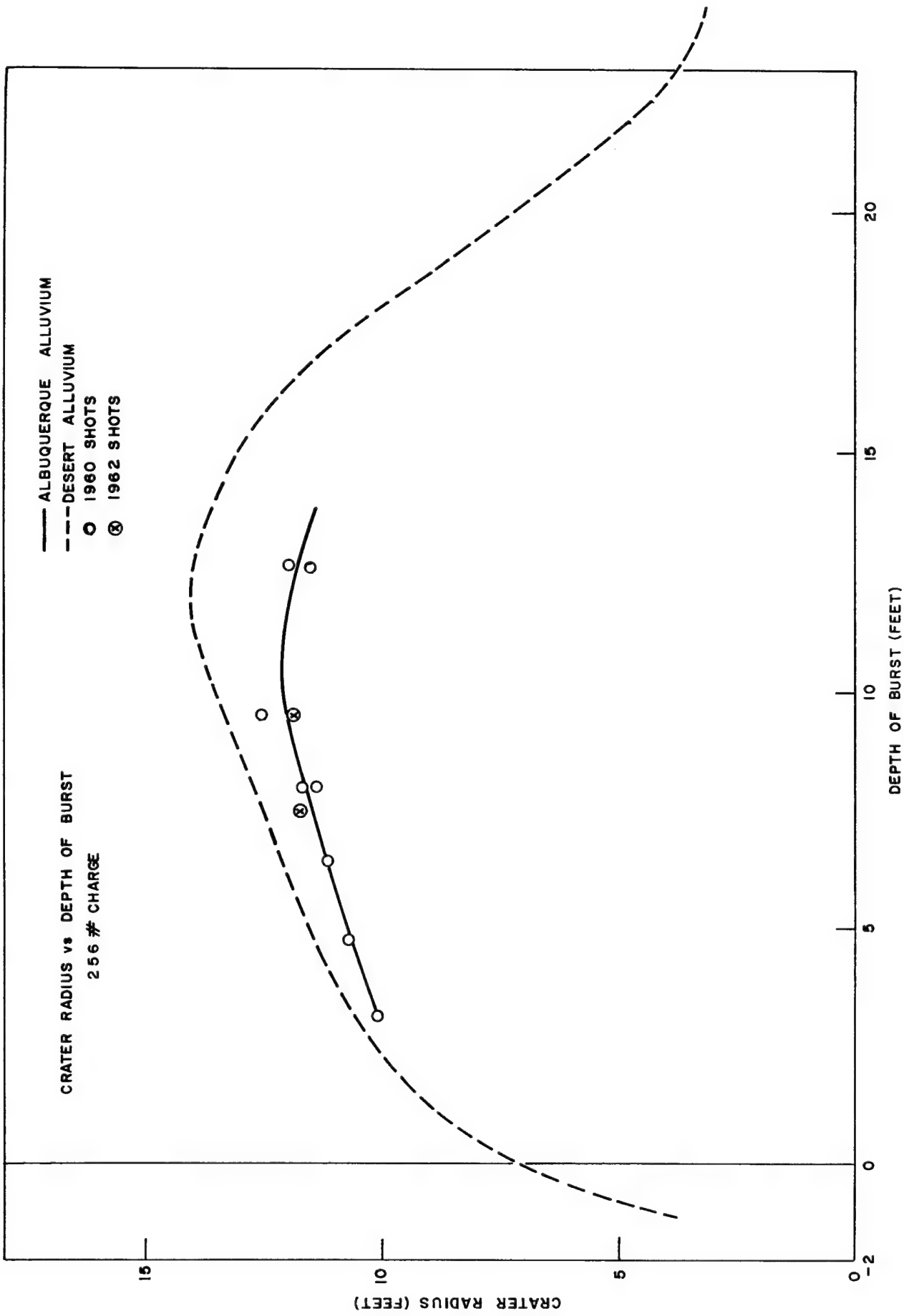

Figure 4.2 Crater radius depth-of-burst curve, 256-pound charges

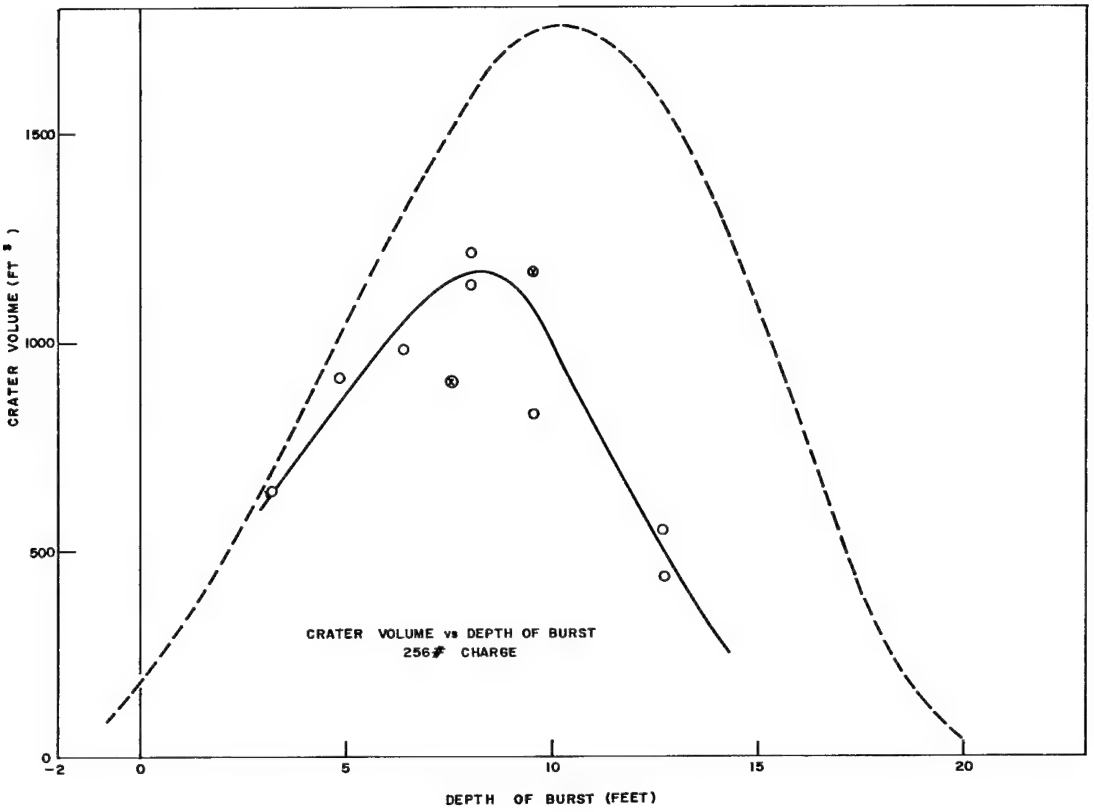

Figure 4.3 Crater volume depth-of-burst curve, 256-pound charges

The difference in the dimensions is a measure of the relative "hardness" of the two soils. The average wet density for the Albuquerque alluvium (101 lb/ft^3) is about the same (99.5 lb/ft^3) as that listed by Piper[9] for the region from the surface to a depth of 16 feet in Area 10, and less than the average (110 lb/ft^3) over a wider range of depths examined for the Project Stagecoach experiment.[10] Since the density of the Albuquerque soil is about the same as or slightly less than that of the NTS alluvium, one must seek some explanation other than density for the source of the differences in crater dimensions. Not enough information is now available to evaluate the relative importance of other soil properties, especially shear strength. Ratios obtained from the curves of Figures 4.1, 4.2, and 4.3, together with subsequent information, can be used to predict the dimensions of row-charge craters in NTS desert alluvium.

4.2 Craters from Rows of Charges

Although row-charge crater data can be considered in terms of either the single charge in the row or in terms of the equivalent line charge, the former has been used in the preparation of information for Figures 4.4 and 4.5. The figures show the ratios of average saddle dimensions to average charge center dimensions as functions of charge spacing and burst depth. The figure identifies the regions of line-charge equivalence and line-charge disparity; it indicates approximately the boundary between the region of explosion containment and the region of cratering.

The region of explosion containment is that from which no crater results. The ground may be disturbed or even mounded, but has no relief below the original level.

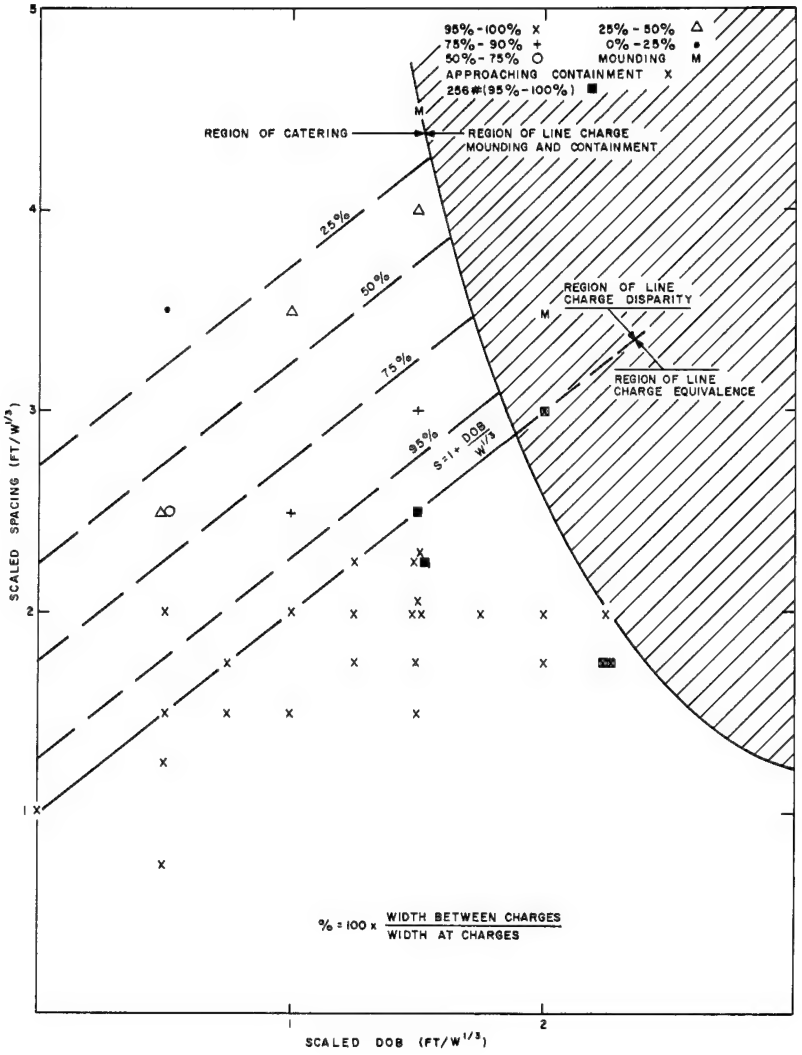

Figure 4.4 Regions of line-charge equivalence and disparity for crater width as a function of scaled spacing and scaled burst depth

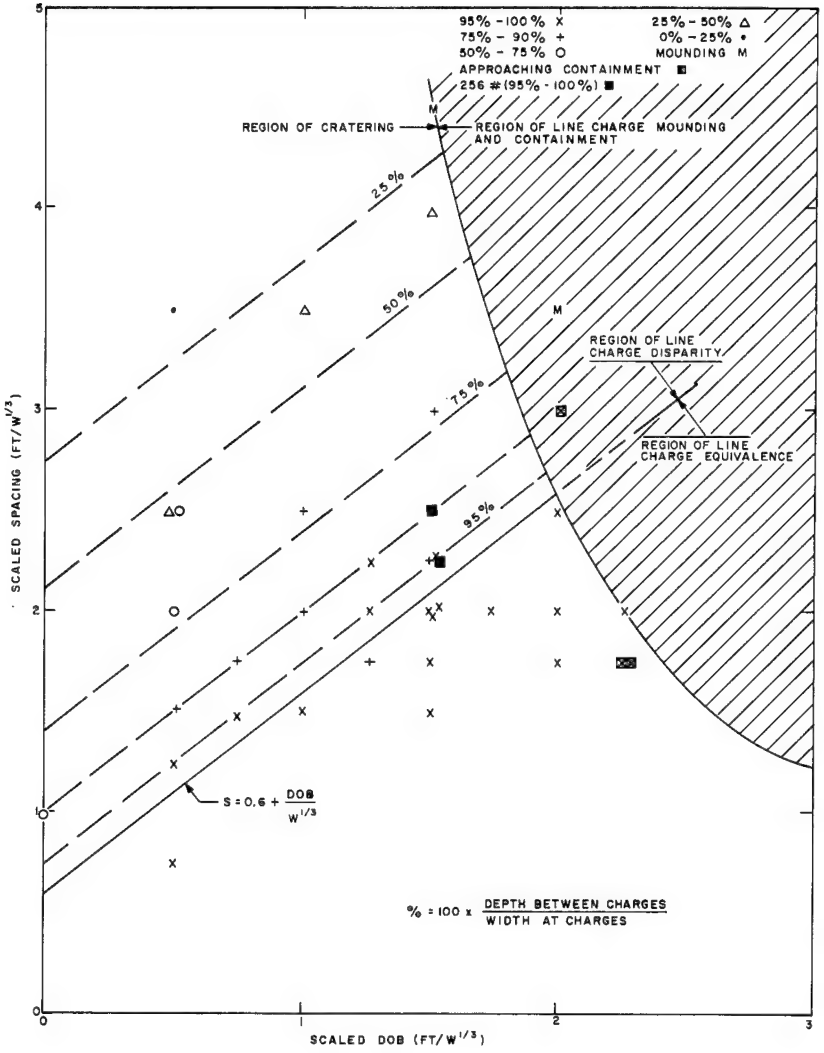

Figure 4.5 Regions of line-charge equivalence and disparity for crater depth as a function of scaled spacing and scaled burst depth

Within the region of cratering are a number of craters which show a mound within a crater or other indication of approaching containment.

The ratios of average saddle dimensions to average charge center dimensions have been delineated throughout the region of line-charge disparity. We have chosen to use straight lines paralleling the boundary of line-charge equivalence to represent lines of constant ratio, even though considerably more data than were obtained in this experiment may show later that a straight line is not the best description of the constant ratio. No shots in this series were fired with spacings so great that separate craters were formed by each charge, that is, that the saddle width and depth were zero.

The remaining region, that of line-charge equivalence, is the only region within which a rigorous comparison with craters from continuous line charges may be made. Using dimensions of only those row charges which showed clear channels, together with similar dimensions from an earlier series using rows of 2-pound charges, the equivalent line charge depth-of-burst curves (linear dimensions proportional to $w^{1/2} = (W/S)^{1/2}$) are given in Figures 4.6, 4.7, and 4.8 for scaled radius, depth, and volume. The maximum dimensions are achieved at scaled-burst depths between 2 and 3 ft/$w^{1/2}$, and are at different scaled-burst depths depending upon whether crater radius, depth, or volume is being considered. As in the case of single-charge craters,[7] the scatter increases greatly between the peak value and containment, and great differences in dimensions are encountered among shots fired at the same burst depth. Because the variations are attributed to the fact that the soil inhomogeneities are large relative to the small charge size, one would anticipate smaller variations with larger charges. Even so, single charge data have shown[10,11] that a penalty of greater uncertainty (larger scatter) is always paid for choosing a burst depth greater than that which gives the maximum crater dimensions.

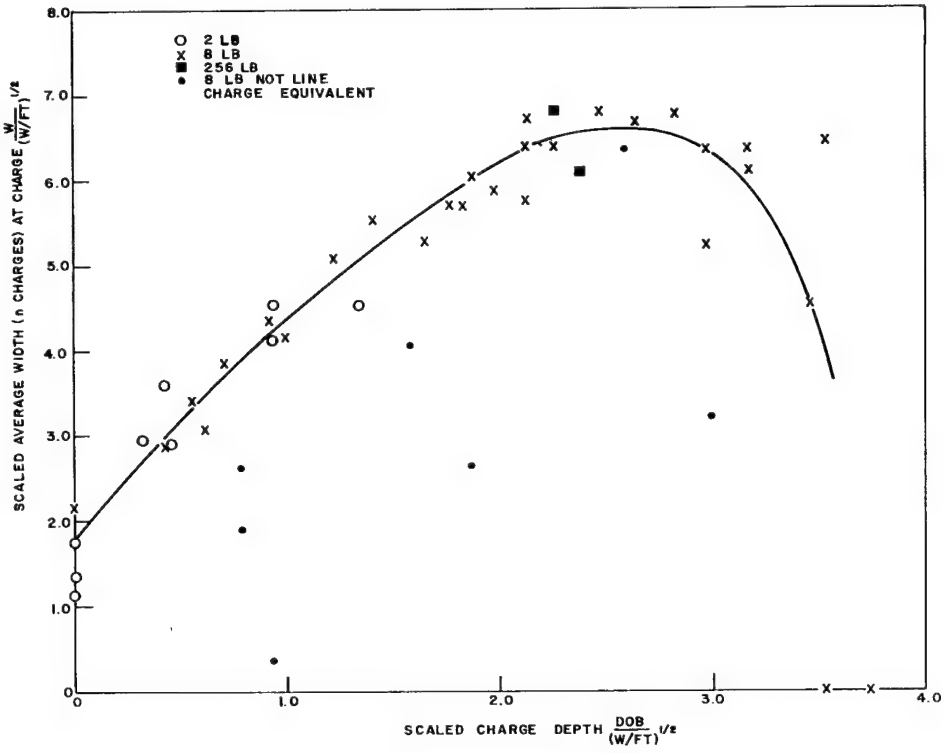

Figure 4.6 Line-charge-equivalent scaled depth-of-burst curve for scaled row-charge crater width

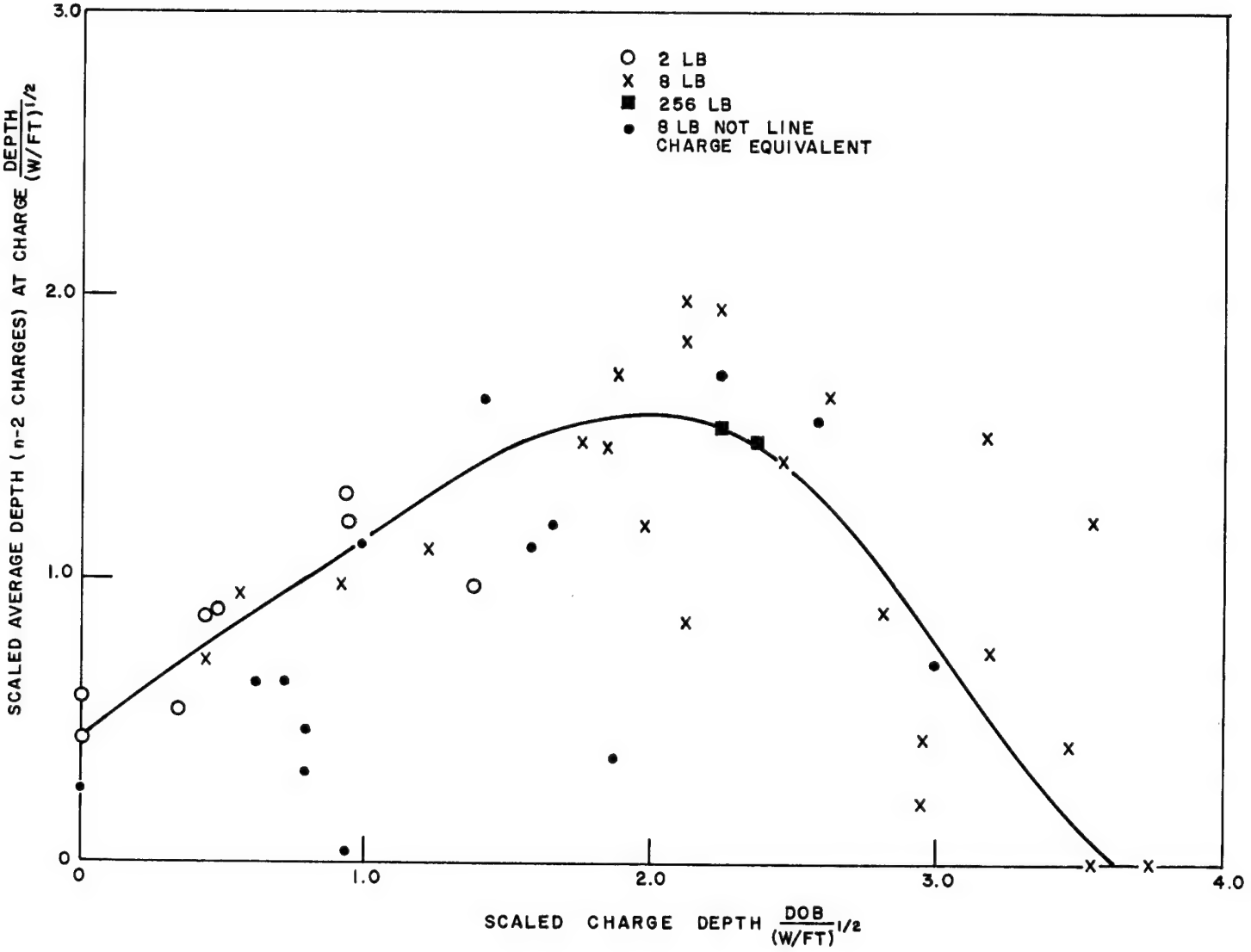

Figure 4.7 Line-charge-equivalent scaled depth-of-burst curves for scaled row-charge crater depth

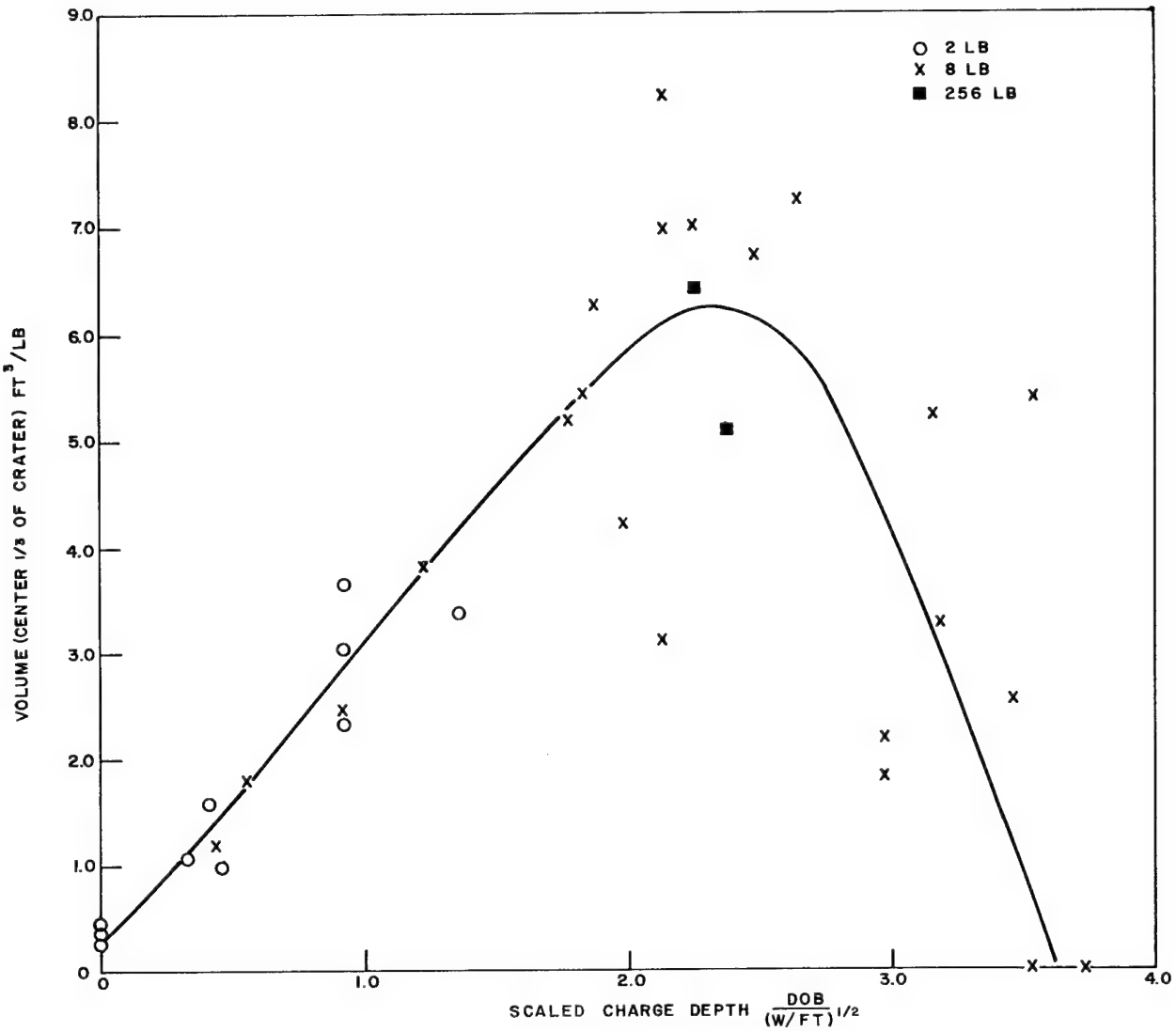

Figure 4.8 Line-charge-equivalent scaled depth-of-burst curve for scaled row charge crater volume

From Figures 4.4 and 4.5, the boundary (limit) of line-charge equivalence can be described as follows

for width: $s \leq 1.0 + \frac{dob}{W^{1/3}}$

for depth: $s \leq 0.6 + \frac{dob}{W^{1/3}}$

where s is the scaled spacing at the boundary in $ft/W^{1/3}$, and dob is the actual burst depth.

Rows of charges spaced closely enough to interact ($S < 3W^{1/3}$) will be contained when

$$\frac{S}{W^{1/3}} > 10.2 \left(\frac{W^{1/3}}{dob}\right)^2 .$$

Note that Figures 4.4 and 4.5 define the largest spacing which will yield a uniform crater and Figures 4.6, 4.7, and 4.8 define the burst depths which maximize the crater dimensions. Together they describe the most efficient employment of chemical explosives. In the figures the region of most efficient employment is most easily defined by the location of the solid squares representing the 256-pound charge craters.

The curved lines in Figures 4.9 and 4.10 indicate the number of charges required at each burst depth and the spacing necessary to give a channel-type crater whose center one-third is two-dimensional as defined by Figure 3.11.

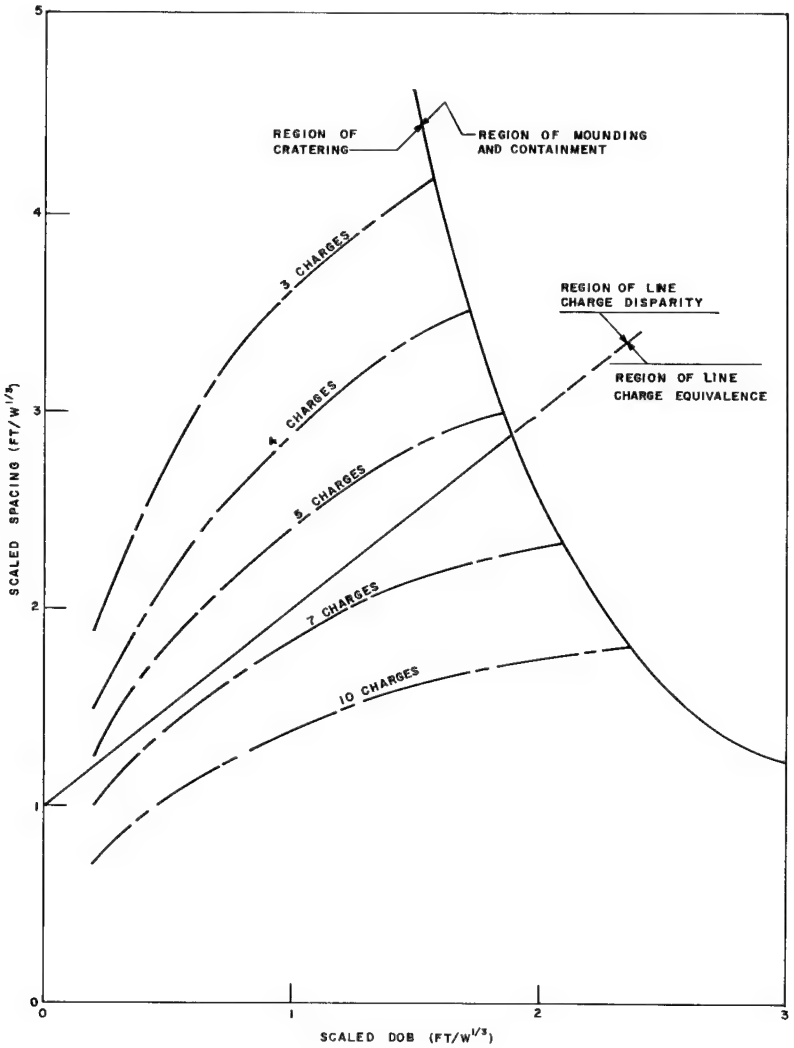

Figure 4.9 Number of charges necessary to give a channel whose width is two dimensional over at least one third its length as a function of scaled spacing and scaled burst depth

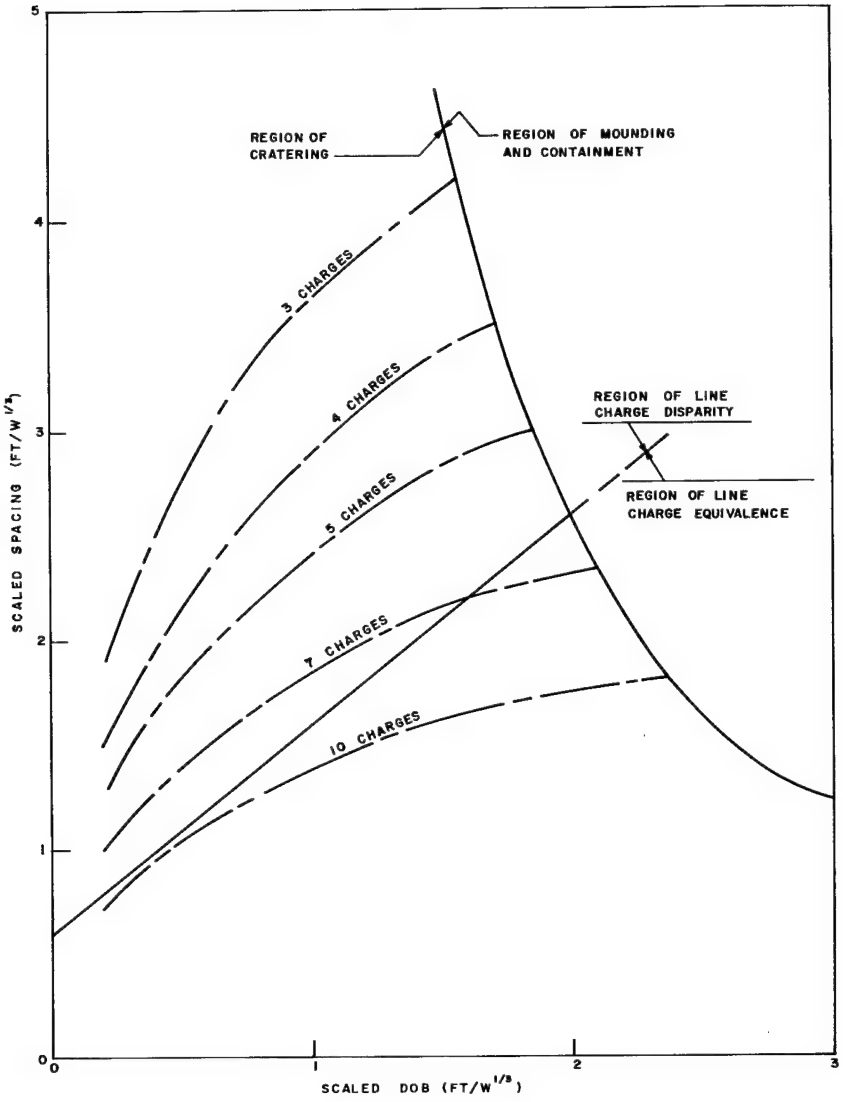

Figure 4.10 Number of charges necessary to give a channel whose depth is two dimensional over at least one third its length as a function of scaled spacing and scaled burst depth

4.3 Craters from Single Charges and Row Charges Compared

For both single and row charges, the crater radius (Figures 4.2, 4.6) is maximized at a burst depth greater than that which maximized crater depth (Figures 4.1, 4.7). Maximum volume (Figures 4.3, 4.8) occurs at a burst depth between those depths which maximize radius and depth. From Figure 4.8, it is clear that the two rows of 256-pound charges were at the depth (9.52 feet) of maximum crater volume. When the most efficient charge spacing was used, the optimum burial depth for row charges was 10 percent greater than the burial depth which optimized crater dimensions from a single charge of the same weight (Figure 4.3). For 256-pound charges

$$\frac{dob_{row}}{dob_{single}} = \frac{9.5}{8.5} = 1.1 \ .$$

Hence, a row-charge crater is optimized at a burst depth 10 percent greater than that which optimizes single charge volume, when, as was the case with the two rows of 256-pound charges, the charge spacing is close to the boundary of line-charge equivalence. A still closer spacing would, of course, result in an increase in the above ratio.

In Figures 4.5 and 4.6, one observes that the 256-pound row charge with the widest spacing (15.87 feet) is at the boundary of line-charge equivalence for uniform crater width which will be referred to here as Case I. The row charge with the closer spacing (14.3 feet) was about 5 percent greater than that which would have been at the boundary of line-charge equivalence for uniform crater depth, here called Case II. A charge spacing of about 13.6 feet would have been closer to line-charge equivalence for crater depth. From the dimensions of 256-pound charge craters from the burst depths above, ratios of radius and depth can be obtained for the two cases:

Case I (Row charges optimized for uniform width)

$$\frac{\frac{1}{2}W_{row}}{R_{single}} = \frac{24.5/2}{11.75} = 1.05$$

$$\frac{D_{row}}{D_{single}} = \frac{6}{5.1} = 1.15$$

Case II (Row charge optimized for uniform depth)

$$\frac{\frac{1}{2}W_{row}}{R_{single}} = \frac{28.8/2}{11.75} = 1.20$$

$$\frac{D_{row}}{D_{single}} = \frac{6.5}{5.1} = 1.25$$

For Cases I and II the spacing can be defined in terms of single-charge crater radius at the burst depth which optimizes crater radius,*

Case I

$$\frac{S}{R_{single}} = \frac{15.87}{12.1} = 1.3$$

Case II

$$\frac{S}{R_{single}} = \frac{13.6}{12.1} = 1.1$$

There is, of course, no assurance that the ratios given here will apply to other media.

*Note in Figure 4.3 that, if the burst depth (8.5 feet) which optimizes crater volume is used in Figure 4.1, the radius is less than the maximum value and the spacing is closer by a corresponding amount.

Craters from single charges are ordinarily considered to be paraboloids of revolution and the cross sections of linear craters to be parabolas. It can be shown that, while craters from single charges in NTS desert alluvium are almost parabolas, they depart from the shape of a parabola toward that of a cone. By comparing $\pi r^2 d/V$ for all such craters, one finds that the value shifts with burst depth from nearly 2.4 at the surface to about 2.1 at the optimum burst depth. Although there is considerable scatter (Figure 4.11) in the shape of the ten 256-pound single-charge craters reported here, there is nothing to refute the observation made on the NTS craters.

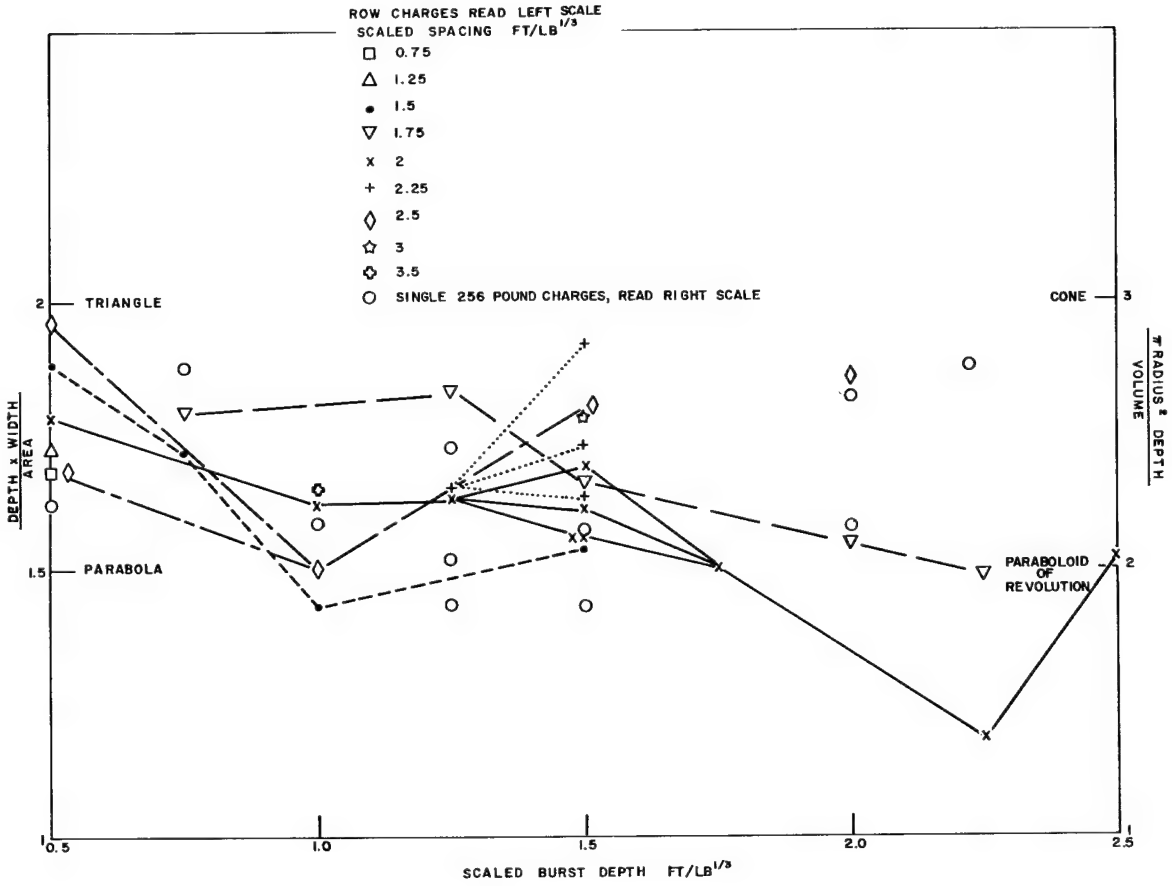

Figure 4.11 Trends in shape of single and row-charge crater profiles with scaled burst depth and scaled charge spacing

Similar scatter was encountered in the shape of the row-charge craters (Figure 4.11). Nonetheless, a similar trend toward a parabola with increased burst depth is discernible. When one examines (Figure 4.12) the trend with spacing at one constant scaled burst depth (1.5 $ft/lb^{1/3}$), a trend from a parabolic cross section toward a triangular one is suggested.

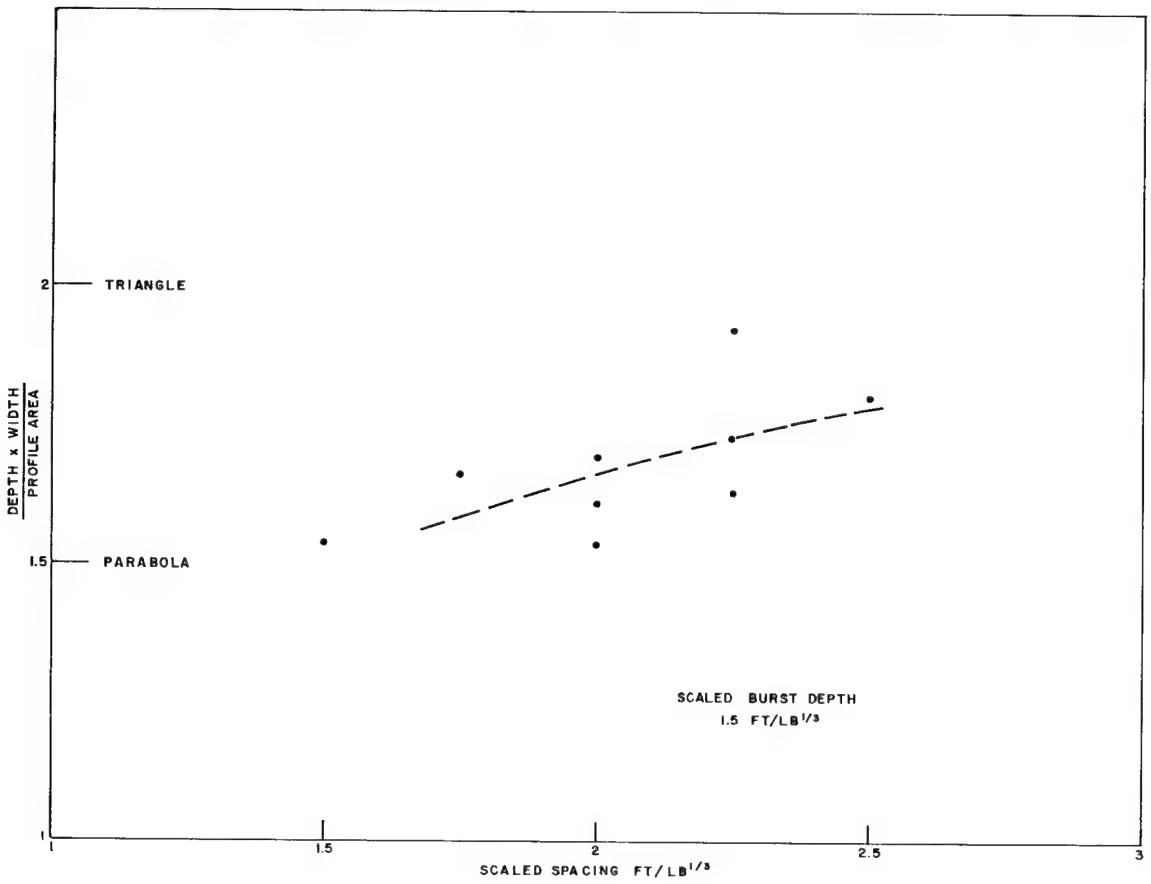

Figure 4.12 Trends in the shape of row-charge crater profiles with scaled spacing at a constant scaled burst depth

4.4 Throwout

4.4.1 Single Charges

The throwout from an explosion in the Albuquerque alluvium ranges from clods, which are relatively insensitive to drag forces, to fine aerosol material the displacement of which is greatly dependent on wind conditions. The fine material may also be influenced by the air blast if, while in its trajectory, it is within the blast wave. The particle size distribution is also a function of burst depth, since a larger percentage of the material ejected by a surface or near surface burst is close to the charge, is crushed more by the shock wave, and is dispersed as fine material. No attempt was made in this experiment to distinguish between that material which emerged as fines or clods since clods were usually further broken on impact.

The ejecta is given its initial velocity by the shock wave followed by an added impetus from the gas pressure. It might be expected that the material which has a high angle of ejection would fall close, but this is precisely the material which has the largest initial velocity. It has been shown[10] that the material in the region near the surface and about one-third of a crater radius from the surface zero is ejected farthest. In the case of 8-pound single charges (Figure 4.13), less material fell at the close distances for the shallowest shot, and less at the farthest distances for the deepest shot. In the case of the 256-pound charges also (Figure 4.14), it has been observed that less material reaches the greater distance and more falls at the closer distances as burial depth is increased.

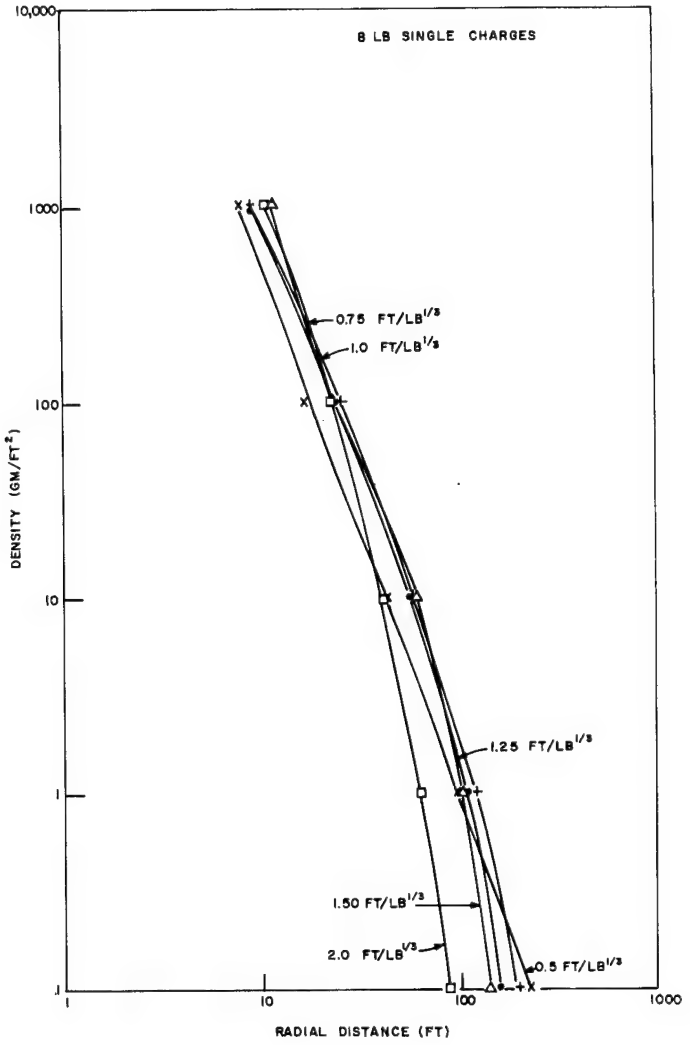

Figure 4.13 Throwout density-distance plots for 8-pound single charges at various burst depths

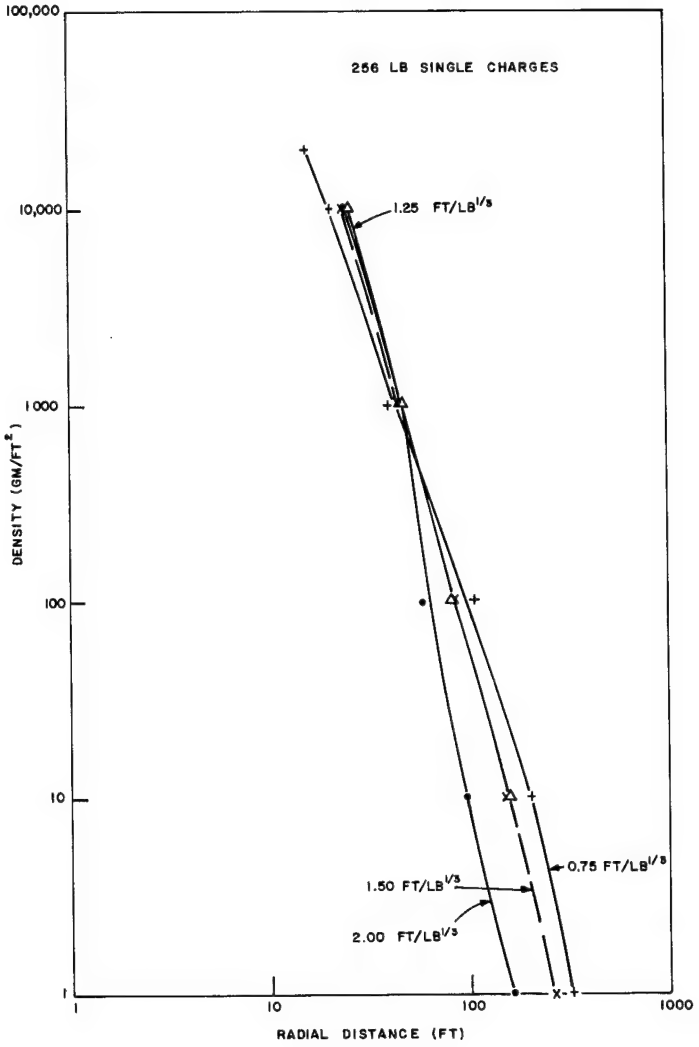

Figure 4.14 Throwout density-distance plots for 256-pound single charges at various burst depths

The accumulated percentage of throwout volume is plotted against the distance from the crater edge in terms of the crater radius (Figure 4.15). The results show that for 256-pound charges three times as many crater radii must be reached for the deepest shot before accounting for 90 percent of the throwout volume as is the case for the two shallower shots. The 90-percent level for the 8-pound charge was reached at nearly four times as many crater radii as for the 256-pound charge at the corresponding burst depth. However, the 50-percent level for the 8-pound charge was reached at only about two times as many radii. These observations suggest that no simple method of normalizing the throwout for the two different charge weights is involved. Clearly, however, the same scaling does not apply to both the crater radius and the radial distance to which the same percentage of total throwout volume is ejected.

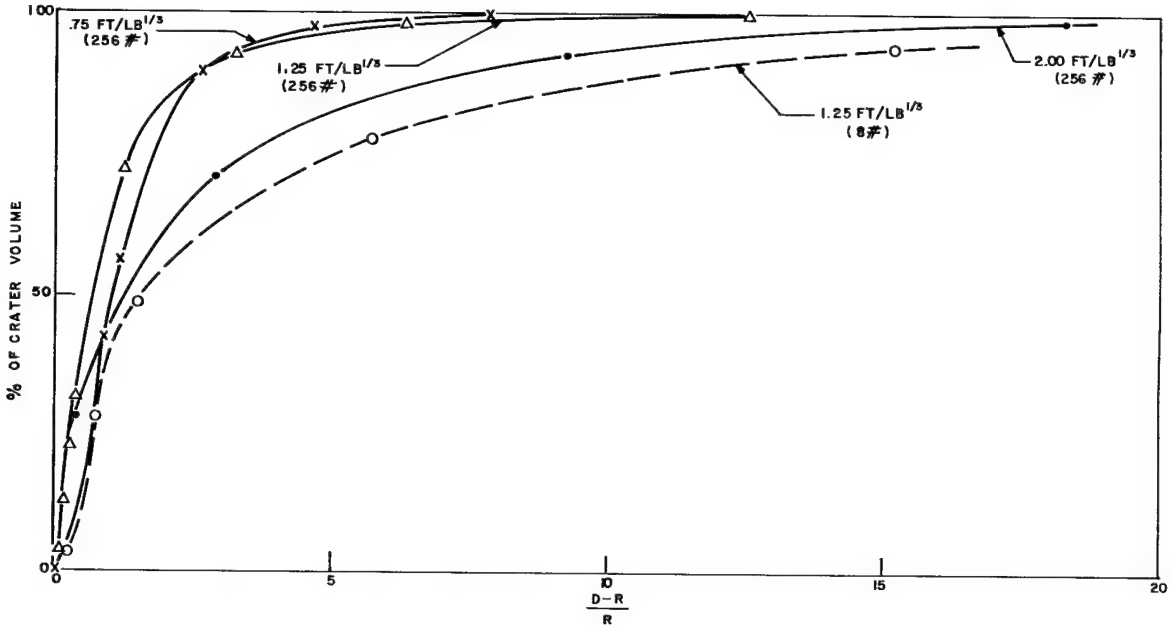

Figure 4.15 Percent of crater volume ejected to a given scaled distance for single charges at three scaled burst depths

4.4.2 Row Charges

The distribution of ejecta from row charges laterally differs from the distribution off the end of the row. Figure 4.16 shows the density-distance curves of ejecta for rows of six 8-pound charges spaced 4 feet apart and buried 2, 2.5, 3, 3.5, and 4 feet deep measured normal to the midpoint of the row. The density-distance curves of ejecta off the end of the row are shown in Figure 4.17. Distances off the end of the row are measured from the end charge.

Certain observations concerning ejecta patterns can be made. First, as mentioned earlier, there is less material ejected off the end of the row. This is especially true only at the closer distances. At the greatest distances, the densities are about the same as those perpendicular to the axis of the row (comparison of Figures 4.16, 4.17). This suggests that most of the material collected at the greatest distances was airborne, in contrast to that which has a ballistic trajectory and falls closer to the crater. Second, the material was ejected laterally to distances which generally decrease as burst depth is increased (Figure 4.16). Exceptions occur at the shallower burst depths where higher densities at the greater distances are obtained at the expense of those at the closer locations. Third, off the end of the row the pattern is either inconclusive or suggest that throwout is maximized at one depth of burst, since the shot at the 3-foot burst depth gave the greatest throwout over most of the range.

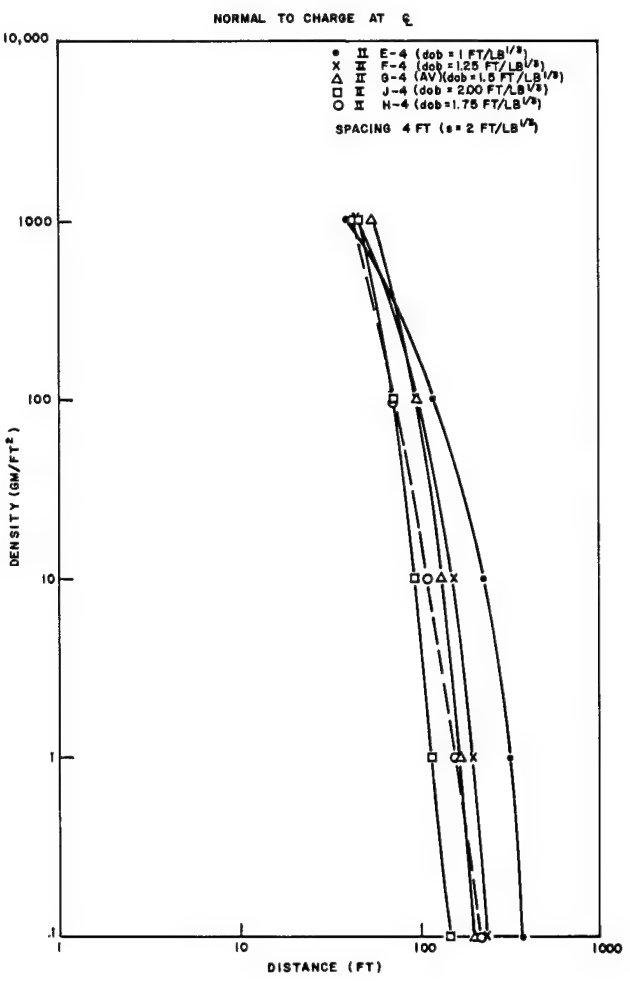

Figure 4.16 Throwout density-distance plots normal to an 8-pound row charge spaced at 4 feet and buried at various scaled burst depths

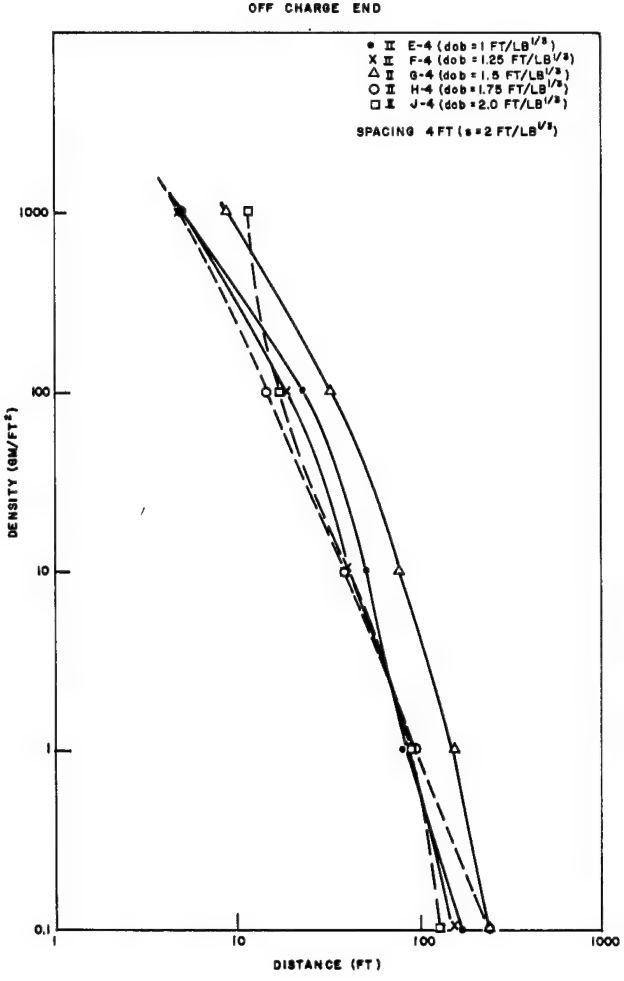

Figure 4.17 Throwout density-distance plots off the end charge of an 8-pound row charge spaced at 4 feet and buried at various scaled burst depths

When charge burst depth is held constant, the influence of charge spacing on throwout is demonstrated. Generally, the greater the spacing the less the density of ejecta perpendicular to the long axis of the row (Figure 4.18) and the greater the density at the intermediate ranges off the ends. Densities off the end show less variation with charge spacing (Figure 4.19).

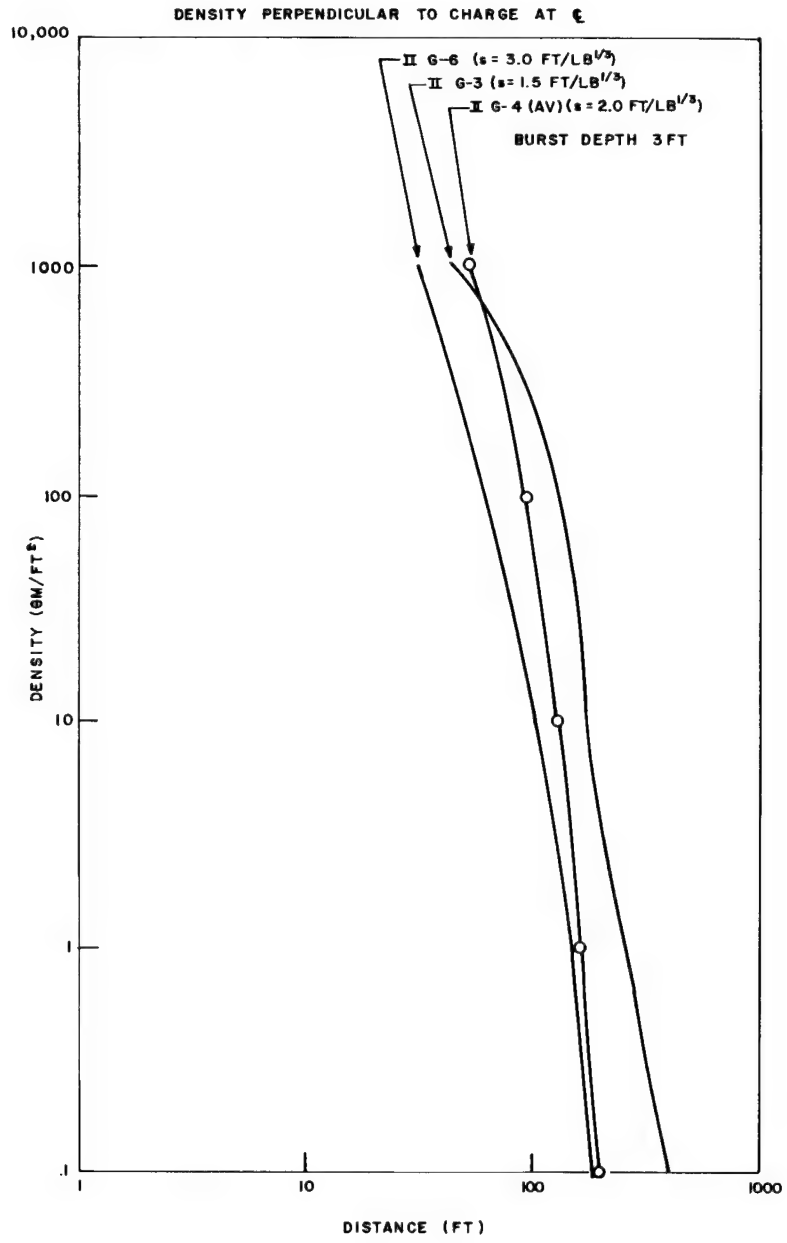

Figure 4.18 Throwout density-distance plots normal to an 8-pound row charge buried at 3 feet with various spacings between the charges

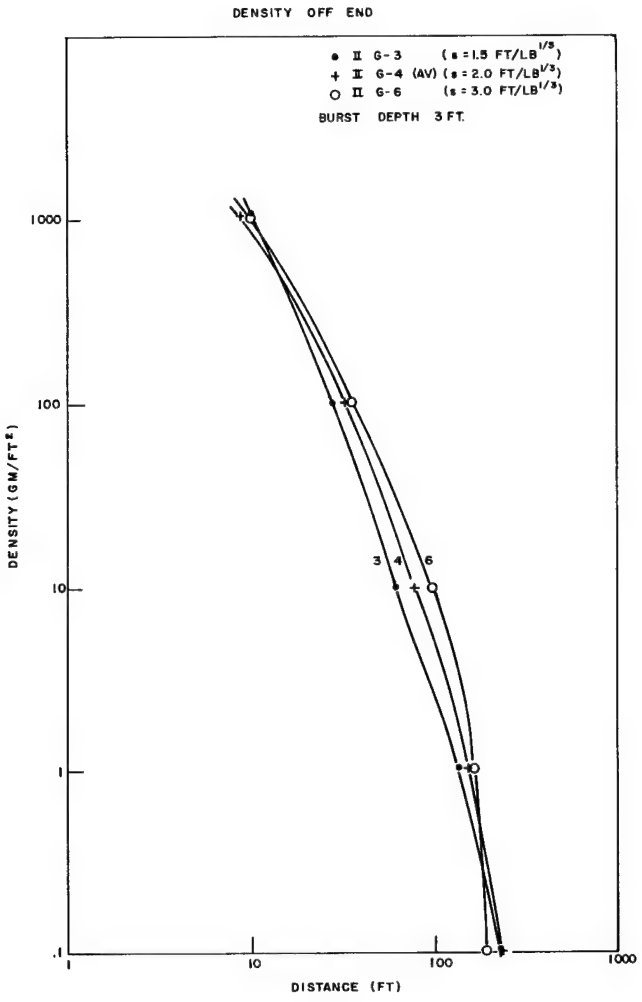

Figure 4.19 Throwout density-distance plots off the end of an 8-pound row charge buried at 3 feet with various spacings between charges

Two 8-pound row charges (II-6-4.5) were exploded at the same cube-root-scaled burst depth and spacing as one of the 256-pound row charges. Unfortunately no throwout measurements were made on either of the two shots. In order to make, for row-charge throwout, a comparison similar to that made in Figure 4.15 for single charges, the results of the 256-pound row-charge throwout may be compared (Figure 4.20) with results of an 8-pound row charge at the same scaled-burst depth but at a slightly smaller spacing (II-G-4). At the very close distances the percentage of throwout is equal to that from the larger charges, and at the greater distances it is considerably less. Obviously, the distance to which a given percentage of total throwout is ejected scales in a different manner from the crater radius.

Figure 4.20 illustrates the effect of varying the scaled burial depth while keeping spacing constant for three shots of 8-pound row charges. It is interesting to note that the percentage of throwout of one of the 8-pound shots (II-J-4) agrees well with that of the larger charge row, even though the smaller charges were buried relatively more deeply. This experiment did not provide enough information to permit us to determine whether a different scaling law for charge burial depth would normalize the percentage ejected to a given scaled distance from row charges.

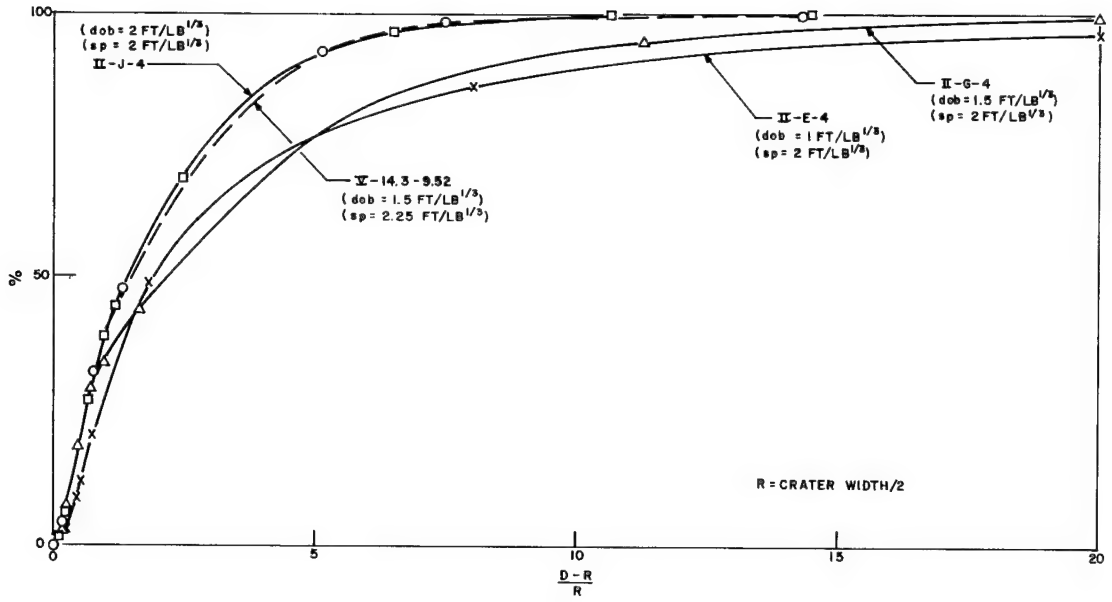

Figure 4.20 Percent of crater volume ejected to a given scaled distance for row charges at nearly the same scaled spacing and at three scaled burst depths

In Figure 4.21 are results similar to Figure 4.20 for the same 256-pound row charge together with those from three rows of 8-pound charges, all at the same cube-root scaled burst depth (1.5 ft/lb$^{1/3}$) but with different charge spacing. All throwout densities for the small charges are less than those of the larger charge, and the same reversal in the trend with charge spacing is observed as was noted earlier in Figure 4.20.

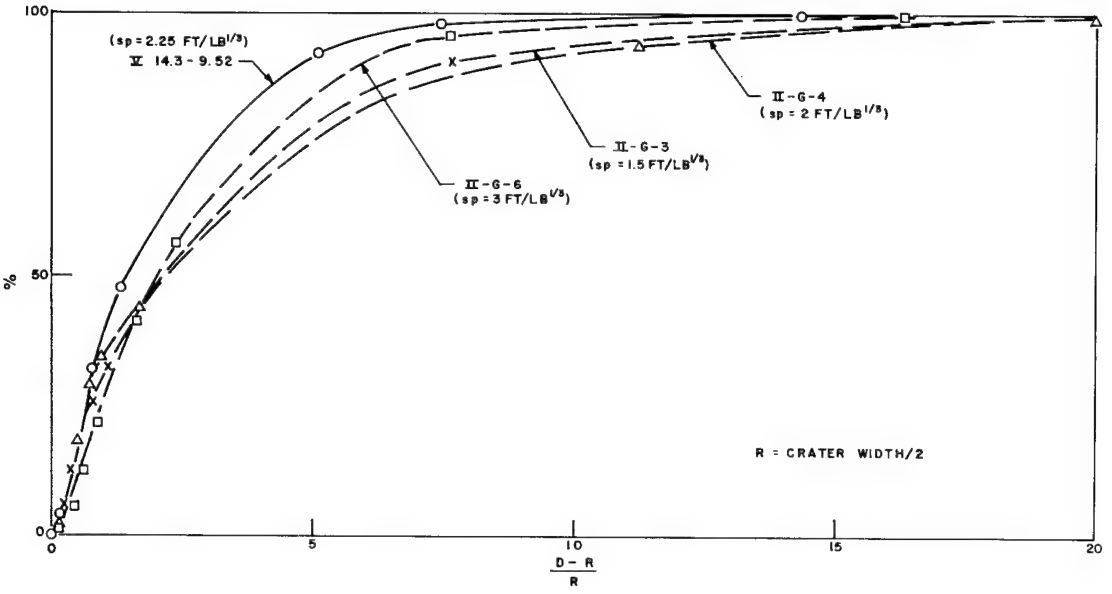

Figure 4.21 Percent of crater volume ejected to a given scaled distance for row charges at a scaled burst depth of 1.5 ft/lb$^{1/3}$ at four different scaled spacings

4.4.3 Comparison of Throwout from Row Charges and Single Charges

The comparison between row- and single-charge throwout is evidenced by Figure 4.22, which compares the throwout-density-versus-distance curve for a single 256-pound charge with that for a row of 256-pound charges, the charges in both cases being buried at 9.52 feet. Values are given for both a line off one end of the row and a line normal to the axis of the row at its midpoint. Again, distances off the end are measured from the end charge and the lateral distances from the axis of the row. At the closest distances the density off the end of the row is the same as would be encountered with a single charge and the density is everywhere else greater for the row charge. Part of the reason for this lies in the fact that the unit crater volume of the single charge (3.21 cu ft/lb) is exactly half that of the row charge (6.42 cu ft/lb). It is interesting to note that the slope of the density-distance curve for the row charge approaches, at the greater distances, that for the single charge.

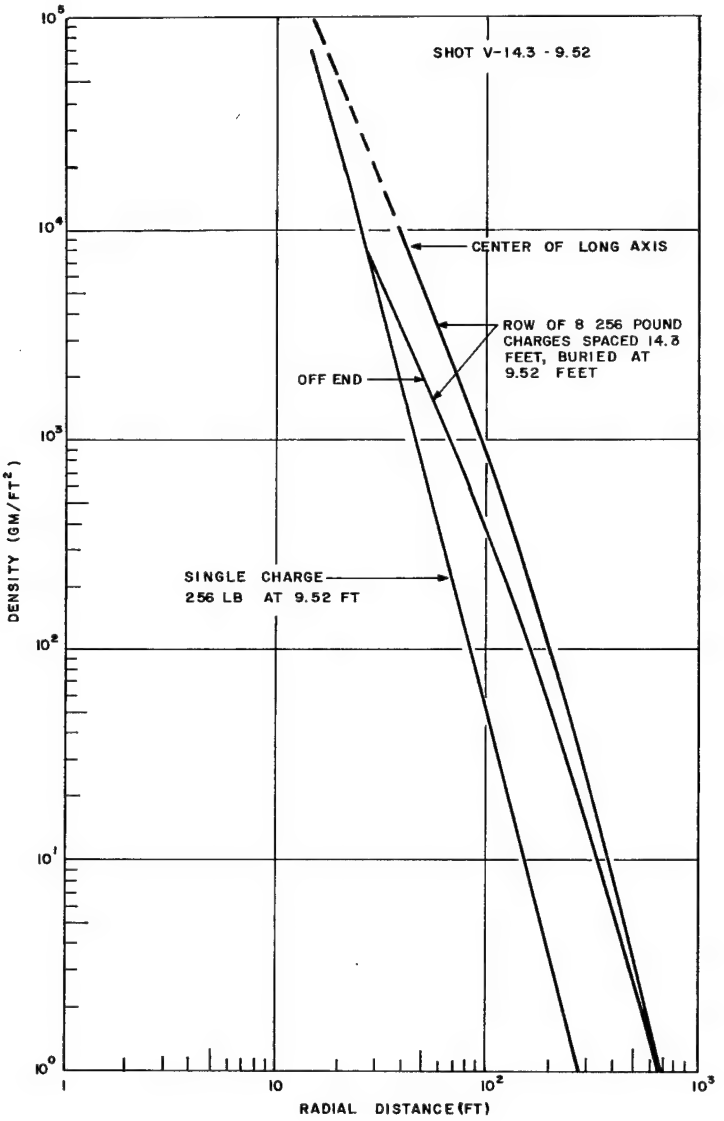

Figure 4.22 Comparison density-distance plot for 256-pound single and row charges

CHAPTER 5. CONCLUSIONS

The wide scatter in the 8-pound single-charge crater dimensions, especially the dimensions for crater depth and volume, is attributed to the relatively greater importance of strength properties of the soil for small charges. Because of the scatter, heavy reliance was placed on the dimensions obtained from 256-pound charge craters in defining the depth-of-burst curves for Albuquerque fan-delta alluvium.

If too few charges are used in a row, the effect approaches that of a single charge. If there are a sufficient number of charges in a row, the crater approaches that of a line-charge crater, provided the spacing between charges meets the requirements for line-charge equivalence. A noticeable lack of throwout off the ends of row charges, similar to that observed on Project Tobaggon, was noted for those charges where the spacing was such that it provided line-charge equivalence. As the spacing was increased above the boundary of line-charge equivalence, the amount of throwout off the ends of the row increased.

A comparison of the depth-of-burst curves for the Albuquerque fan-delta alluvium with the NTS desert alluvium shows that the Albuquerque material is a "harder" one. Crater dimensions are smaller and the peaks of the depth-of-burst curves appear at a shallower burst depth in the case of the Albuquerque material. Ratios obtained from this comparison can be used to predict the results of row-charge craters in the NTS desert alluvium.

The region of line-charge equivalence of row-charge craters is defined as that of spacing and burst depth which gives a crater of uniform dimension, either width or depth. The boundary of line-charge equivalence is obtained where, for width, the scaled charge spacing approximately equals $1 + dob/W^{1/3}$. For crater depth the value is $S/W^{1/3} = 0.6 + dob/W^{1/3}$. As the spacing is increased beyond this value, there is an increasing difference between the crater dimension at a point between charges in the row and that measured at the charge location.

The optimum burst depth for row charges was found to be 10 percent greater than that for an equal size single charge.

A row-charge crater with a uniform width was obtained where the charge spacing is 30 percent greater than the maximum single-charge crater radius. A uniform crater depth is obtained where the spacing is 10 percent greater than the single-charge maximum radius.

At the spacing which is 30 percent greater than the maximum single-charge crater radius, one-half the width of the row-charge crater is 5 percent greater than the single-charge crater radius which results from a burst at the depth which maximizes crater volume; the row-charge crater depth at the same spacing is 15 percent greater than the single-charge crater depth which results from a burst at the depth which maximizes crater volume. At the spacing which is 10 percent greater, one-half the row-charge crater width is 20 percent greater and the row-charge crater depth is 25 percent greater than the single-charge crater radius and depth, respectively, which result from a burst at the depth which maximizes crater volume.

The 256-pound single charges ejected less throwout material to the greater distances and more to the closer distances as burial depth was increased.

Although there was less material ejected off the end of the row-charge crater, the densities at the greatest distances are about the same as those normal to the charge. This is probably because the material blown to the greatest distances is more dependent upon wind transport than that which falls at the closer distances. Normal to the axis of the row charge, the material is ejected to distances which decrease as burst depth is increased. Densities of throwout off the end of a row charge show little variation with charge spacing. Normal to the axis of the row charge, however, a larger spacing results in a lesser density of ejecta. Off the

end of a row charge at the closest distances, the density of ejecta is the same for single charges and row charges. Everywhere else the density of material is greater in the case of the row charge. This is in part because the volume of crater per pound of explosive is greater by a factor of two in the case of the row charge than in the case of the single charge.

The burst depth and spacing for the most efficient employment of row charges was defined. The loss in cratering efficiency as a result of failing to work at the optimum burst depth or spacing can be evaluated from the information obtained from this experiment.

LIST OF REFERENCES

1. "Ditching and Field Clearing with Dynamite," E. I. du Pont de Nemours and Company (Inc.), Wilmington, Delaware, 1955.

2. Hahneman, Ditching a Swamp with Dynamite for a Banana Plantation, Engineering News Record, November 8, 1928.

3. Mainevsky, Formulas for Using Dynamite in Canal Excavation, Civil Engineering, December 1933.

4. Vortman, L. J., and L. N. Schofield, High Explosive Cratering in Fan-Delta Alluvium, SCTM 60-59(51), Sandia Corporation, 1959.

5. Carlson, R. H., High-Explosive Ditching from Linear Charges, SC-4483(RR), Sandia Corporation, July 1961.

6. Merritt, M. L., B. F. Murphey, and L. J. Vortman, Cratering with Chemical Explosives, Proceedings of the Second Plowshare Symposium, Part II, Excavation, UCRL-5676, May 14, 1959.

7. Chabai, A. J., Crater Scaling Laws for Desert Alluvium, SC-4391(RR), Sandia Corporation, 1959.

8. Chabai, A. J., Gravity Scaling Laws for Explosion Craters, SC-4541(RR), Sandia Corporation, 1960.

9. Piper, Arthur M., Geologic, Hydrologic, and Thermal Features of the Sites, Operations Windstorm and Jangle, Project 1(8)a, WT-343, United States Geological Survey, Portland, Oregon, May 1952.

10. Vortman, L. J., et al., 20-Ton HE Cratering Experiments in Desert Alluvium, Project Stagecoach, Final Report, SC-4596(RR), Sandia Corporation, May 1962.

11. Murphey, B. F., High Explosive Crater Studies: Desert Alluvium, SC-4614(RR), Sandia Corporation, May 1961.

APPENDIX A

SINGLE-CHARGE CRATER TOPOGRAPHY

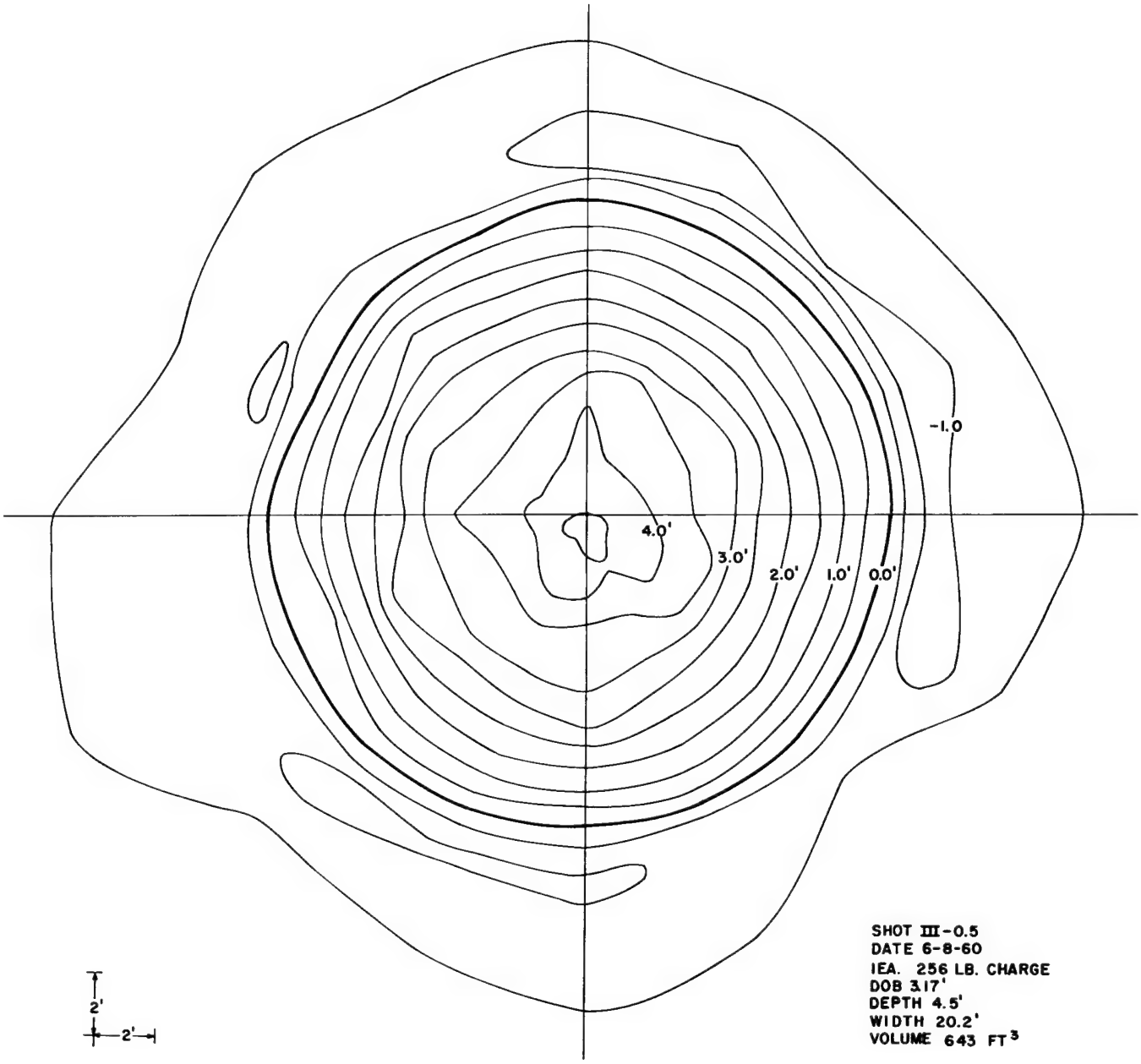

Figure A.1 Crater topography 256-pound charge buried 3.17 feet

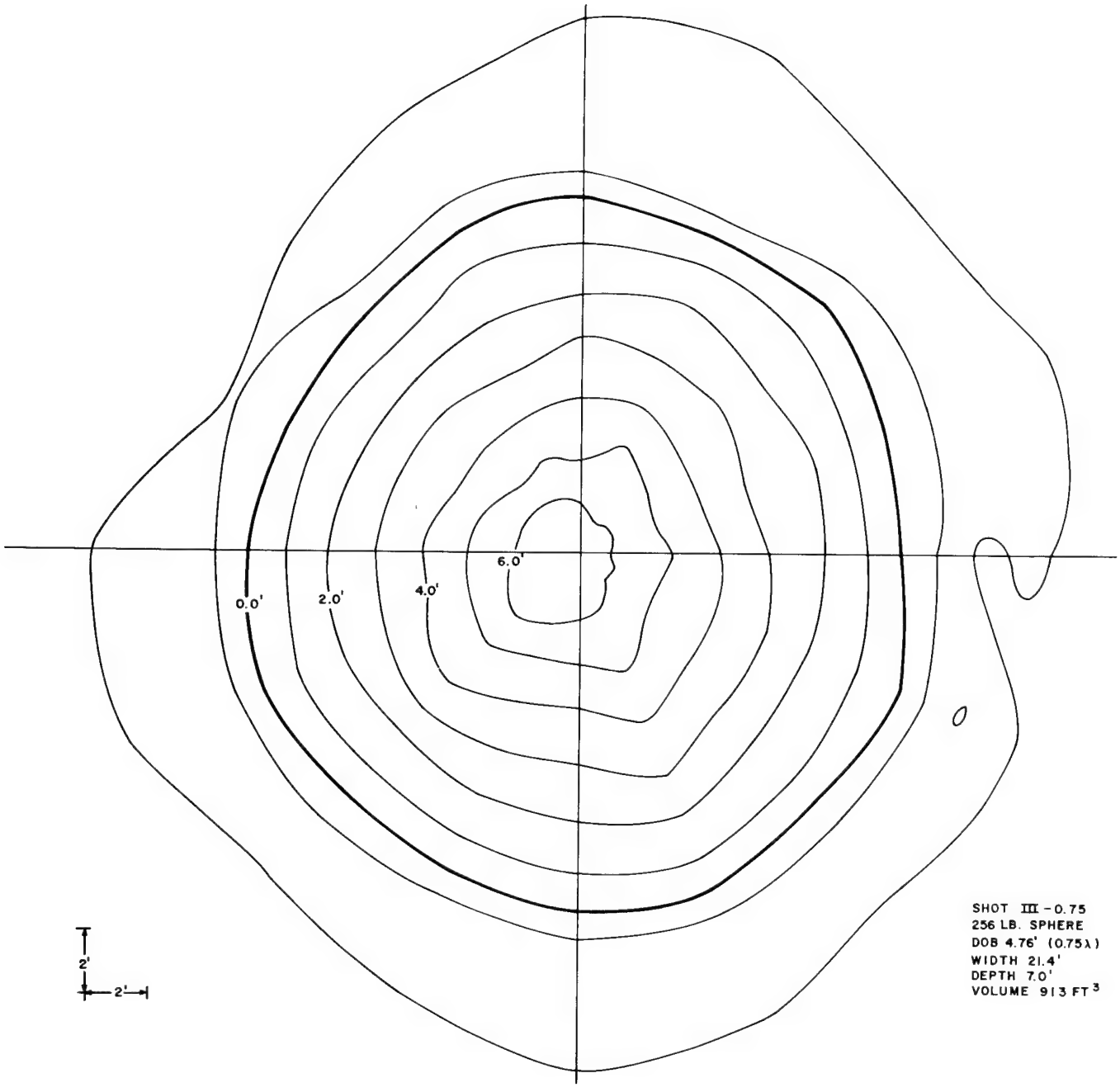

Figure A.2 Crater topography 256-pound charge buried 4.76 feet

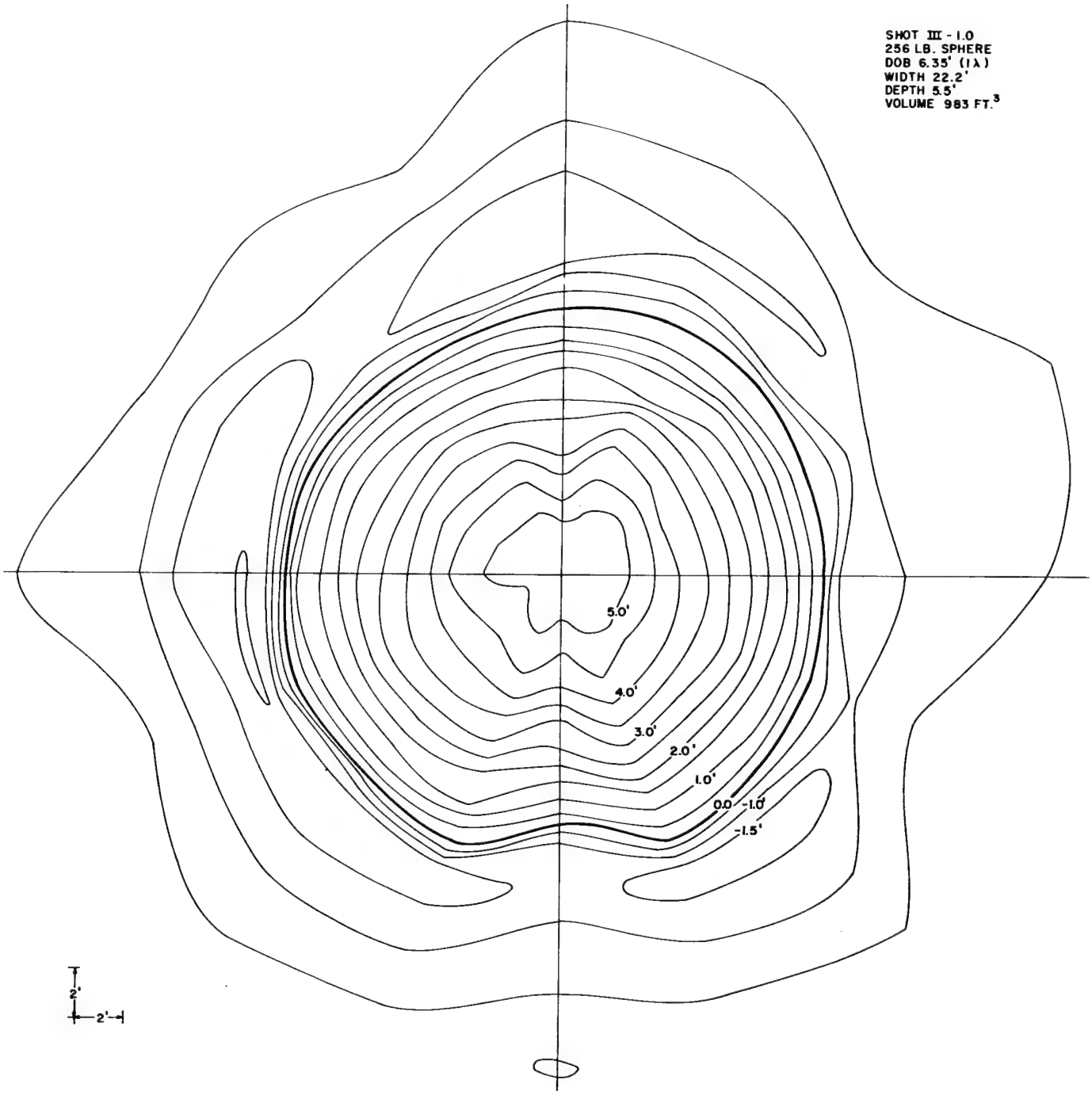

Figure A.3 Crater topography 256-pound charge buried 6.35 feet

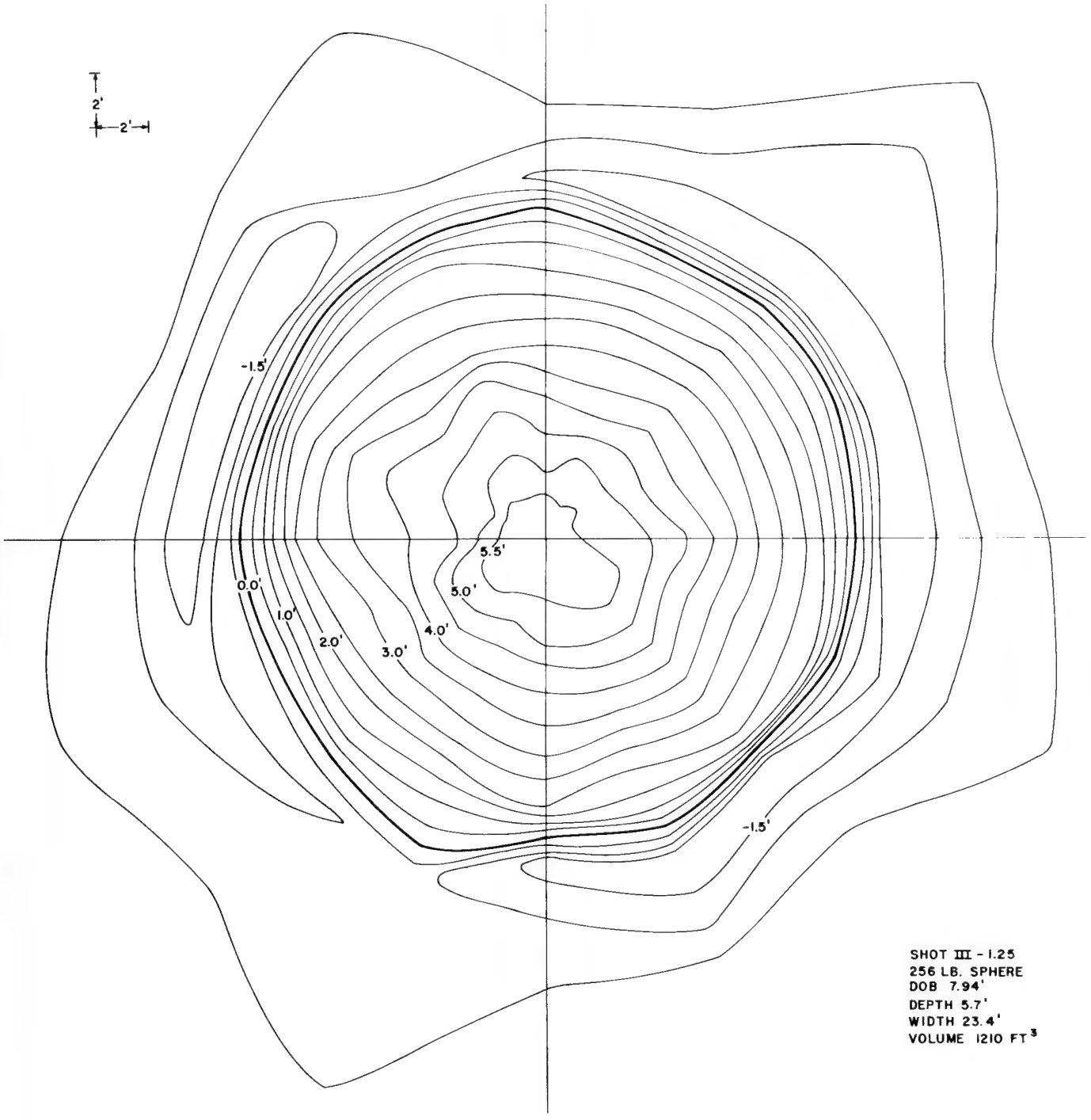

Figure A.4 Crater topography 256-pound charge buried 7.94 feet

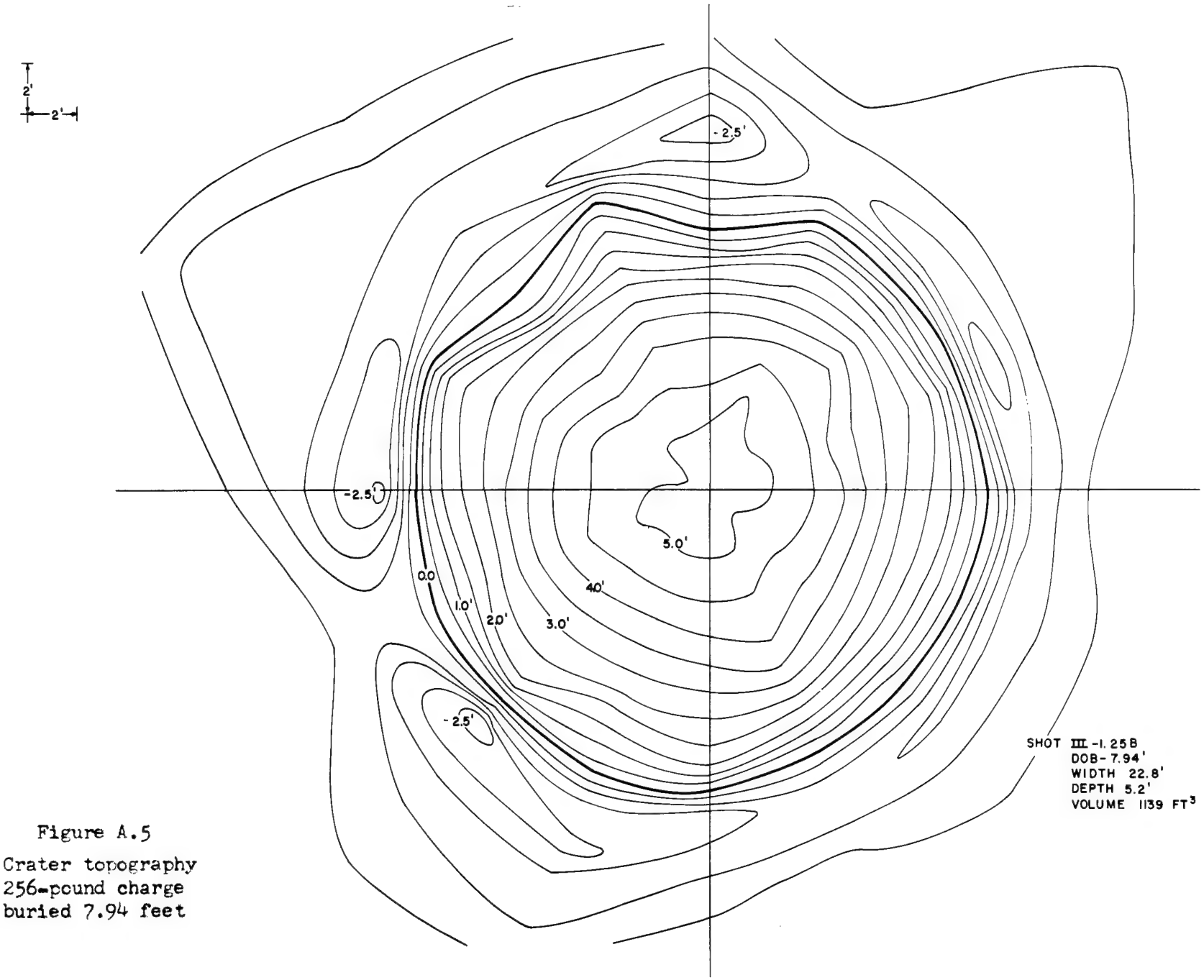

Figure A.5

Crater topography
256-pound charge
buried 7.94 feet

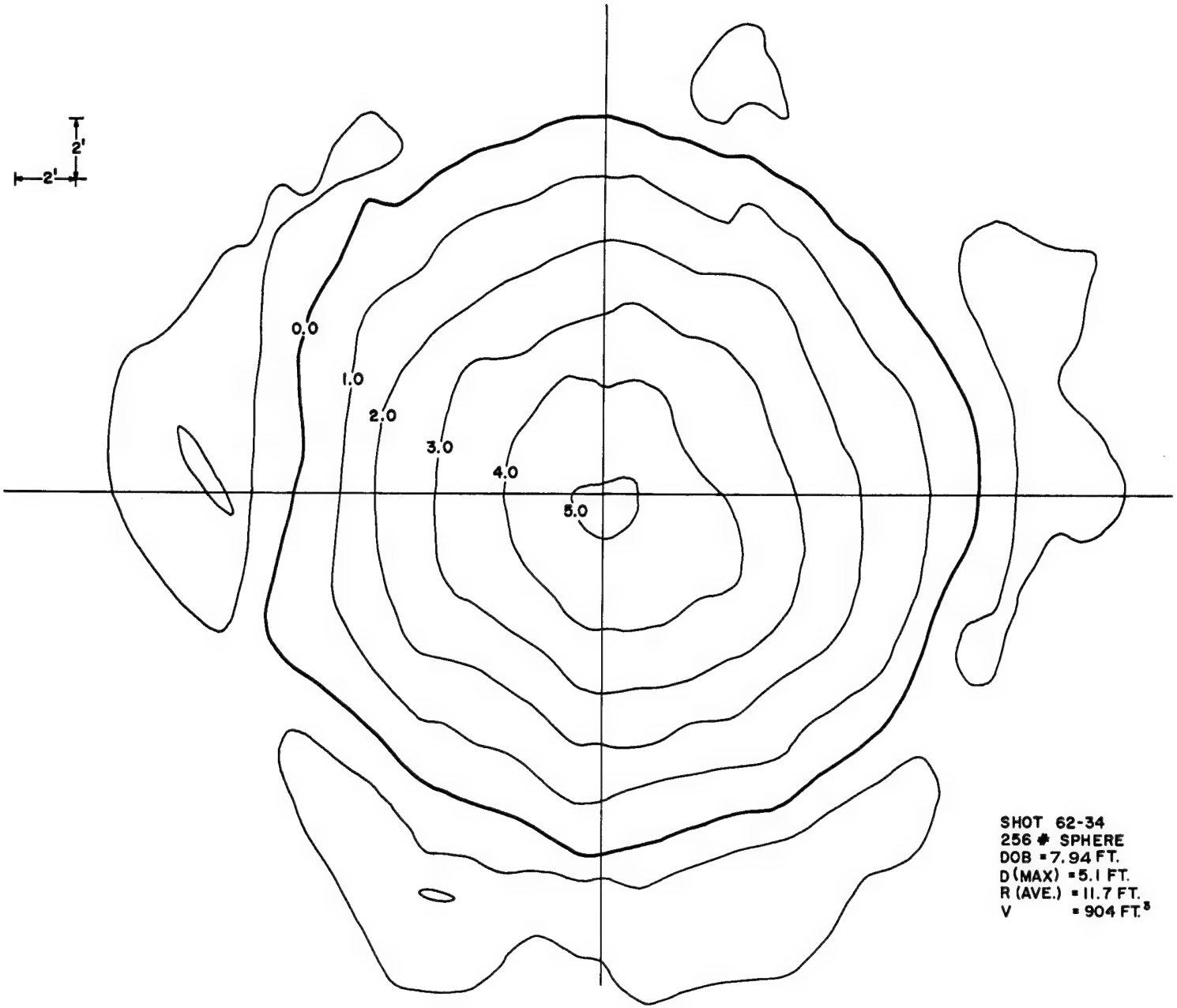

Figure A.6 Crater topography 256-pound charge buried 7.94 feet

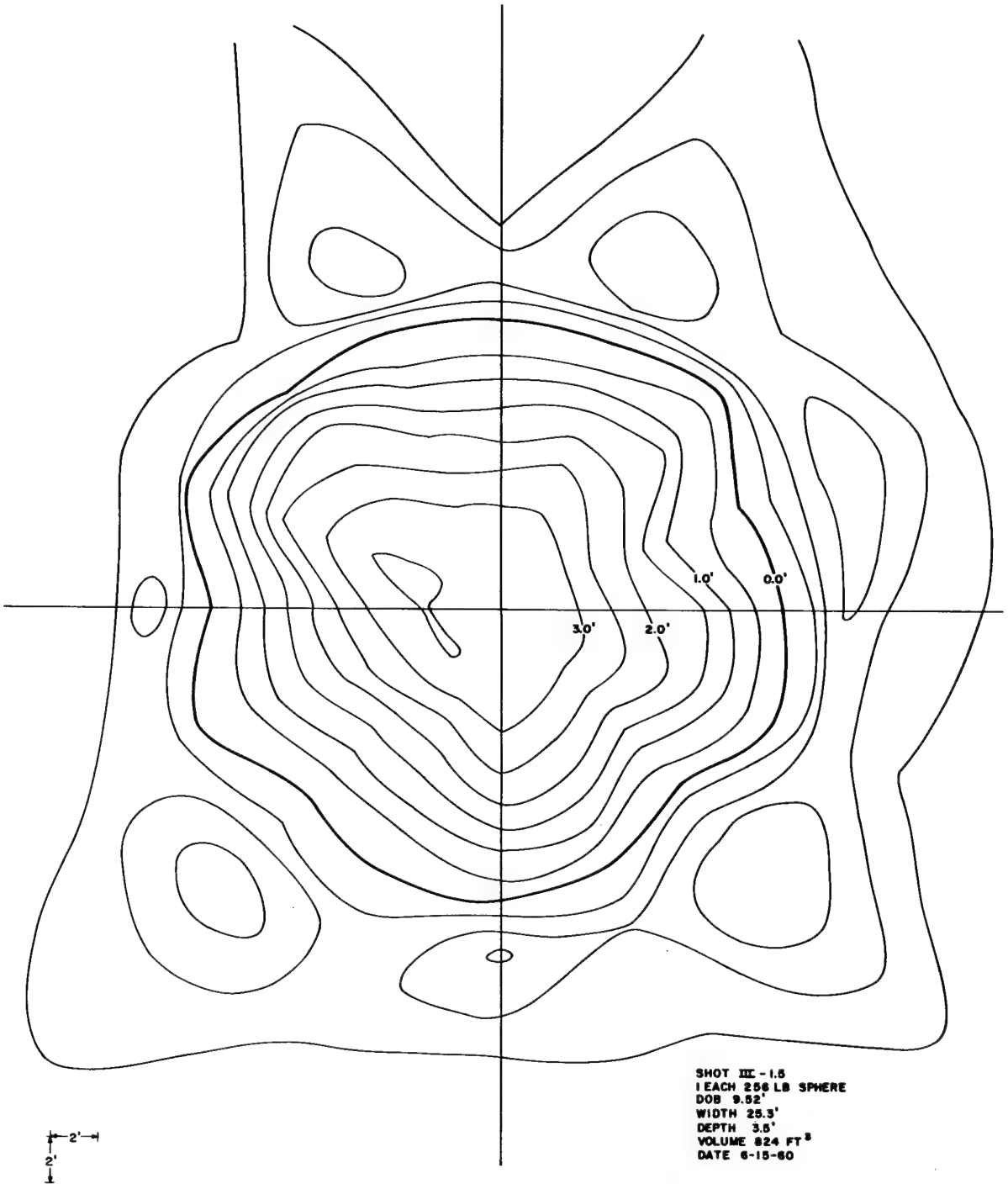

Figure A.7 Crater topography 256-pound charge buried 9.52 feet

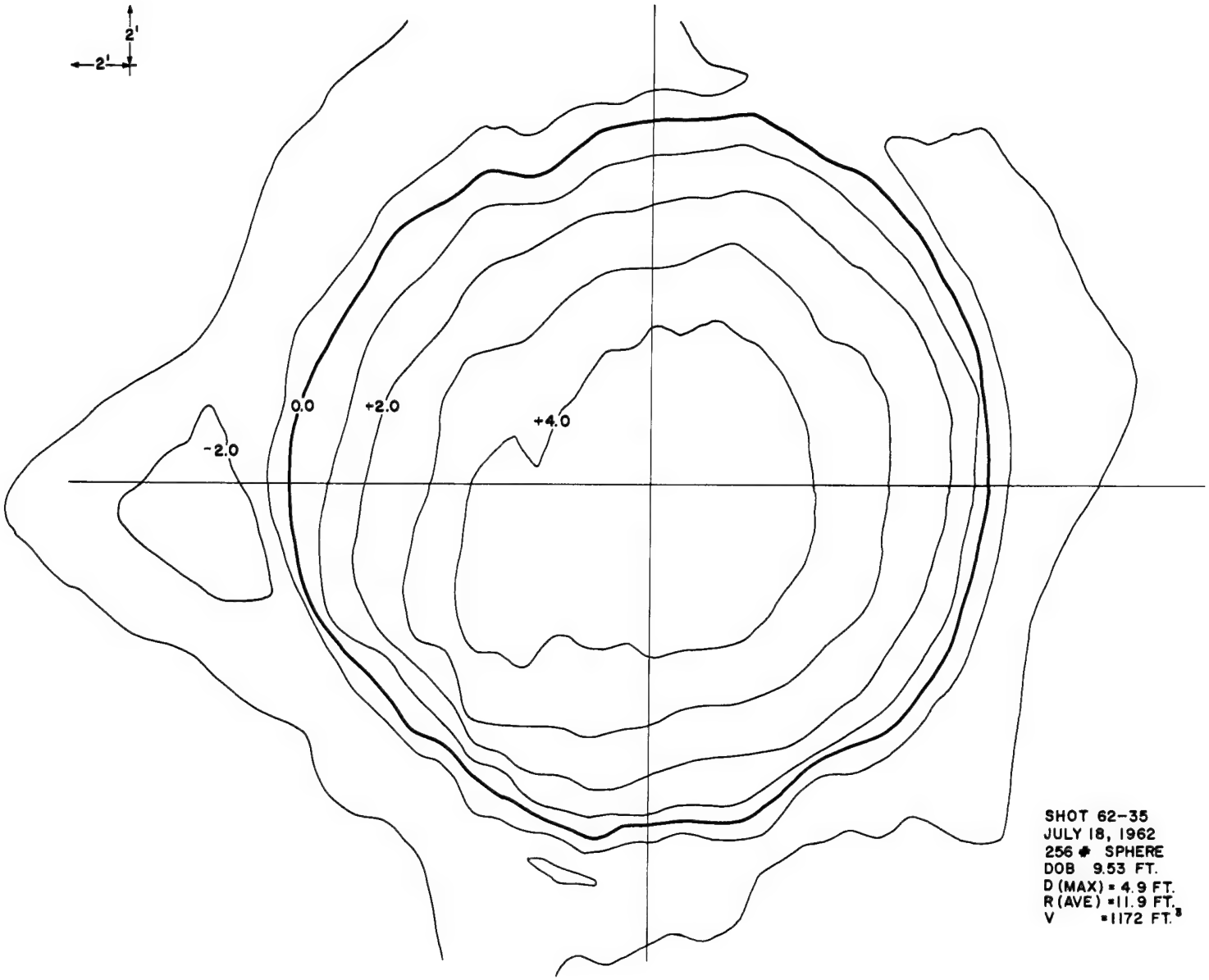

Figure A.8 Crater topography 256-pound charge buried 9.53 feet

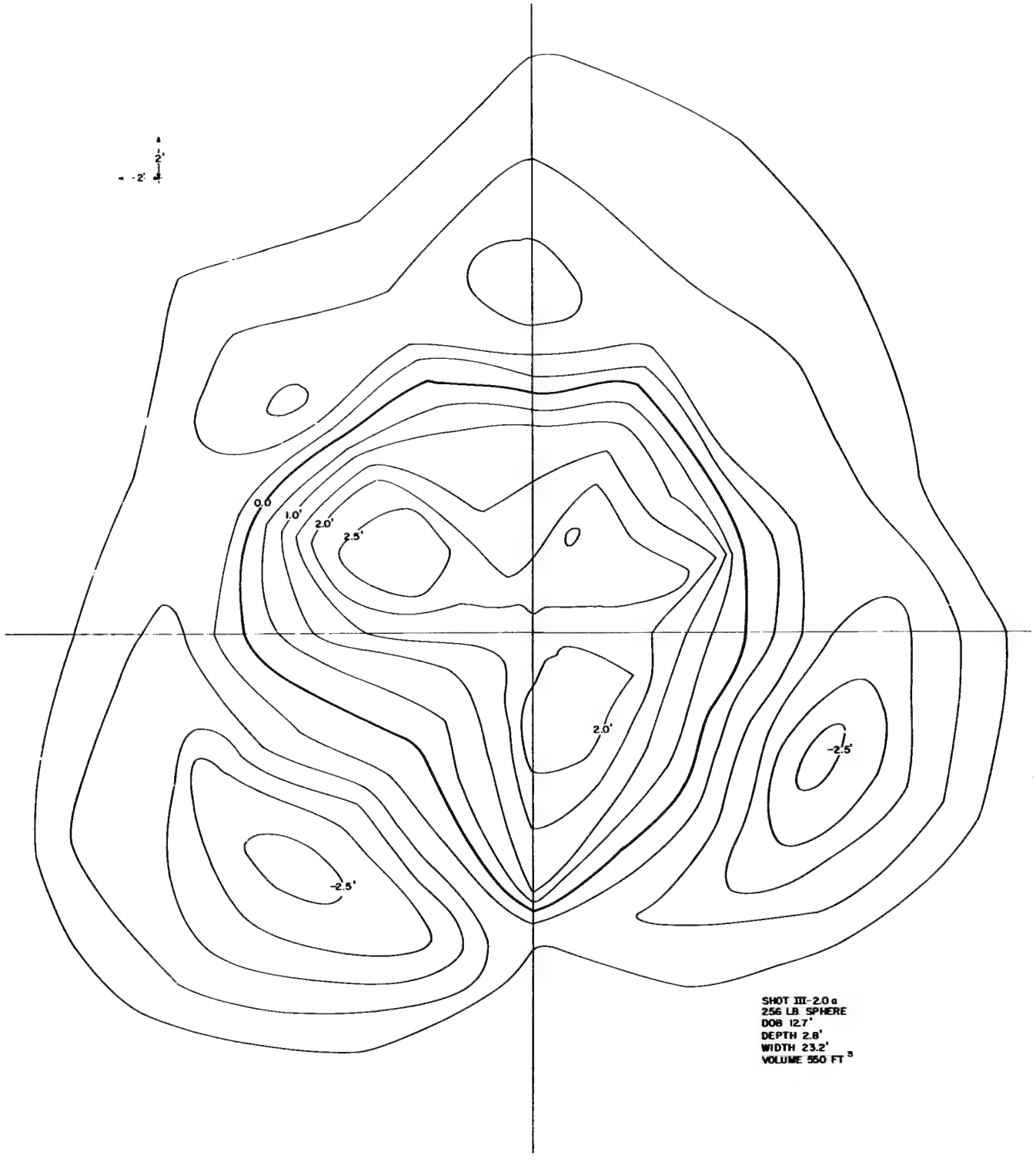

Figure A.9 Crater topography 256-pound charge buried 12.7 feet

Figure A.10

Crater topography
256-pound charge
buried 12.7 feet

APPENDIX B

ROW-CHARGE CRATER TOPOGRAPHY

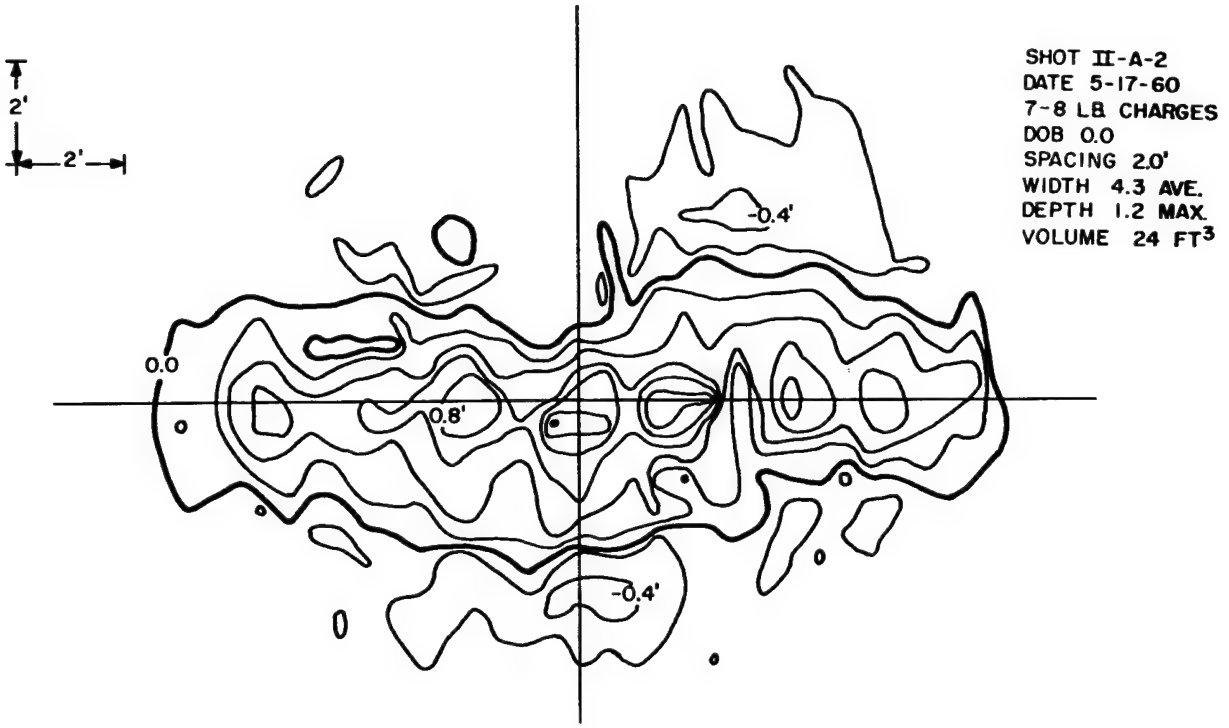

Figure B.1 Crater topography 8-pound row charge buried 0 feet, spaced 2 feet

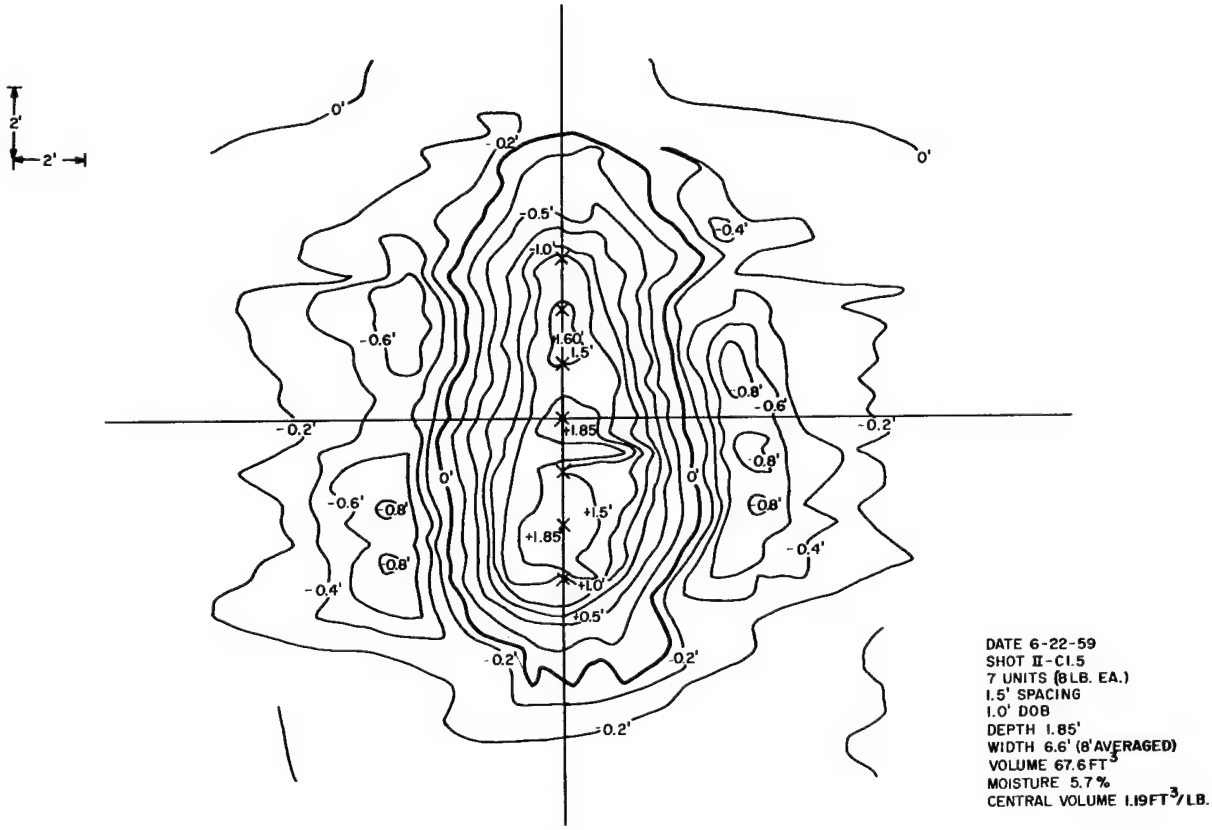

Figure B.2 Crater topography 8-pound row charge buried 1 foot, spaced 1.5 feet

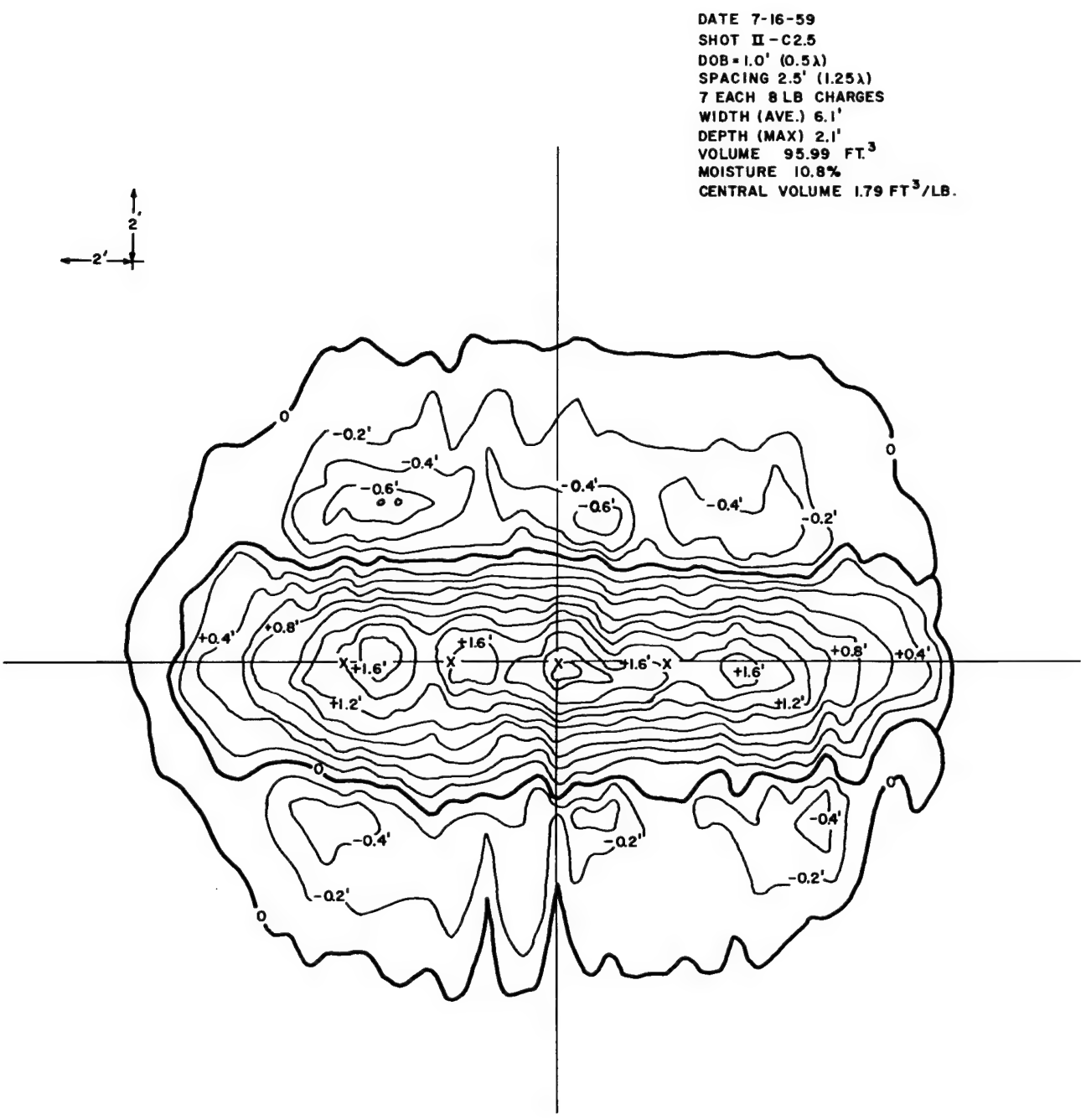

Figure B.3 Crater topography 8-pound row charge buried 1 foot, spaced 2.5 feet

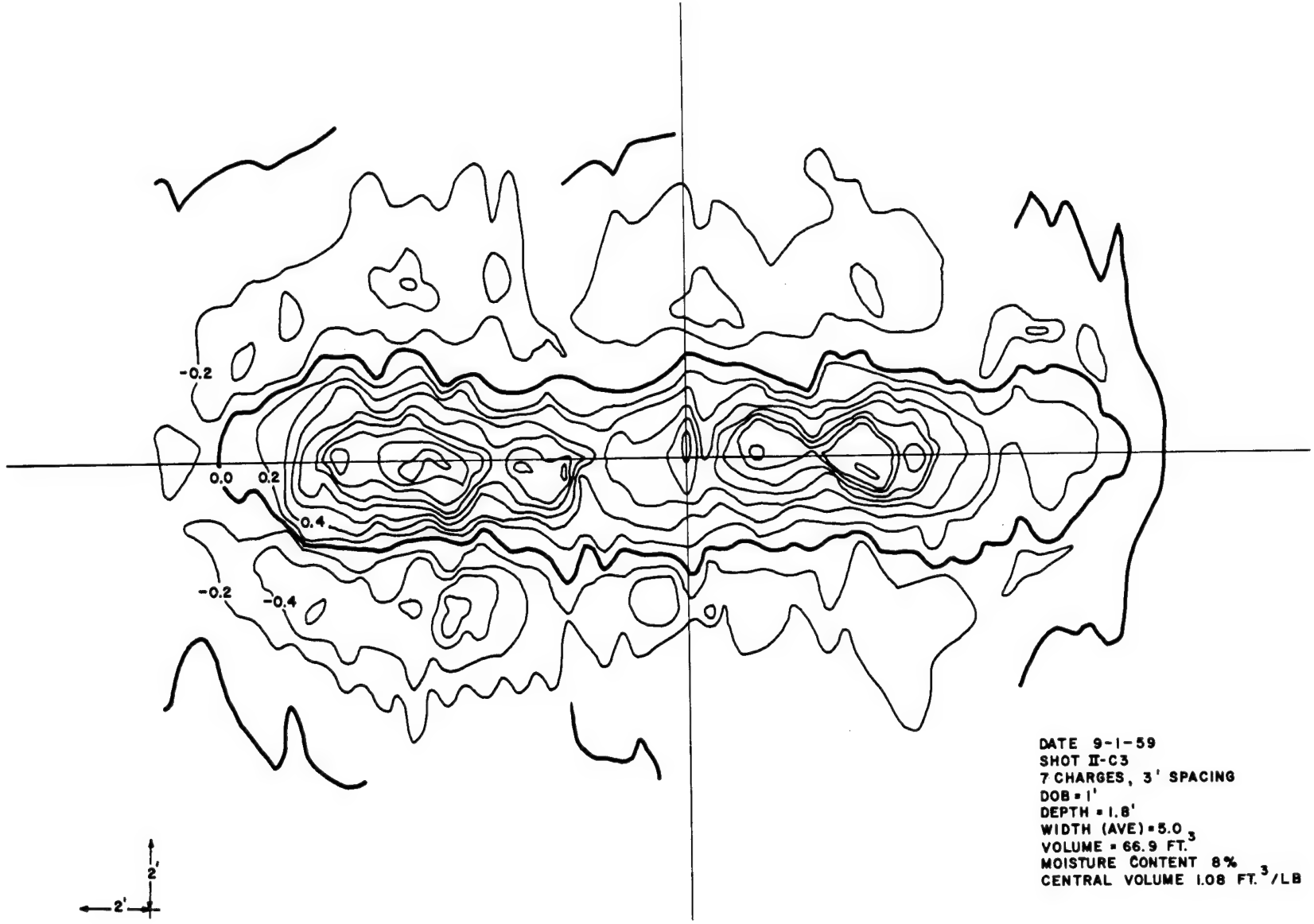

Figure B.4 Crater topography 8-pound row charge buried 1 foot, spaced 3 feet

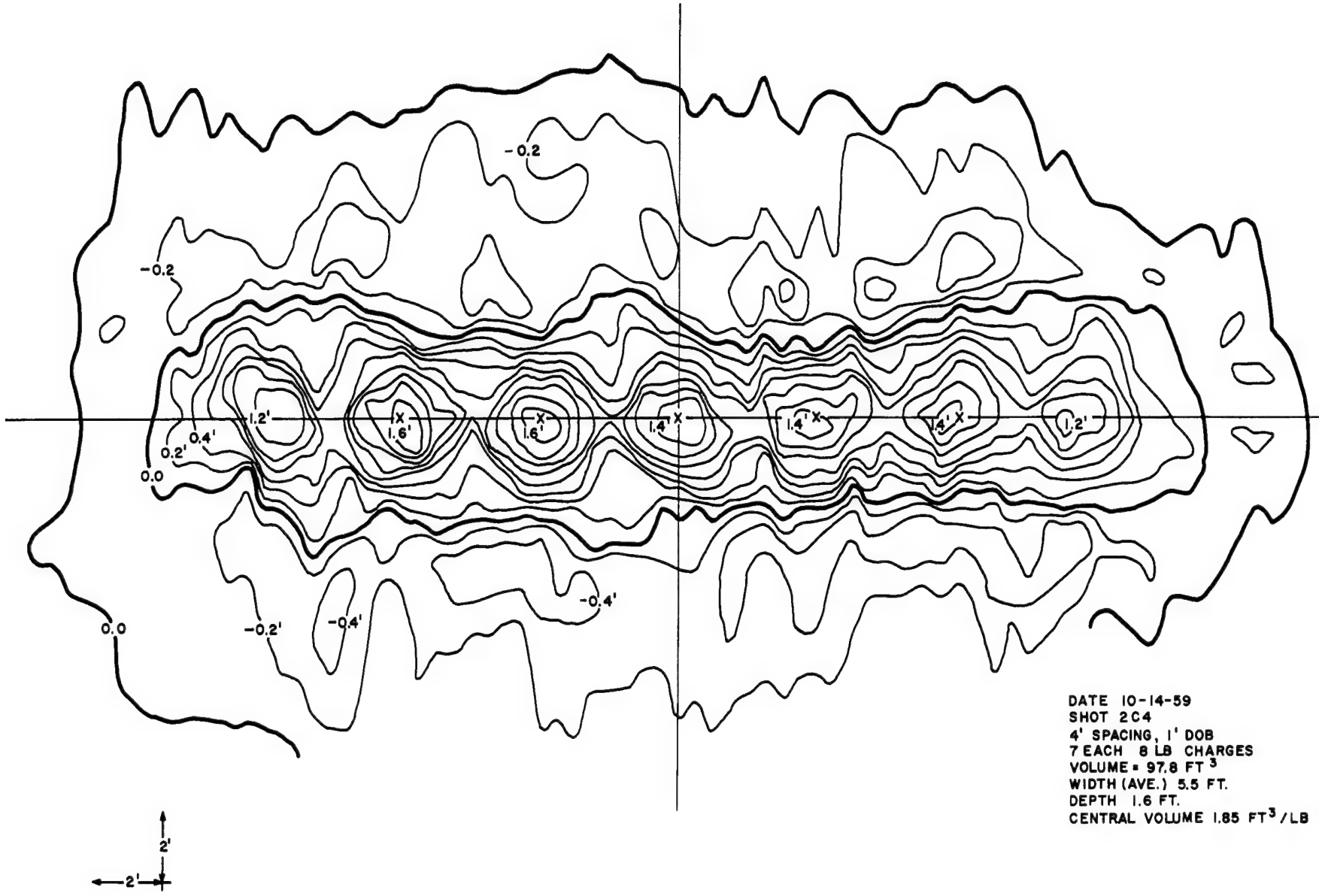

Figure B.5 Crater topography 8-pound row charge buried 1 foot, spaced 4 feet

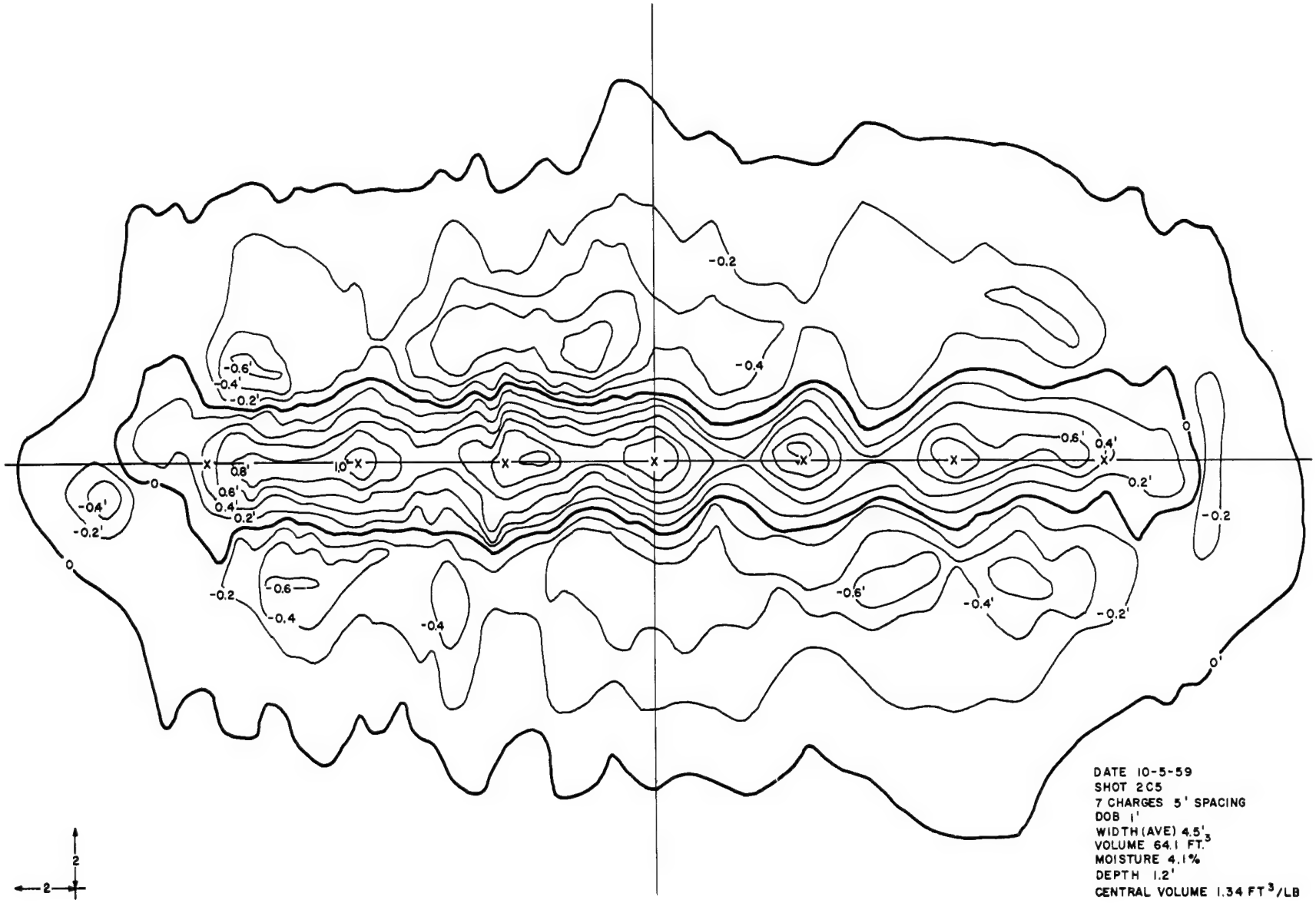

Figure B.6 Crater topography 8-pound row charge buried 1 foot, spaced 5 feet

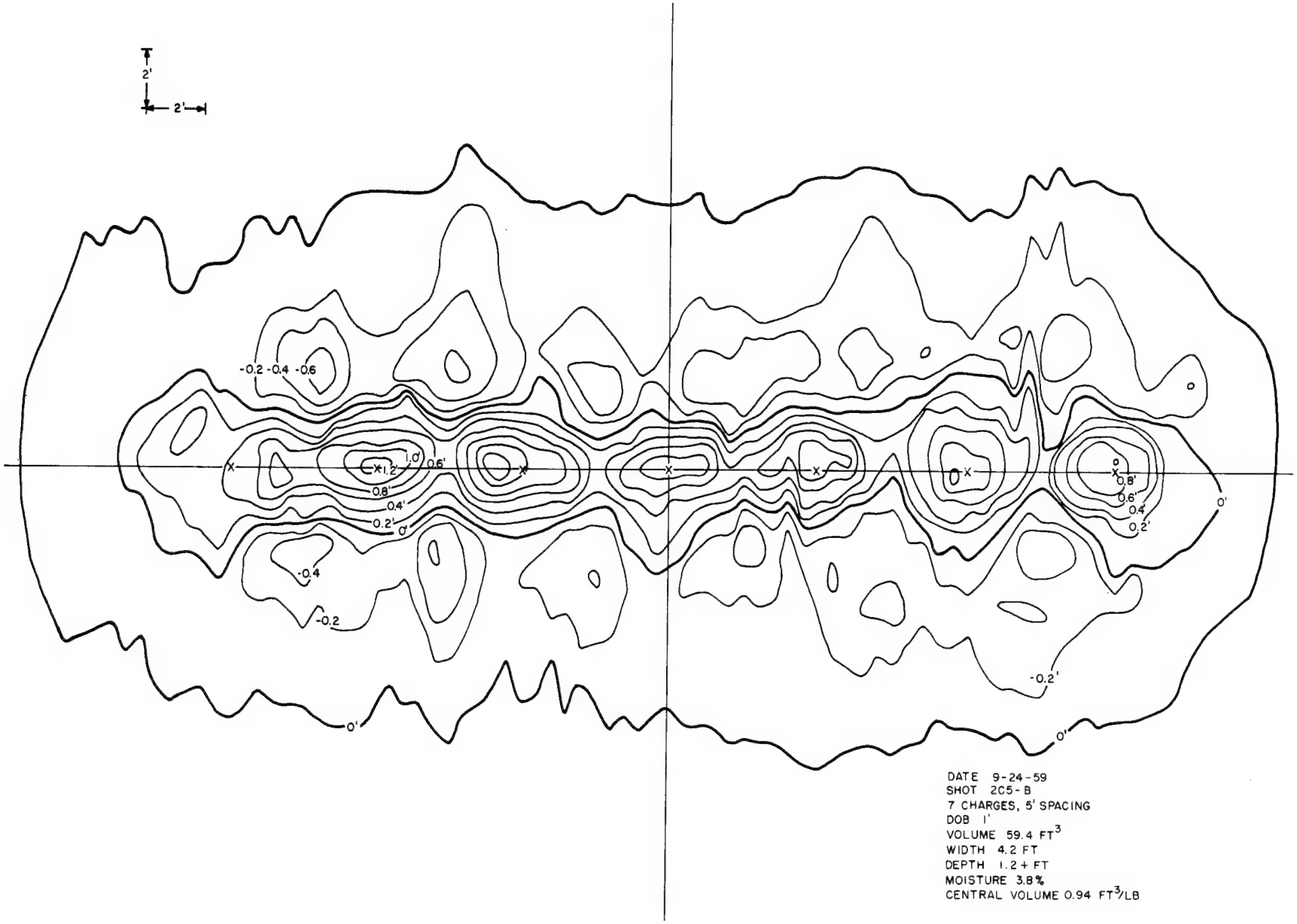

Figure B.7 Crater topography 8-pound row charge buried 1 foot, spaced 5 feet

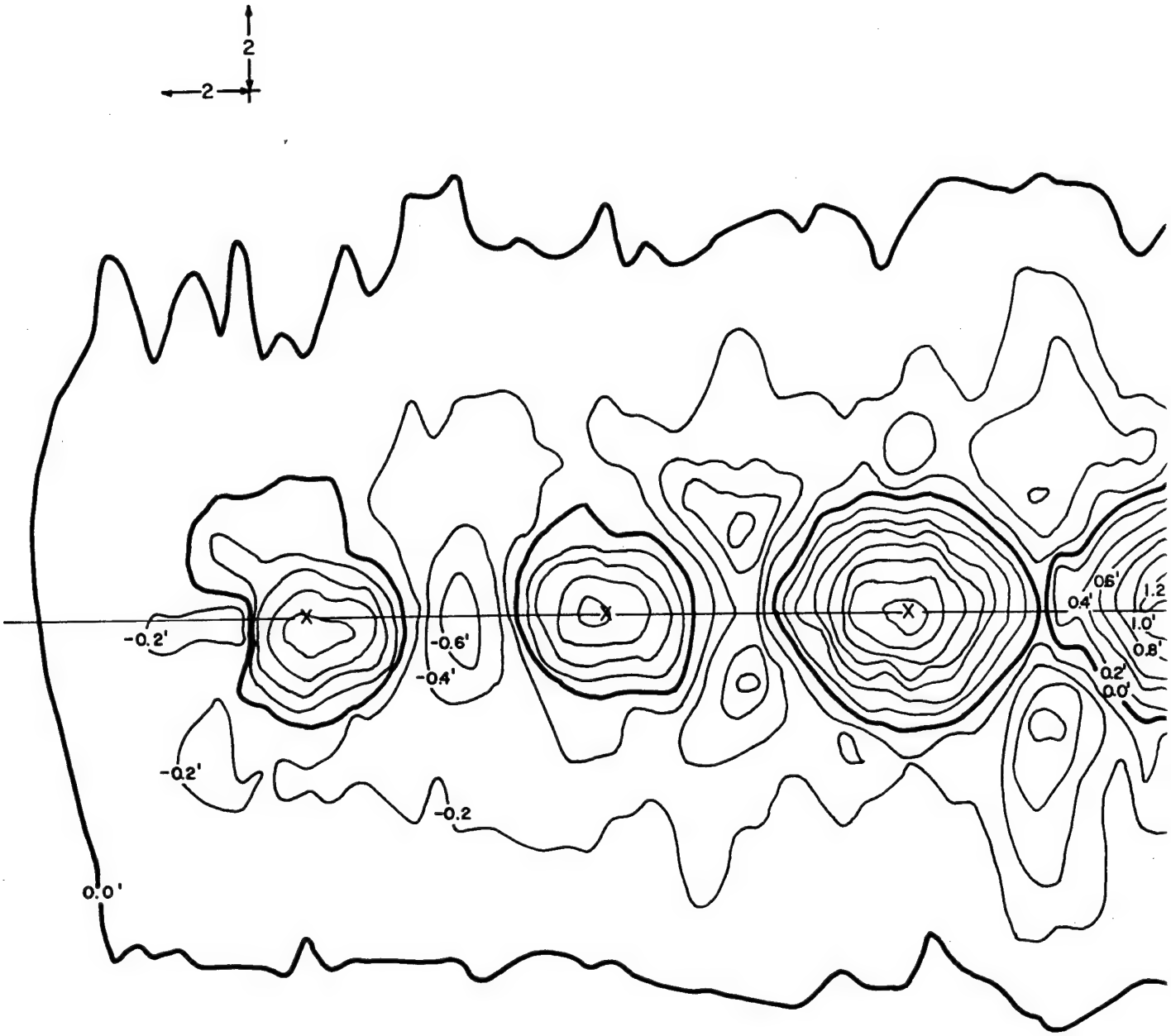

Figure B.8 Crater topography

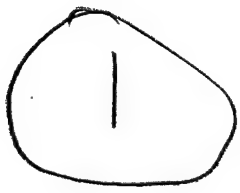

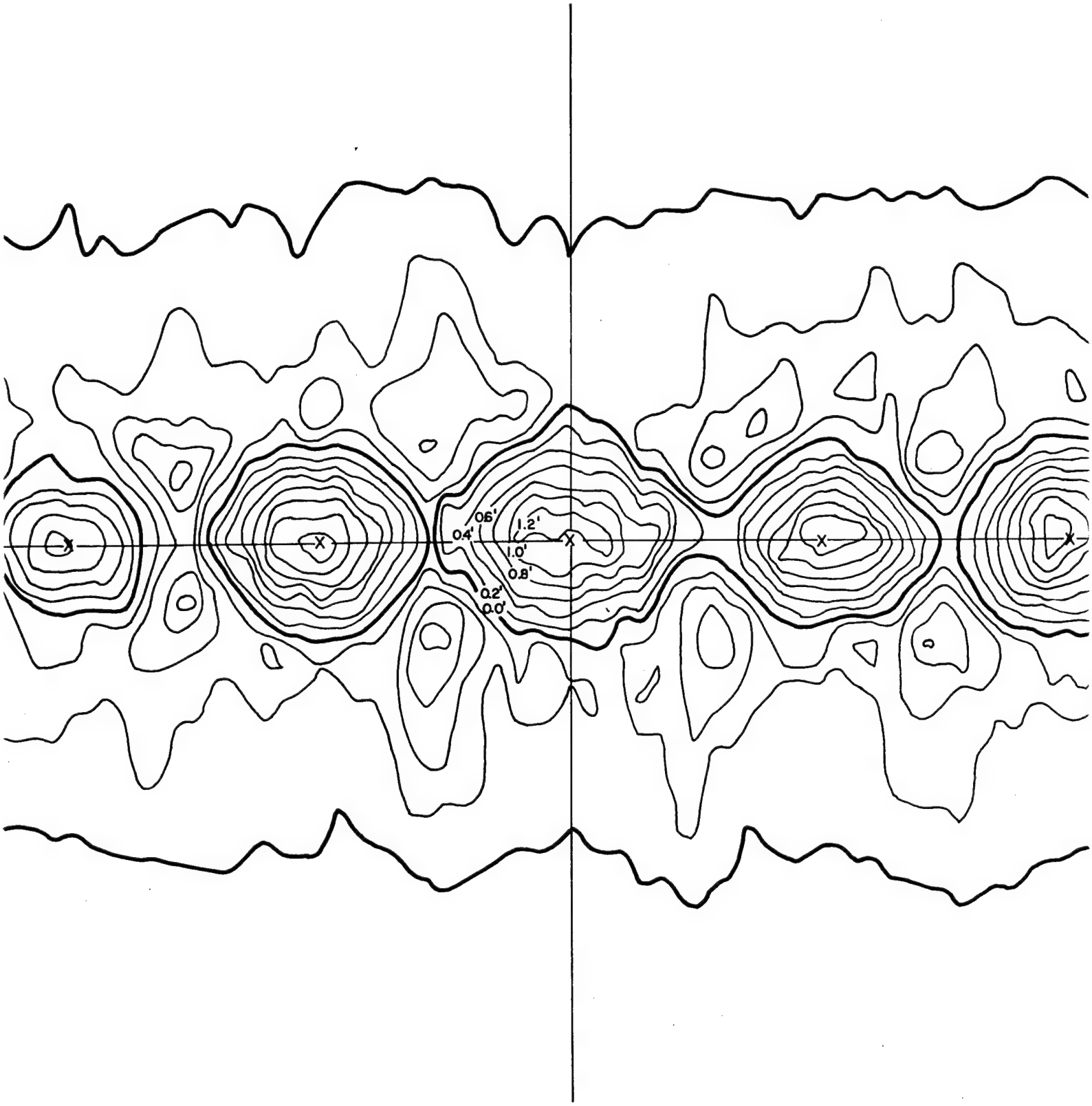

Figure B.8 Crater topography 8-pound row charge buried 1 foot, spaced 7 feet

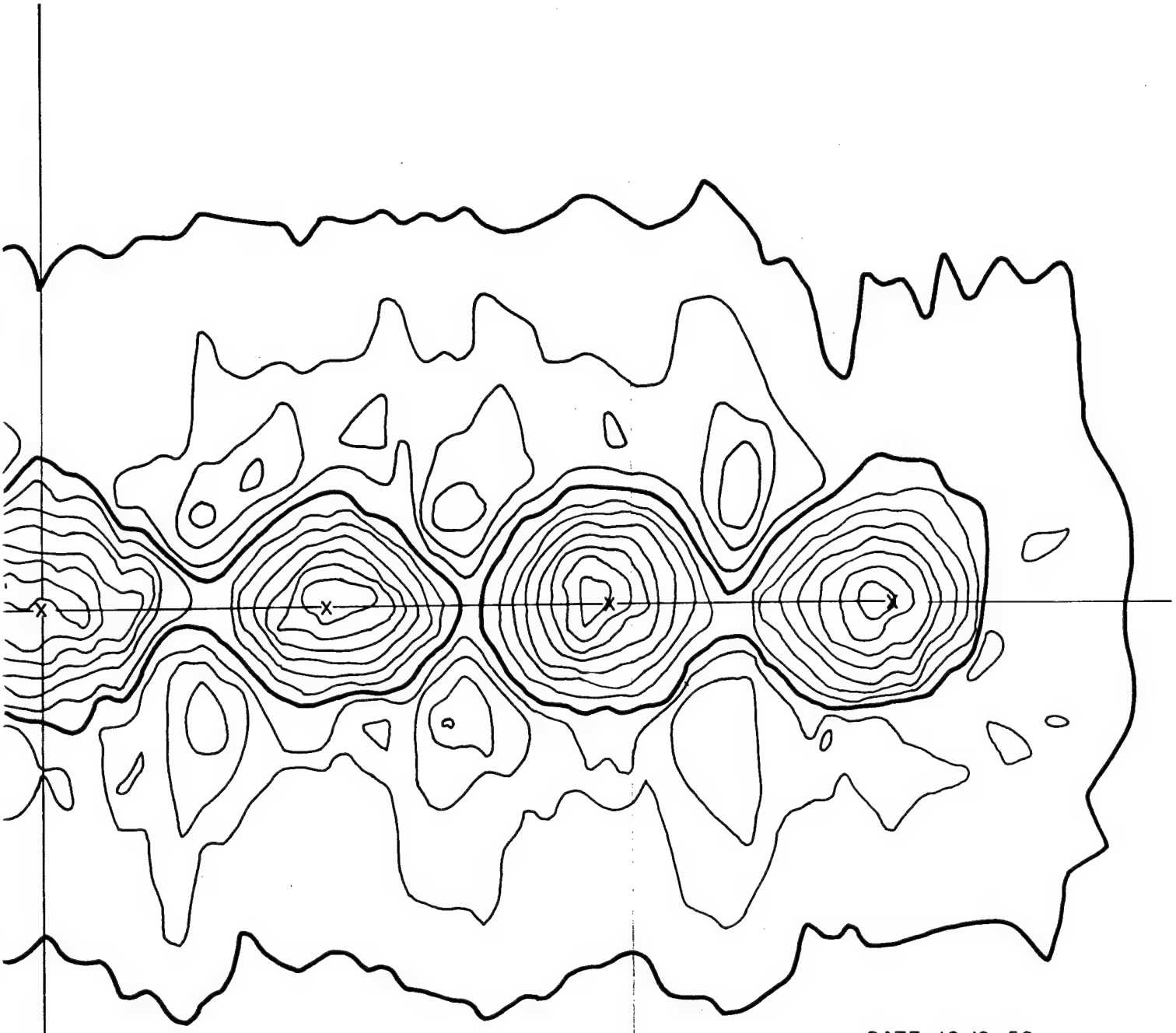

DATE 10-16-59
SHOT II-C 7
7 EA. 8 LB CHARGES
CHARGE SPACING 7'
DEPTH OF BURST 1'
DEPTH 1.4'
VOLUME 90.0 FT^3
WIDTH 5.6'
CENTRAL VOLUME 1.94 FT^3/LB

8-pound row charge buried 1 foot, spaced 7 feet

3

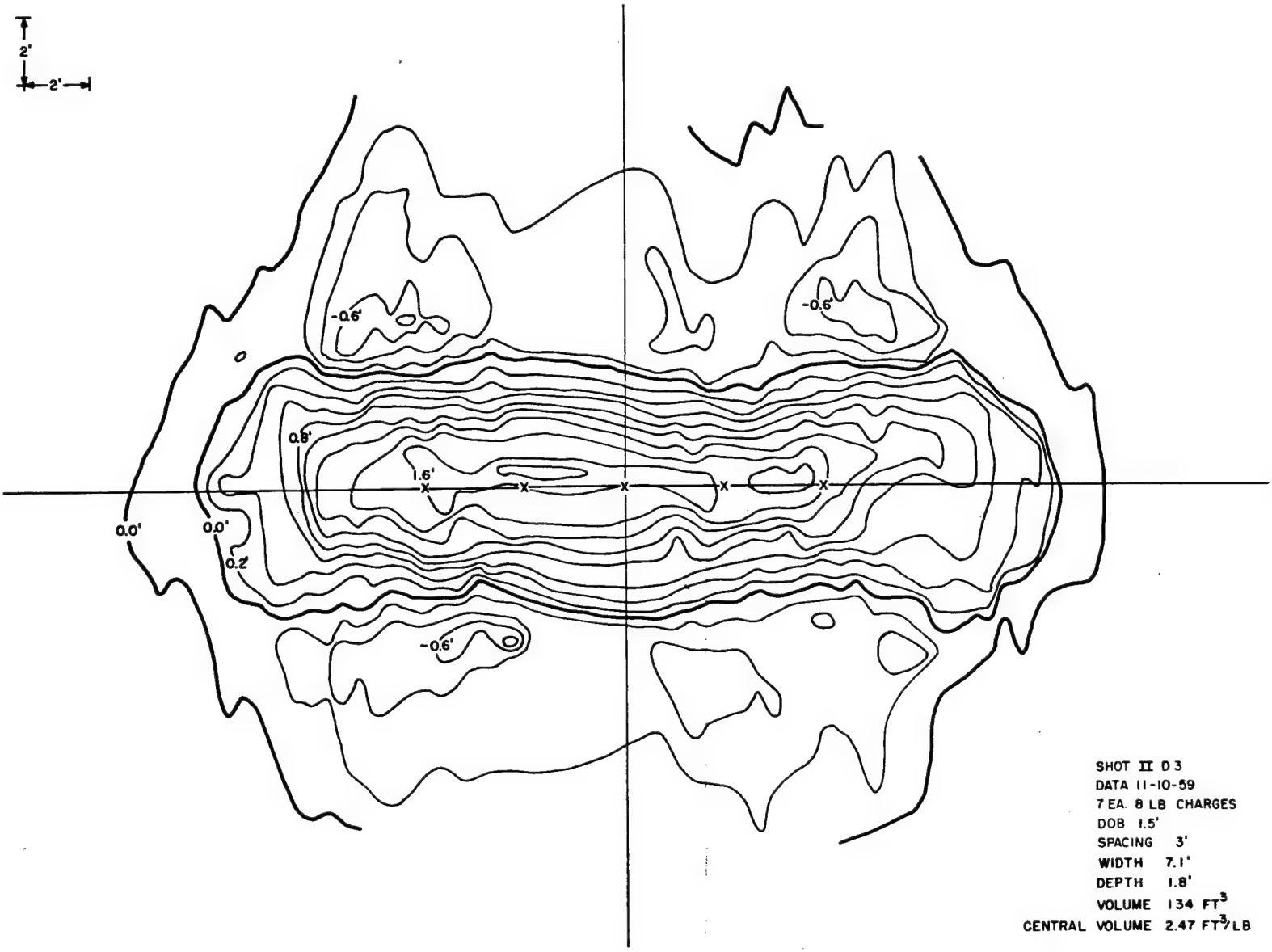

Figure B.9 Crater topography 8-pound row charge buried 1.5 feet, spaced 3 feet

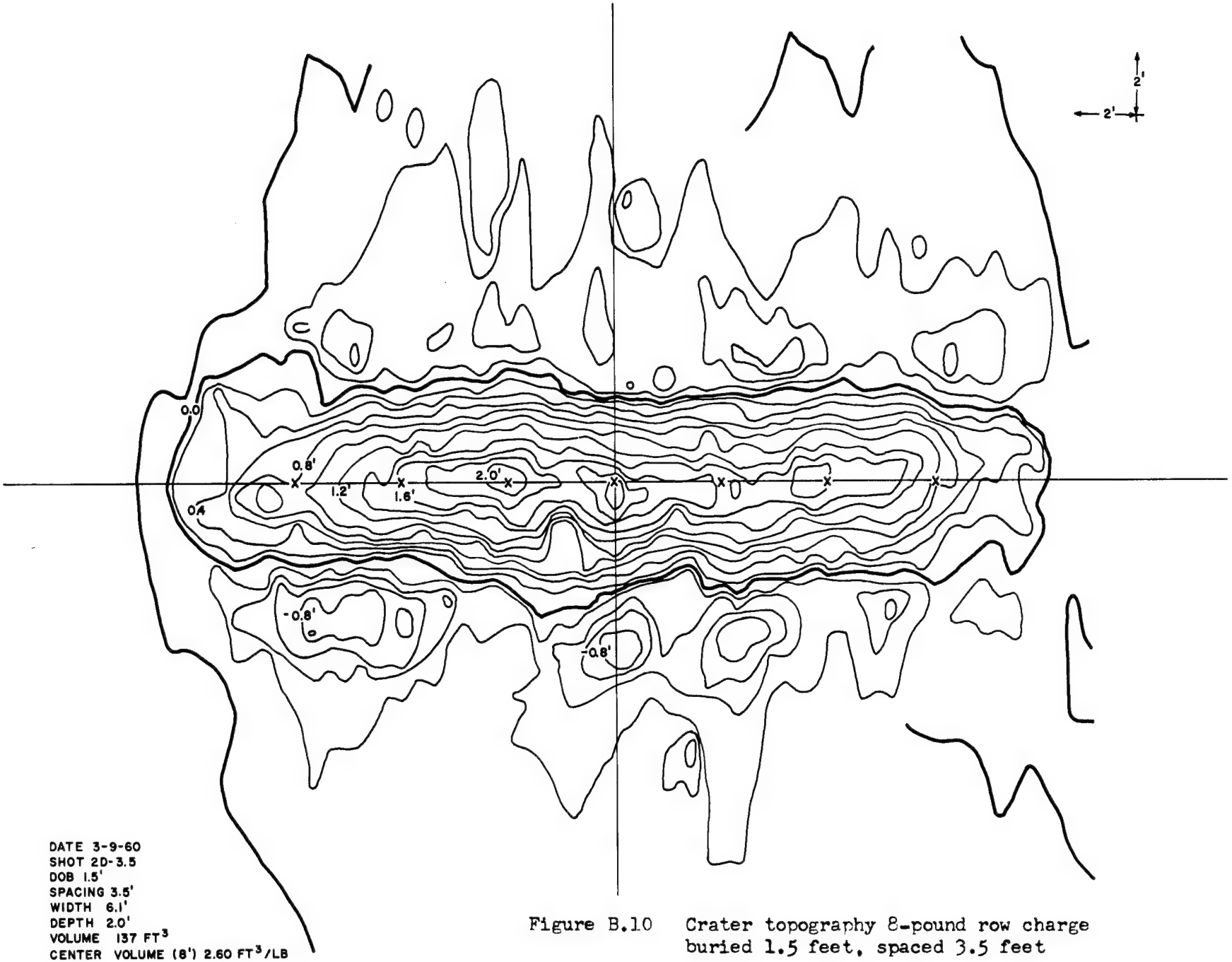

Figure B.10 Crater topography 8-pound row charge buried 1.5 feet, spaced 3.5 feet

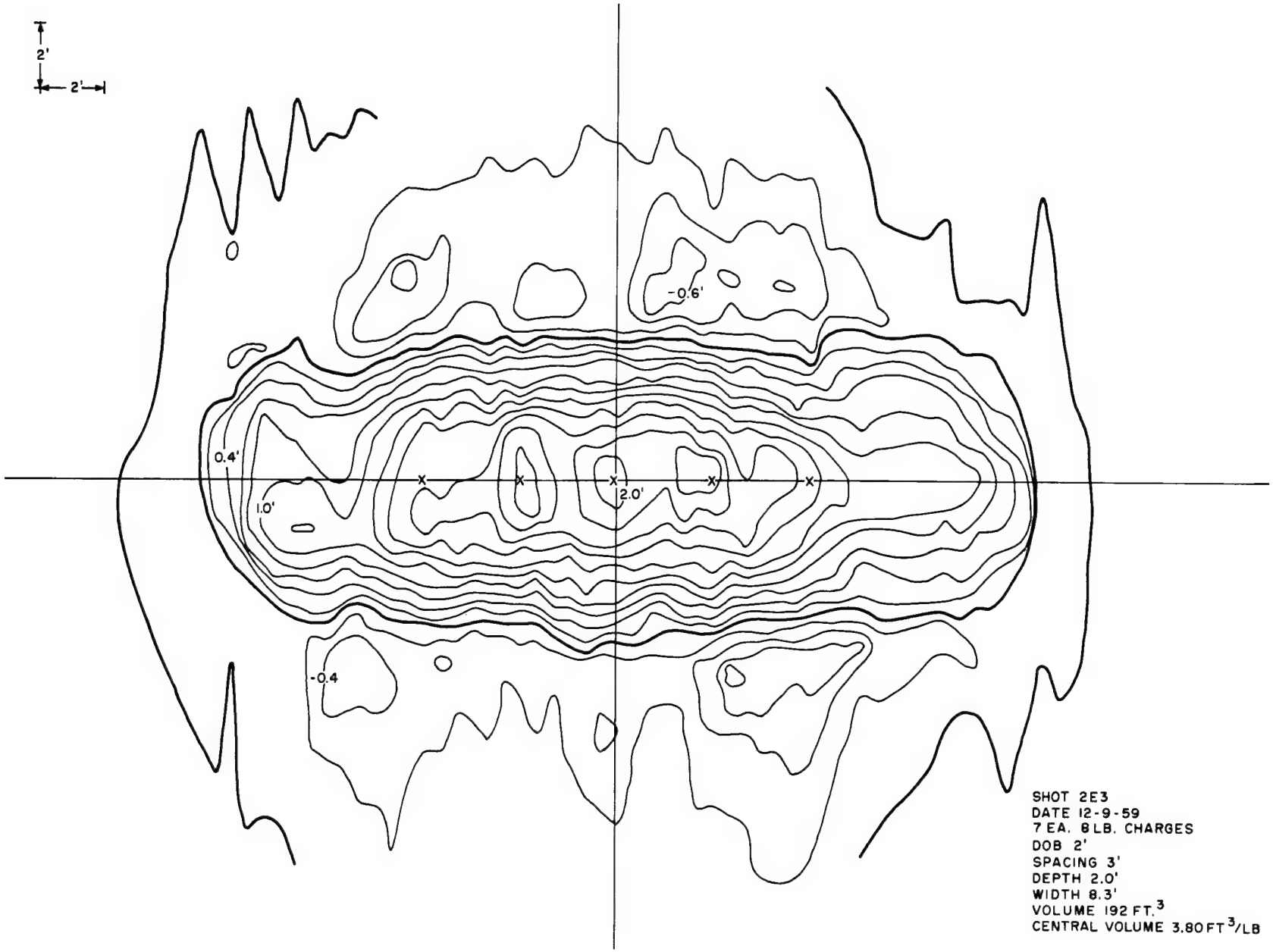

Figure B.11 Crater topography 8-pound row charge buried 2 feet, spaced 3 feet

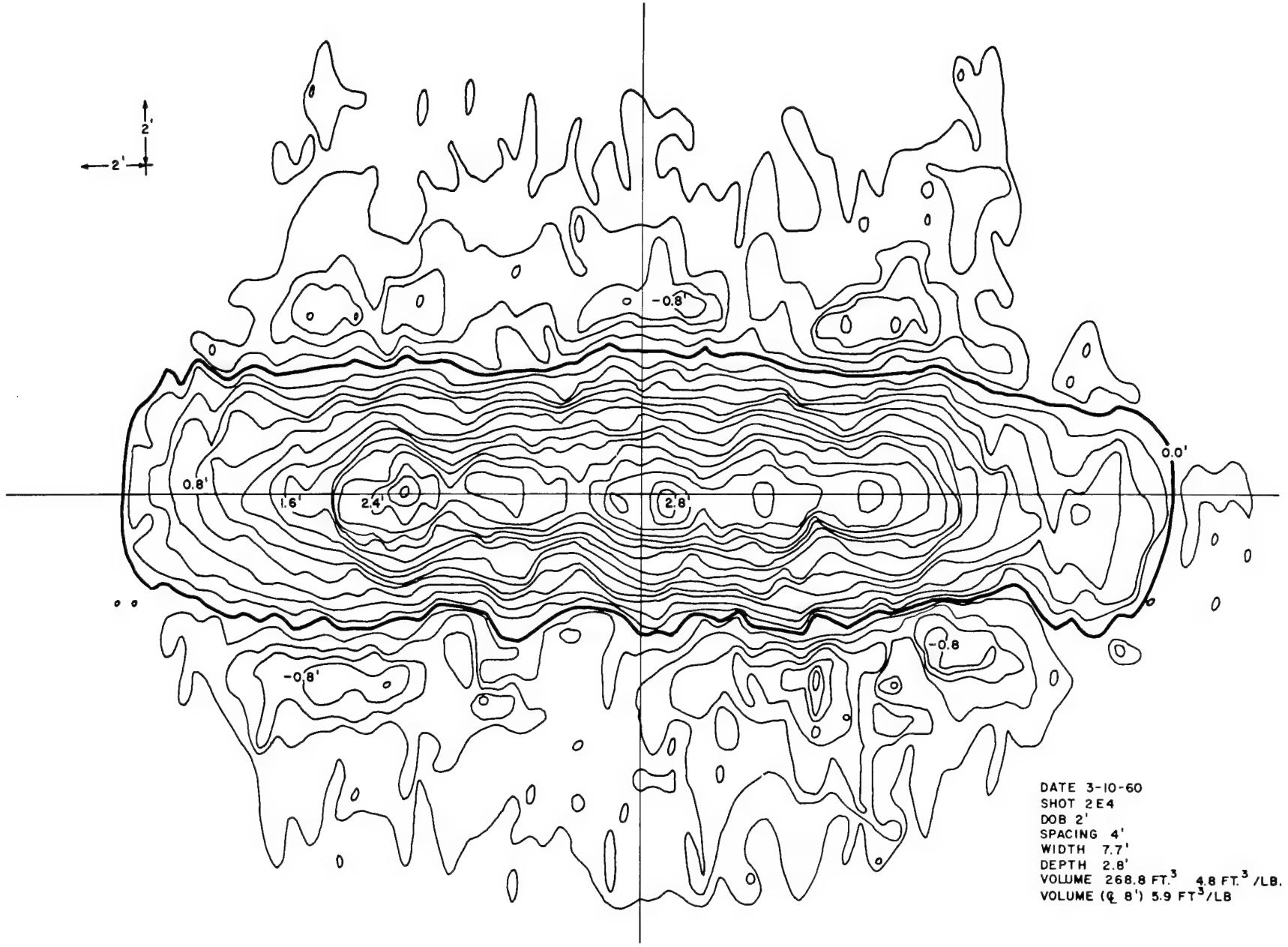

Figure B.12 Crater topography 8-pound row charge buried 2 feet, spaced 4 feet

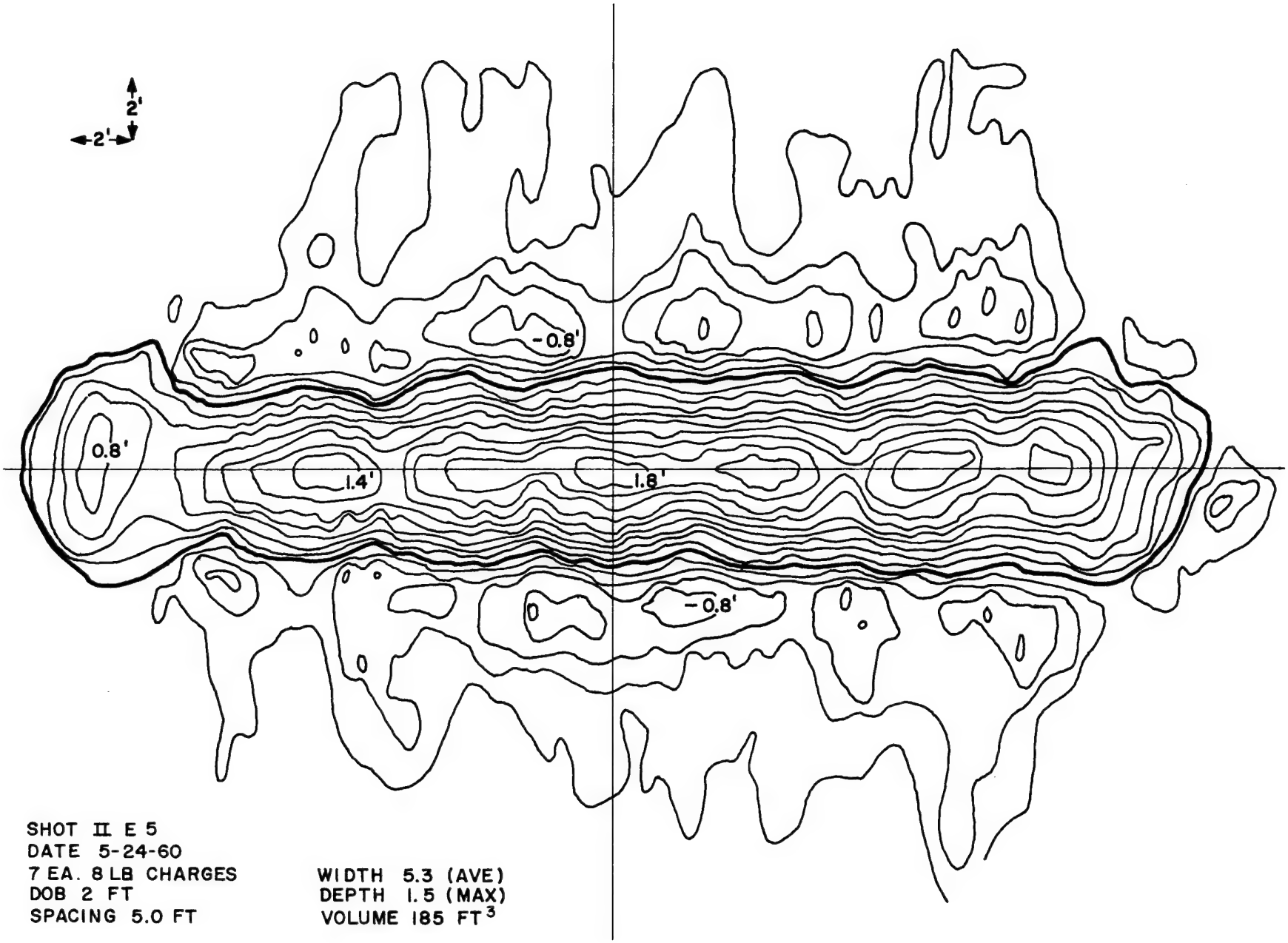

Figure B.13 Crater topography 8-pound row charge buried 2 feet, spaced 5 feet

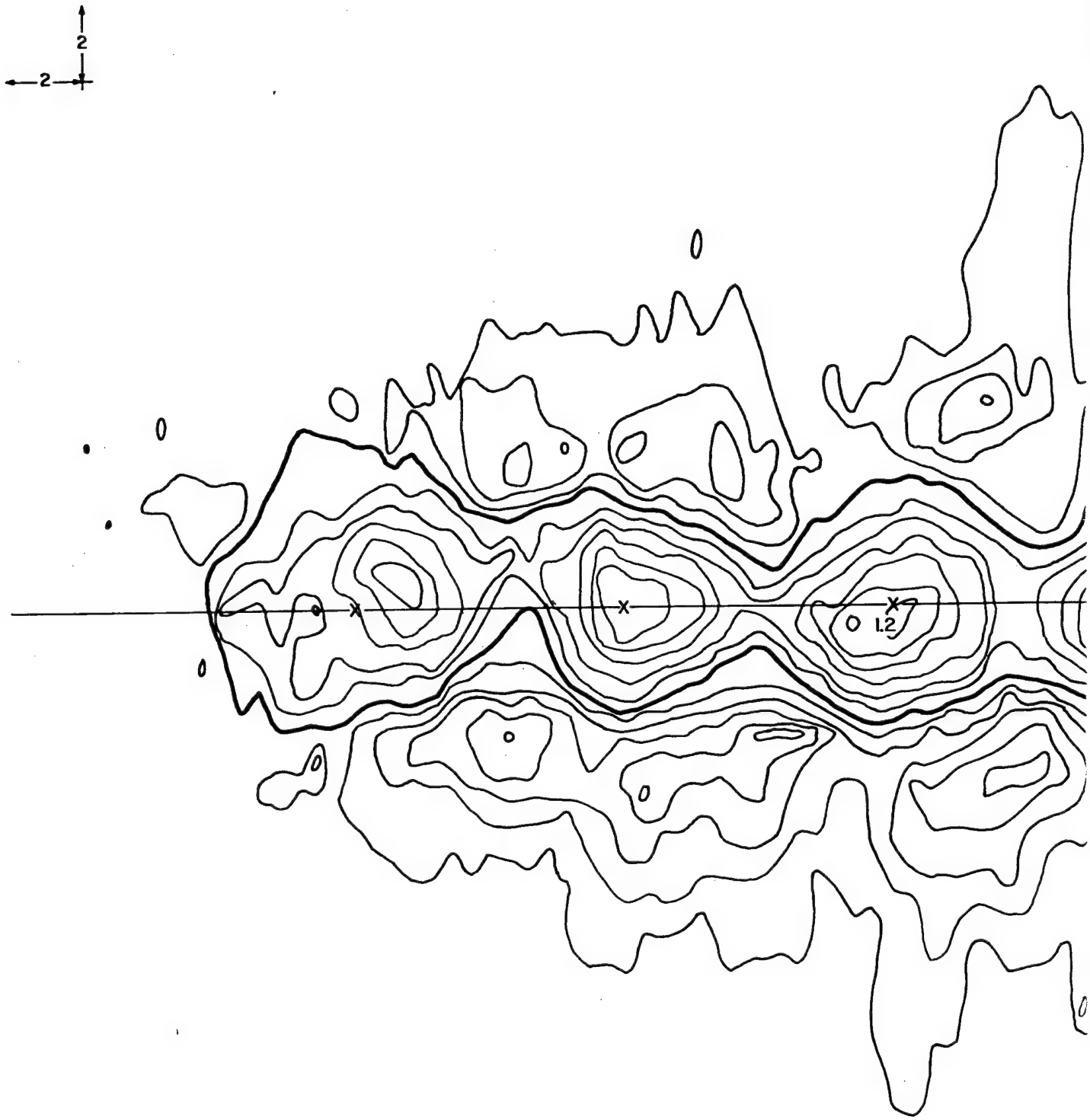

Figure B.14 Crater topography 8-po

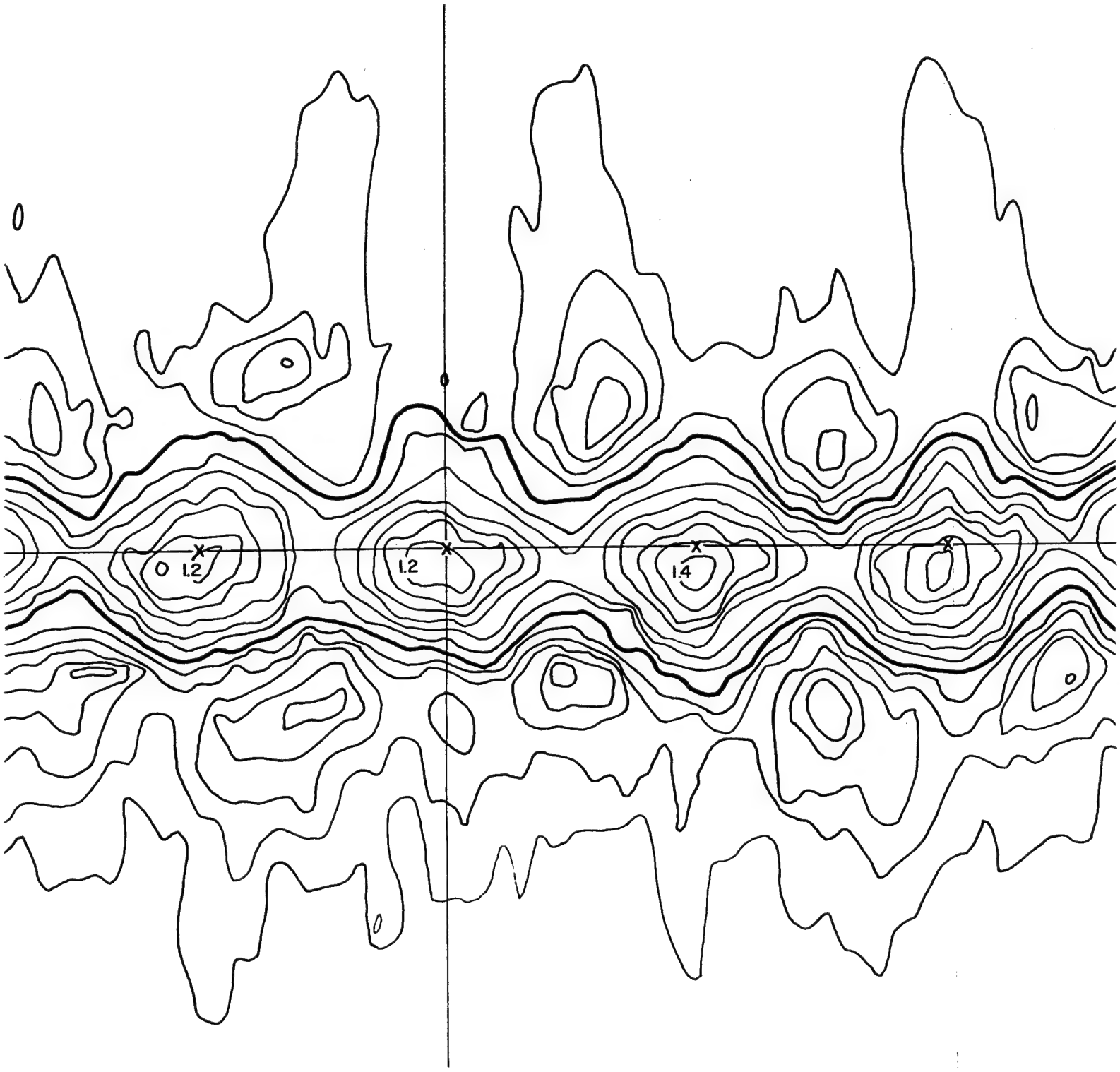

ure B.14 Crater topography 8-pound row charge buried 2 feet, spaced 7 feet

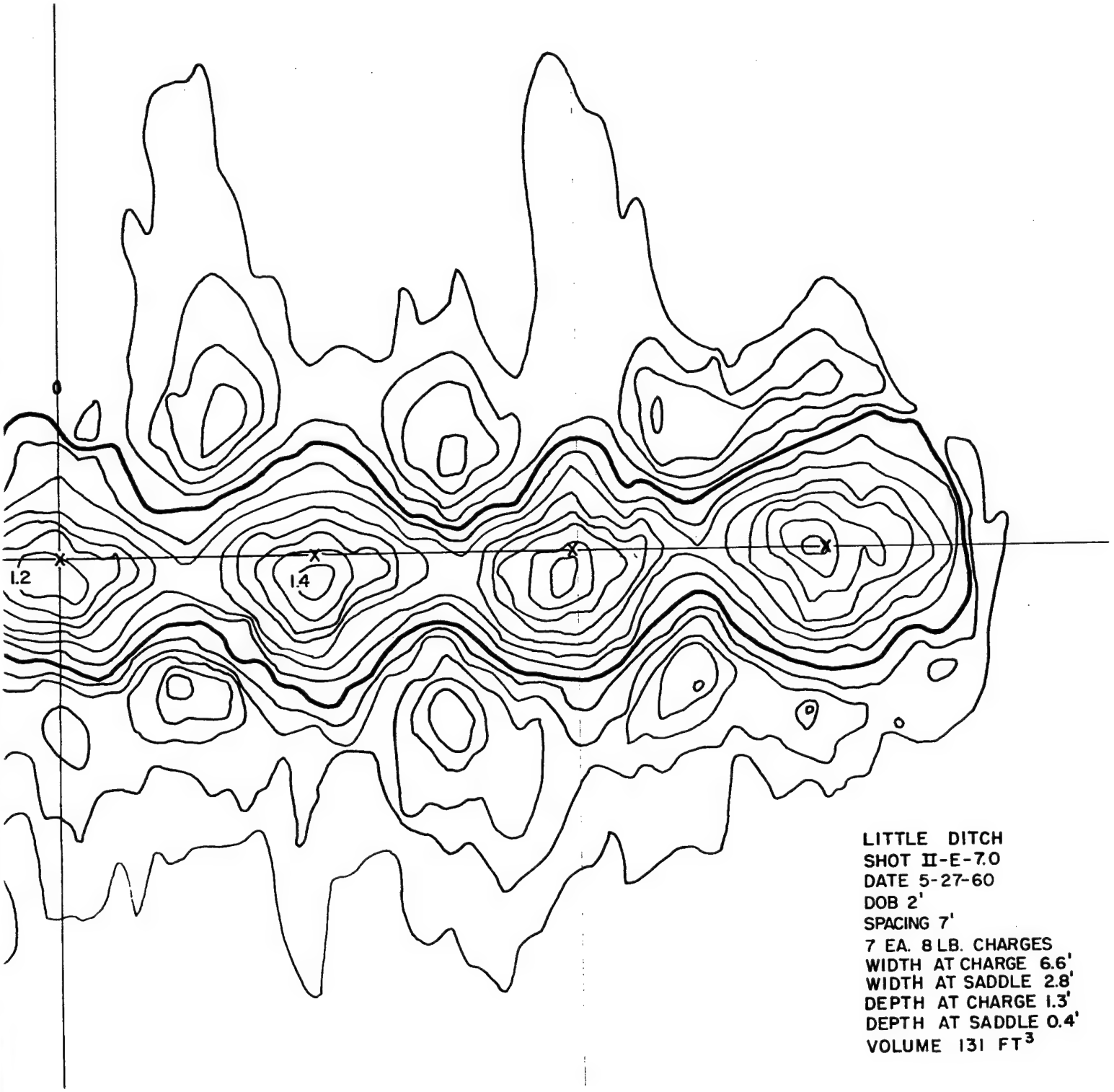

nd row charge buried 2 feet, spaced 7 feet

(3)

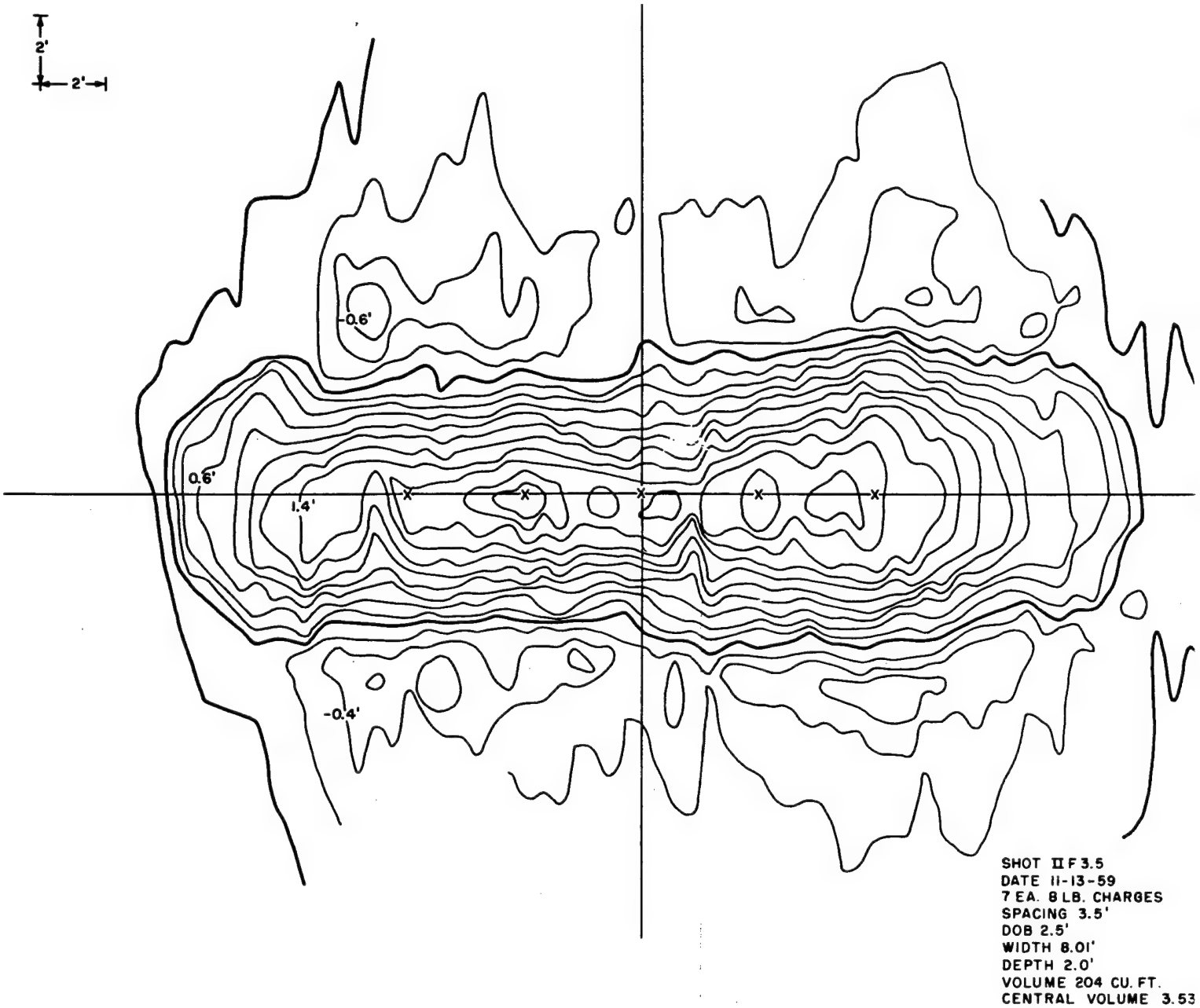

Figure B.15 Crater topography 8-pound row charge buried 2.5 feet, spaced 3.5 feet

SHOT II F 3.5
DATE 11-13-59
7 EA. 8 LB. CHARGES
SPACING 3.5'
DOB 2.5'
WIDTH 8.01'
DEPTH 2.0'
VOLUME 204 CU. FT.
CENTRAL VOLUME 3.53 FT^3/LB

phy 8-pound row charge
t, spaced 3.5 feet

(2)

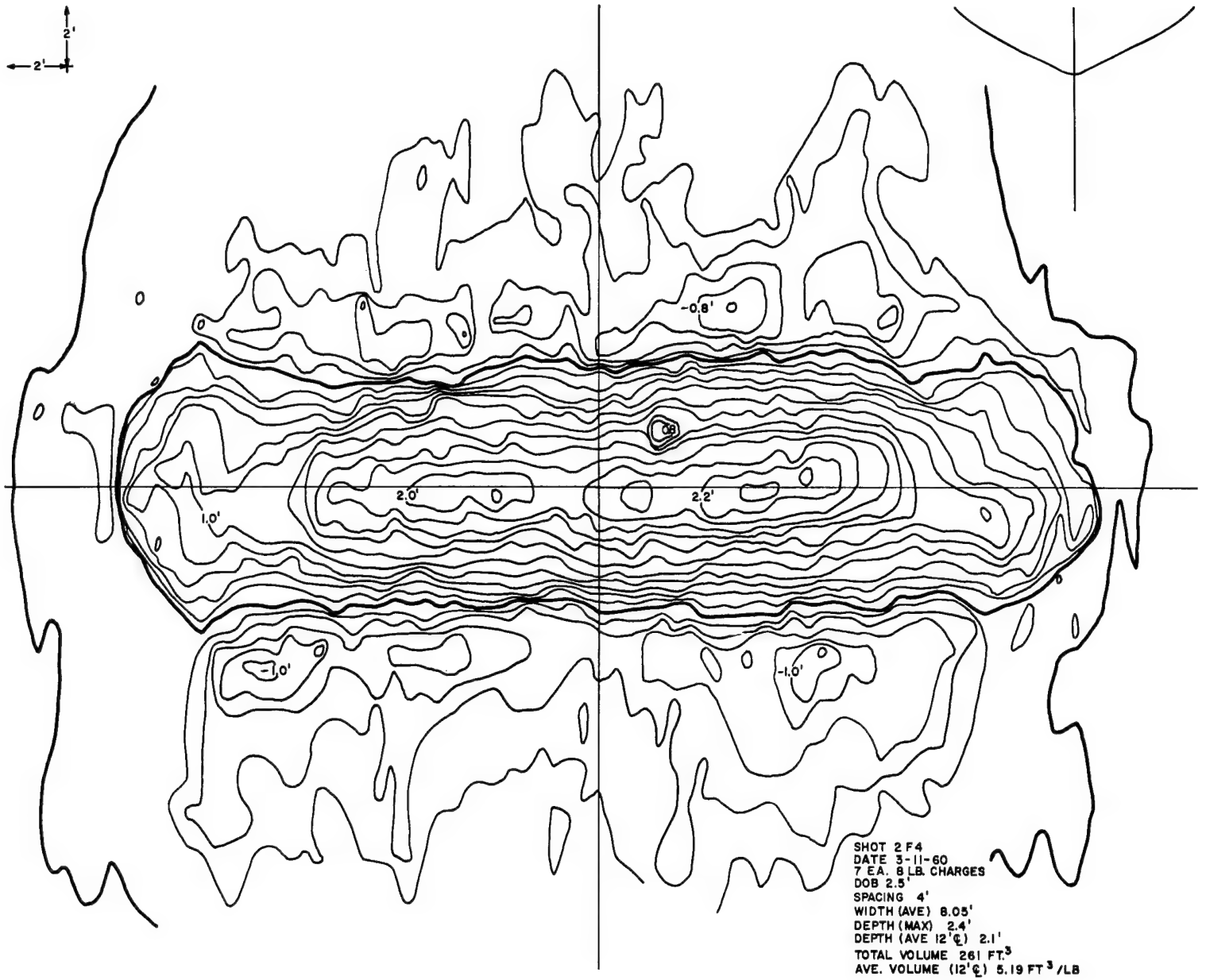

Figure B.16 Crater topography 8-pound row charge buried 2.5 feet, spaced 4 feet

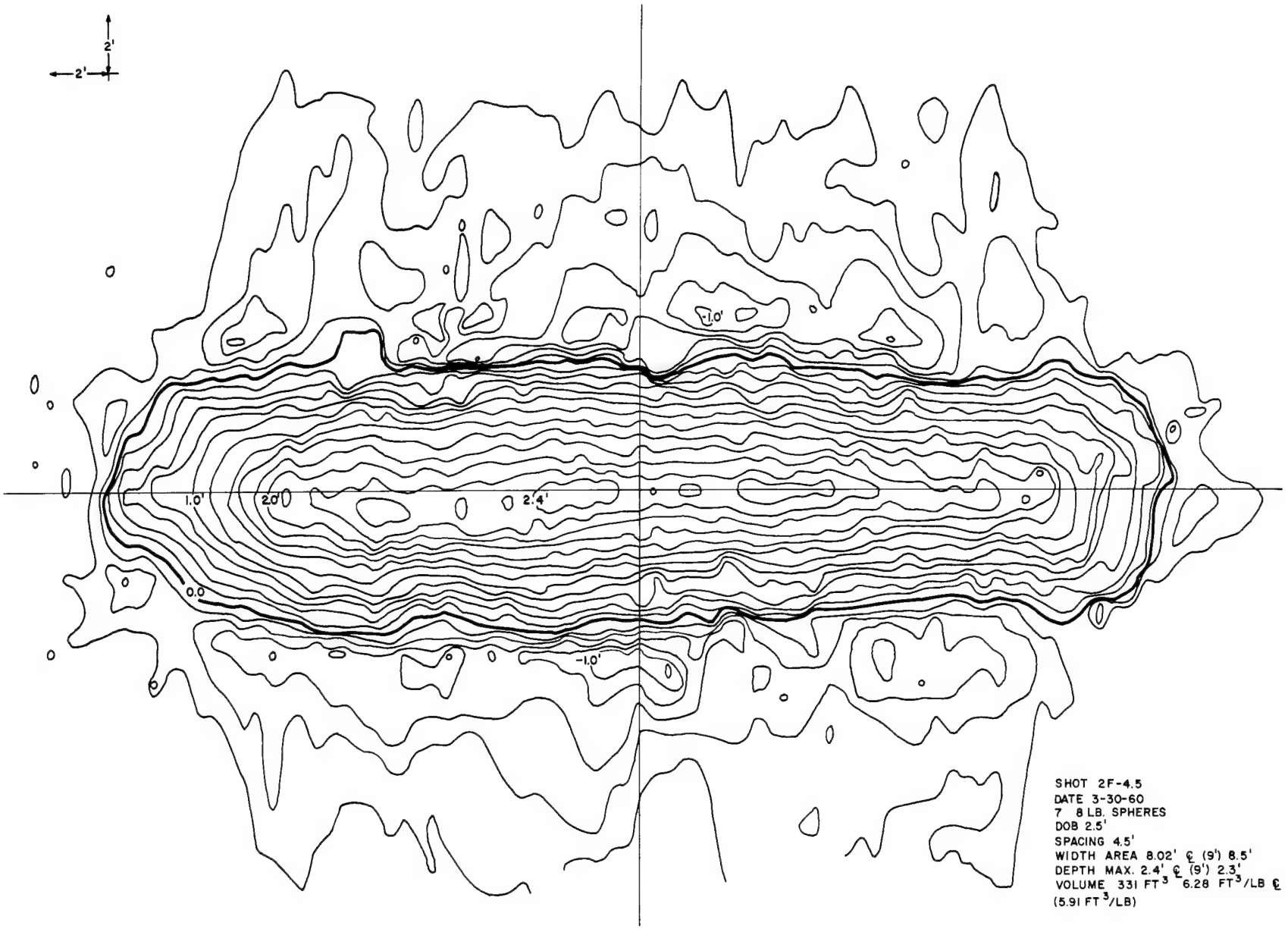

Figure B.17 Crater topography 8-pound row charge buried 2.5 feet, spaced 4.5 feet

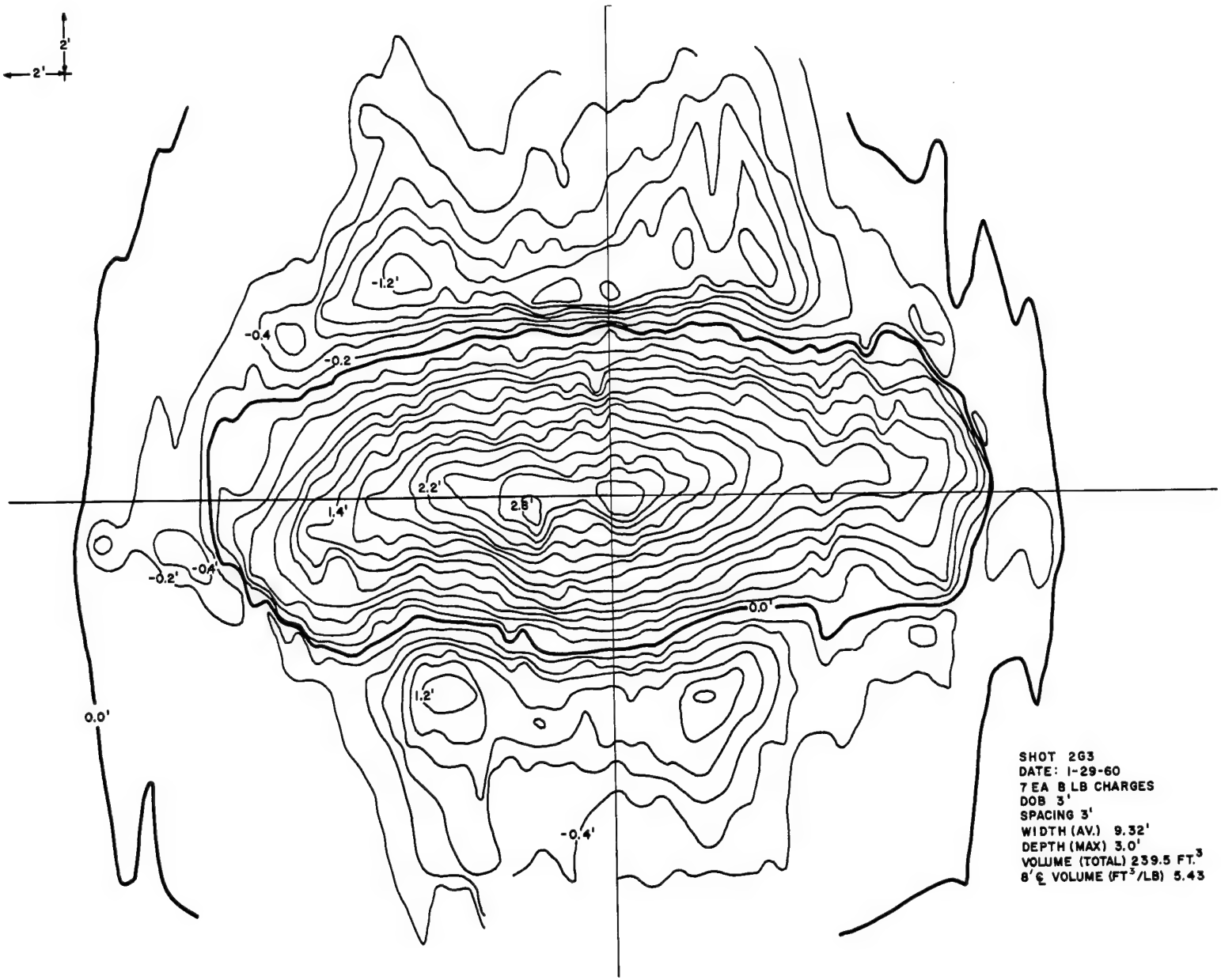

Figure B.18 Crater topography 8-pound row charge buried 3 feet, spaced 3 feet

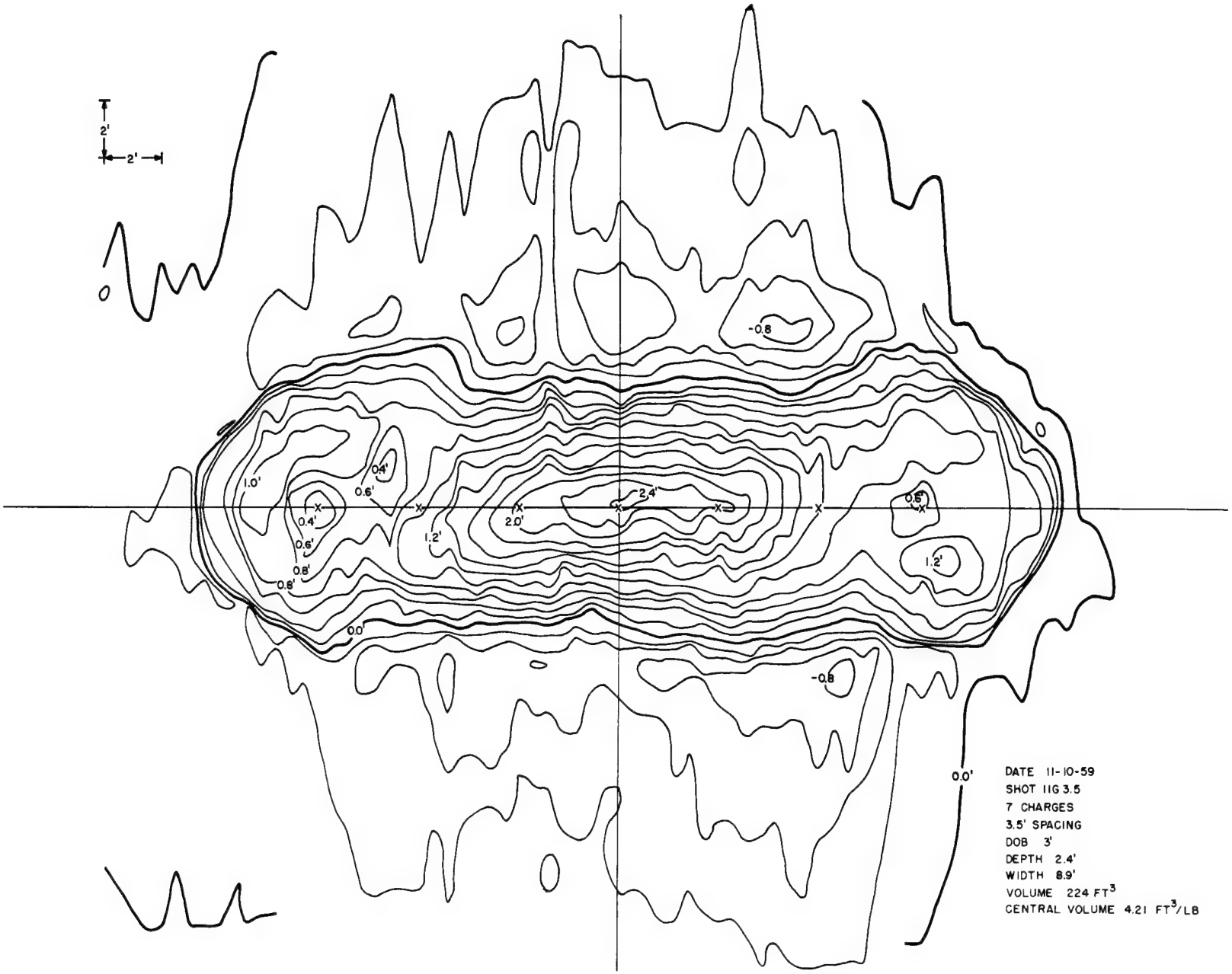

Figure B.19 Crater topography 8-pound row charge buried 3 feet, spaced 3.5 feet

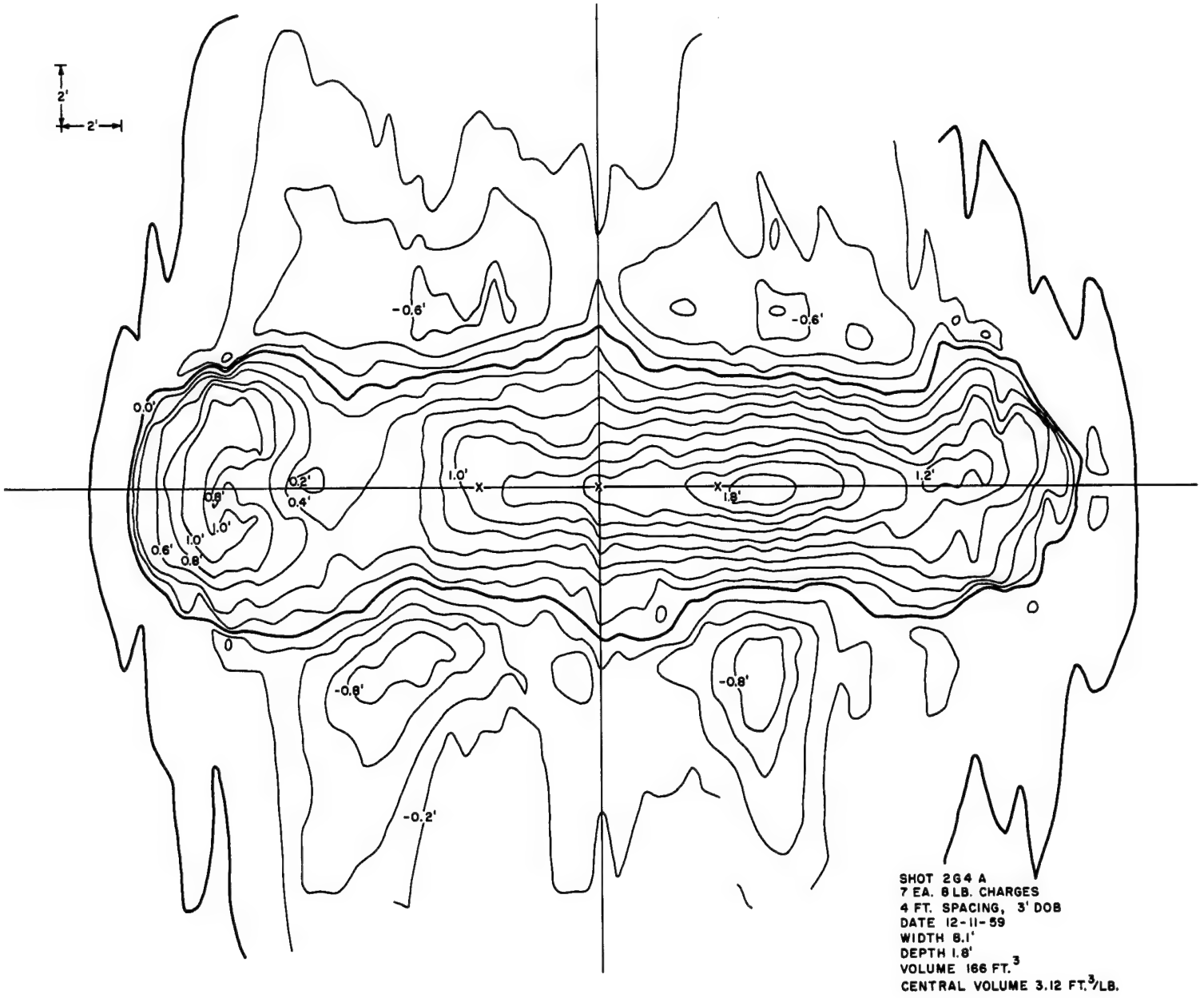

Figure B.20 Crater topography 8-pound row charge buried 3 feet, spaced 4 feet

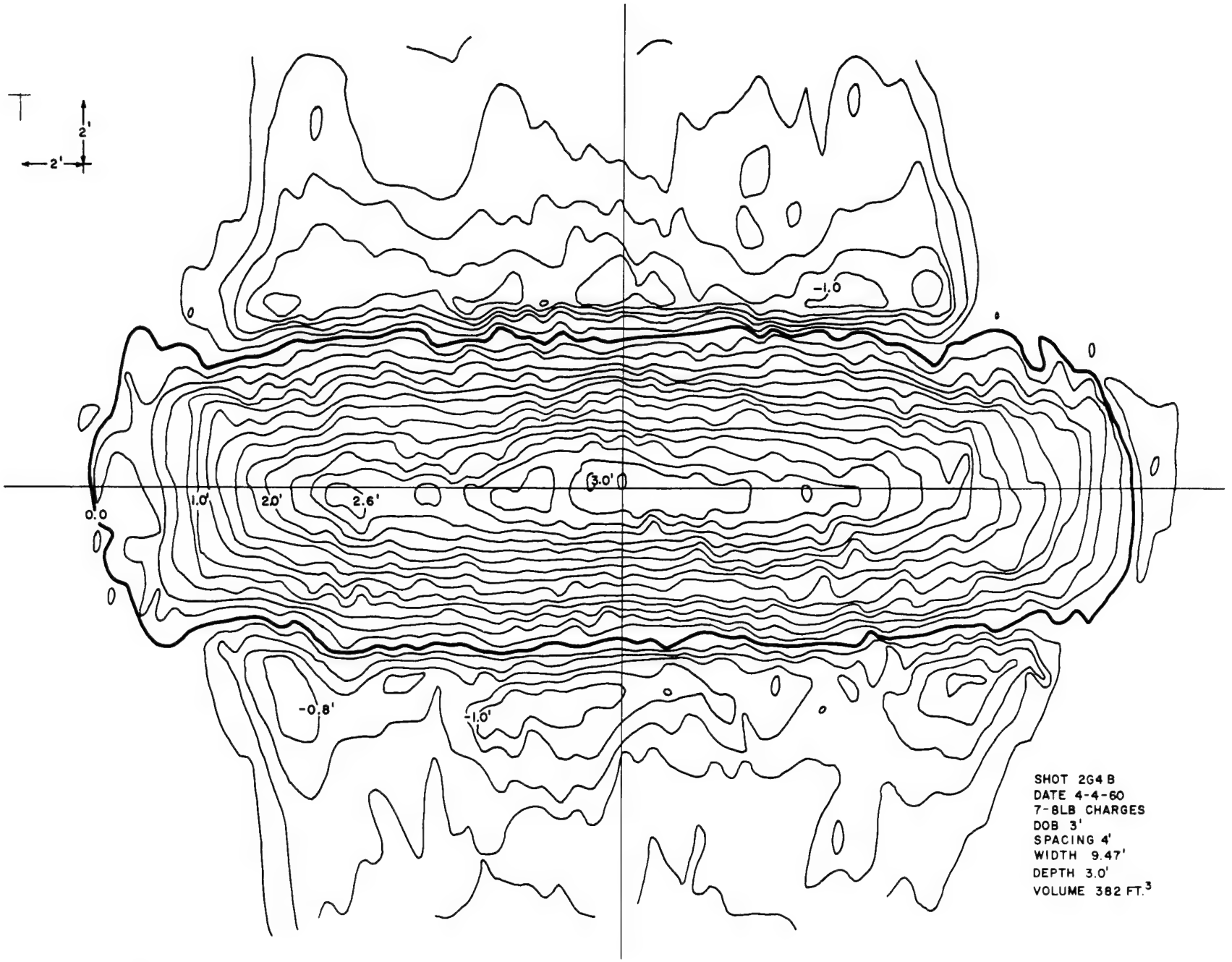

Figure B.21 Crater topography 8-pound row charge buried 3 feet, spaced 4 feet

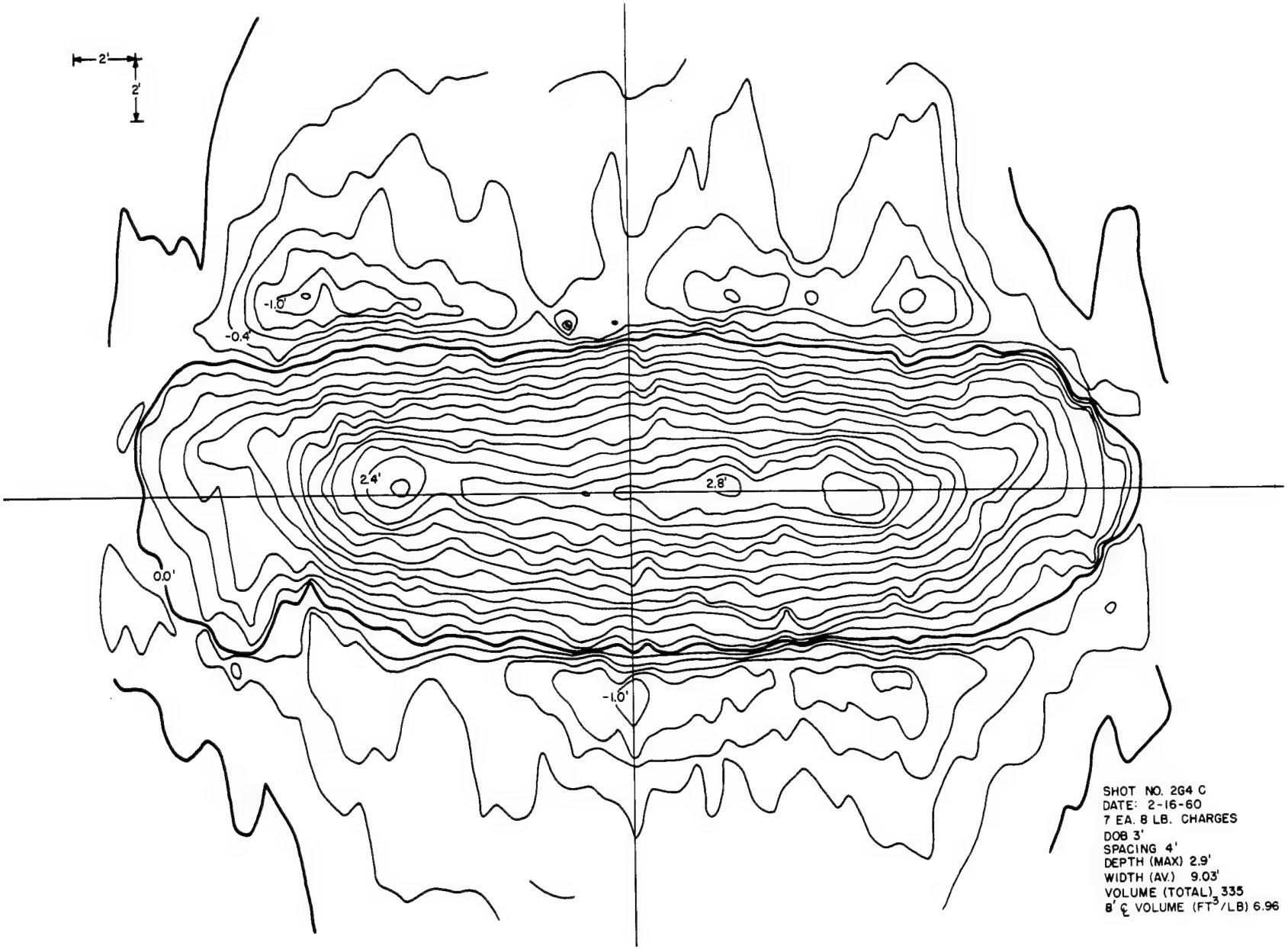

Figure B.22 Crater topography 8-pound row charge buried 3 feet, spaced 4 feet

Figure B.24 Crater topo
buried 3 fe

(1)

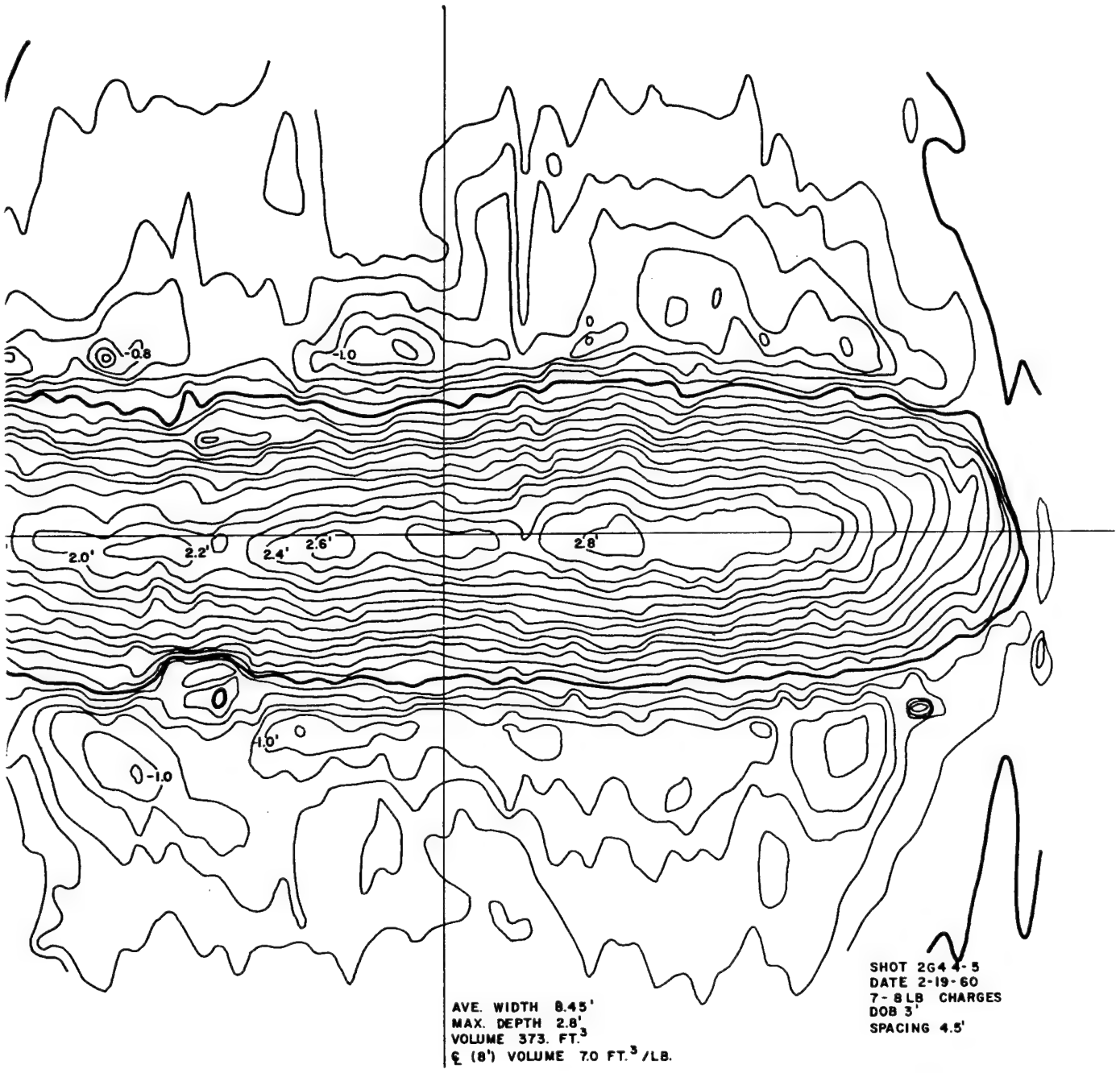

Figure B.24 Crater topography 8-pound row charge buried 3 feet, spaced 4.5 feet

2

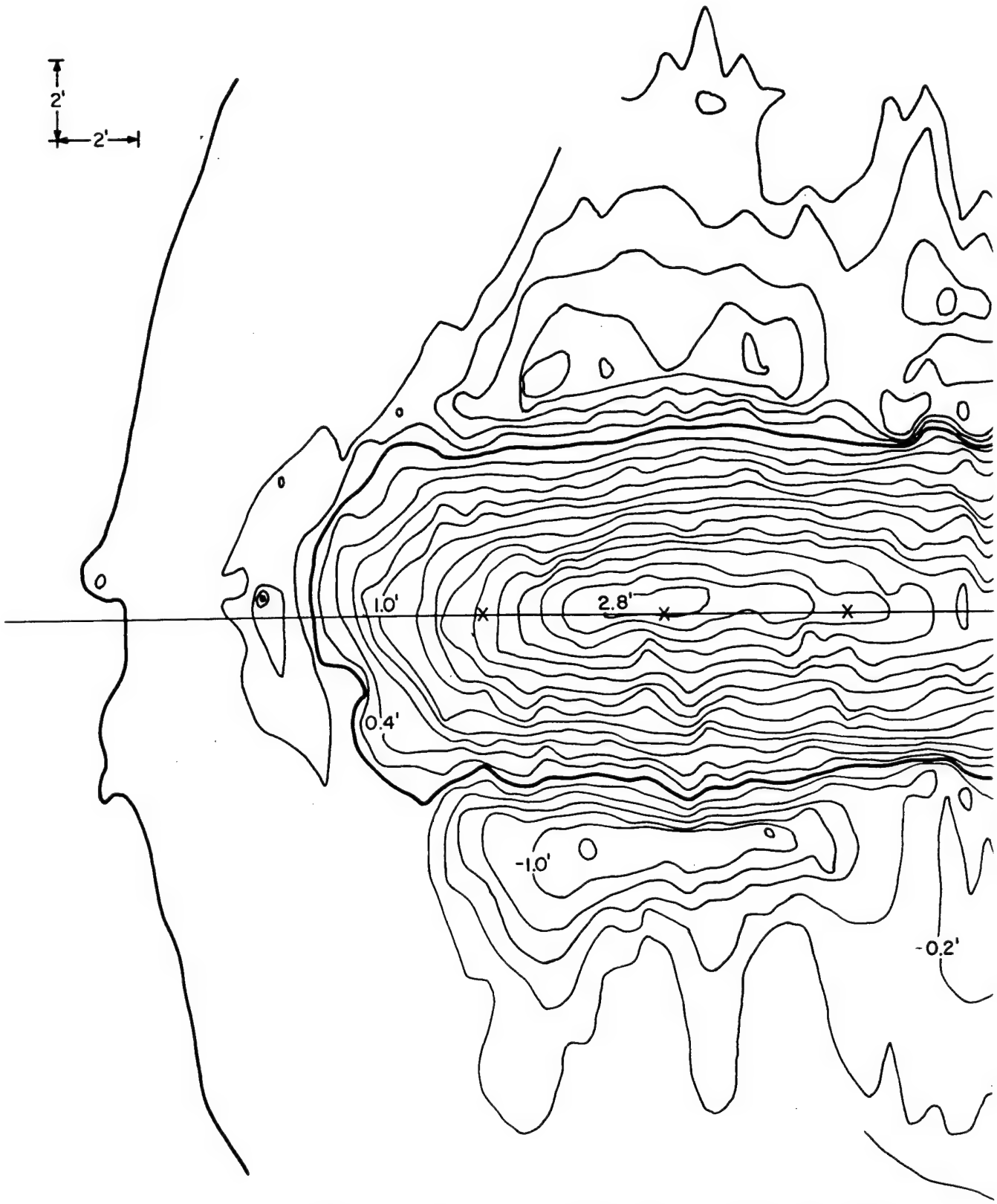

Figure B.23 Crater topography 8-pound row charge buried 3 feet, spaced 4.5 feet

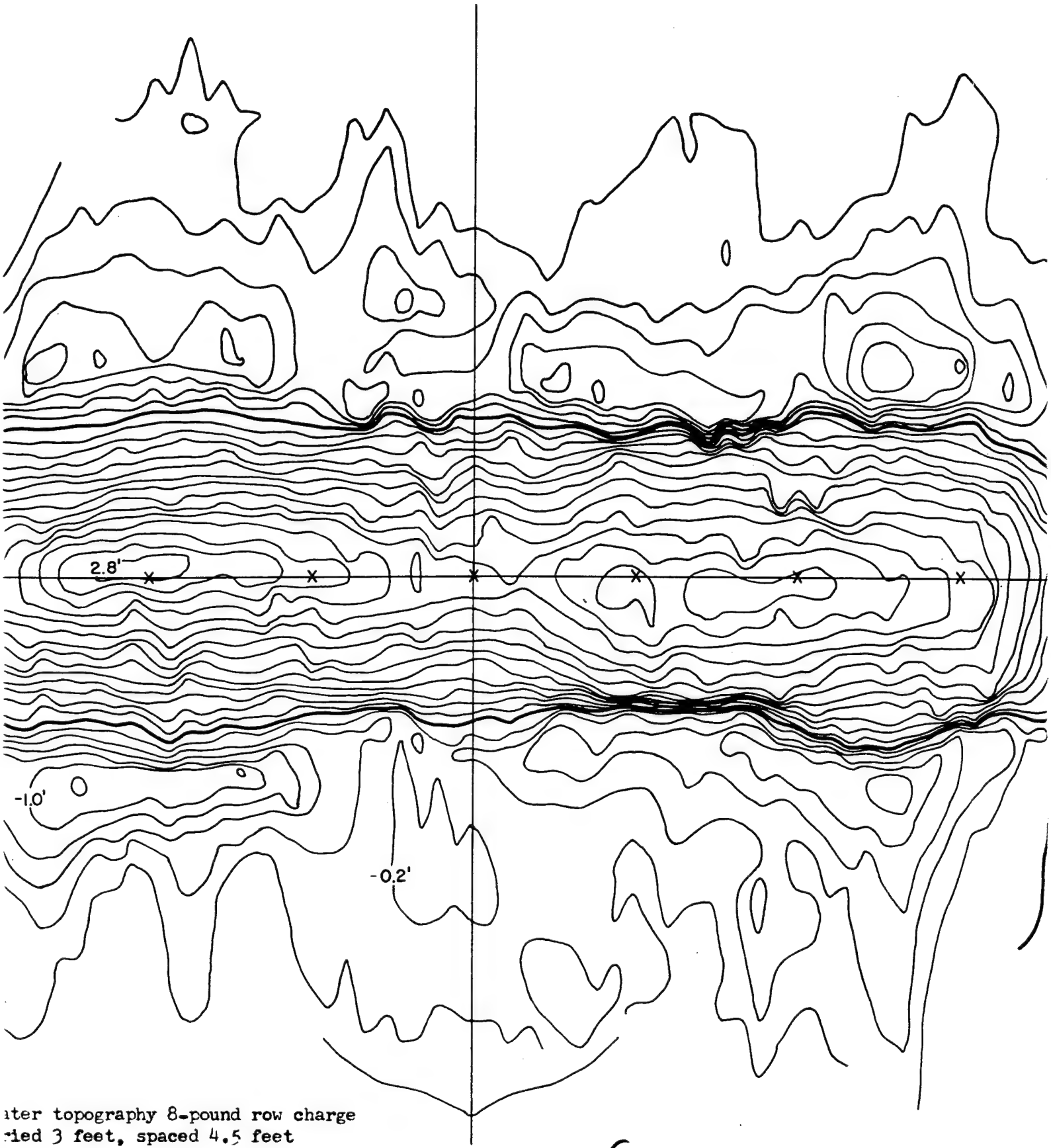

ıter topography 8-pound row charge
ried 3 feet, spaced 4.5 feet

(2)

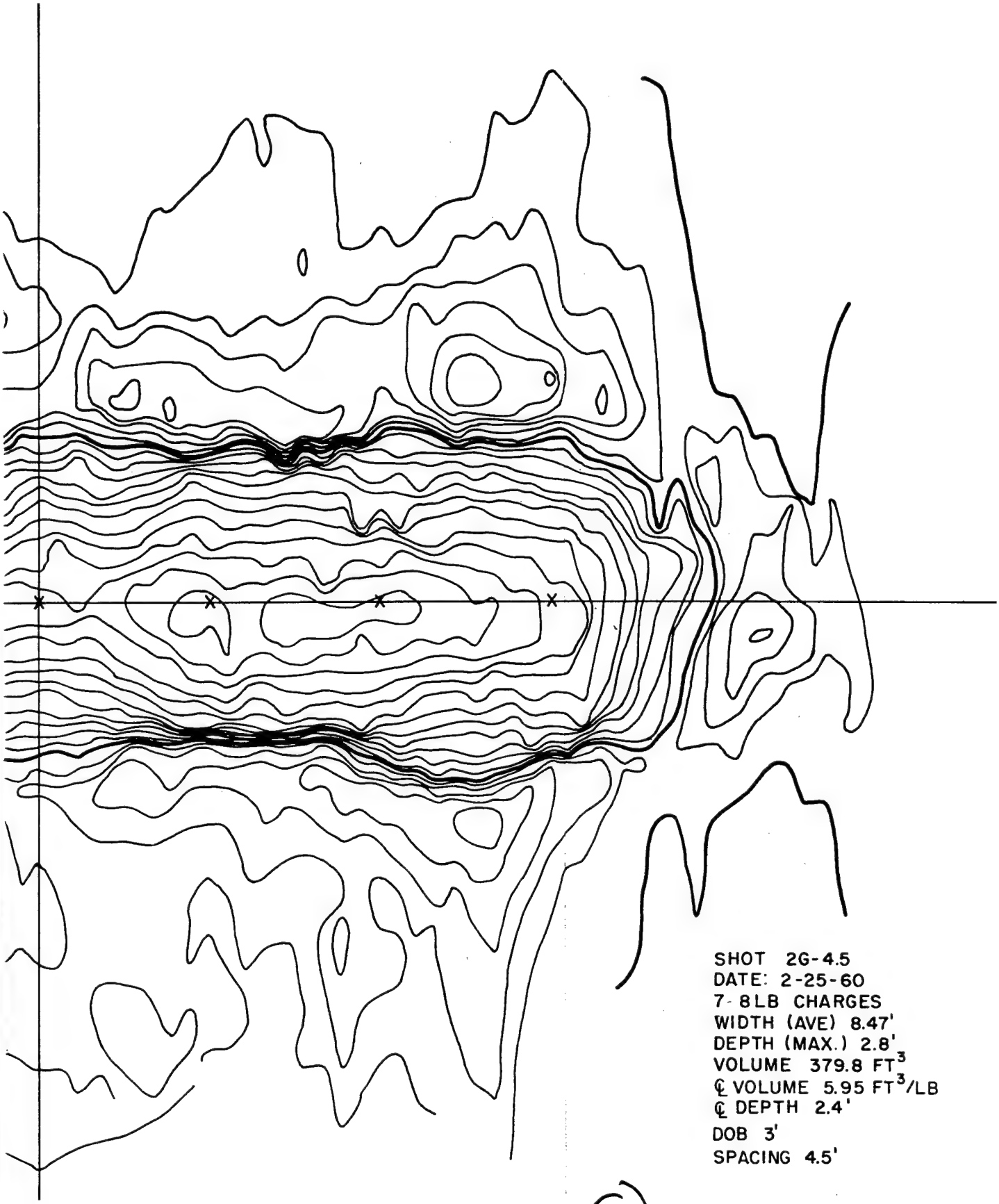

SHOT 2G-4.5
DATE: 2-25-60
7-8LB CHARGES
WIDTH (AVE) 8.47'
DEPTH (MAX.) 2.8'
VOLUME 379.8 FT^3
℄ VOLUME 5.95 FT^3/LB
℄ DEPTH 2.4'
DOB 3'
SPACING 4.5'

3

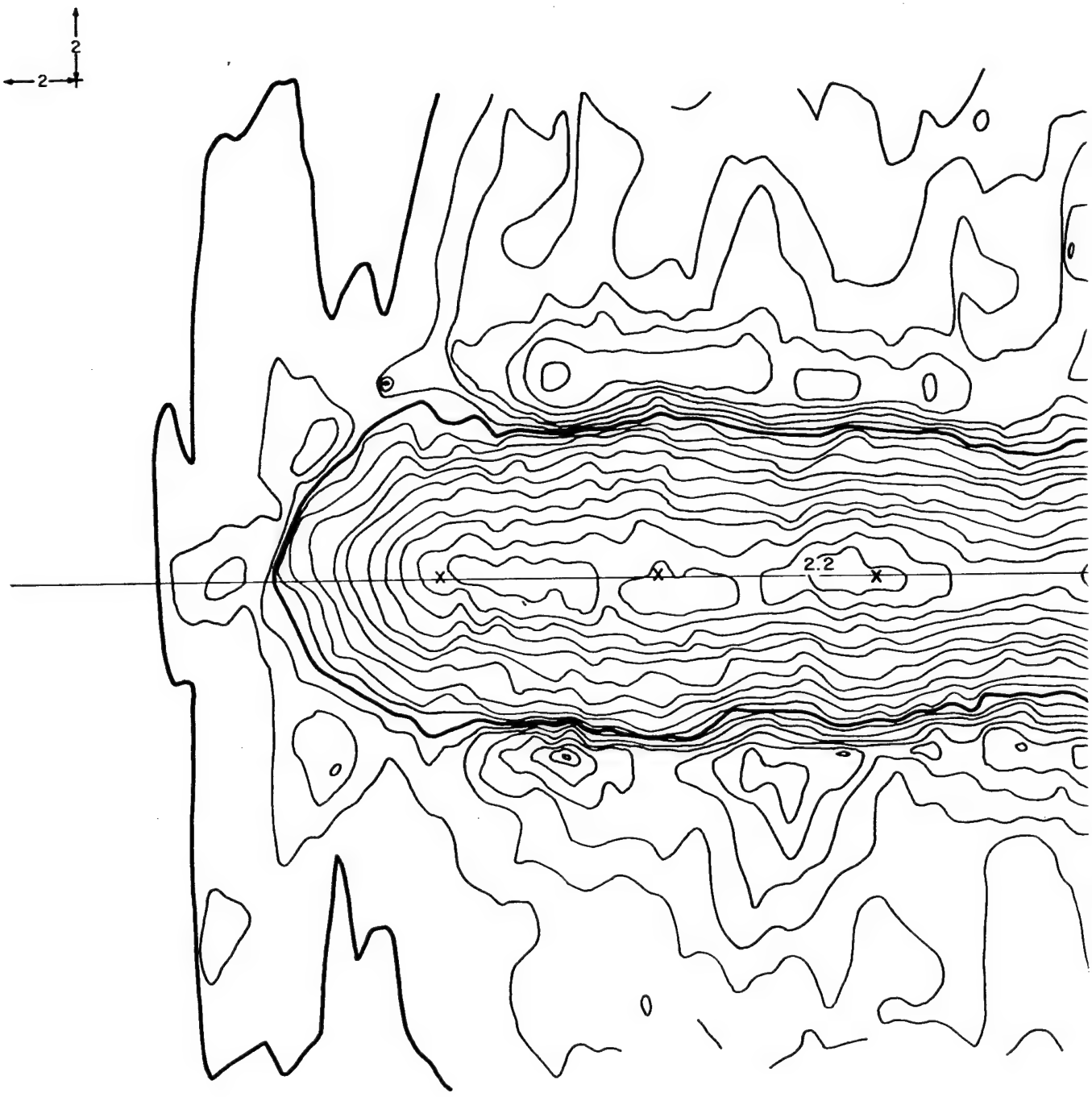

Figure B.25 Crater topography 8-poun

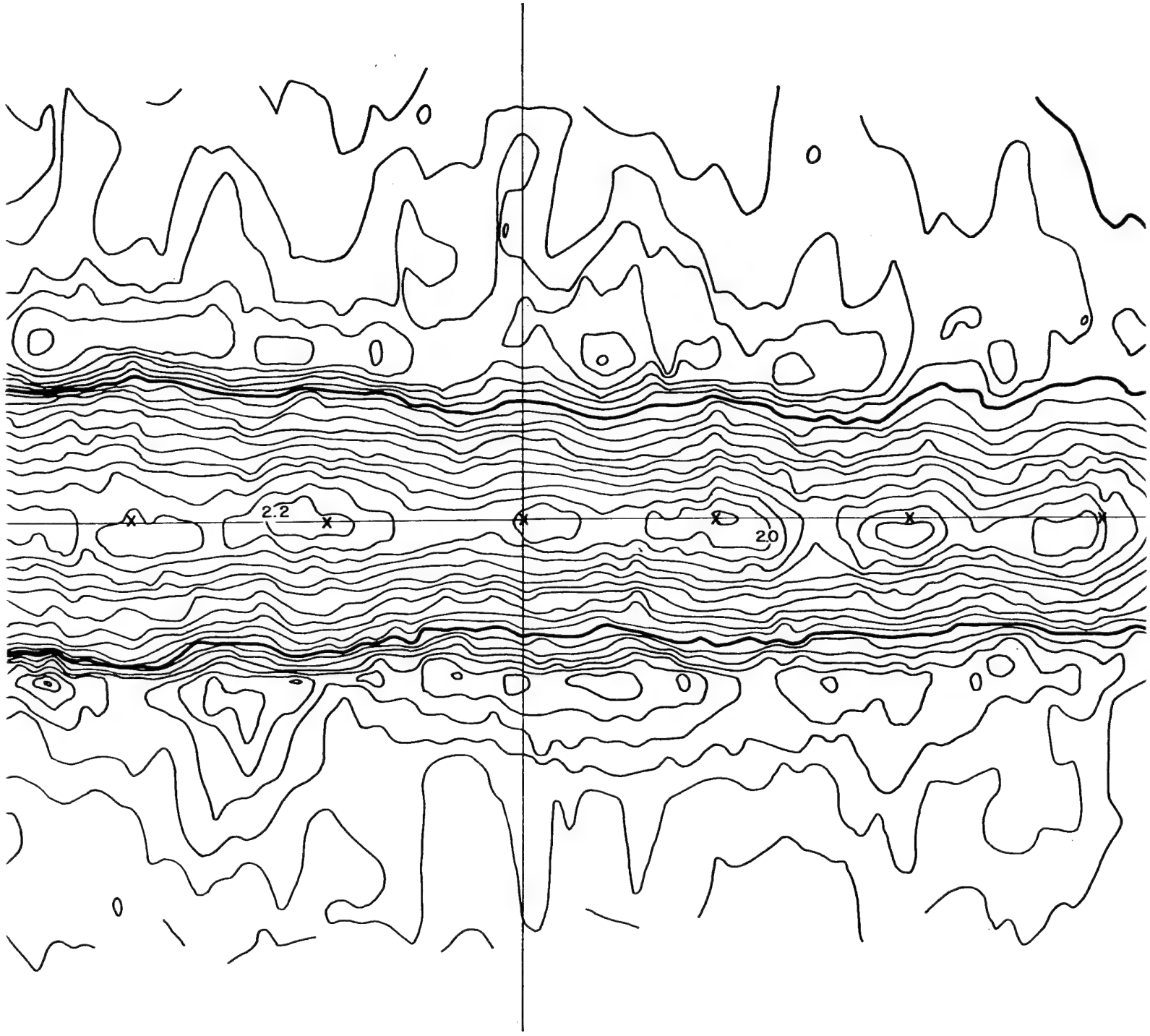

Figure B.25 Crater topography 8-pound row charge buried 3 feet, spaced 6 feet

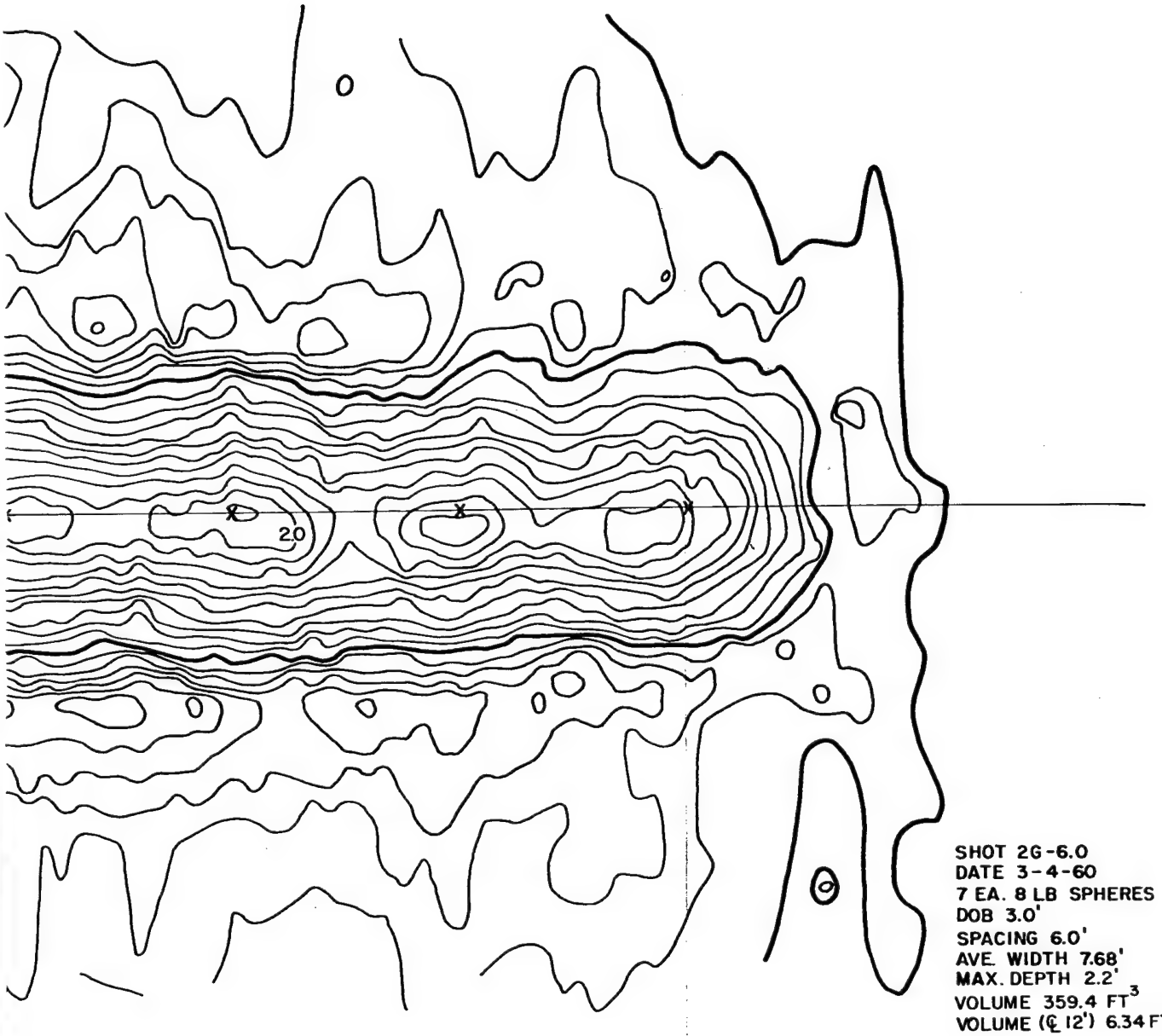

row charge buried 3 feet, spaced 6 feet

3

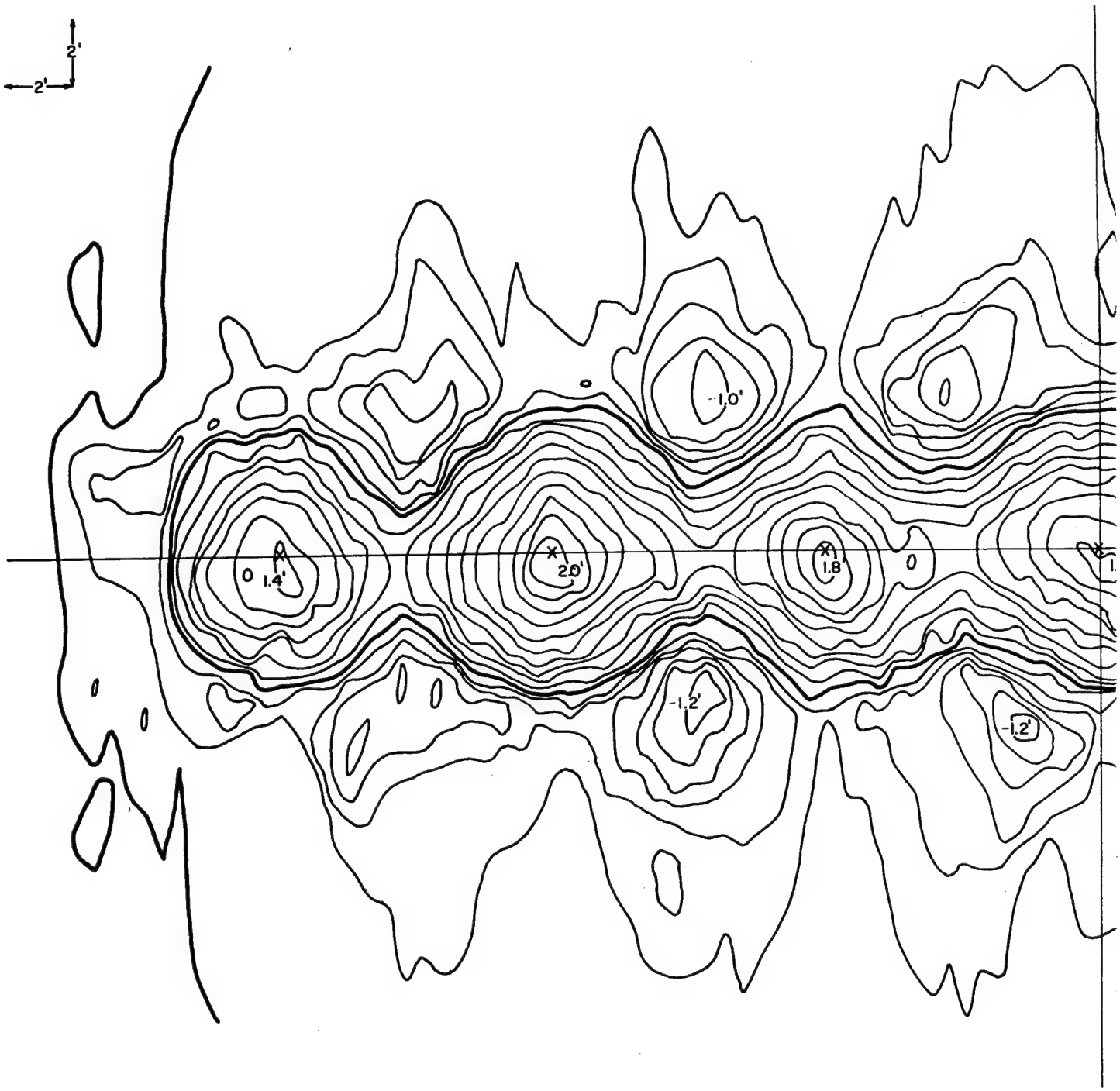

Figure B.26 Crater topography 8-pound

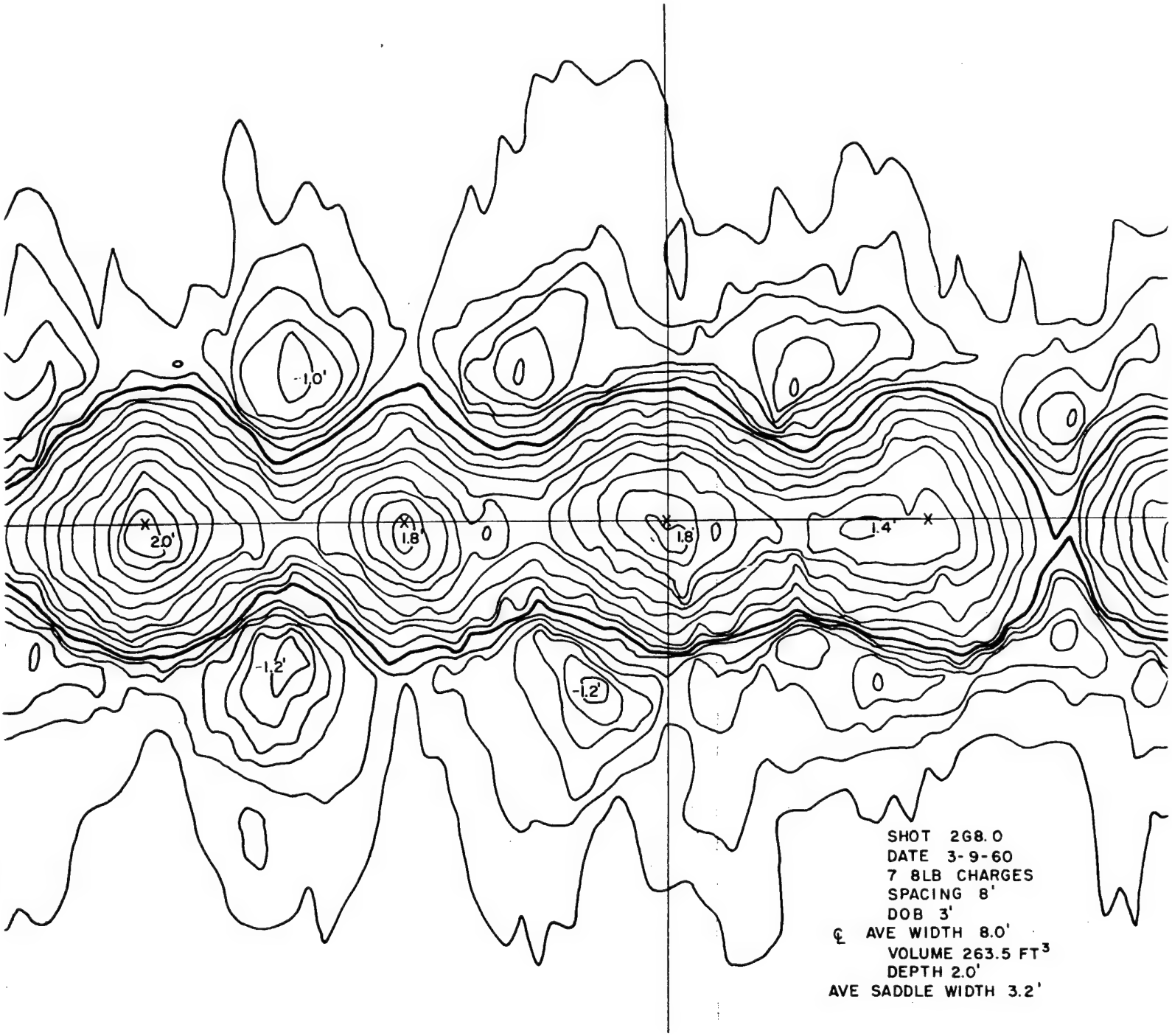

Figure B.26 Crater topography 8-pound row charge buried 3 feet, spaced 8 feet

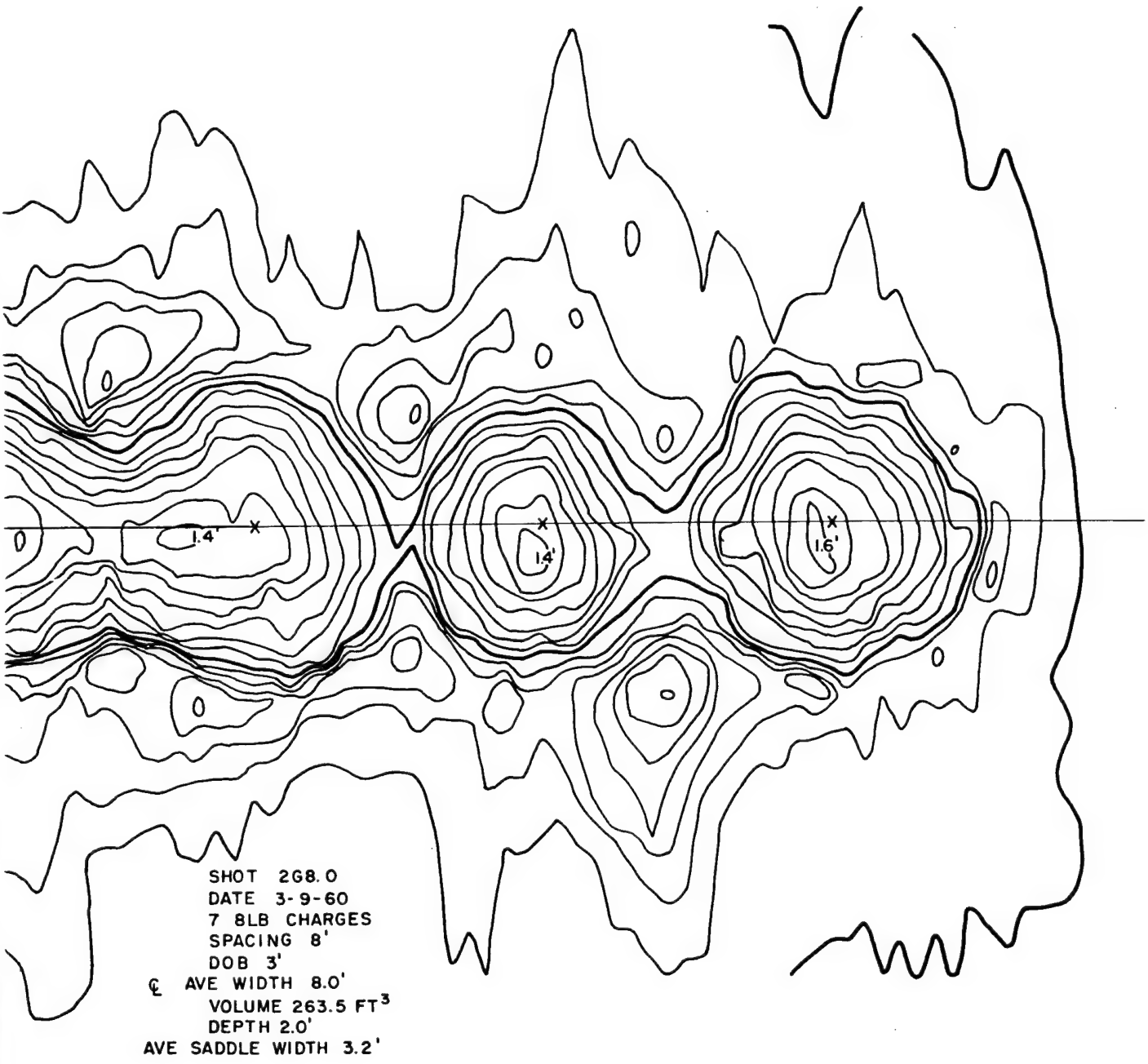

w charge buried 3 feet, spaced 8 feet

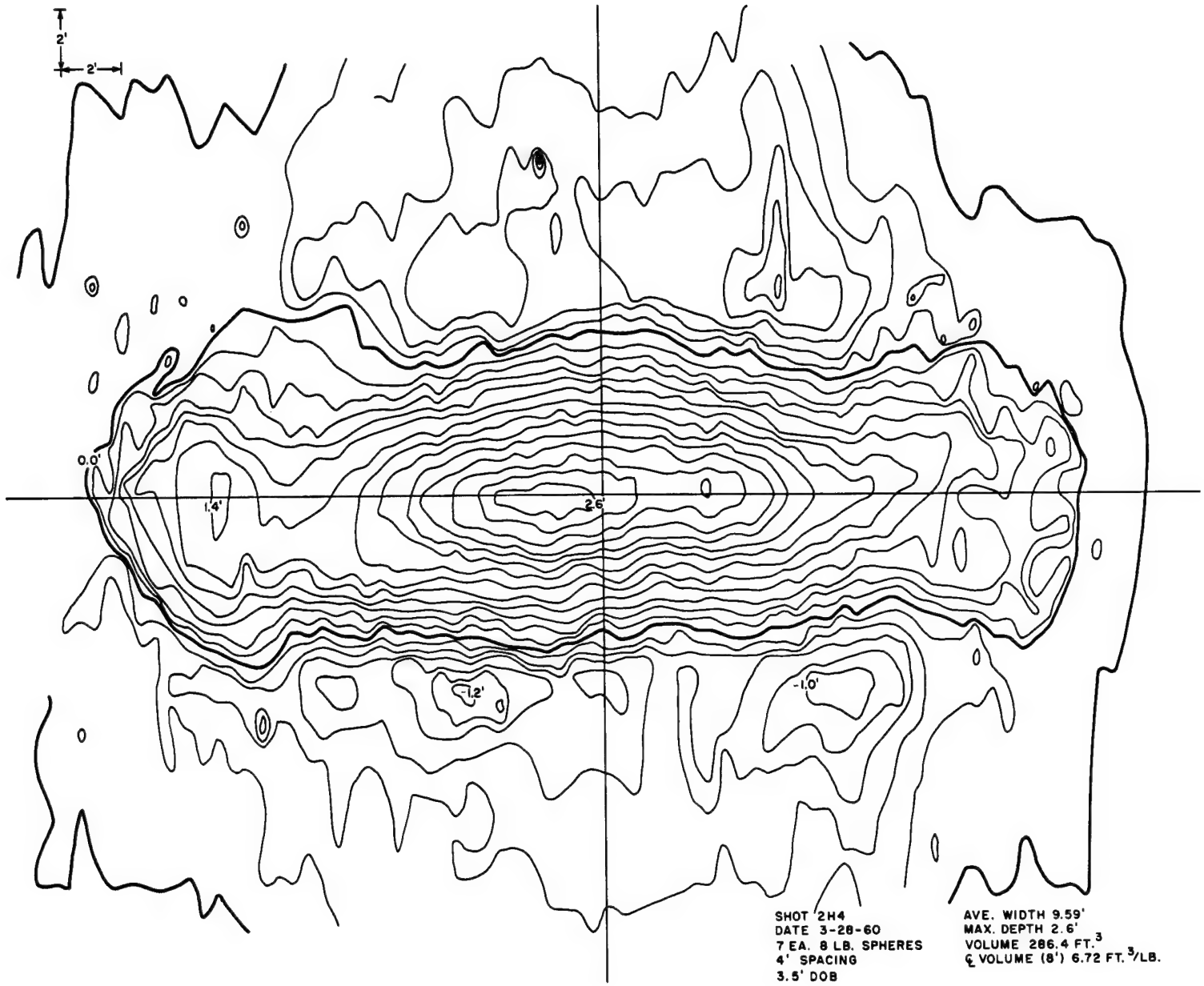

Figure B.27 Crater topography 8-pound row charge buried 3.5 feet, spaced 4 feet

Figure B.28 Crater topography 8-pound row charge buried 4 feet, spaced 3.5 feet

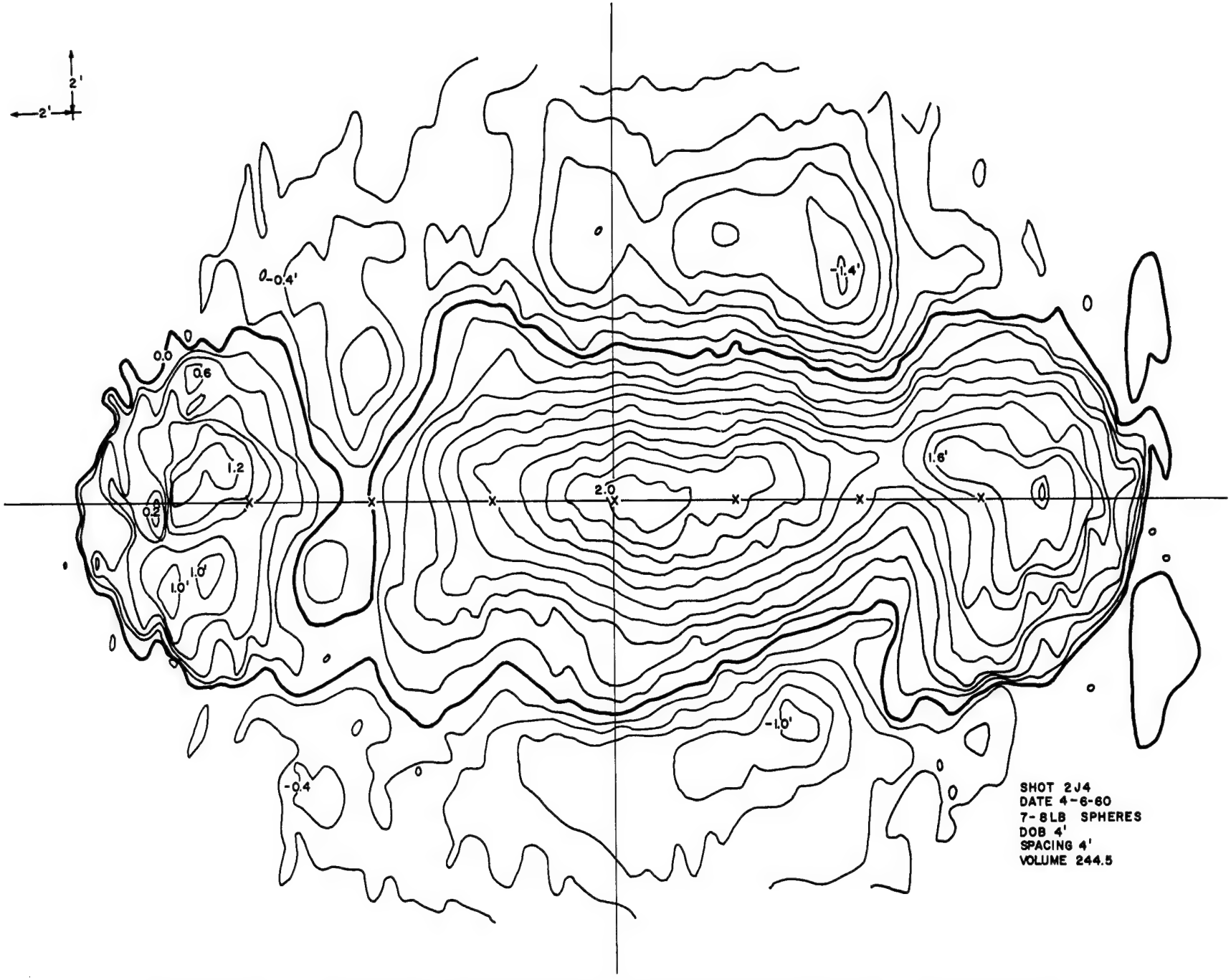

Figure B.29 Crater topography 8-pound row charge buried 4 feet, spaced 4 feet

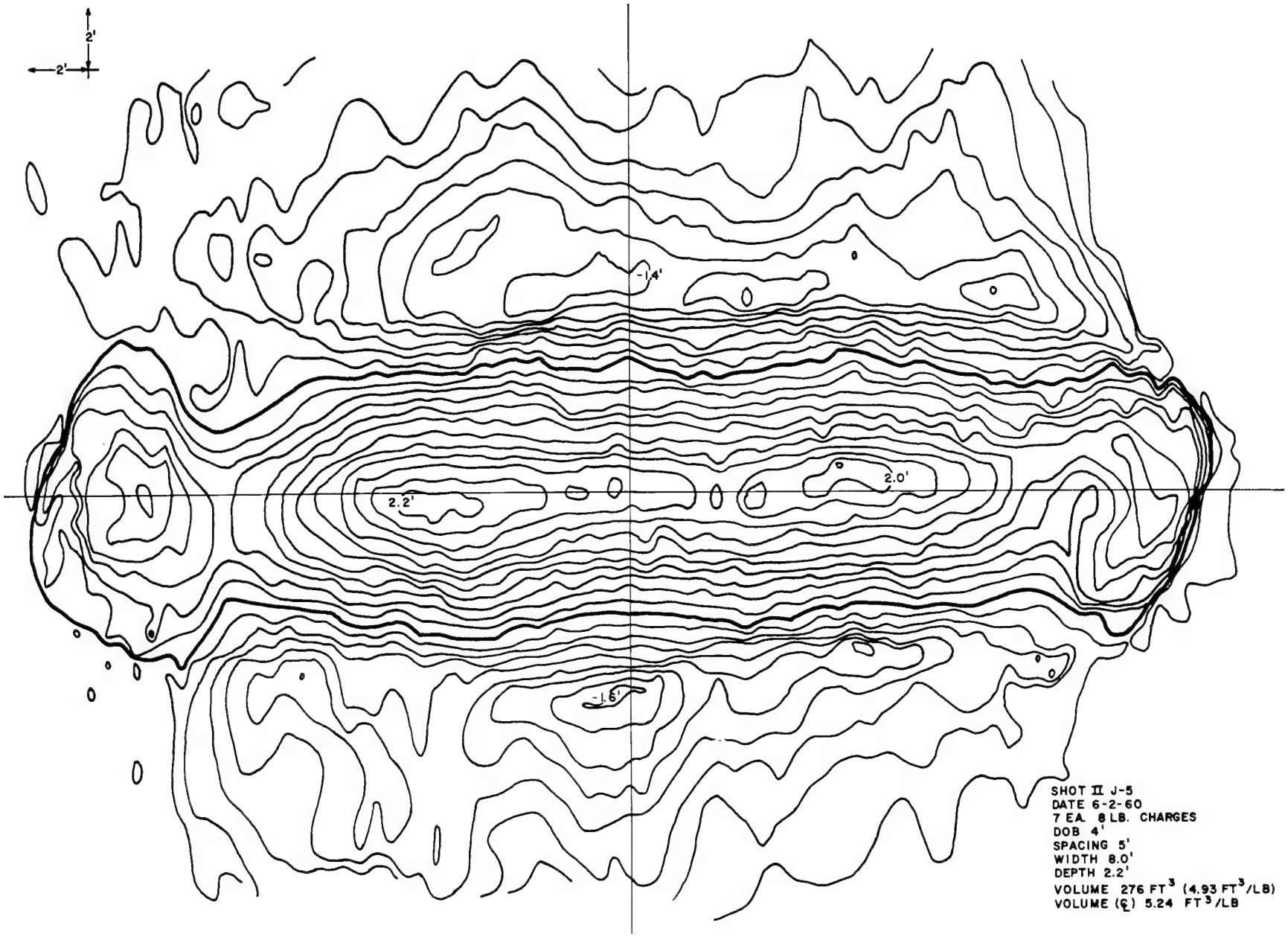

Figure B.30 Crater topography 8-pound row charge buried 4 feet, spaced 5 feet

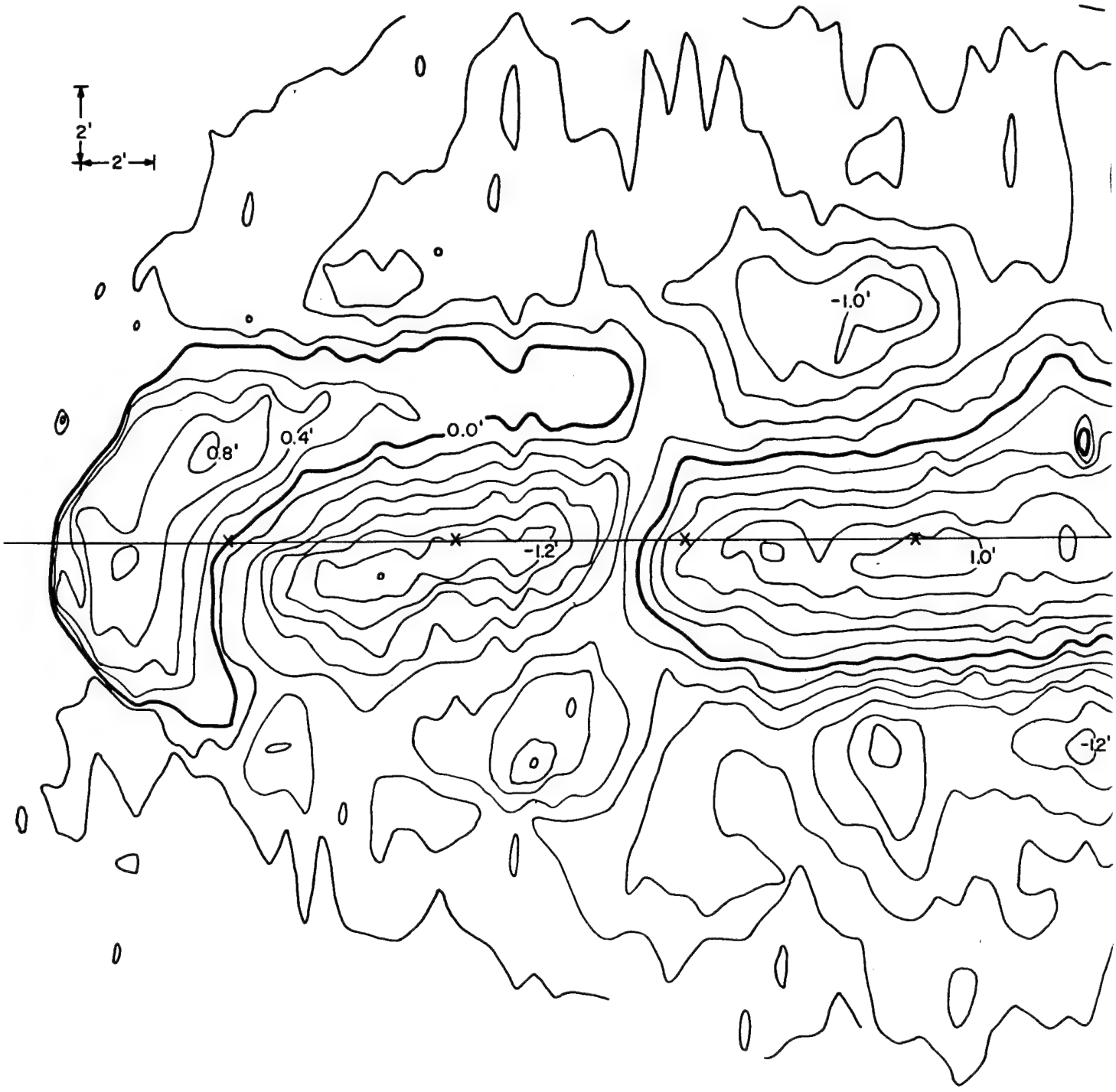

Figure B.31 Crater topography 8-

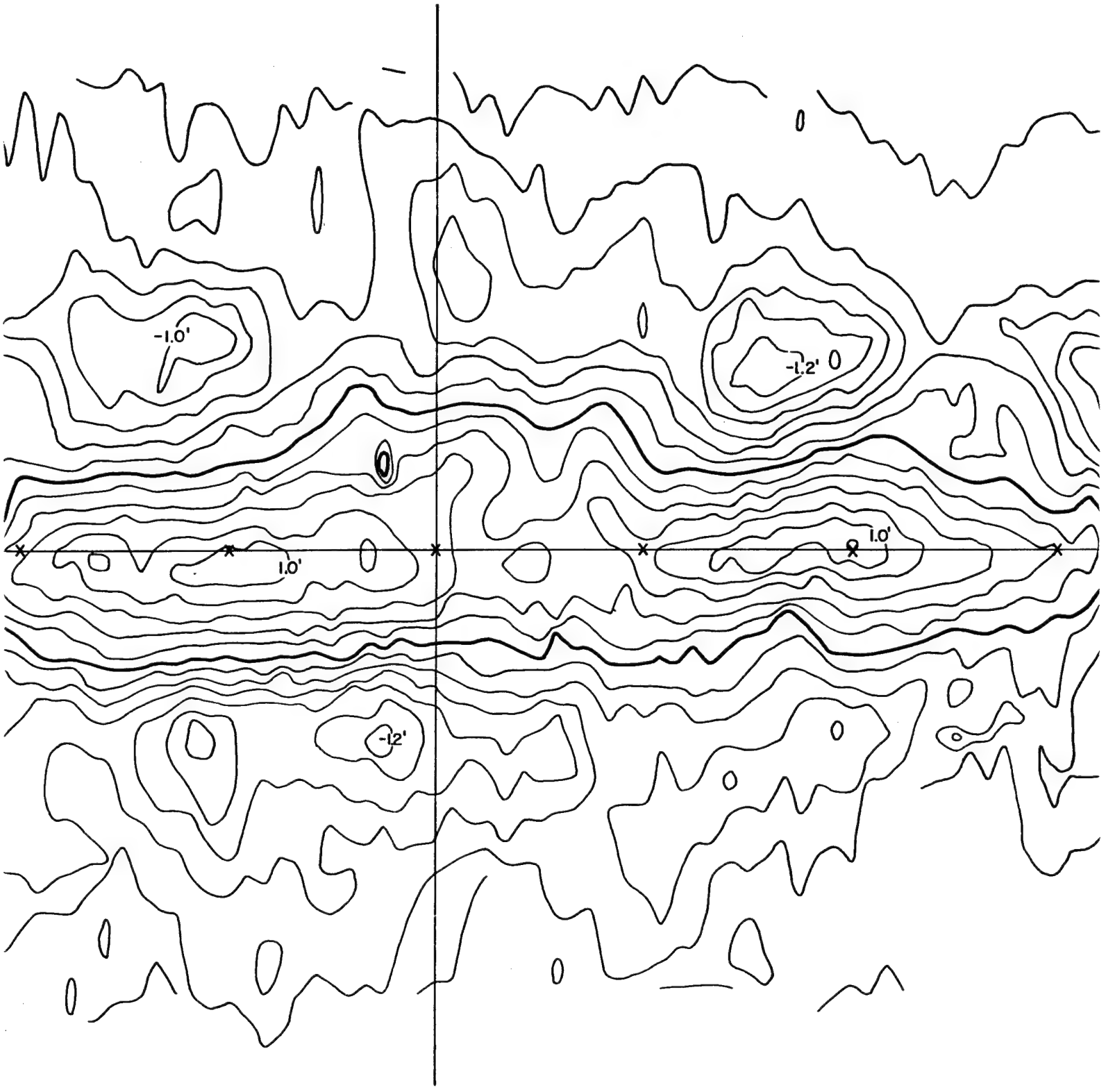

Figure B.31 Crater topography 8-pound row charge buried 4 feet, spaced 6 feet

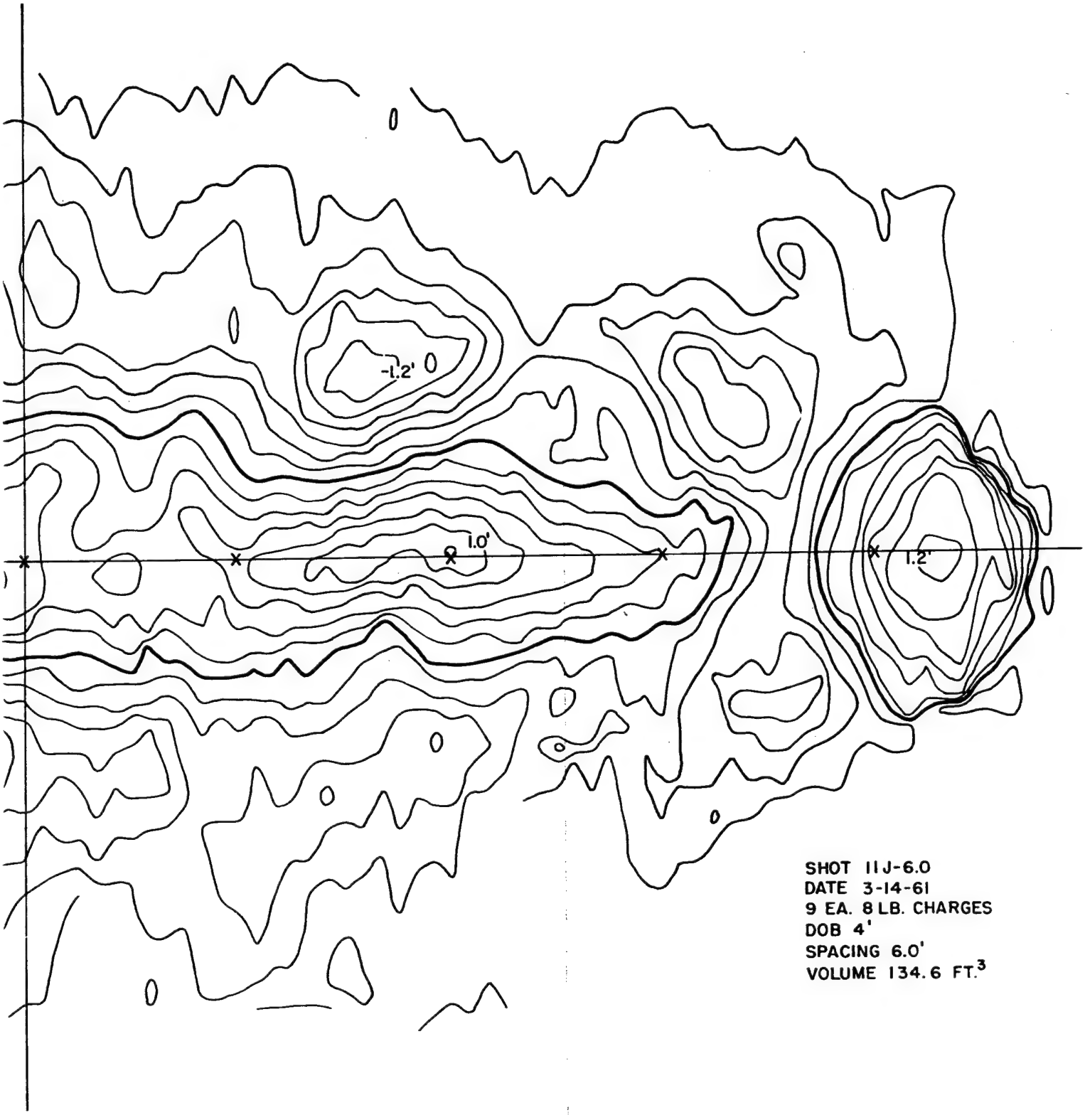

ɔound row charge buried 4 feet, spaced 6 feet

3

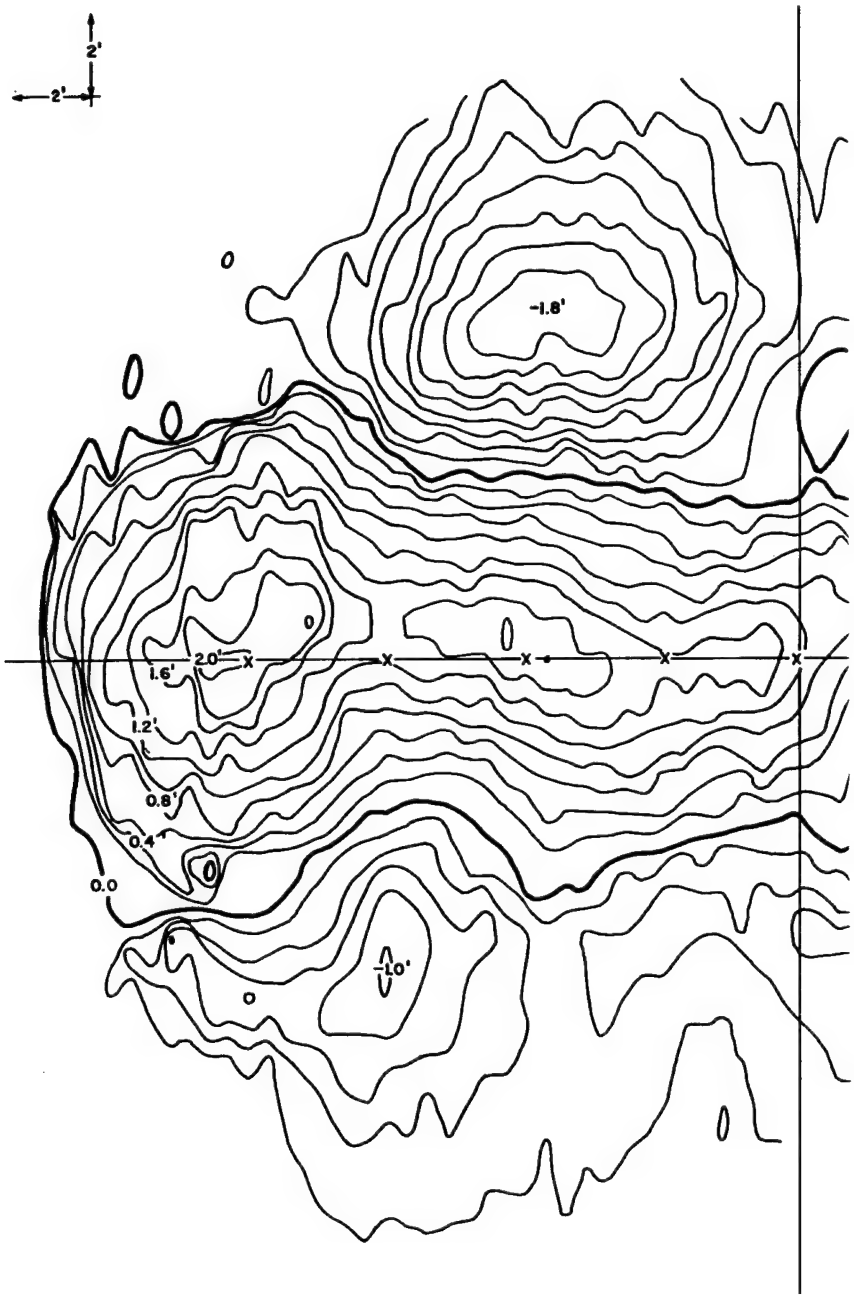

Figure B.32 Crater topography 8-pound

B.32 Crater topography 8-pound row charge buried 4.5 feet, spaced 3.5 feet

Figure B.33 Crater topography 8-pound row charge buried 4.5 feet, spaced 3.5 feet

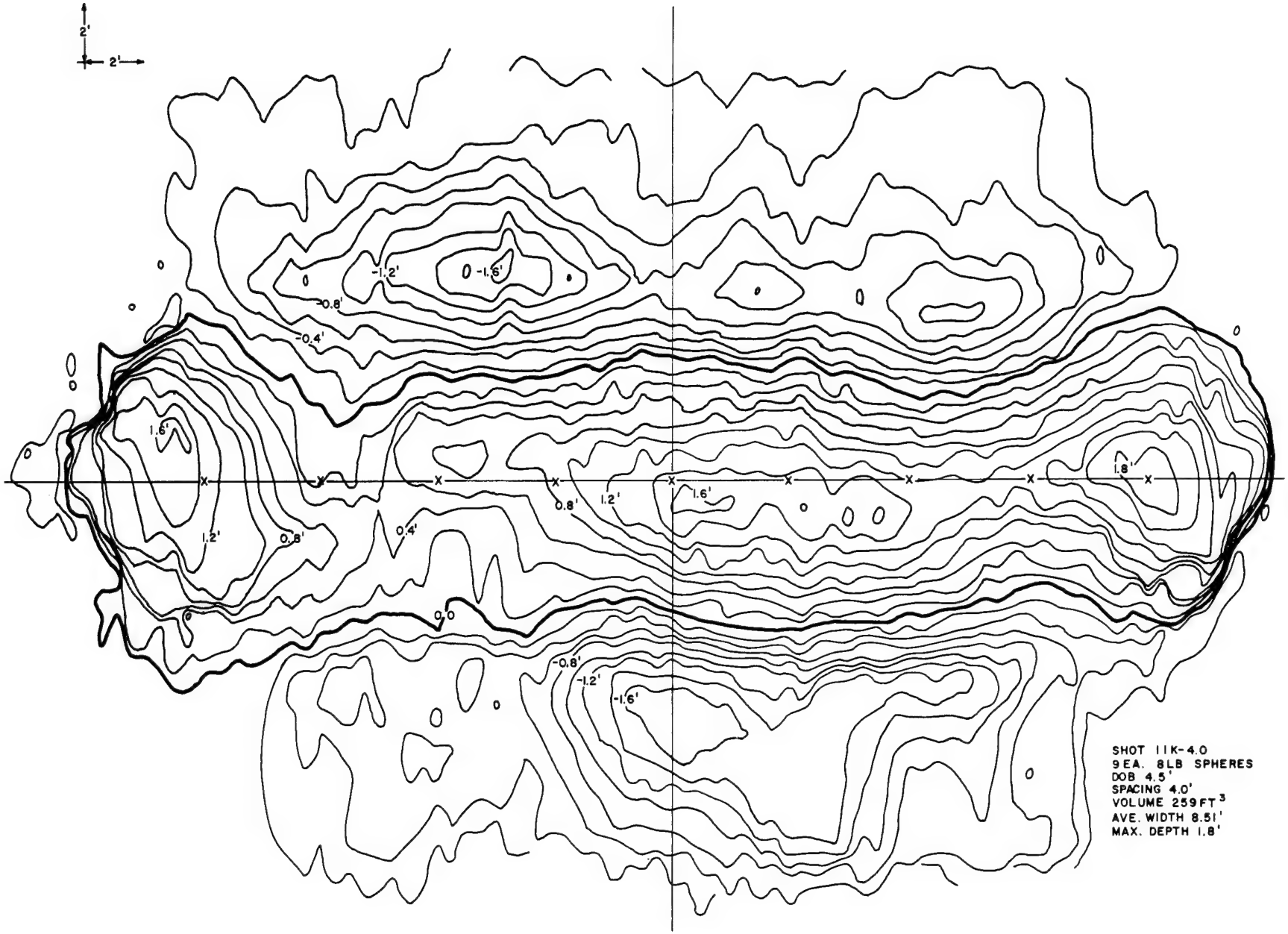

Figure B.34 Crater topography 8-pound row charge buried 4.5 feet, spaced 4.0 feet

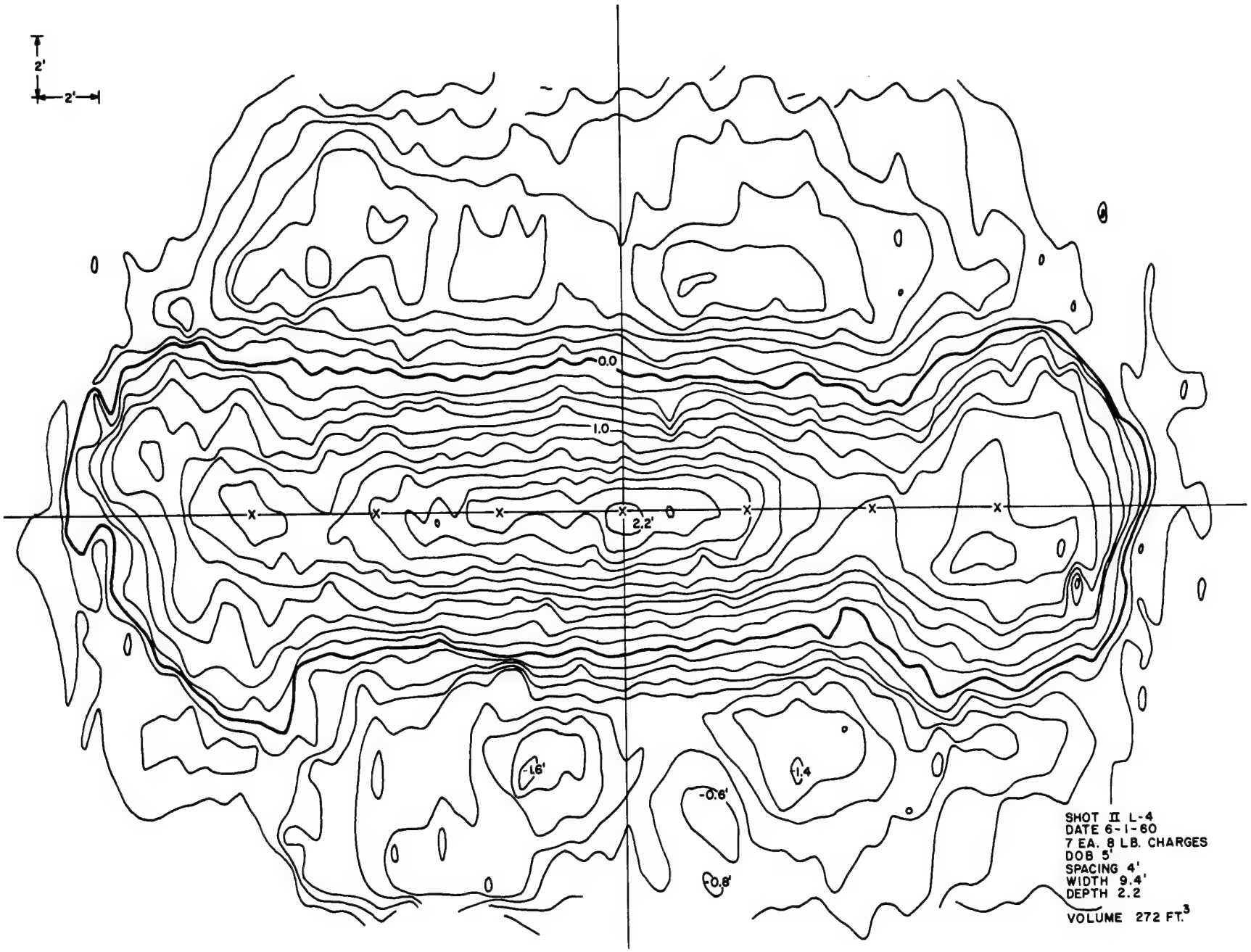

Figure B.35 Crater topography 8-pound row charge buried 5 feet, spaced 4 feet

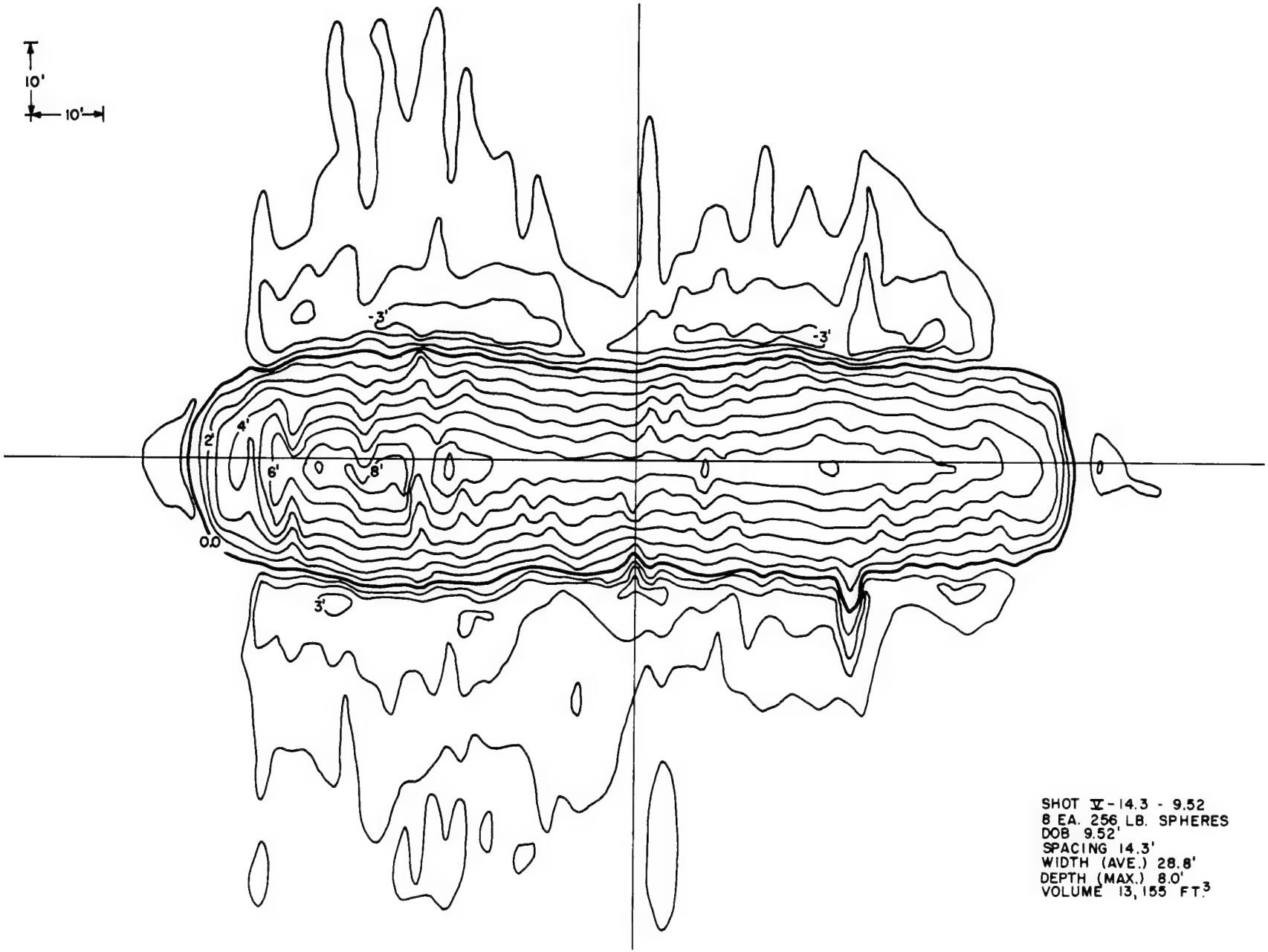

Figure B.36 Crater topography 256-pound row charge buried 9.52 feet, spaced 14.3 feet

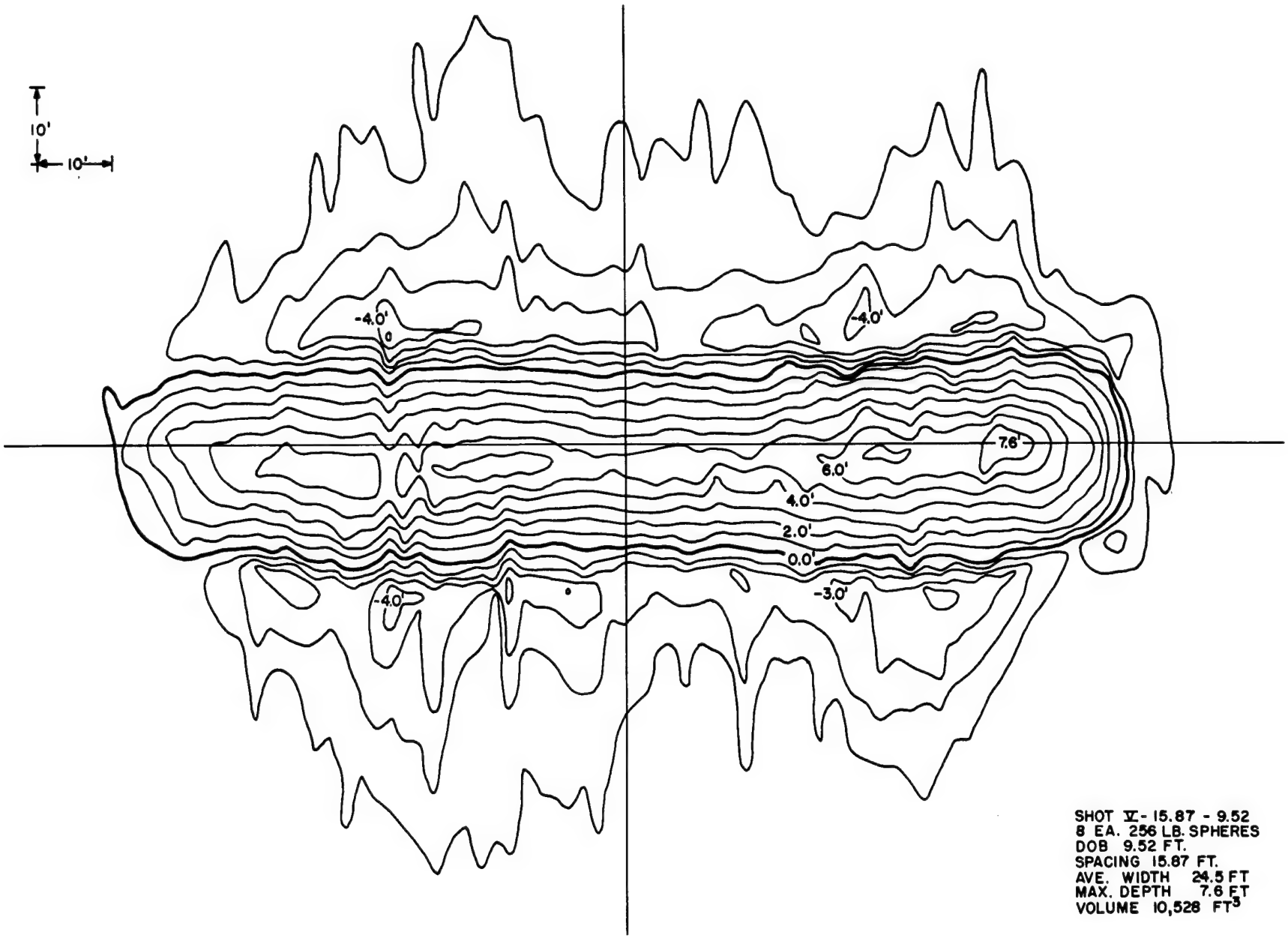

Figure B.37 Crater topography 256-pound row charge buried 9.52 feet, spaced 15.87 feet

APPENDIX C

CRATER PROFILES

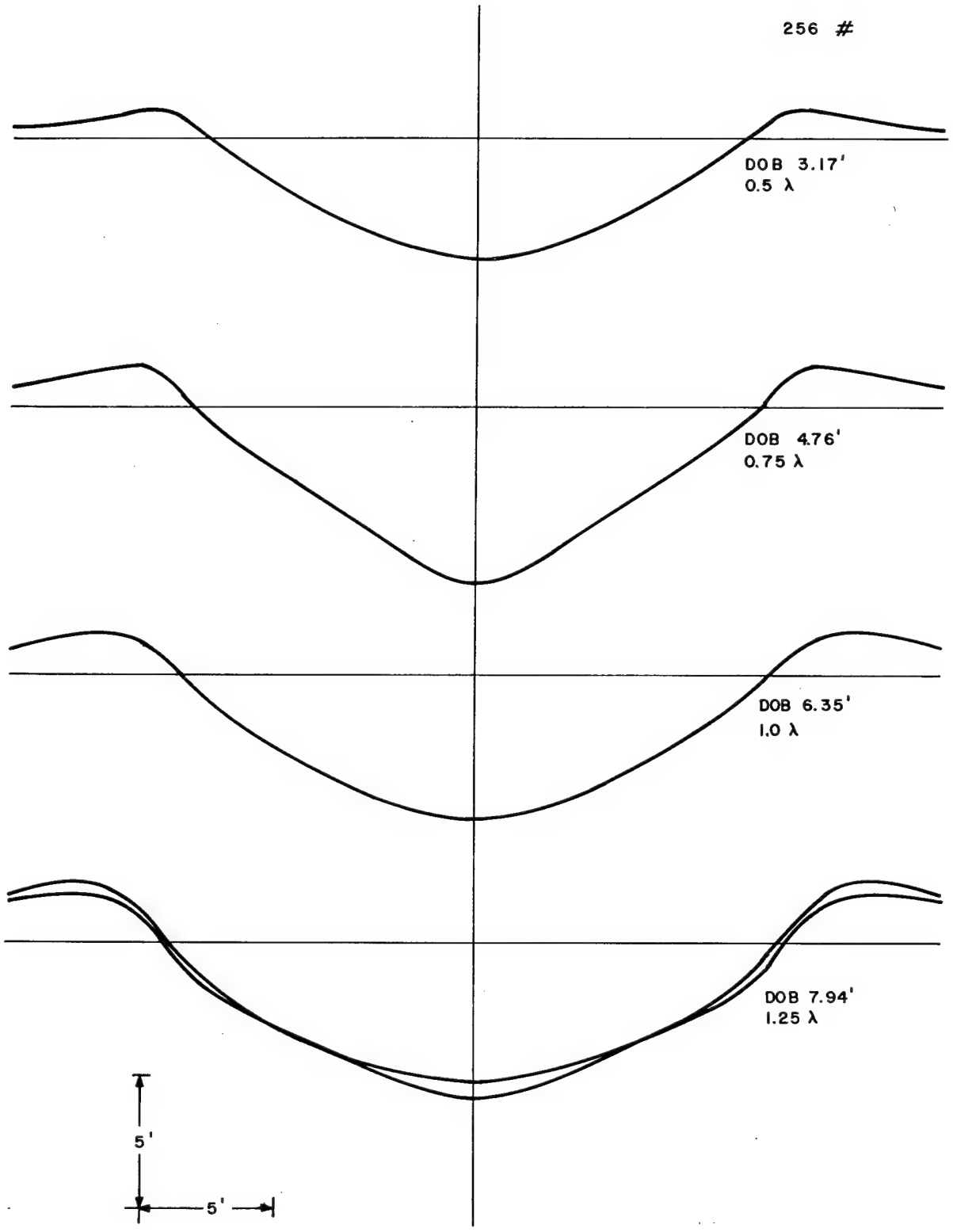

Figure C.1 Profiles of 256-pound single-charge craters

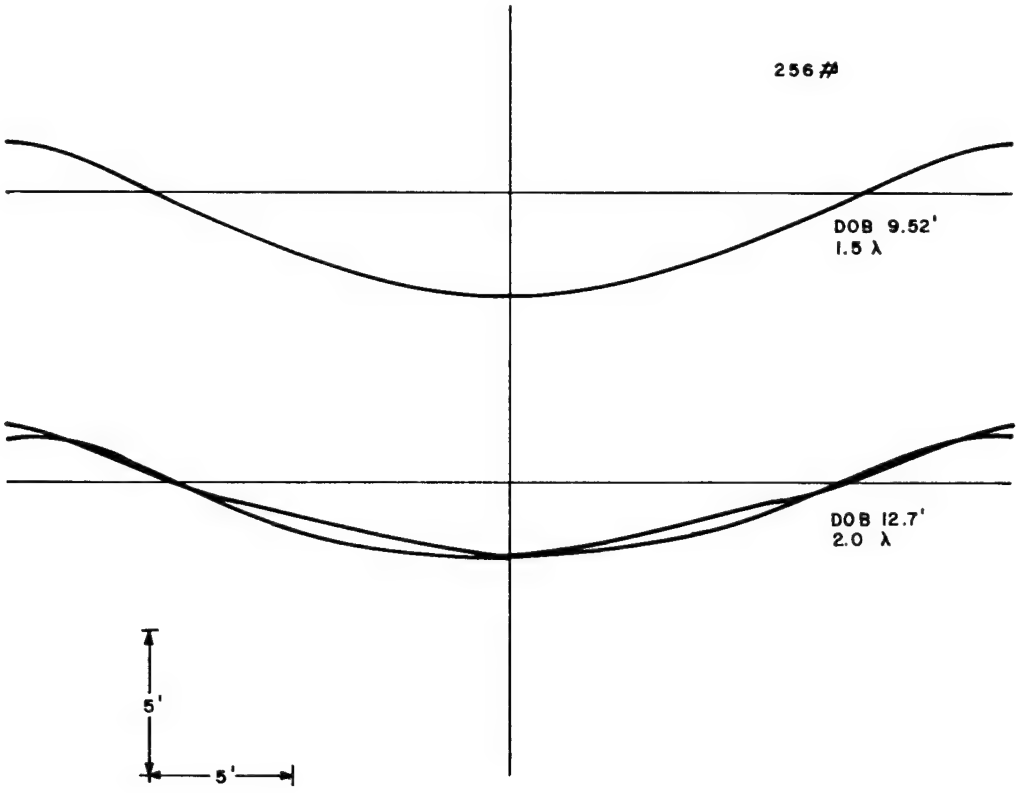

Figure C.2 Profiles of 256-pound single-charge craters

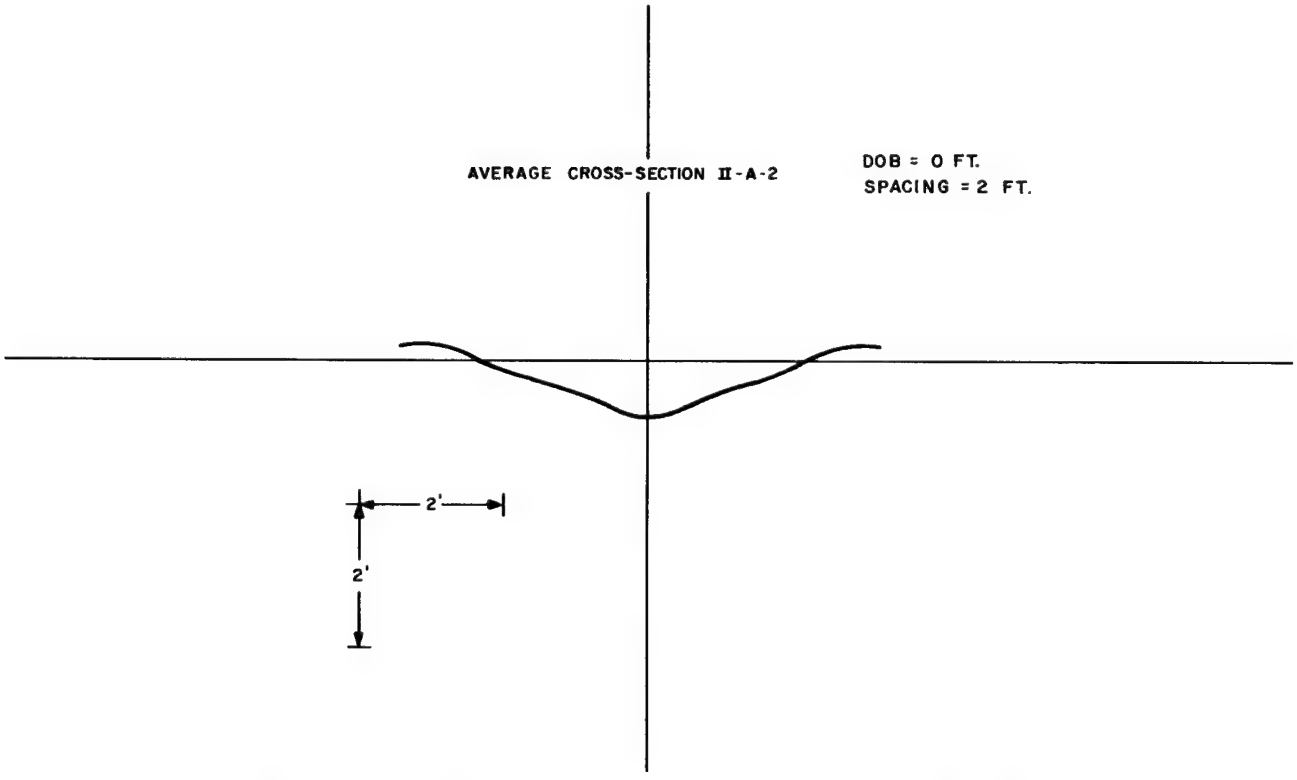

Figure C.3 Average lateral cross-section profile of 8-pound row-charge craters

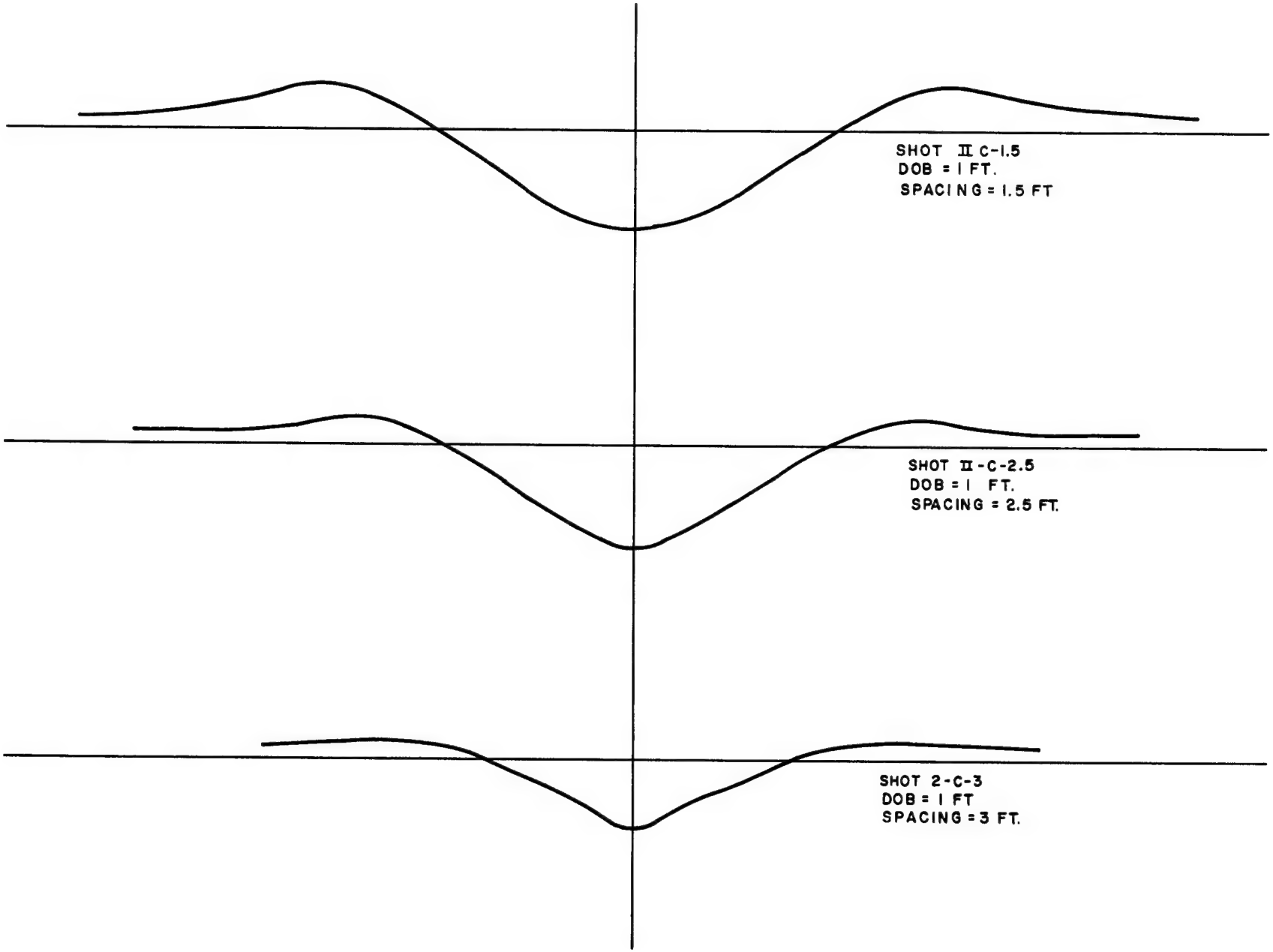

Figure C.4 Average lateral cross-section profiles of 8-pound row-charge craters

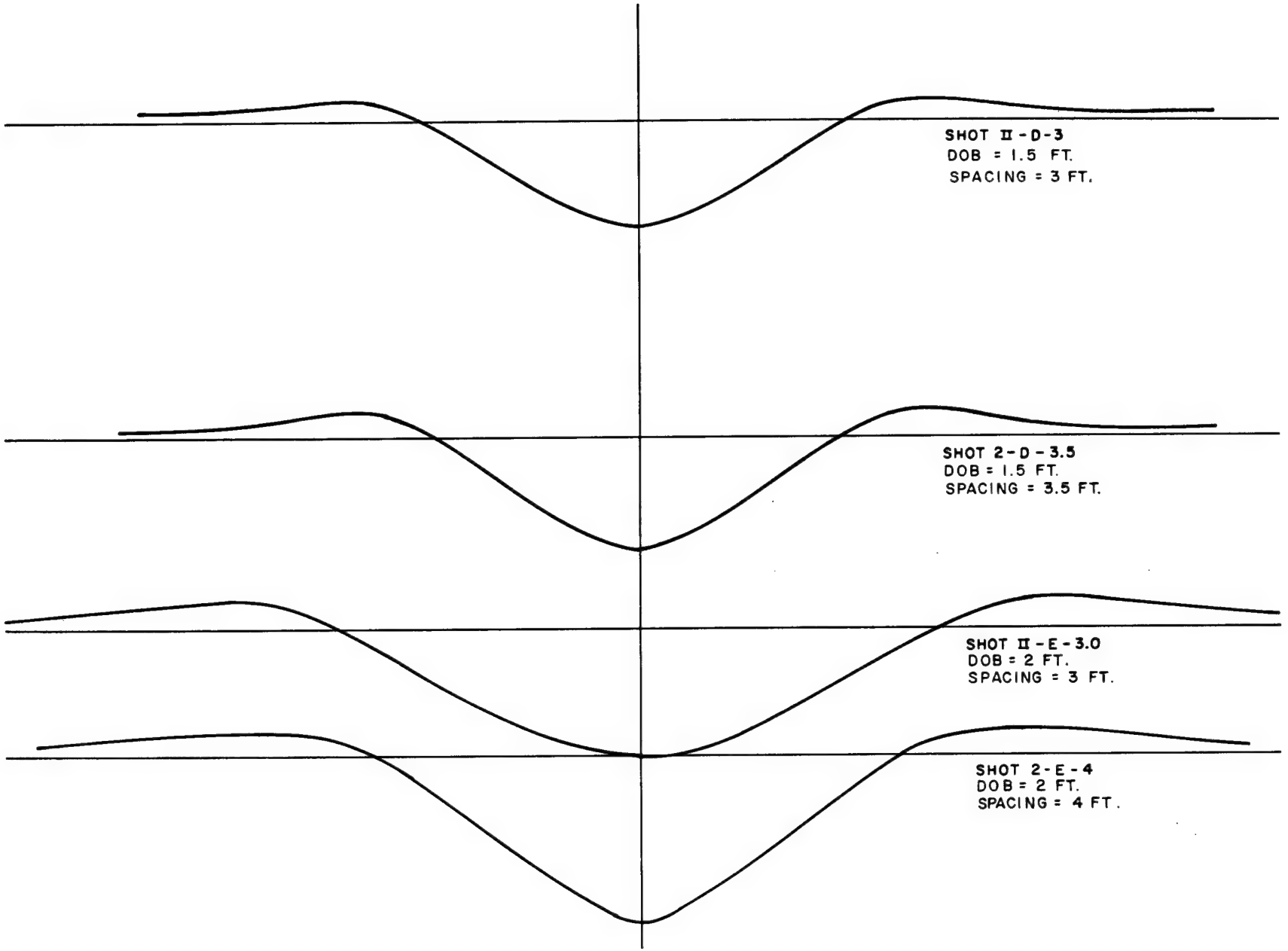

Figure C.5 Average lateral cross-section profiles of 8-pound row-charge craters

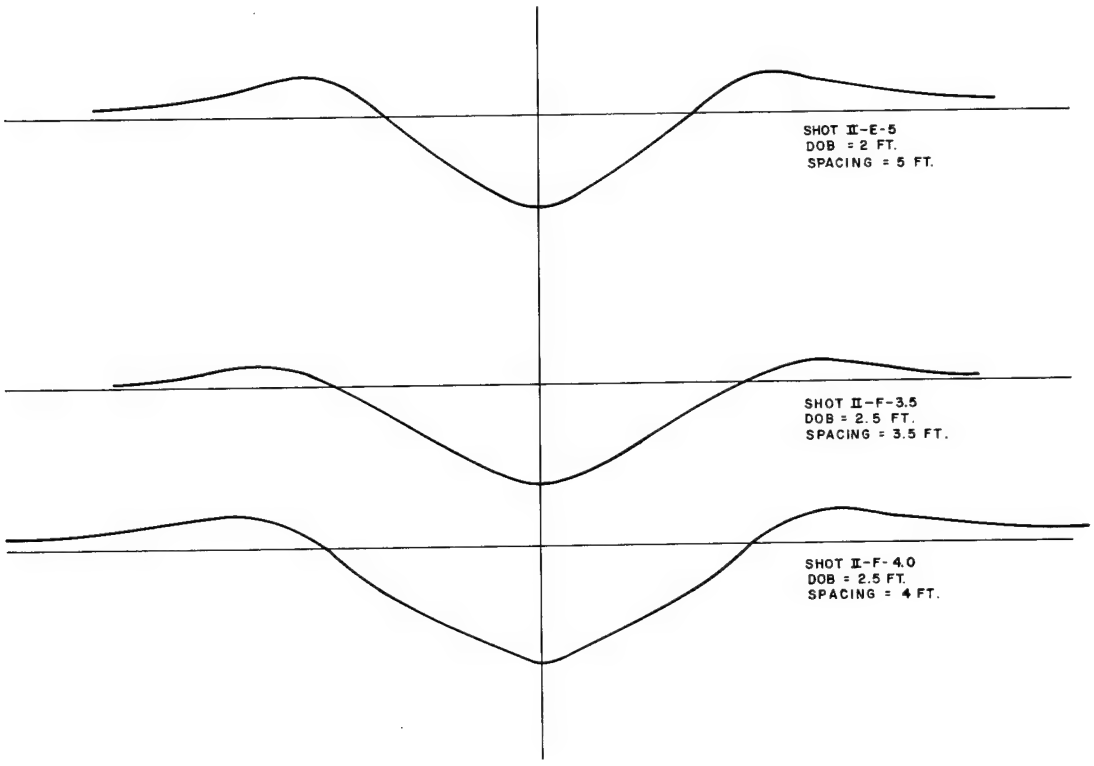

Figure C.6 Average lateral cross-section profiles of 8-pound row-charge craters

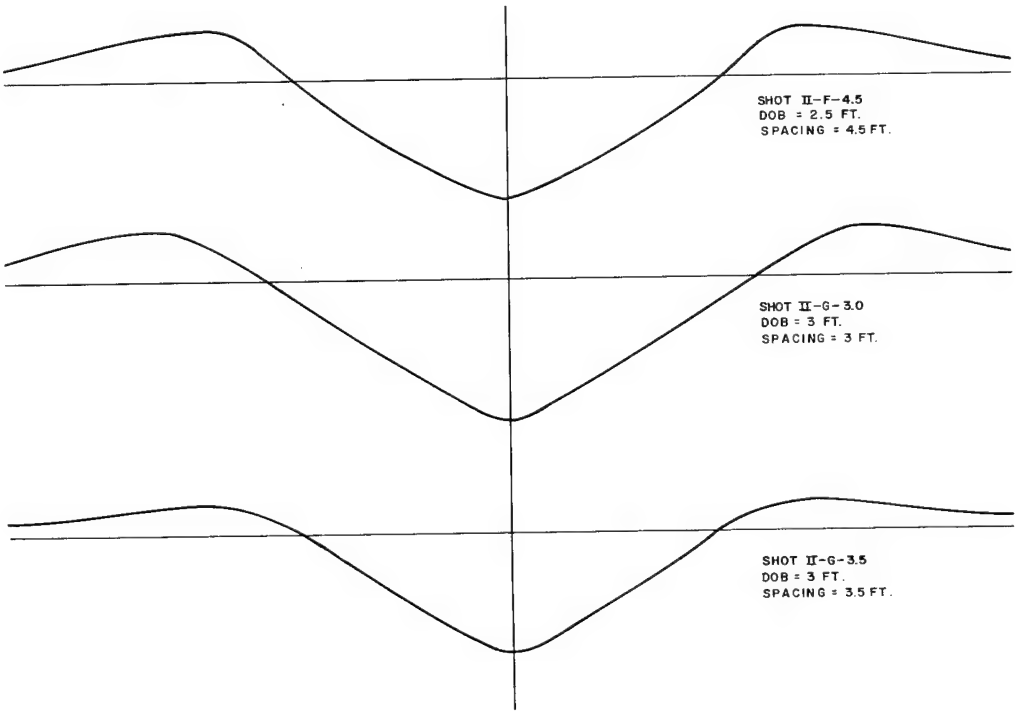

Figure C.7 Average lateral cross-section profiles of 8-pound row-charge craters

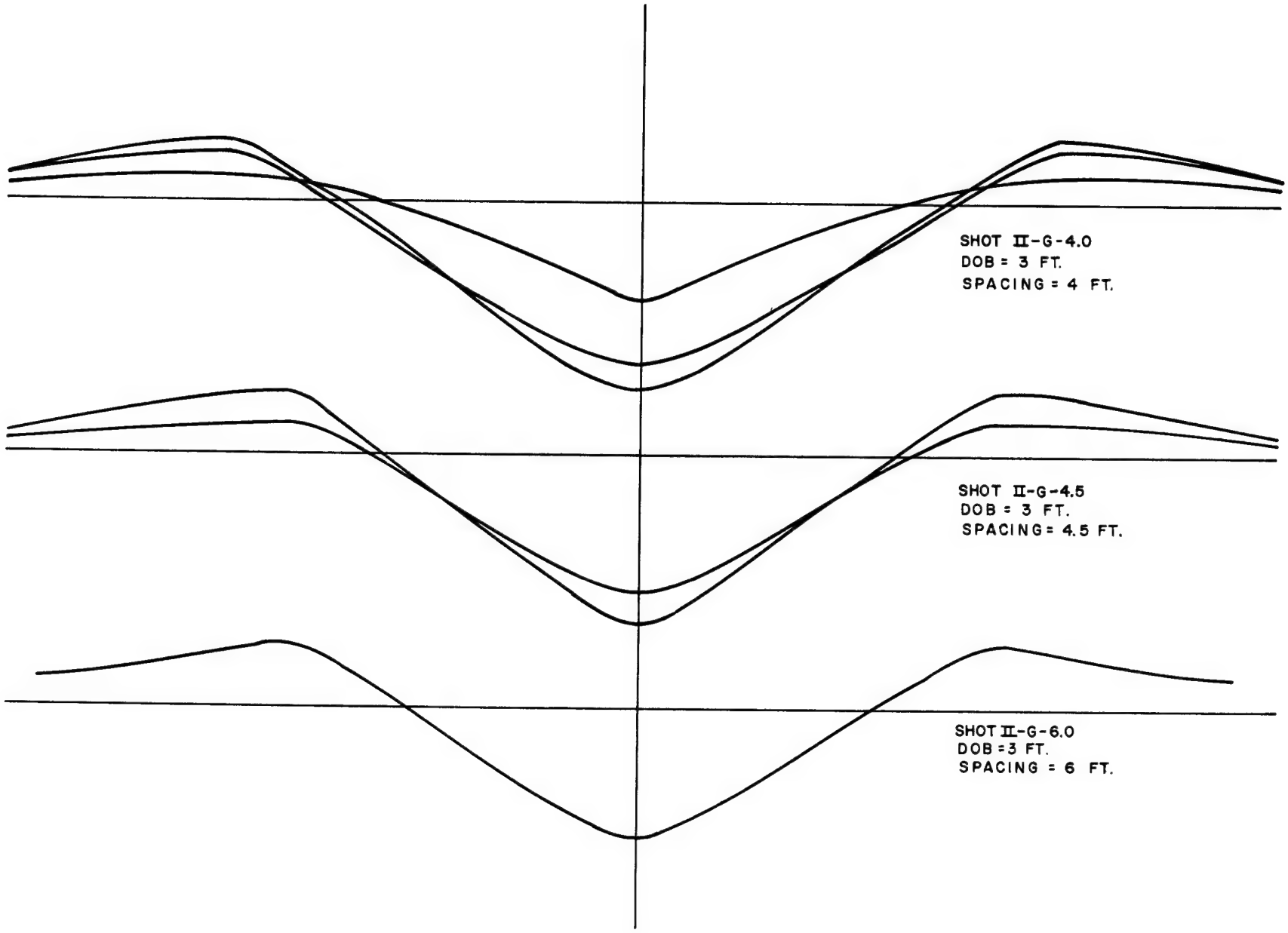

Figure C.8 Average lateral cross-section profiles of 8-pound row-charge craters

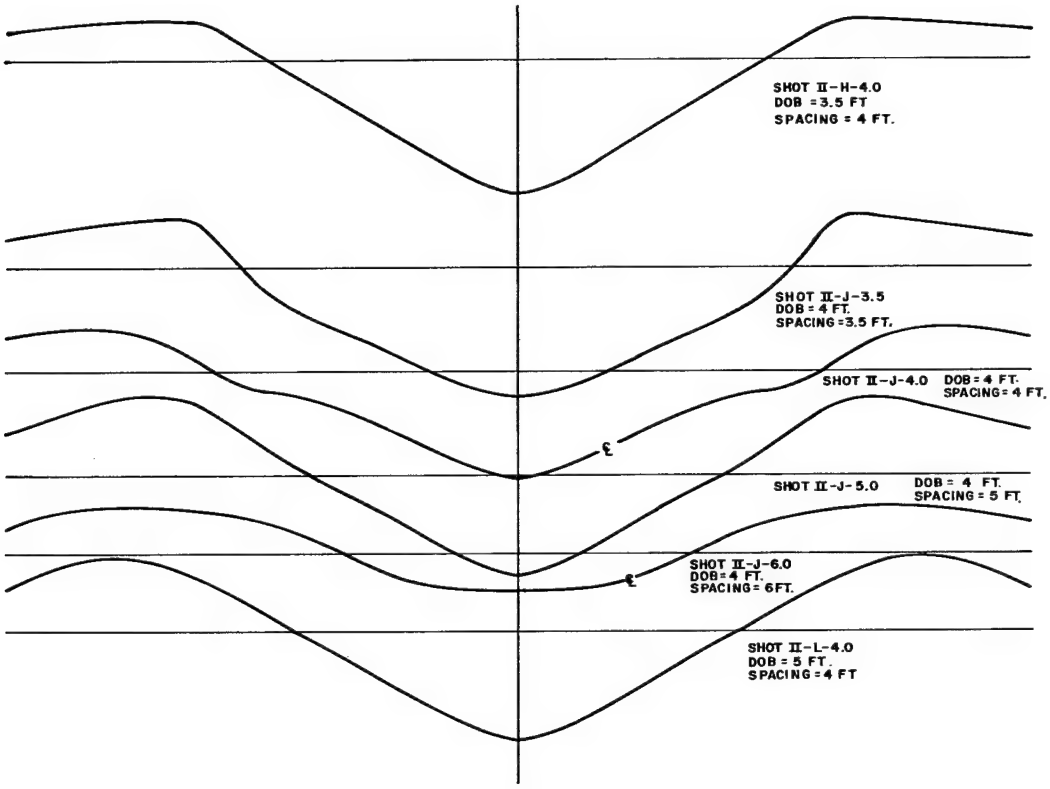

Figure C.9 Average lateral cross-section profiles of 8-pound row-charge craters

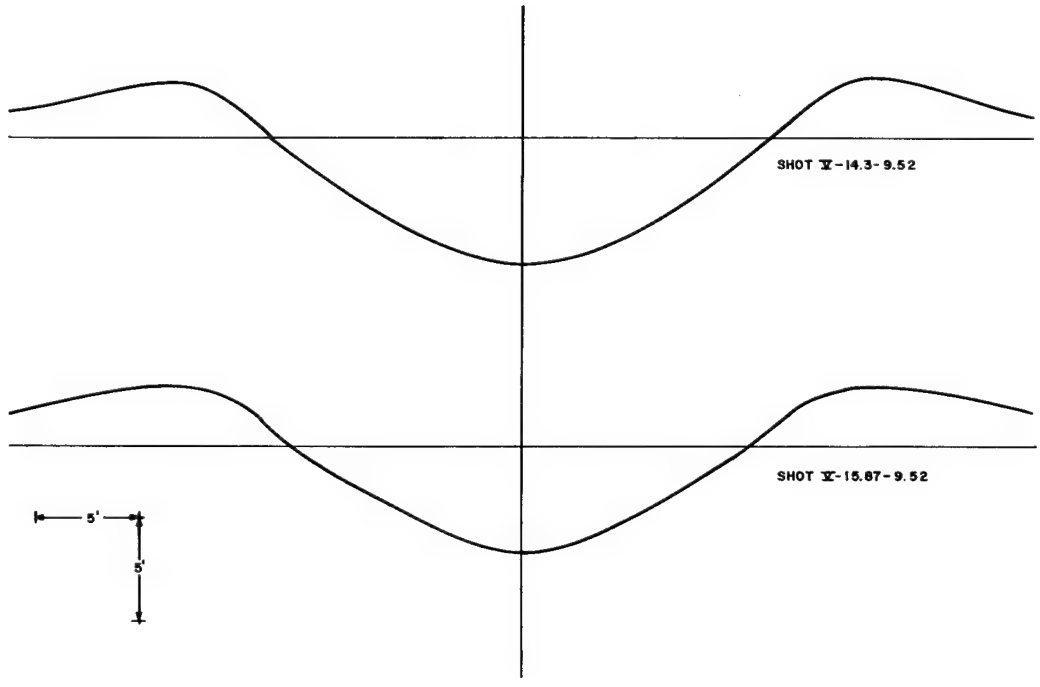

Figure C.10 Average lateral cross-section profiles of 256-pound row-charge craters

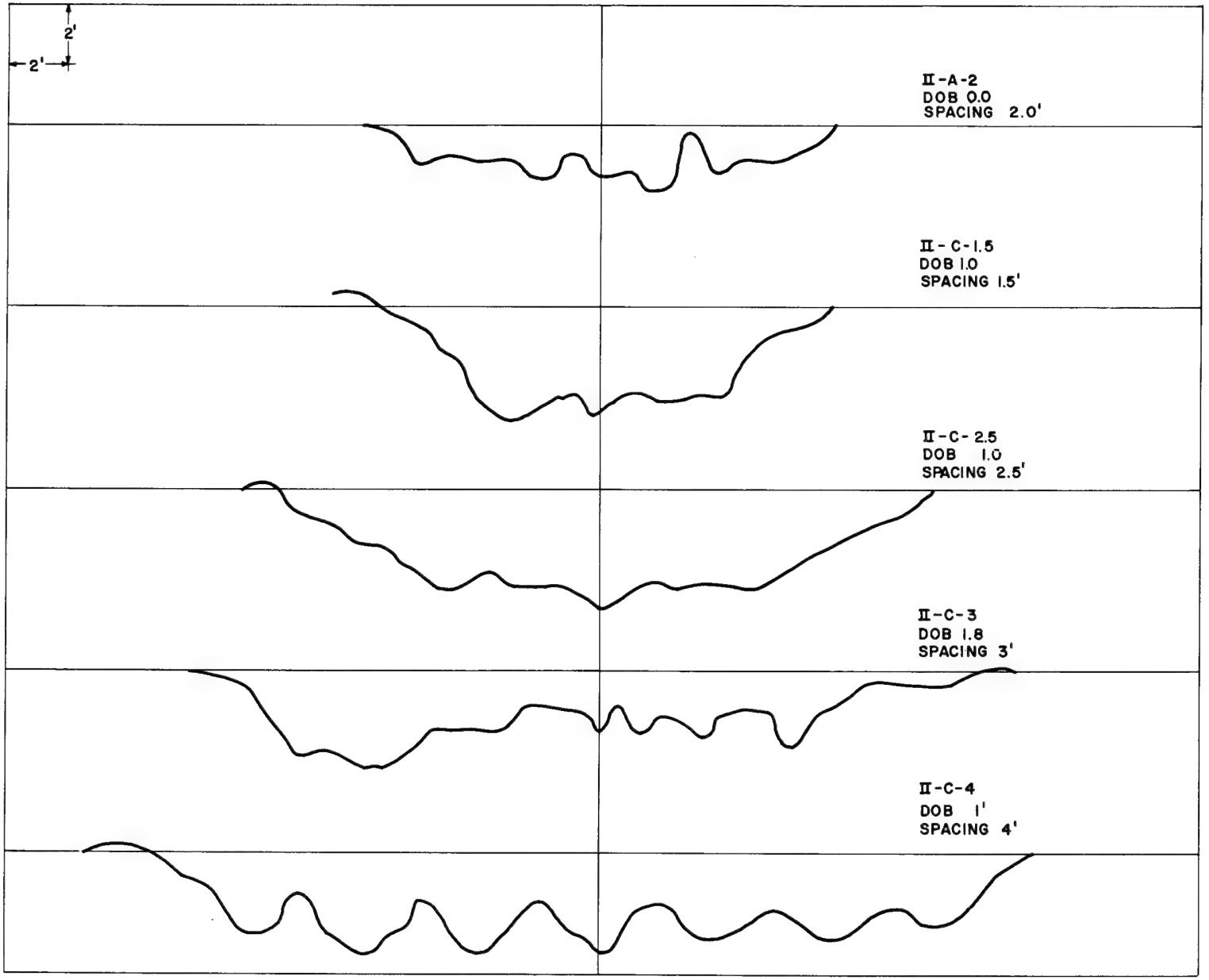

Figure C.11 Longitudinal cross-section profiles of row-charge craters

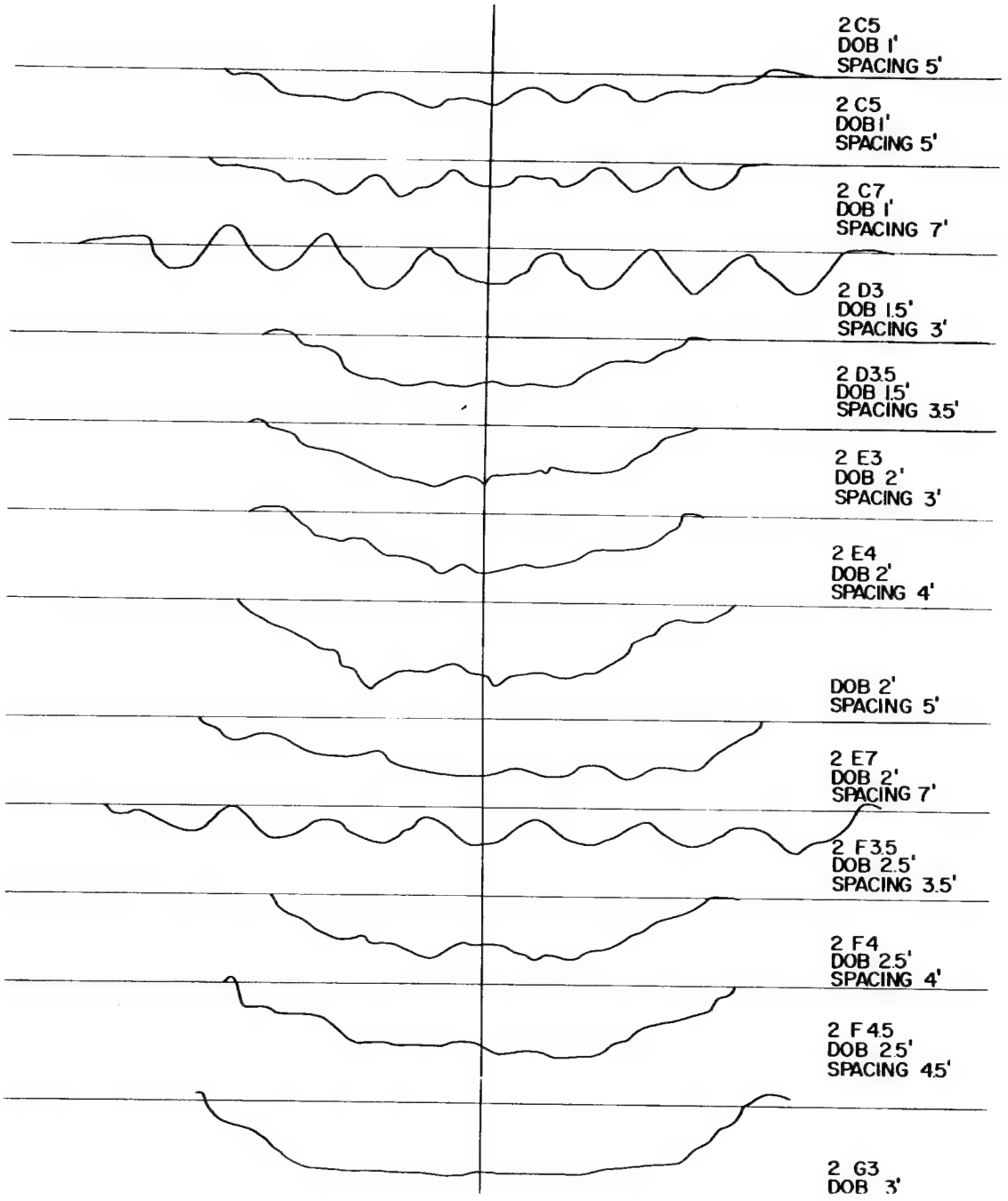
2 C5
DOB 1'
SPACING 5'
2 C5
DOB 1'
SPACING 5'
2 C7
DOB 1'
SPACING 7'
2 D3
DOB 1.5'
SPACING 3'
2 D3.5
DOB 1.5'
SPACING 3.5'
2 E3
DOB 2'
SPACING 3'
2 E4
DOB 2'
SPACING 4'
DOB 2'
SPACING 5'
2 E7
DOB 2'
SPACING 7'
2 F3.5
DOB 2.5'
SPACING 3.5'
2 F4
DOB 2.5'
SPACING 4'
2 F4.5
DOB 2.5'
SPACING 4.5'
2 G3
DOB 3'

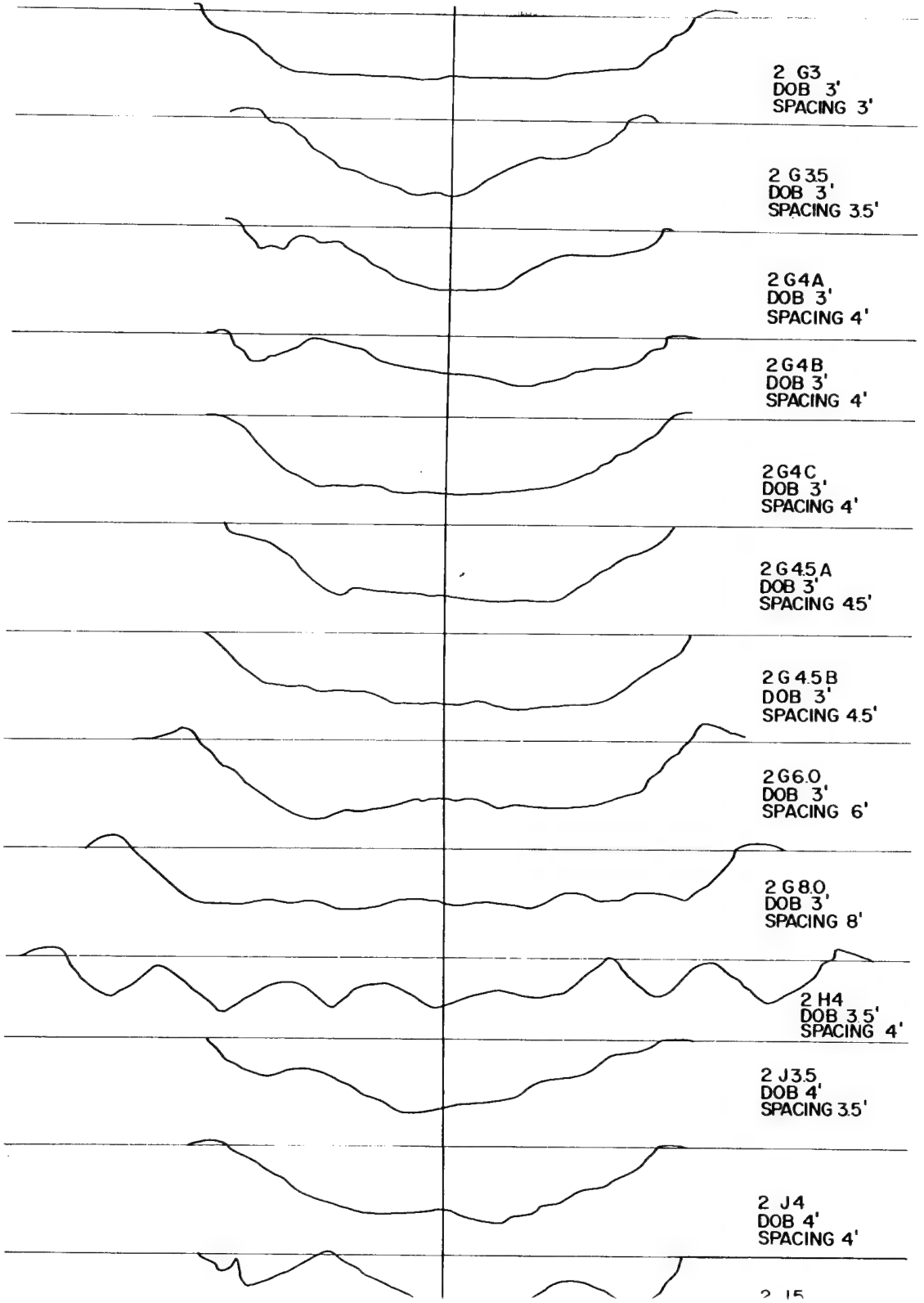
2 G3
DOB 3'
SPACING 3'
2 G3.5
DOB 3'
SPACING 3.5'
2 G4A
DOB 3'
SPACING 4'
2 G4B
DOB 3'
SPACING 4'
2 G4C
DOB 3'
SPACING 4'
2 G4.5A
DOB 3'
SPACING 4.5'
2 G4.5B
DOB 3'
SPACING 4.5'
2 G6.0
DOB 3'
SPACING 6'
2 G8.0
DOB 3'
SPACING 8'
2 H4
DOB 3.5'
SPACING 4'
2 J3.5
DOB 4'
SPACING 3.5'
2 J4
DOB 4'
SPACING 4'

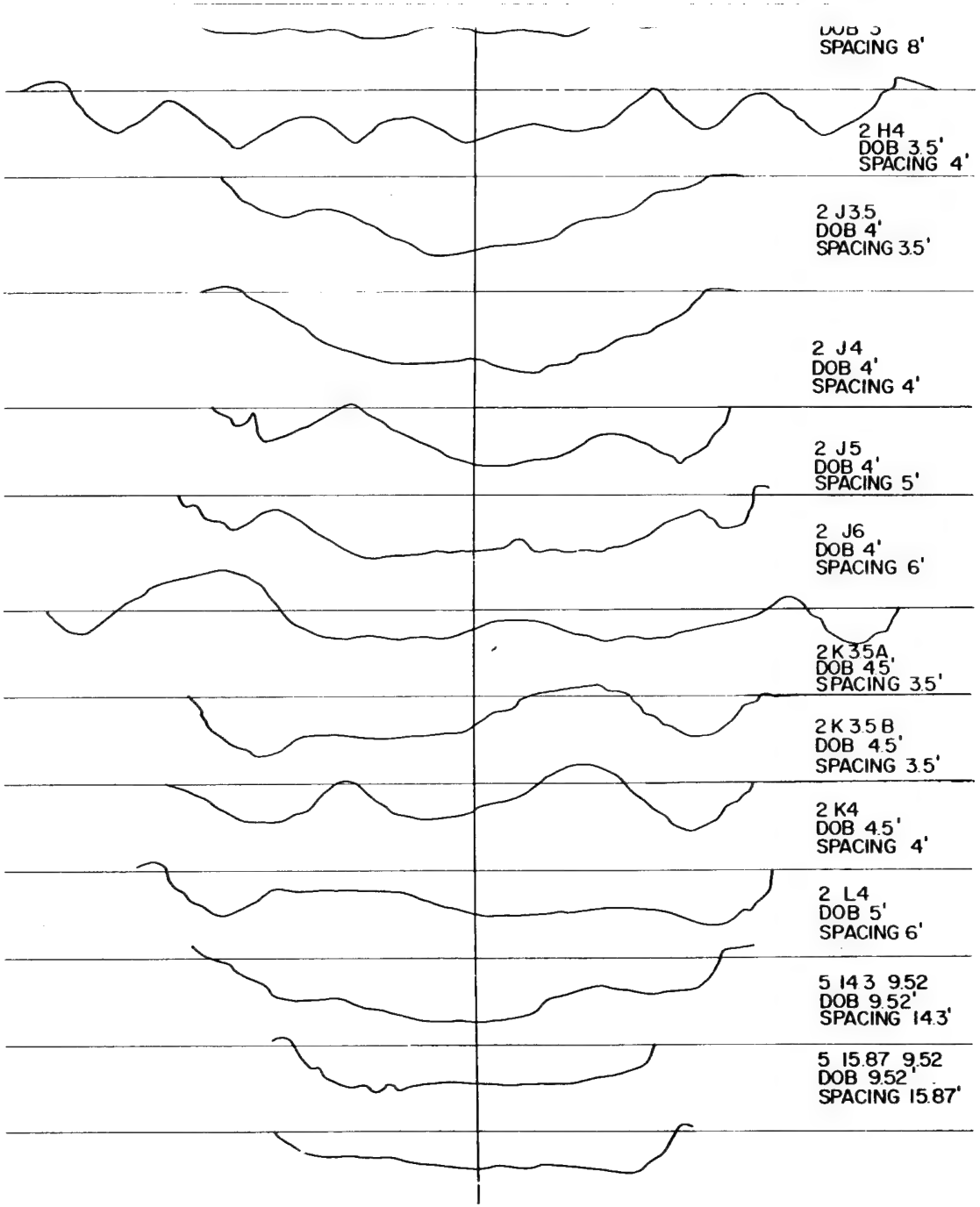

Figure C.12 Longitudinal cross-section profiles of row-charge craters

APPENDIX D

THROWOUT DEPOSITION

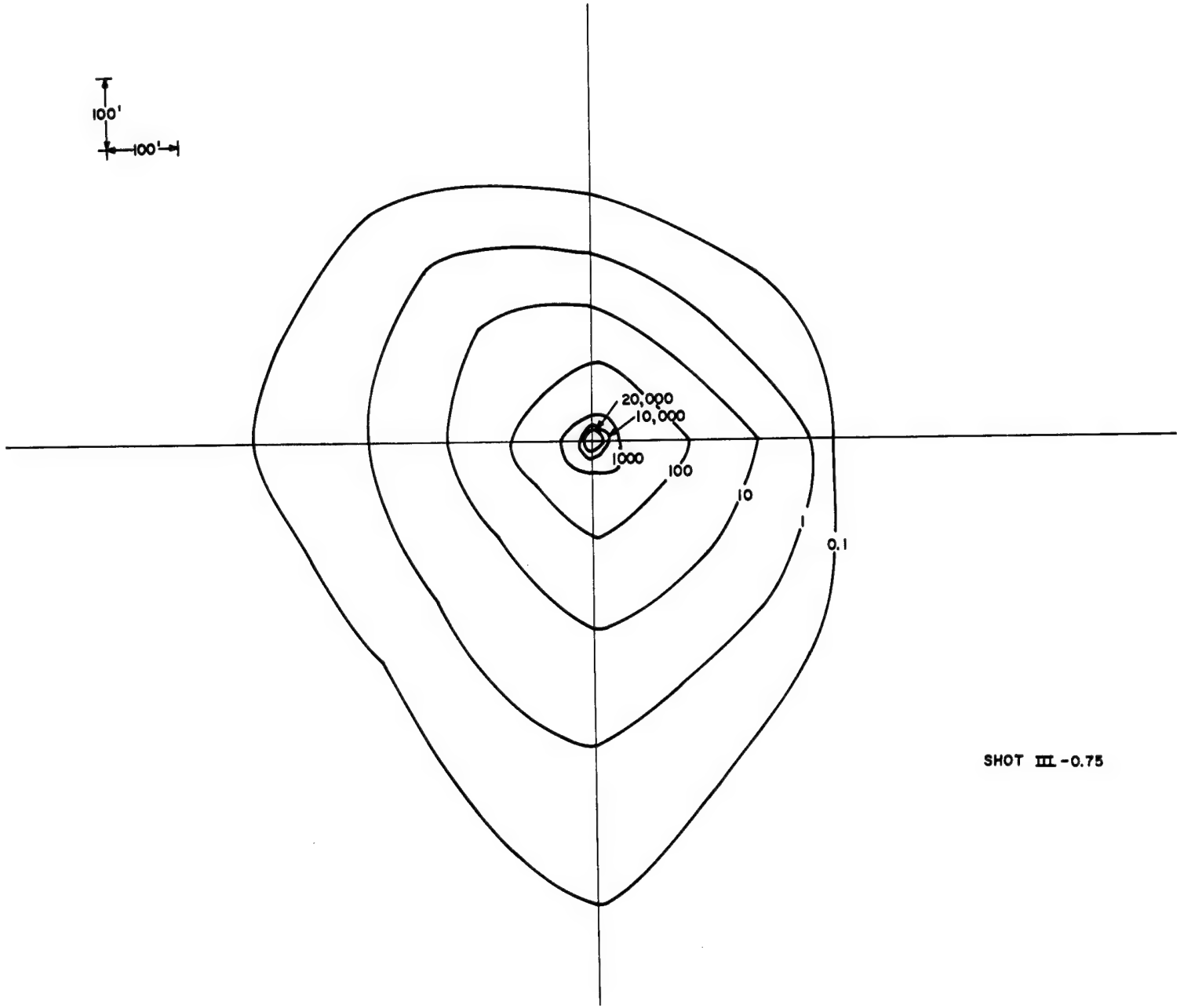

Figure D.1 Throwout deposition, 256-pound single charge, buried at 4.76 feet--contours are in gm/ft^2

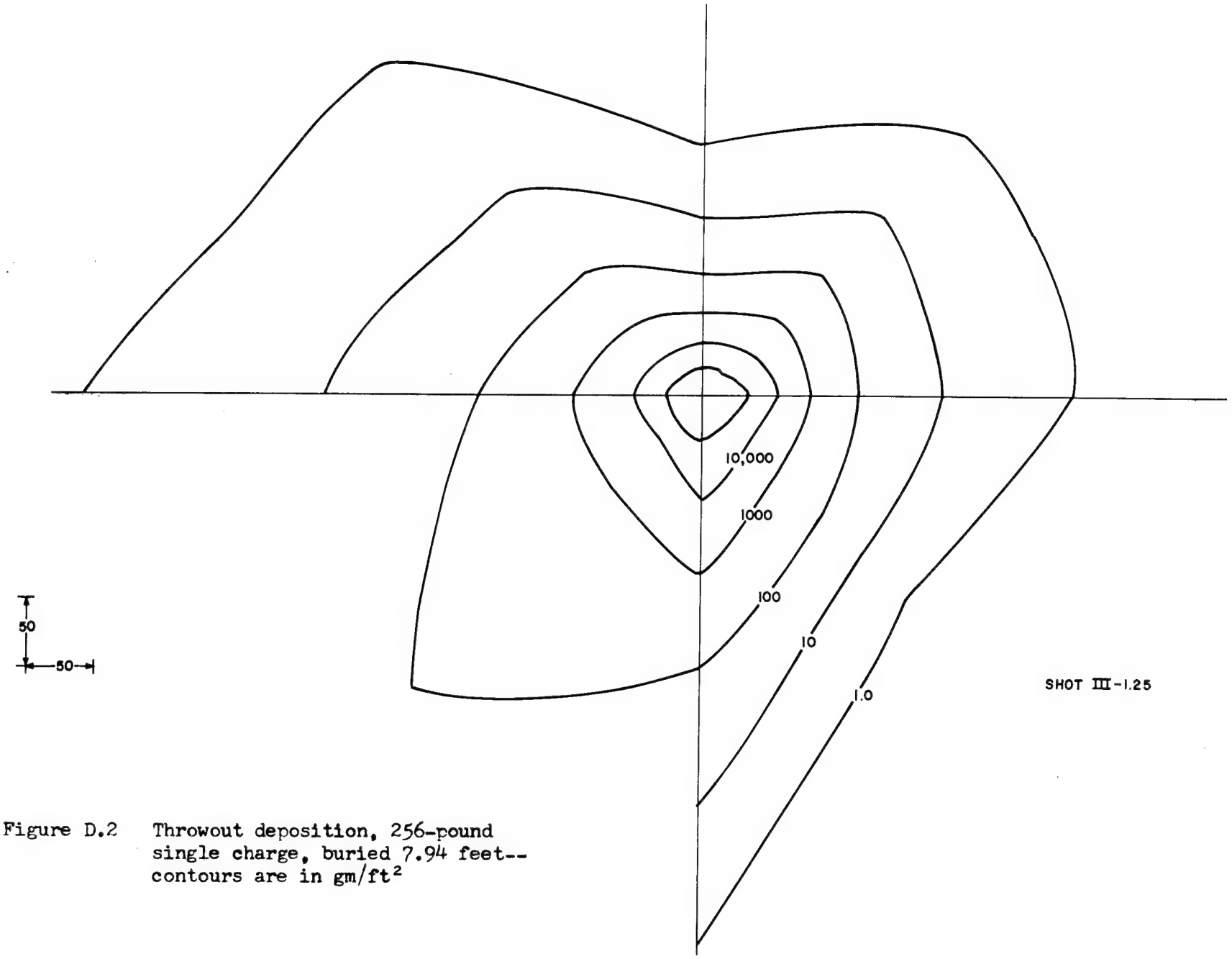

Figure D.2 Throwout deposition, 256-pound single charge, buried 7.94 feet--contours are in gm/ft^2

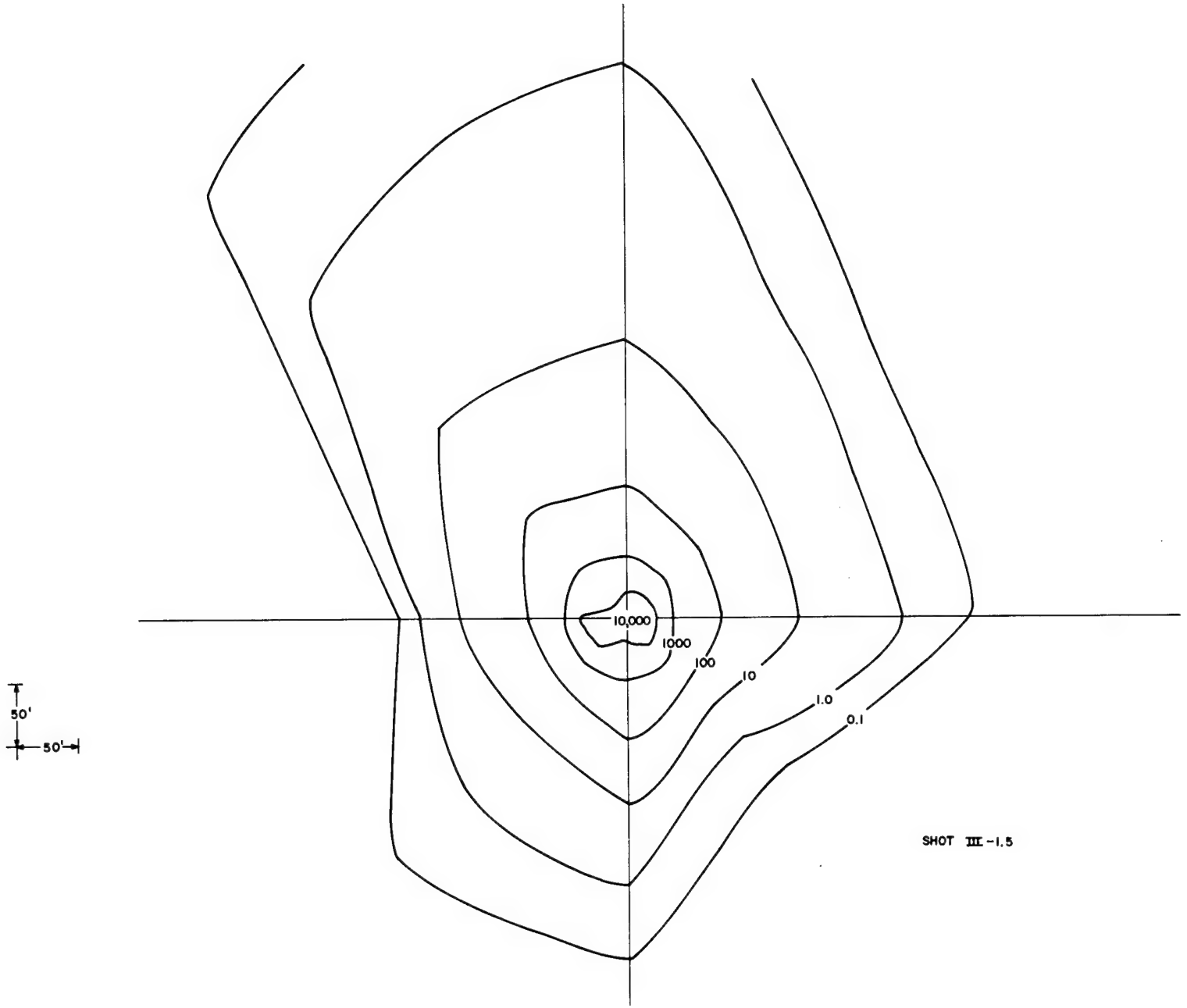

Figure D.3 Throwout deposition, 256-pound single charge, buried at 9.52 feet--contours are in gm/ft^2

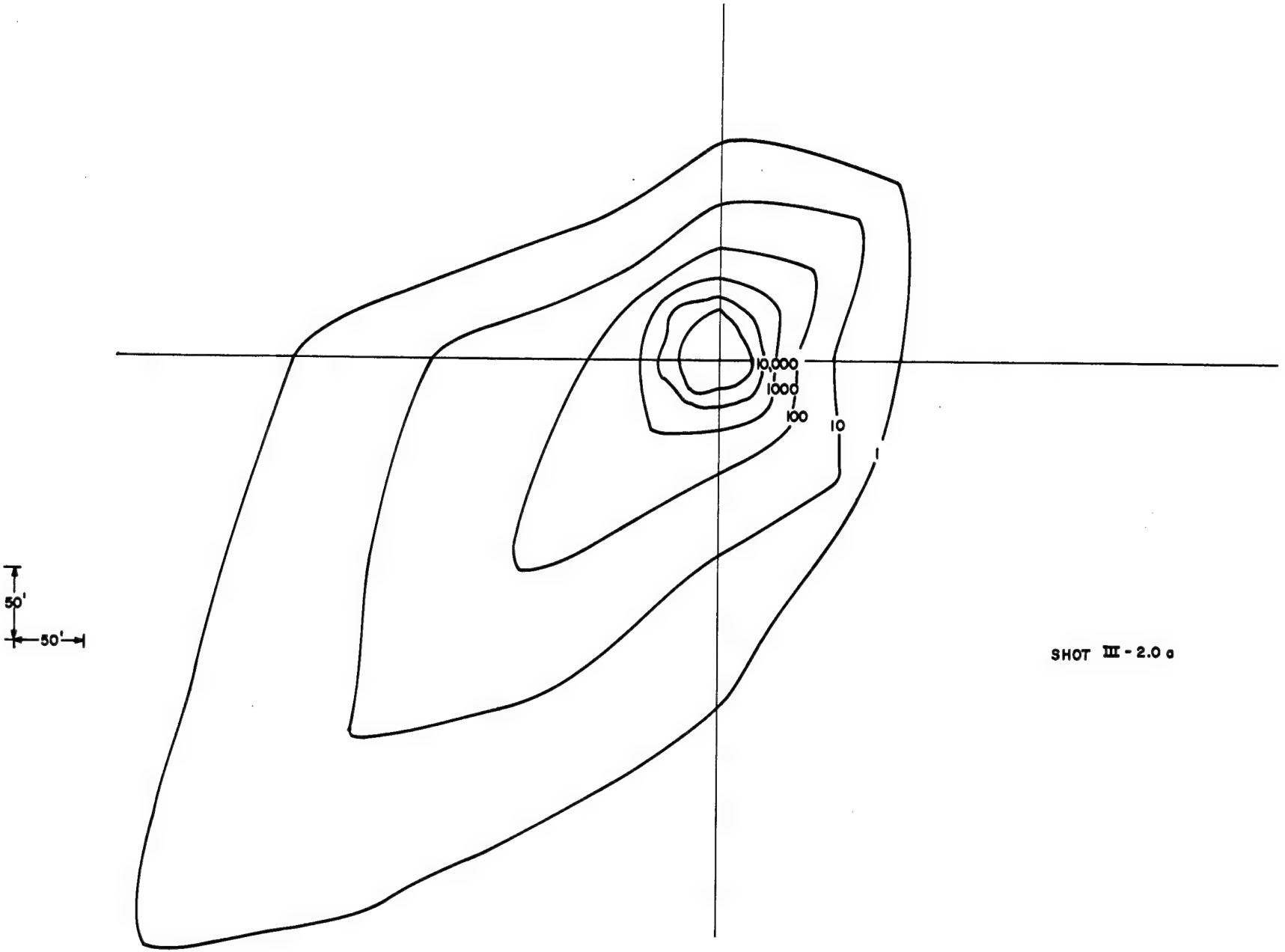

Figure D.4 Throwout deposition, 256-pound single charge, buried at 12.7 feet--contours are in gm/ft^2

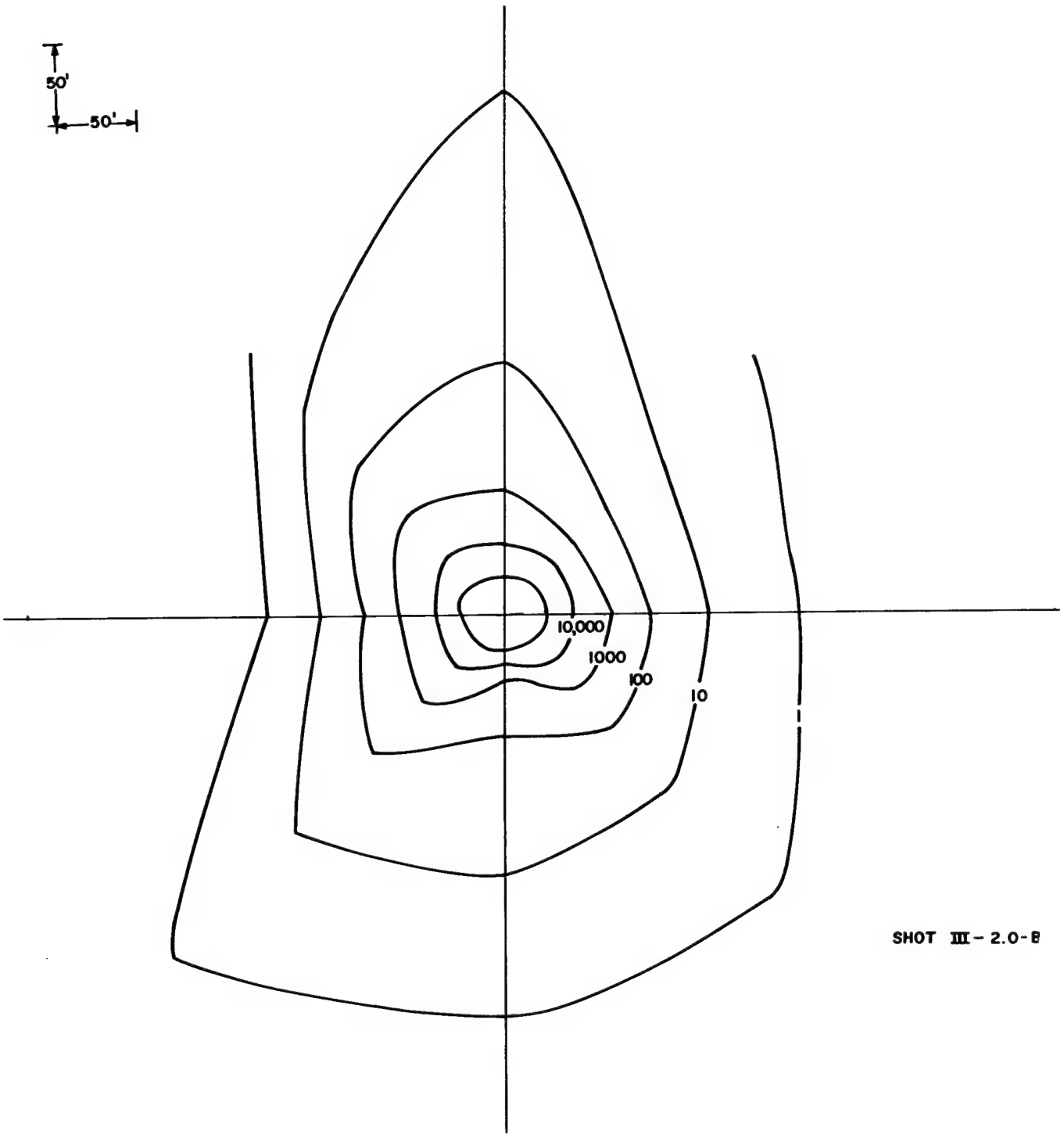

Figure D.5 Throwout deposition, 256-pound single charge, buried at 12.7 feet--contours are in gm/ft^2

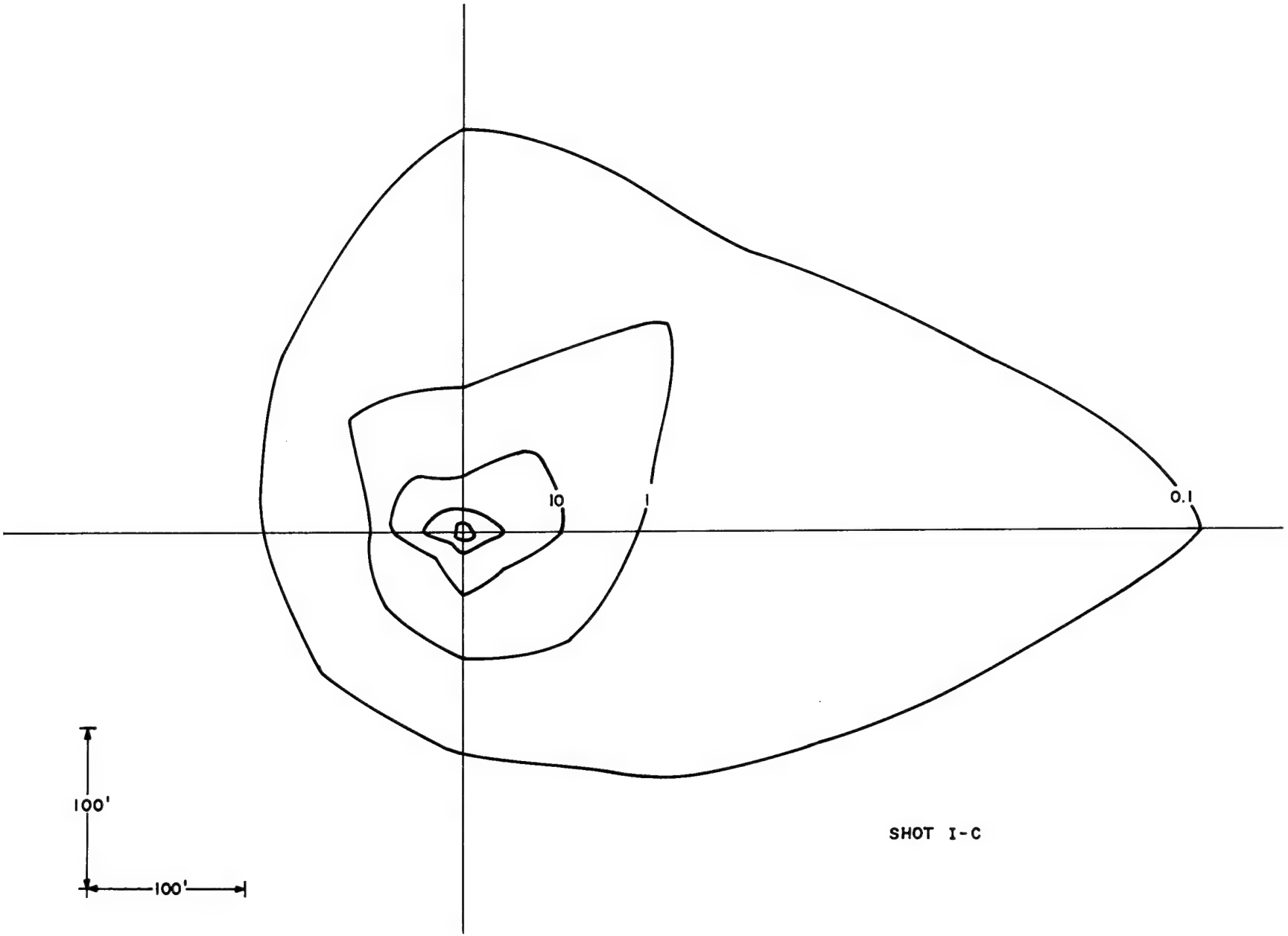

Figure D.6 Throwout deposition, 8-pound single charge, buried at 1 foot--contours are in gm/ft^2

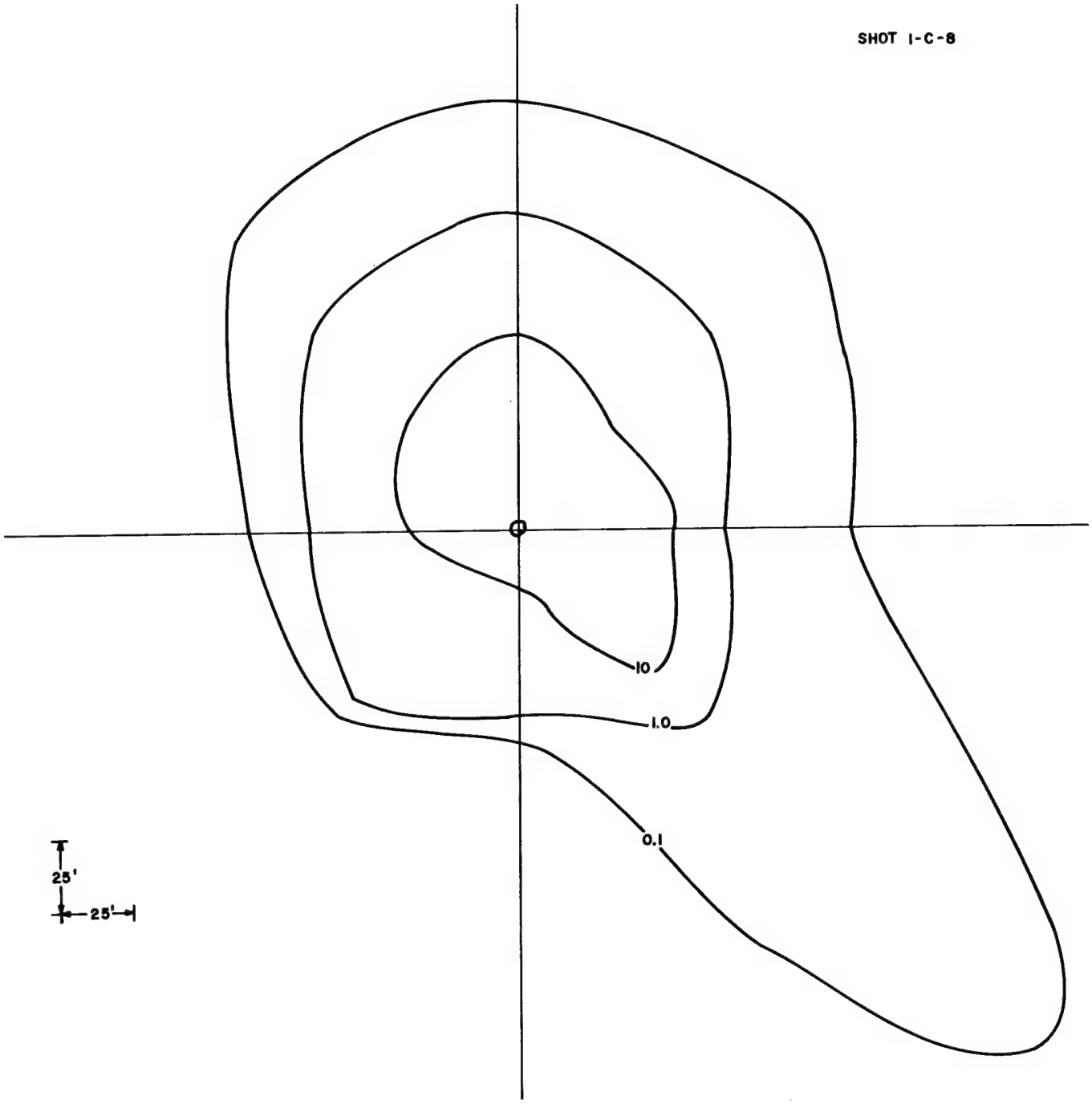

Figure D.7 Throwout deposition, 8-pound single charge, buried 1 foot--contours are in gm/ft^2

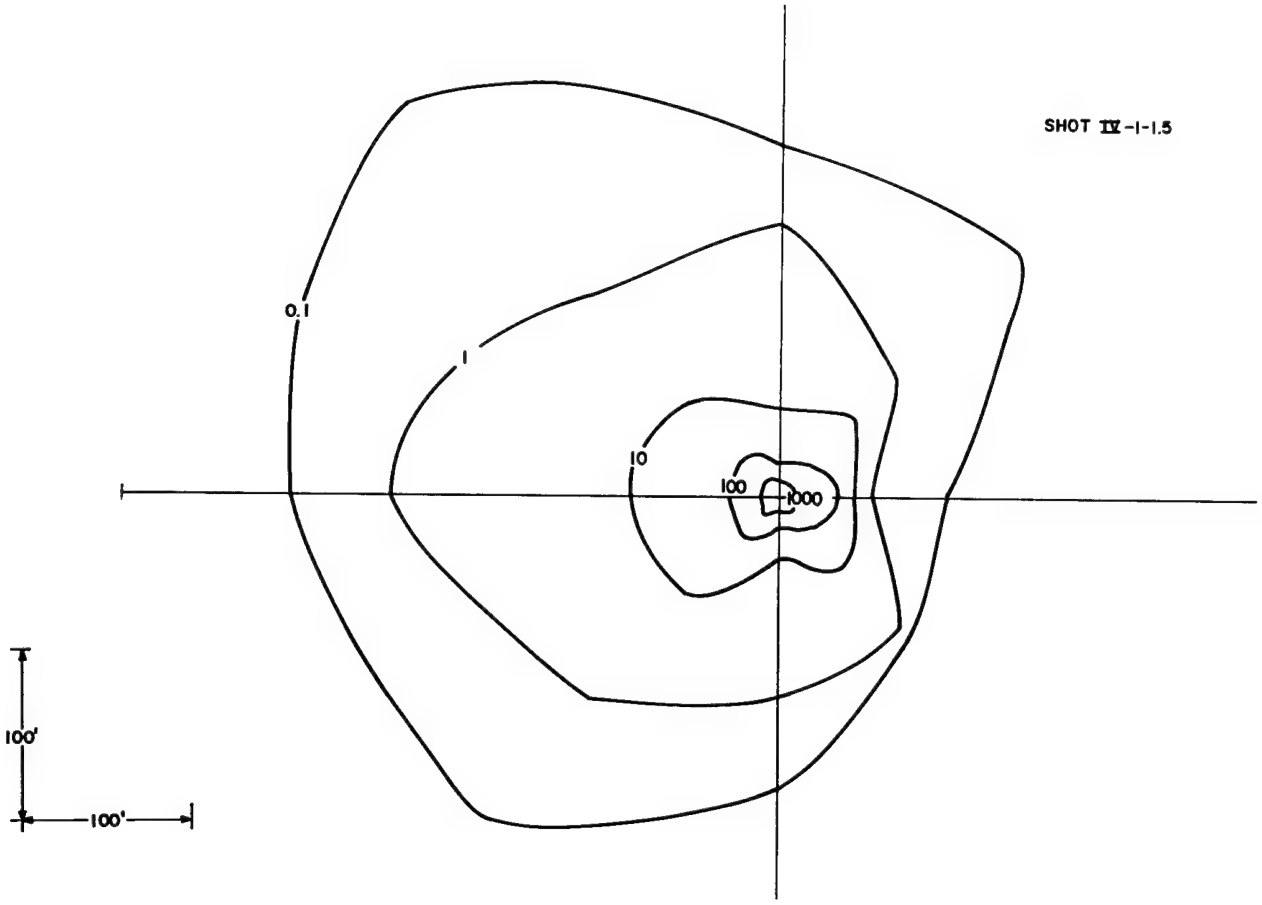

Figure D.8 Throwout deposition, 8-pound single charge, buried at 1.5 feet--contours are in gm/ft^2

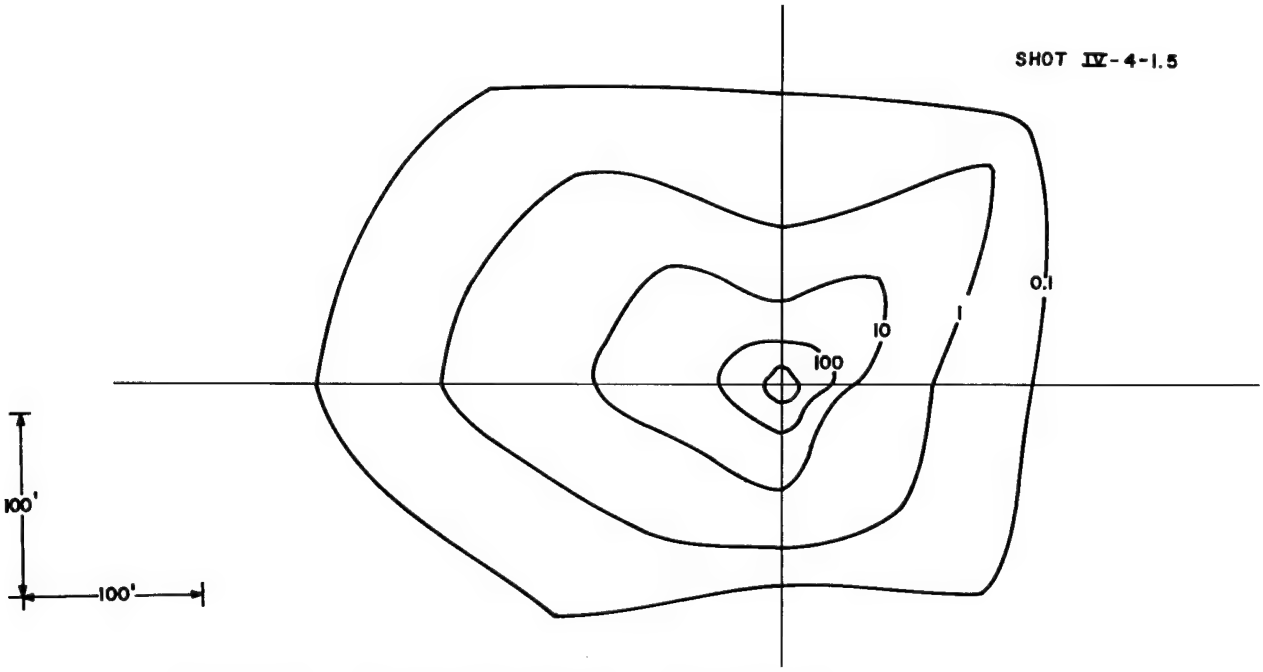

Figure D.9 Throwout deposition, 8-pound single charge, buried at 1.5 feet--contours are in gm/ft^2

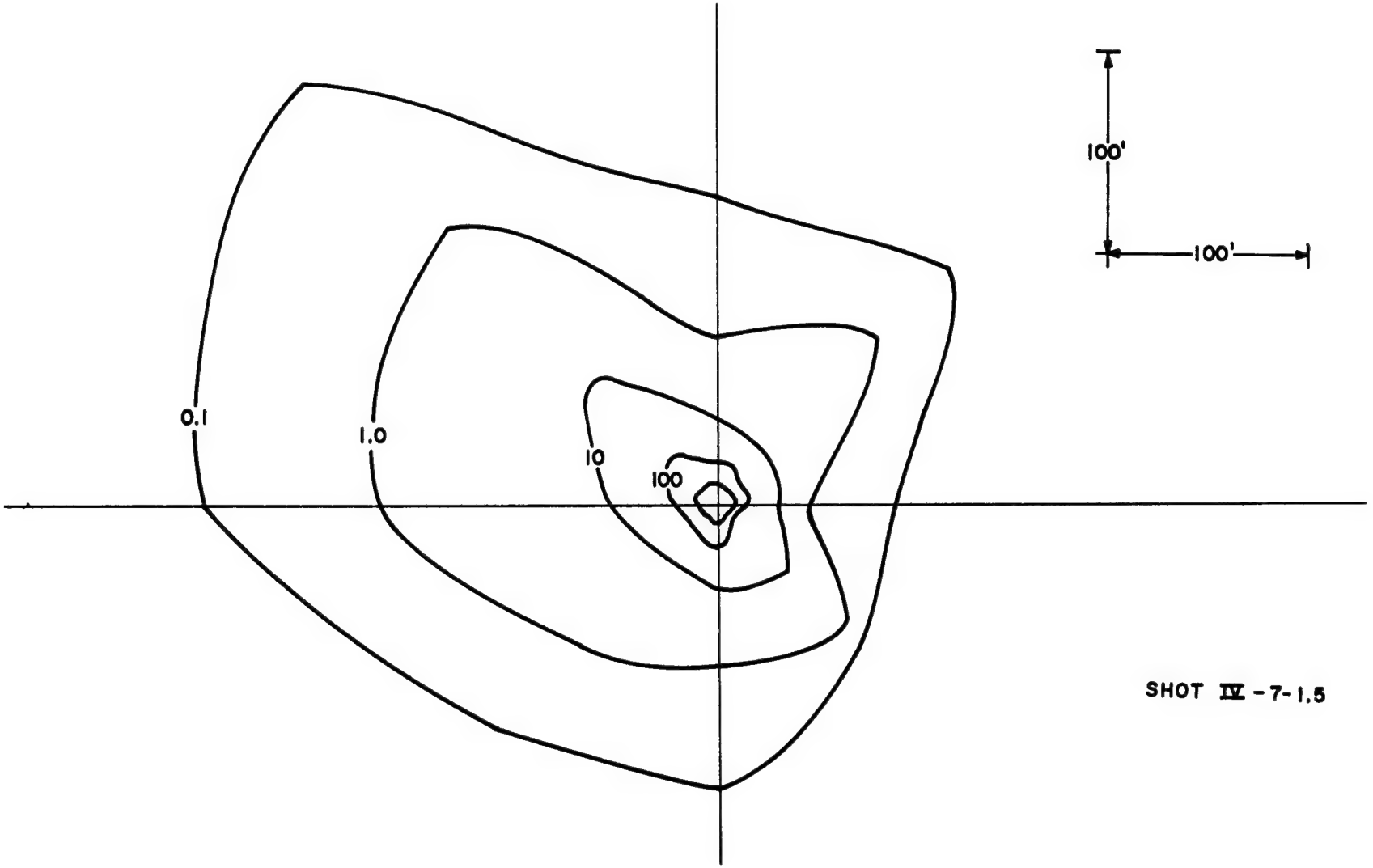

Figure D.10 Throwout deposition, 8-pound single charge, buried at 1.5 feet--contours are in gm/ft^2

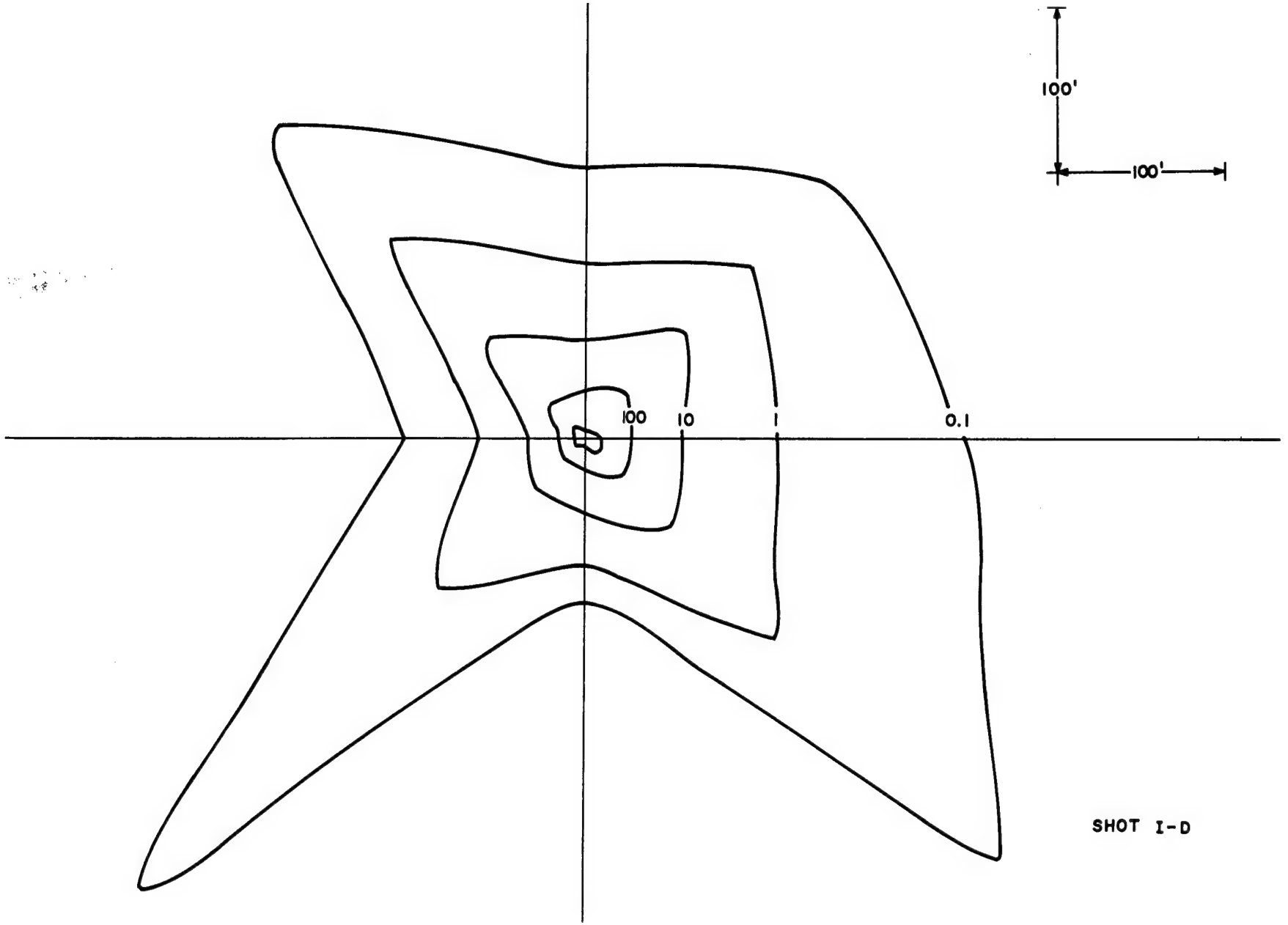

Figure D.11 Throwout deposition, 8-pound single charge, buried at 1.5 feet--contours are in gm/ft^2

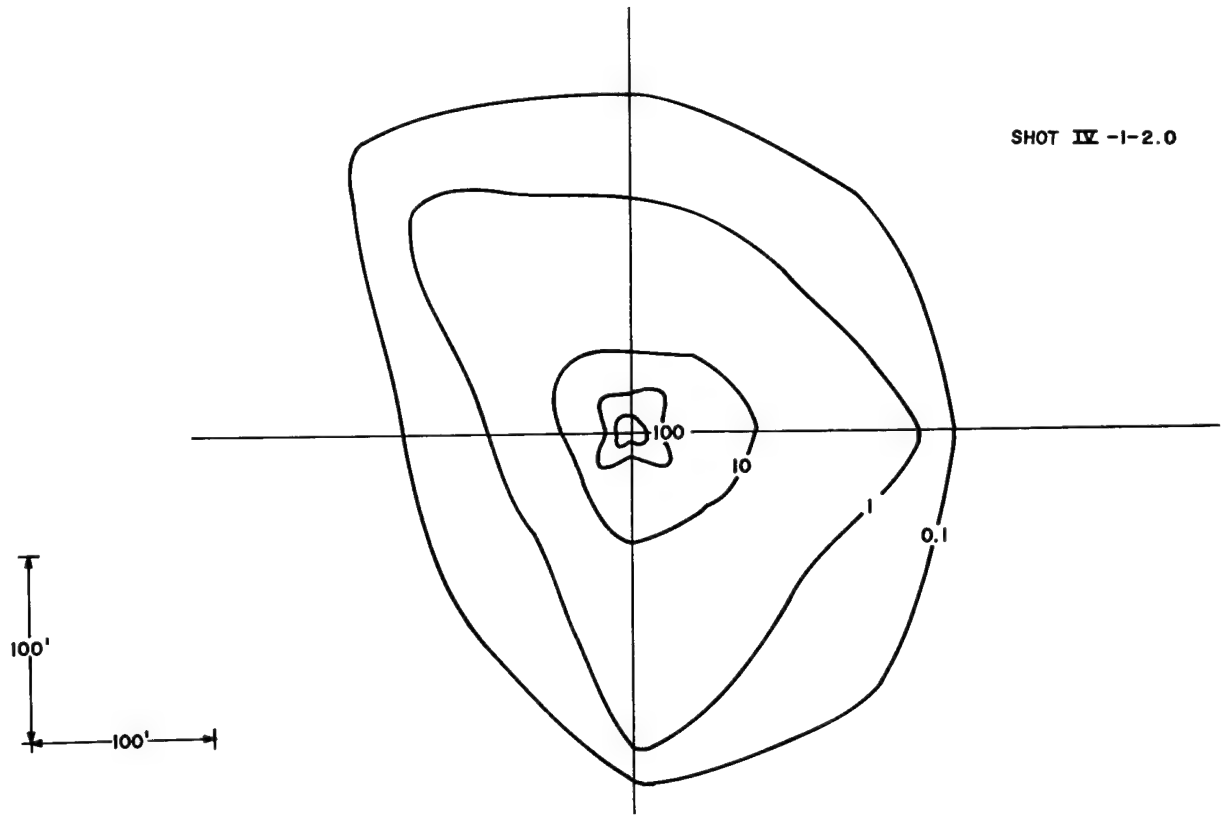

Figure D.12 Throwout deposition, 8-pound single charge, buried at 2 feet--contours are in gm/ft²

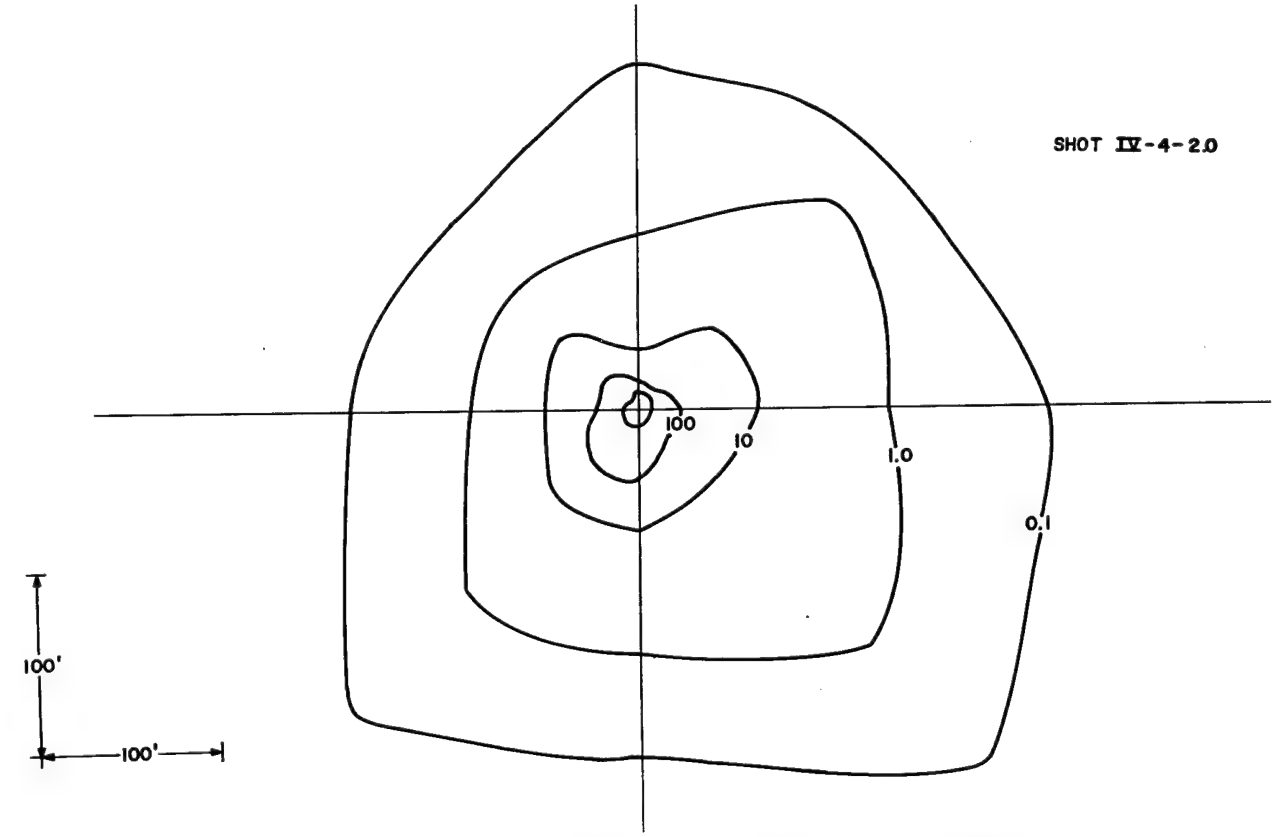

Figure D.13 Throwout deposition, 8-pound single charge, buried at 2 feet--contours are in gm/ft²

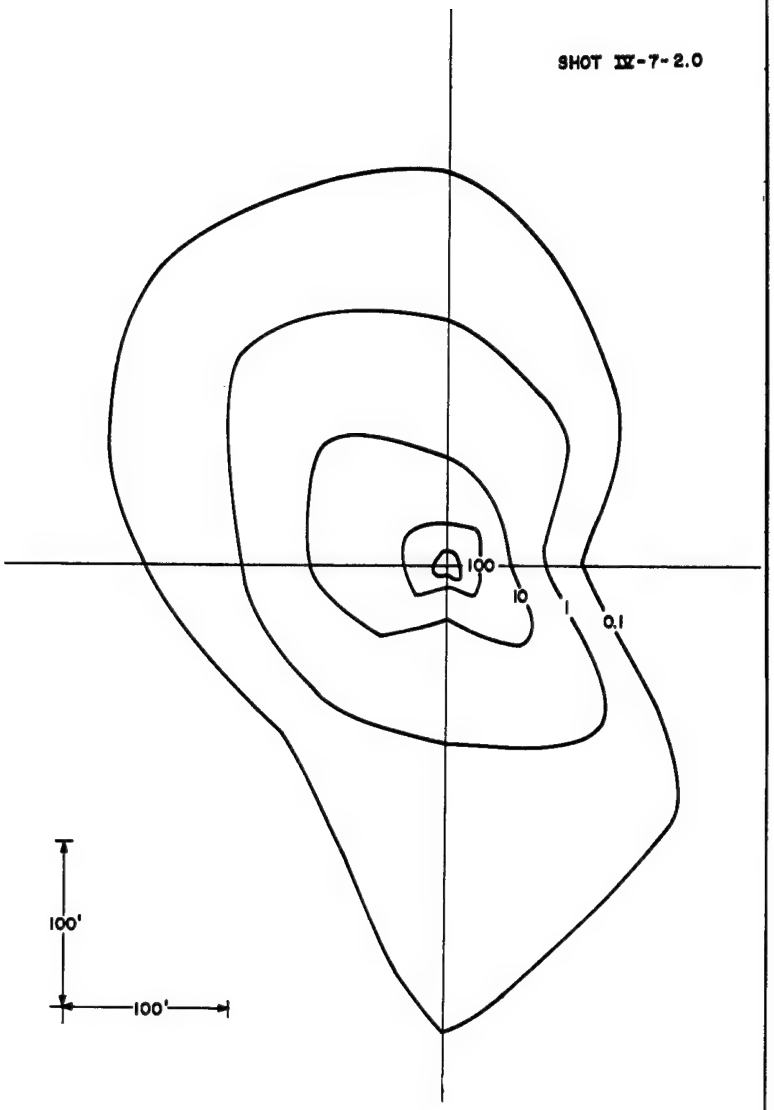

Figure D.14 Throwout deposition, 8-pound single charge, buried at 2 feet--contours are in gm/ft²

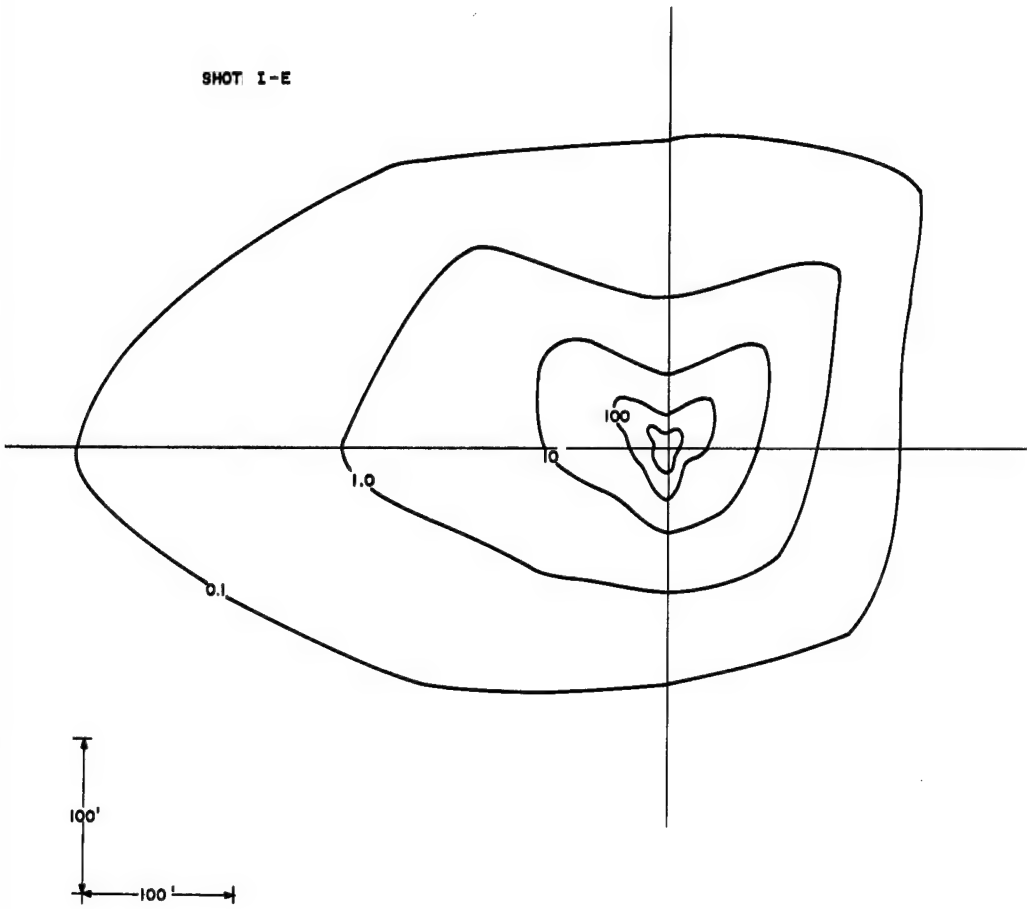

Figure D.15 Throwout deposition, 8-pound single charge, buried at 2 feet--contours are in gm/ft²

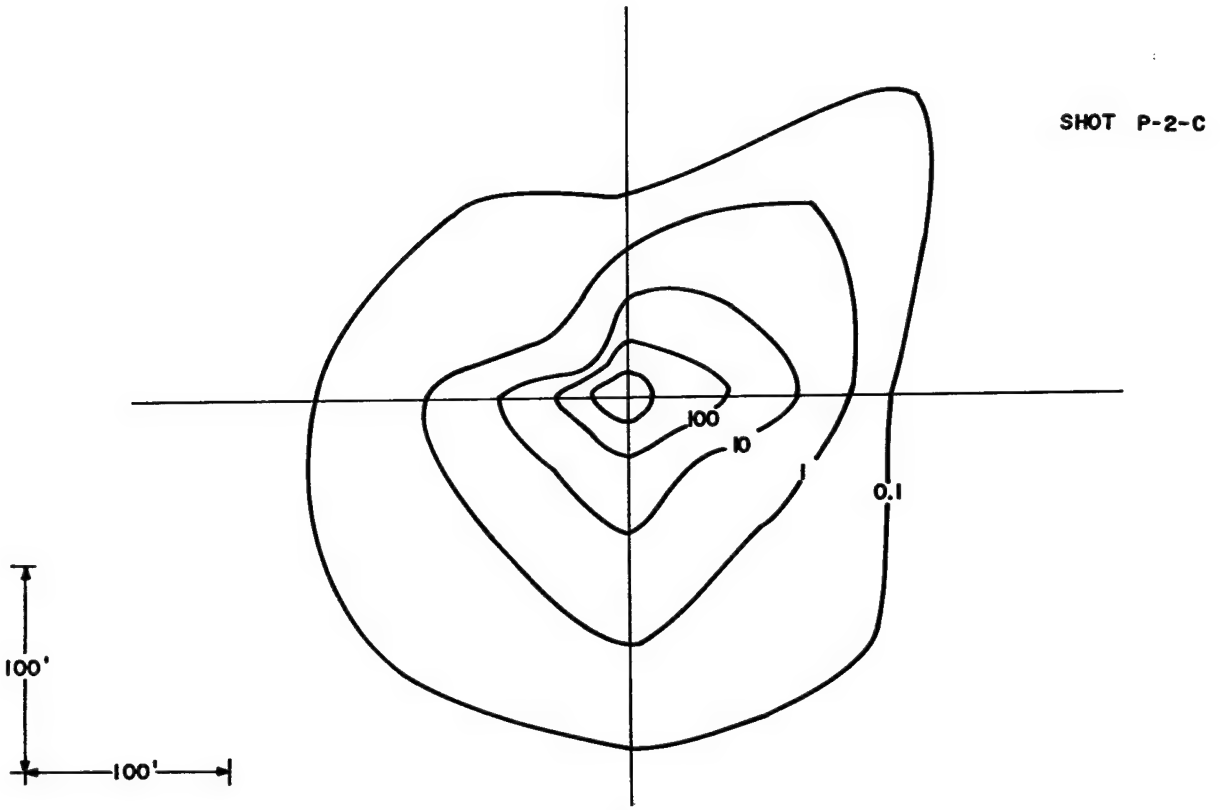

Figure D.16 Throwout deposition, 8-pound single charge, buried at 2 feet--contours are in gm/ft^2

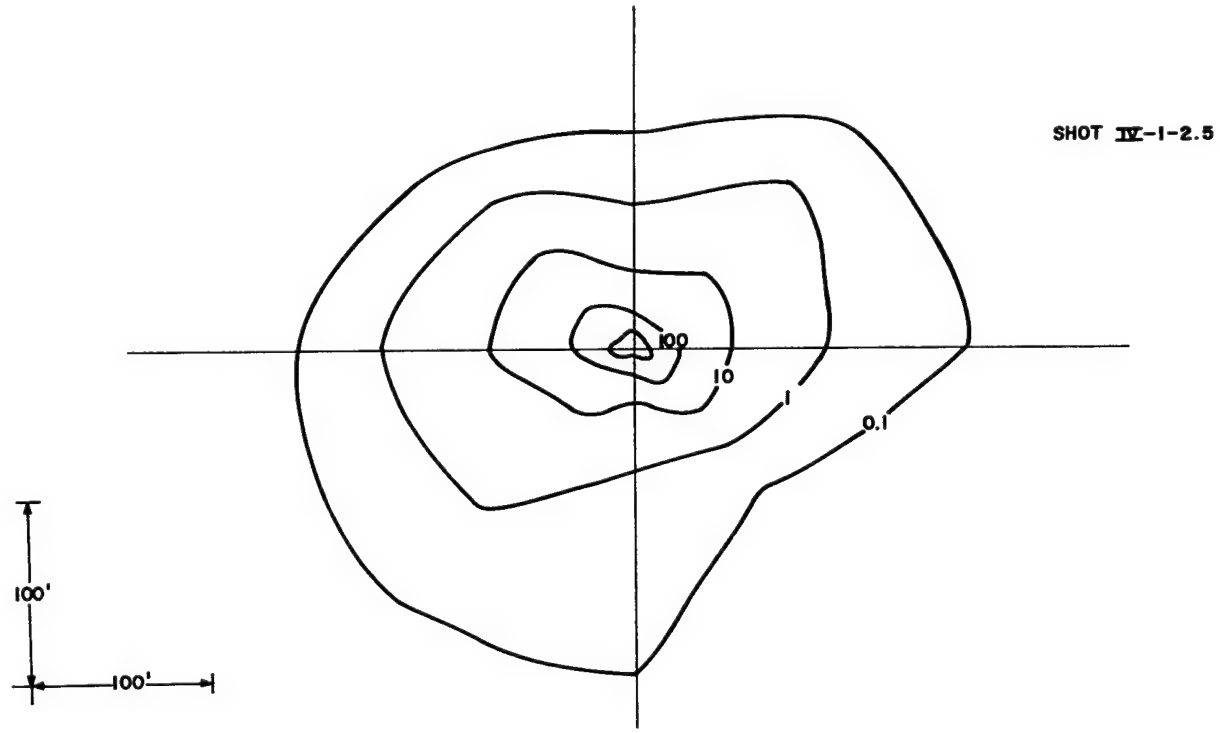

Figure D.17 Throwout deposition, 8-pound single charge, buried at 2.5 feet--contours are in gm/ft^2

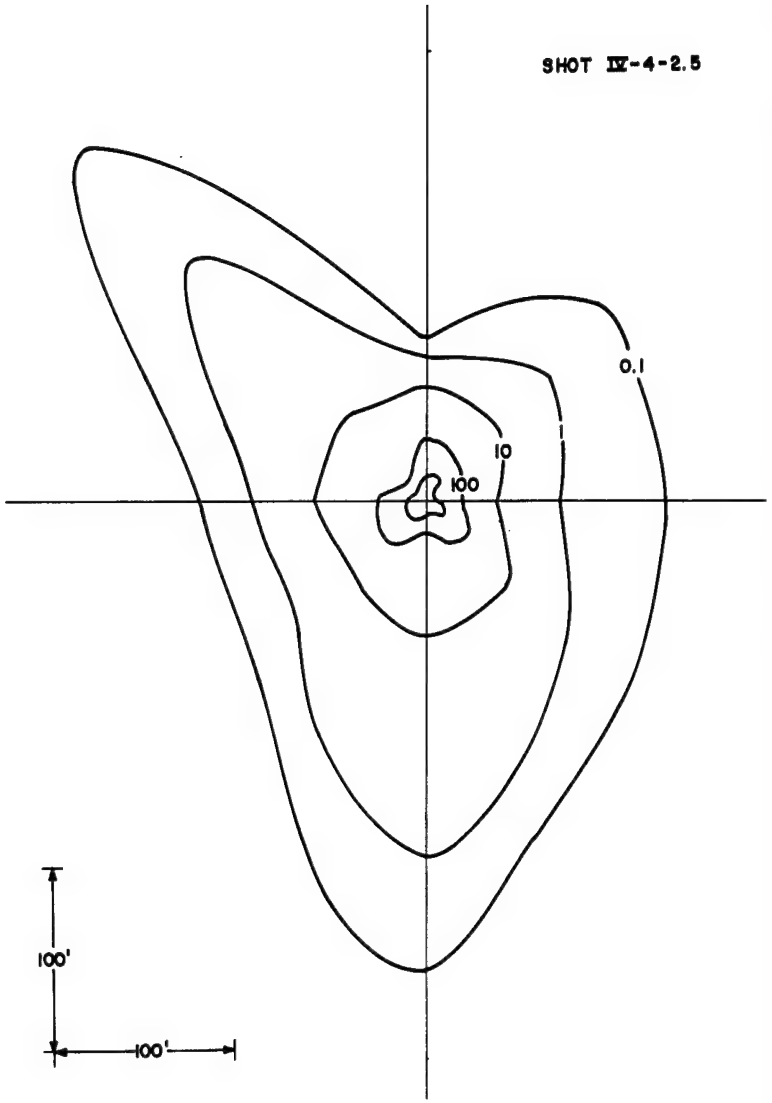

Figure D.18 Throwout deposition, 8-pound single charge, buried at 2.5 feet--contours are in gm/ft^2

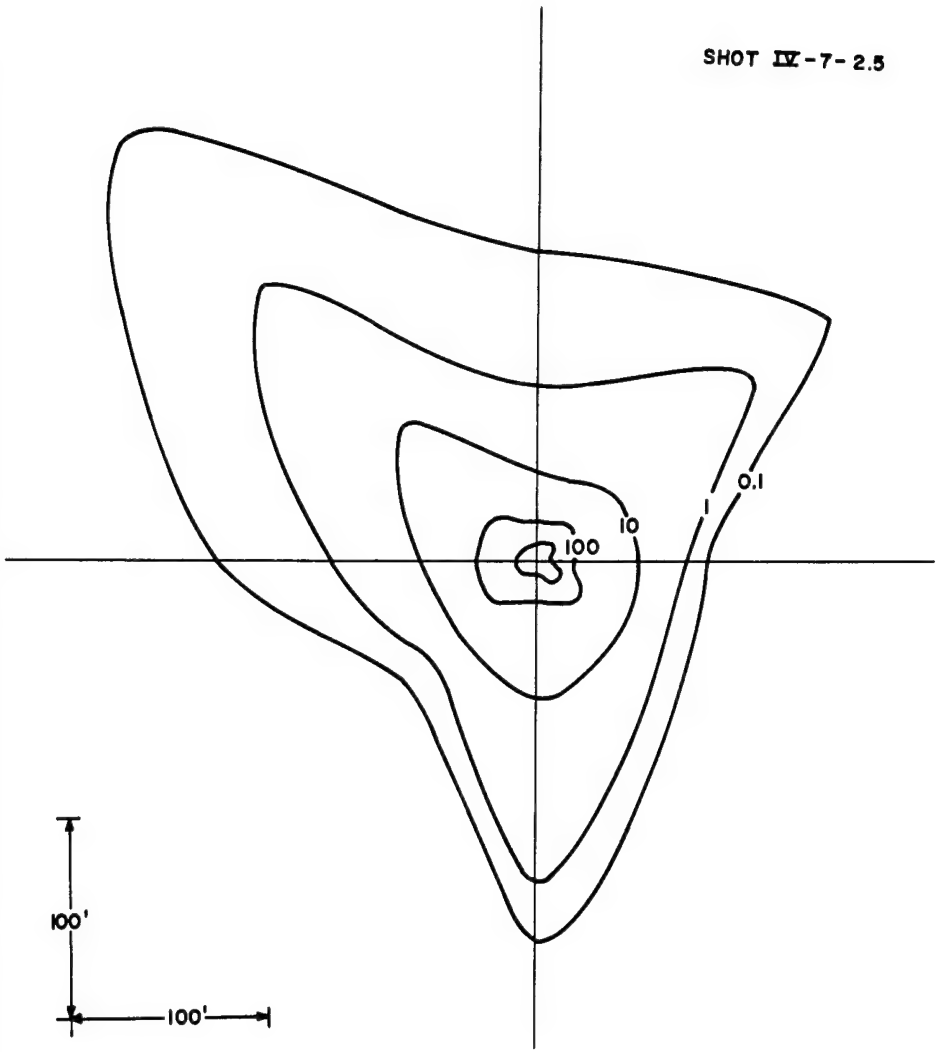

Figure D.19 Throwout deposition, 8-pound single charge, buried at 2.5 feet--contours are in gm/ft^2

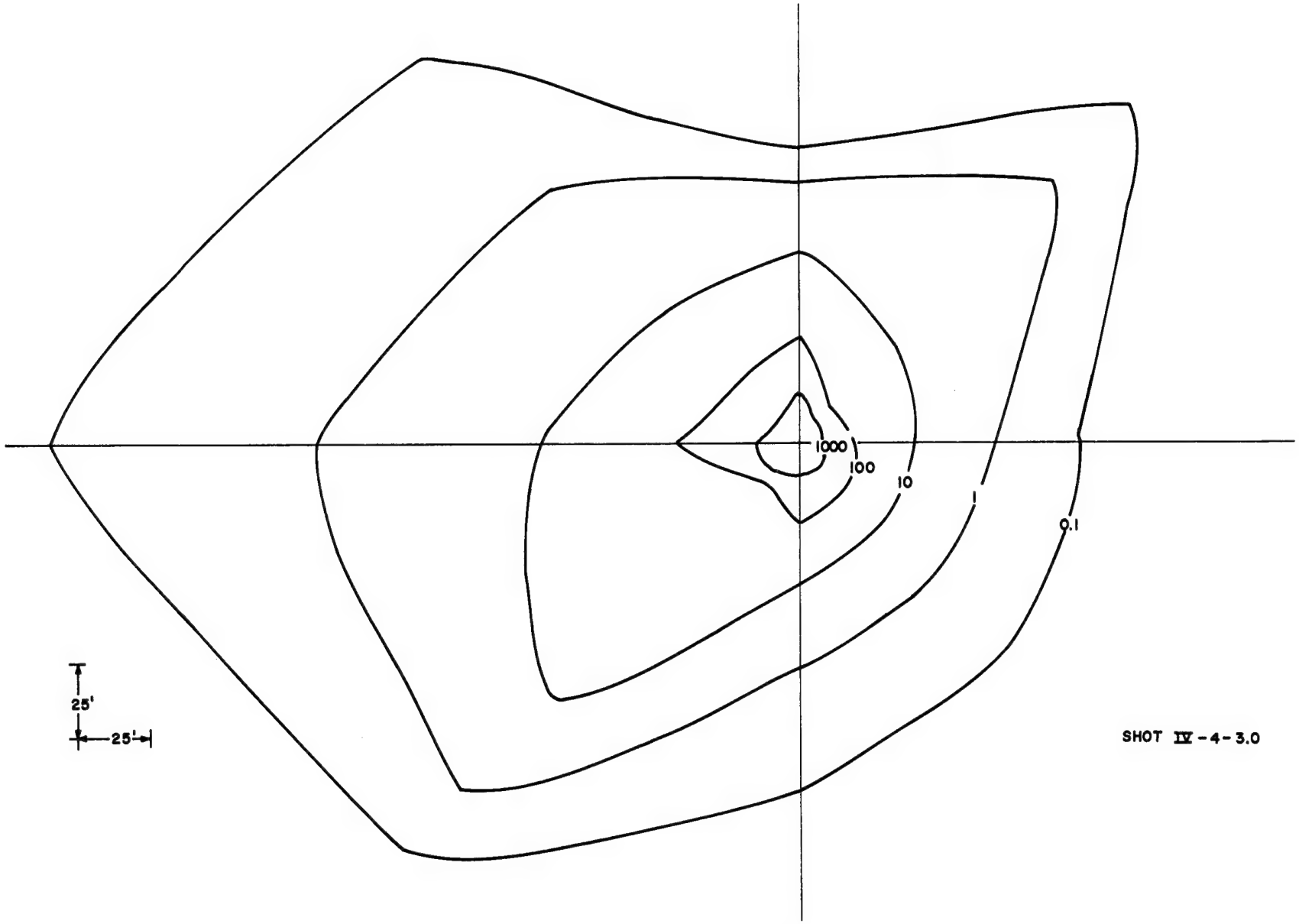

Figure D.20 Throwout deposition, 8-pound single charge, buried at 3 feet--contours are in gm/ft^2

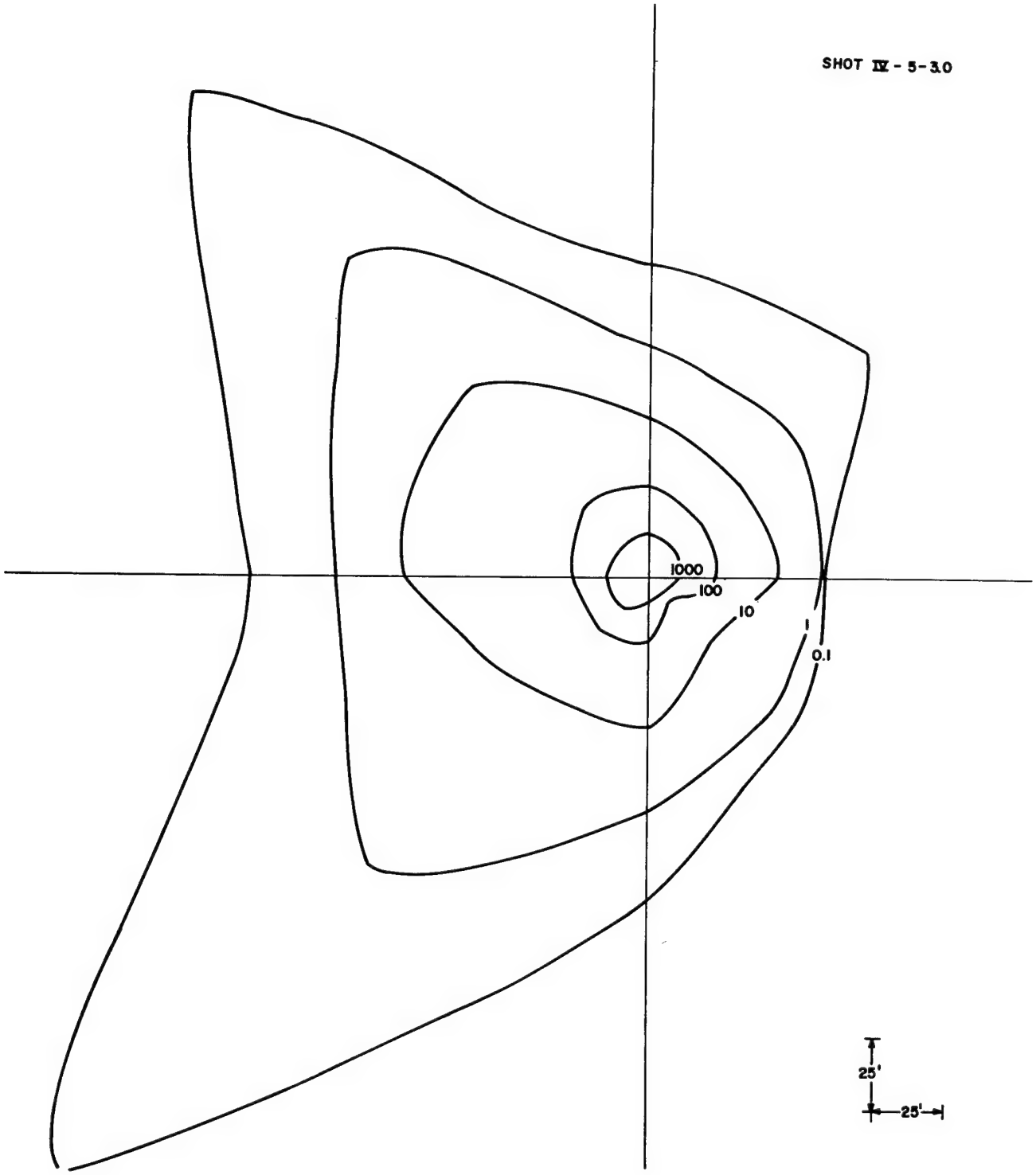

Figure D.21 Throwout deposition, 8-pound single charge, buried at 3 feet--contours are in gm/ft^2

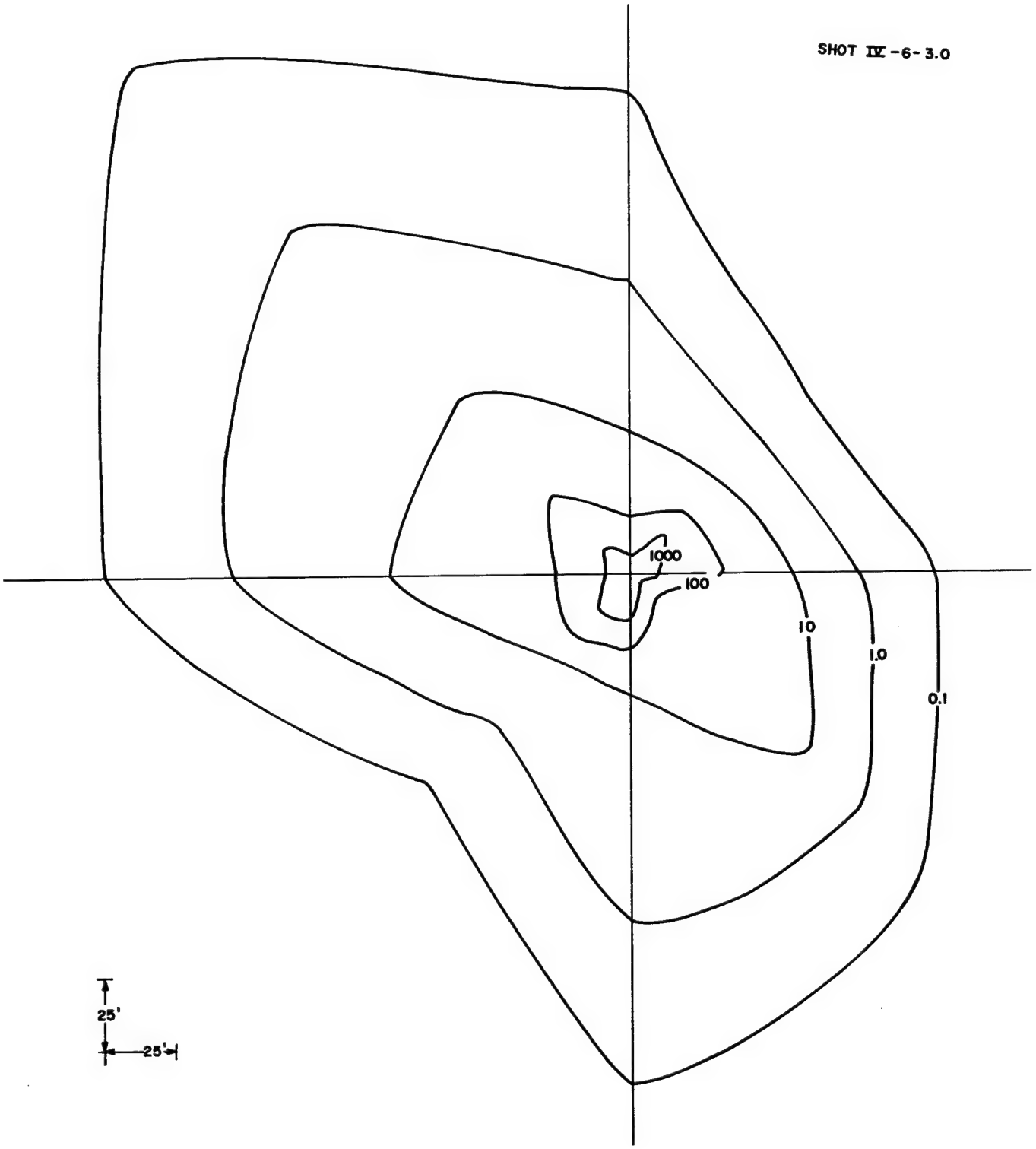

Figure D.22 Throwout deposition, 8-pound single charge buried at 3 feet--contours are in gm/ft^2

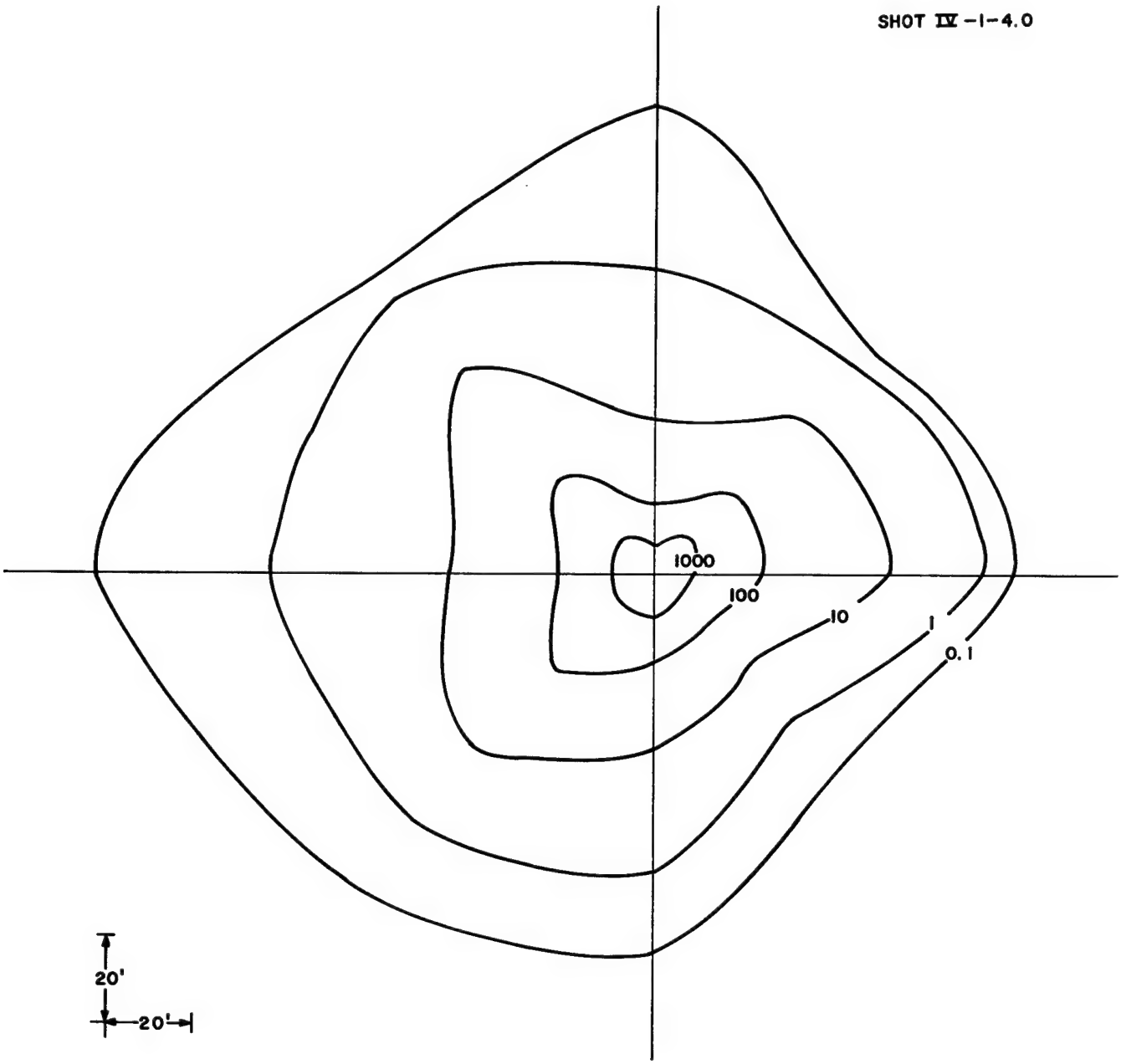

Figure D.23 Throwout deposition, 8-pound single charge, buried at 4 feet--contours are in gm/ft^2

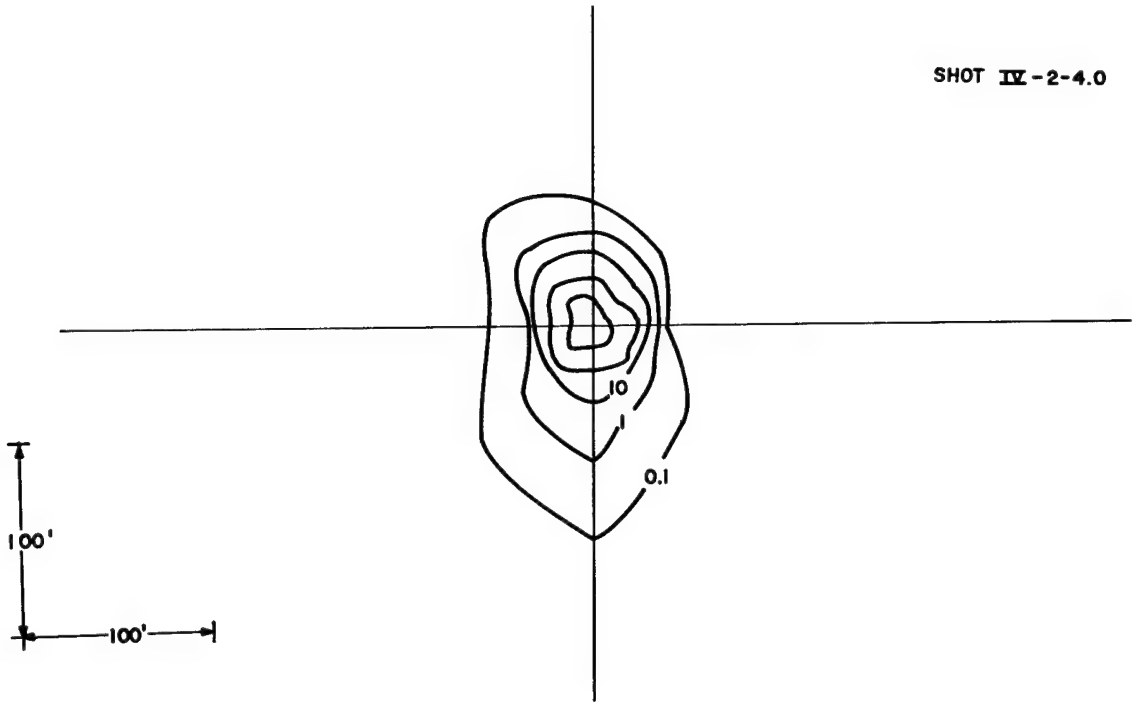

Figure D.24 Throwout deposition, 8-pound single charge, buried at 4 feet--contours are in gm/ft²

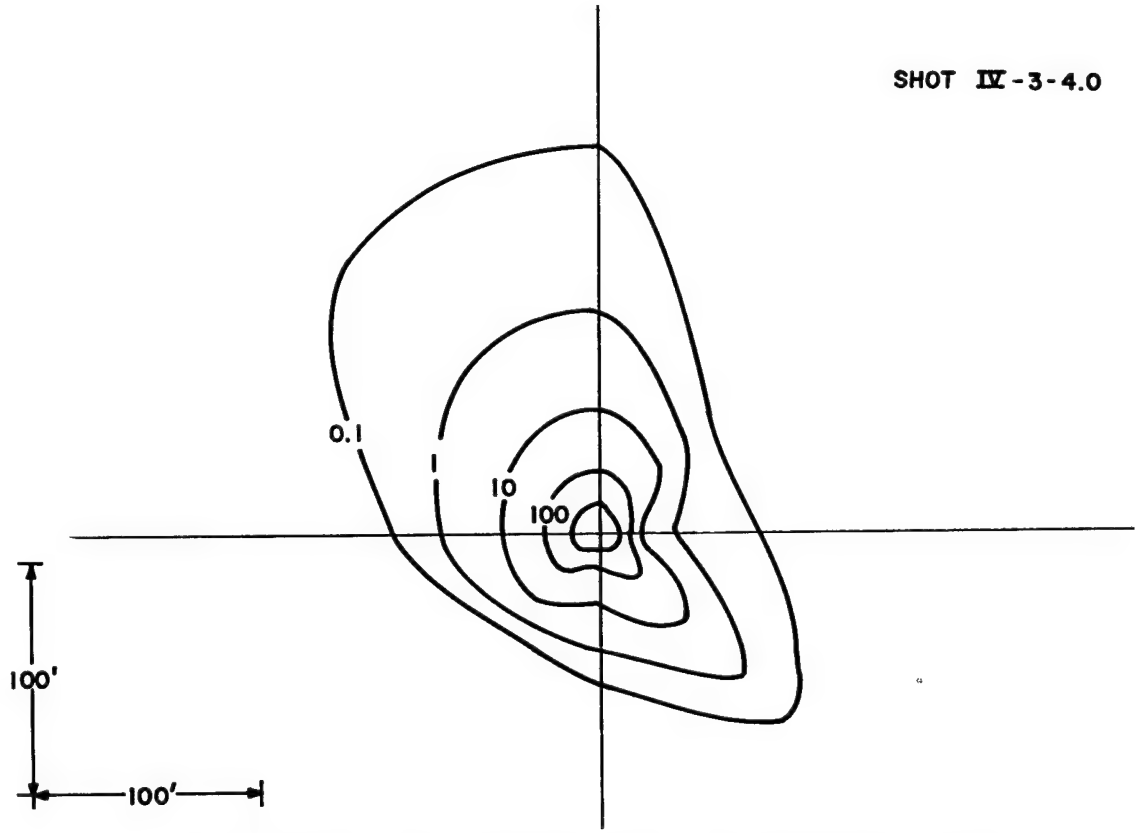

Figure D.25 Throwout deposition, 8-pound single charge, buried at 4 feet--contours are in gm/ft²

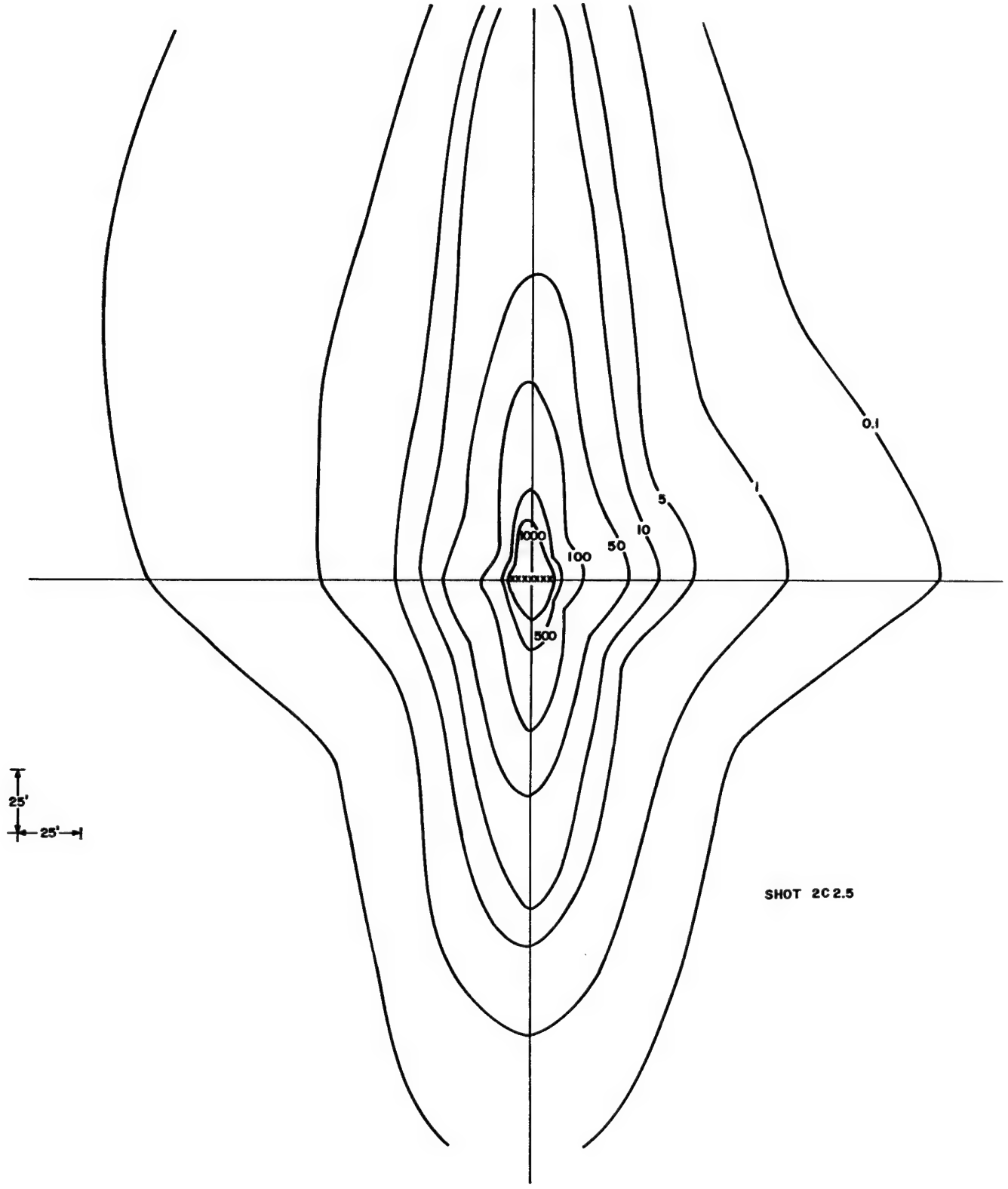

Figure D.26 Throwout deposition, 8-pound row charge, buried 1 foot, spaced 2.5 feet--contours are in gm/ft^2

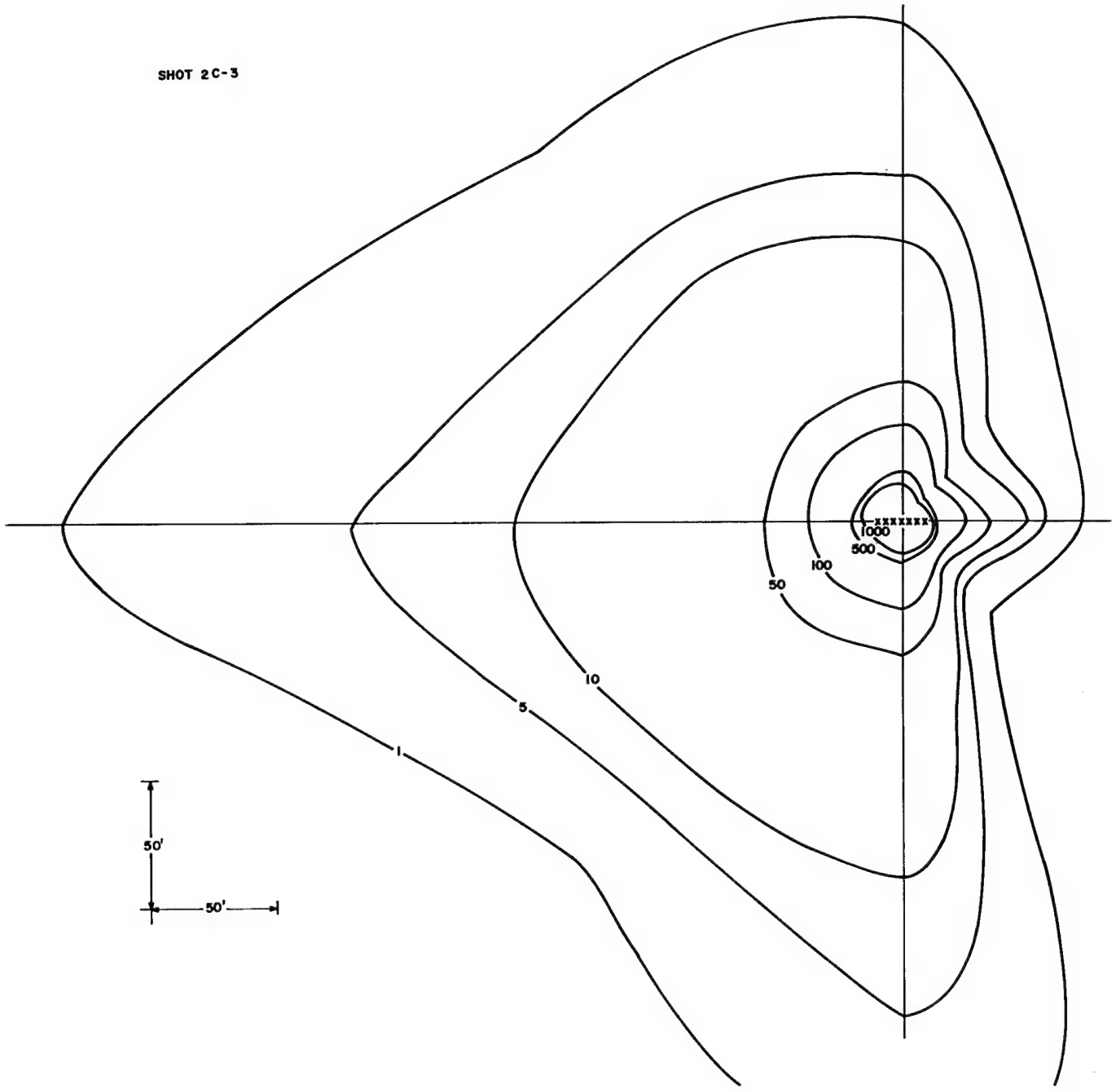

Figure D.27 Throwout deposition, 8-pound row charge, buried 1 foot, spaced 3 feet--contours are in gm/ft^2

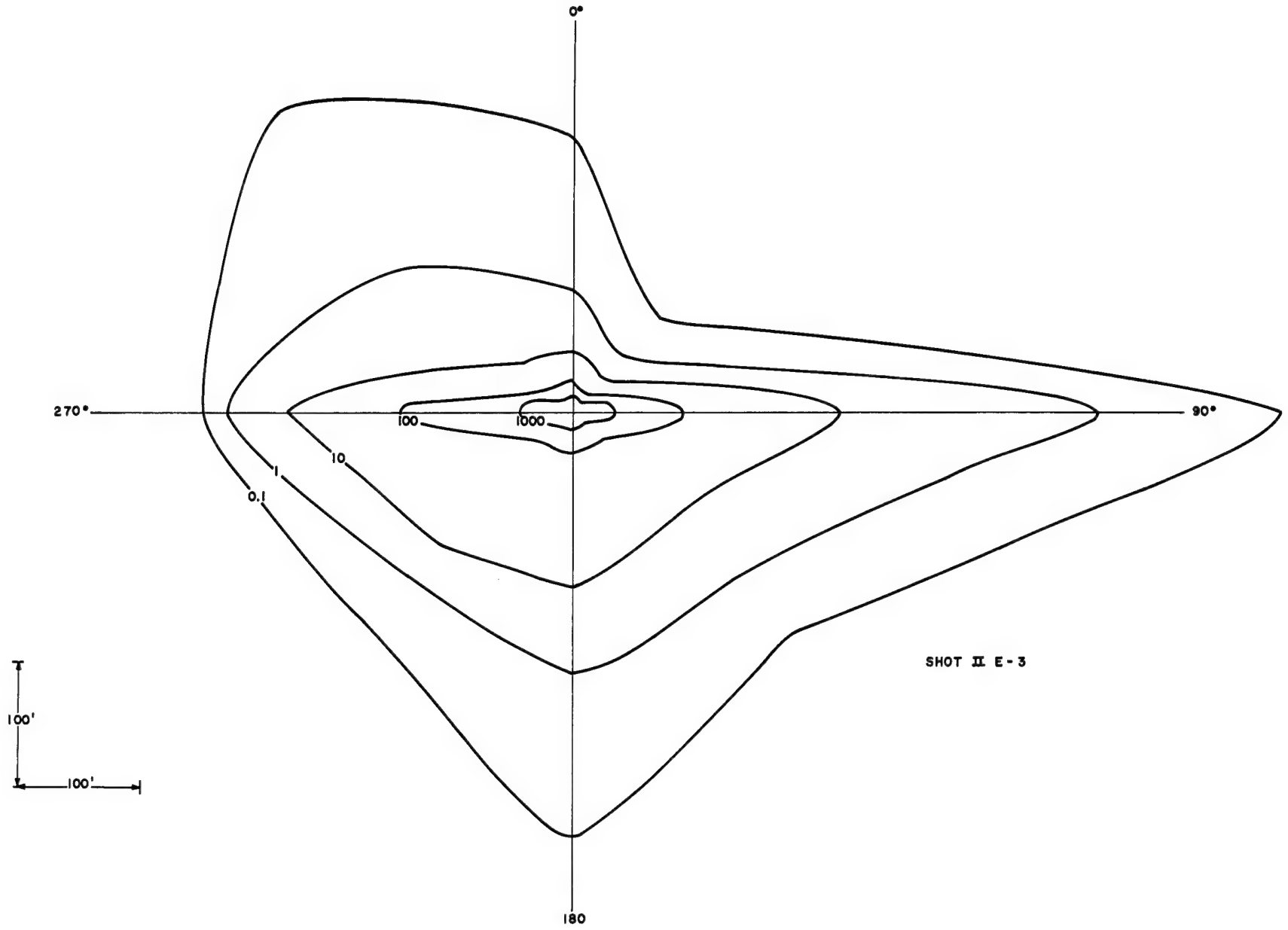

Figure D.28 Throwout deposition, 8-pound row charge, buried 2 feet, spaced 3 feet--contours are in gm/ft^2

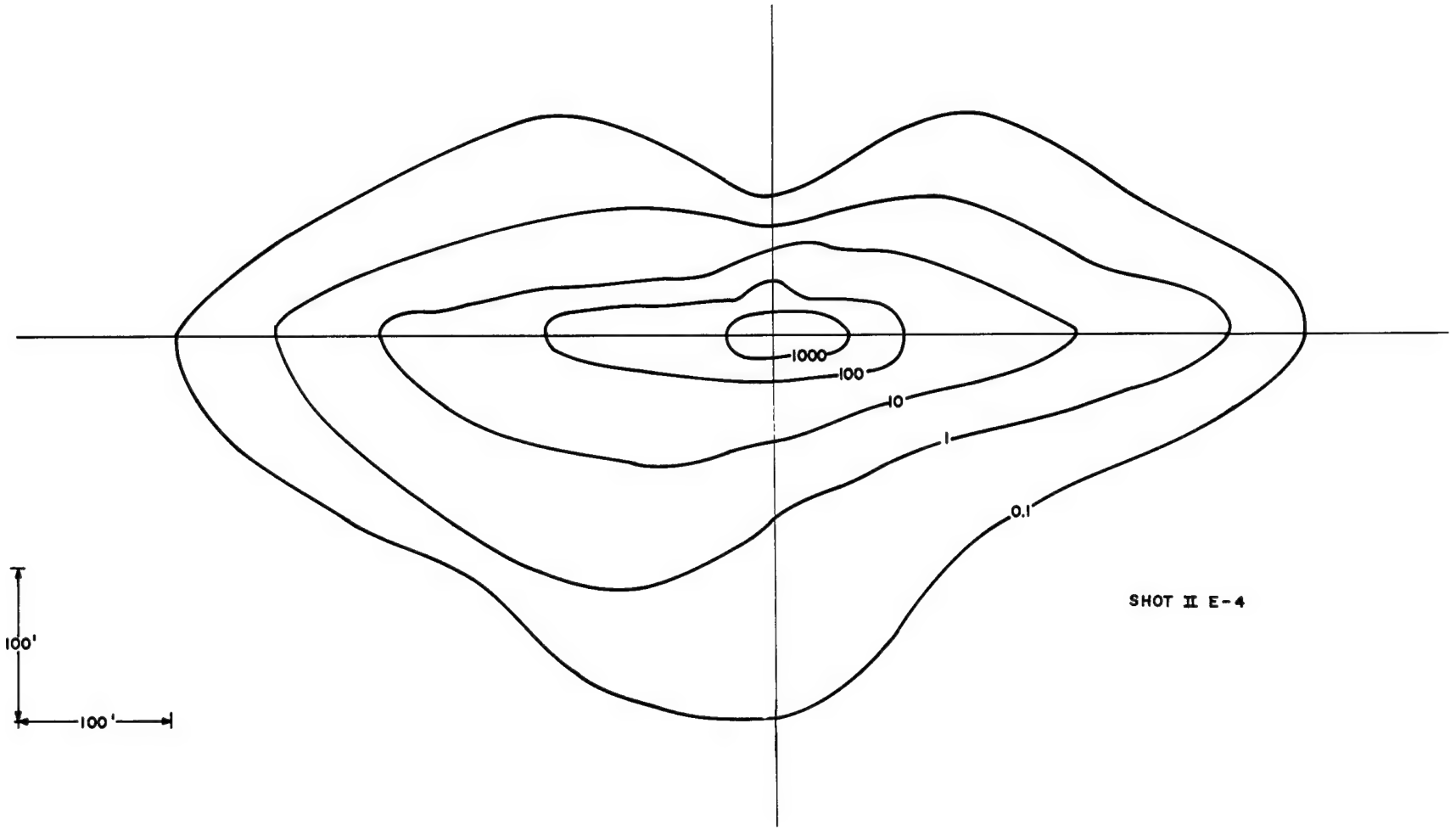

Figure D.29 Throwout deposition, 8-pound row charge, buried 2 feet, spaced 4 feet--contours are in gm/ft^2

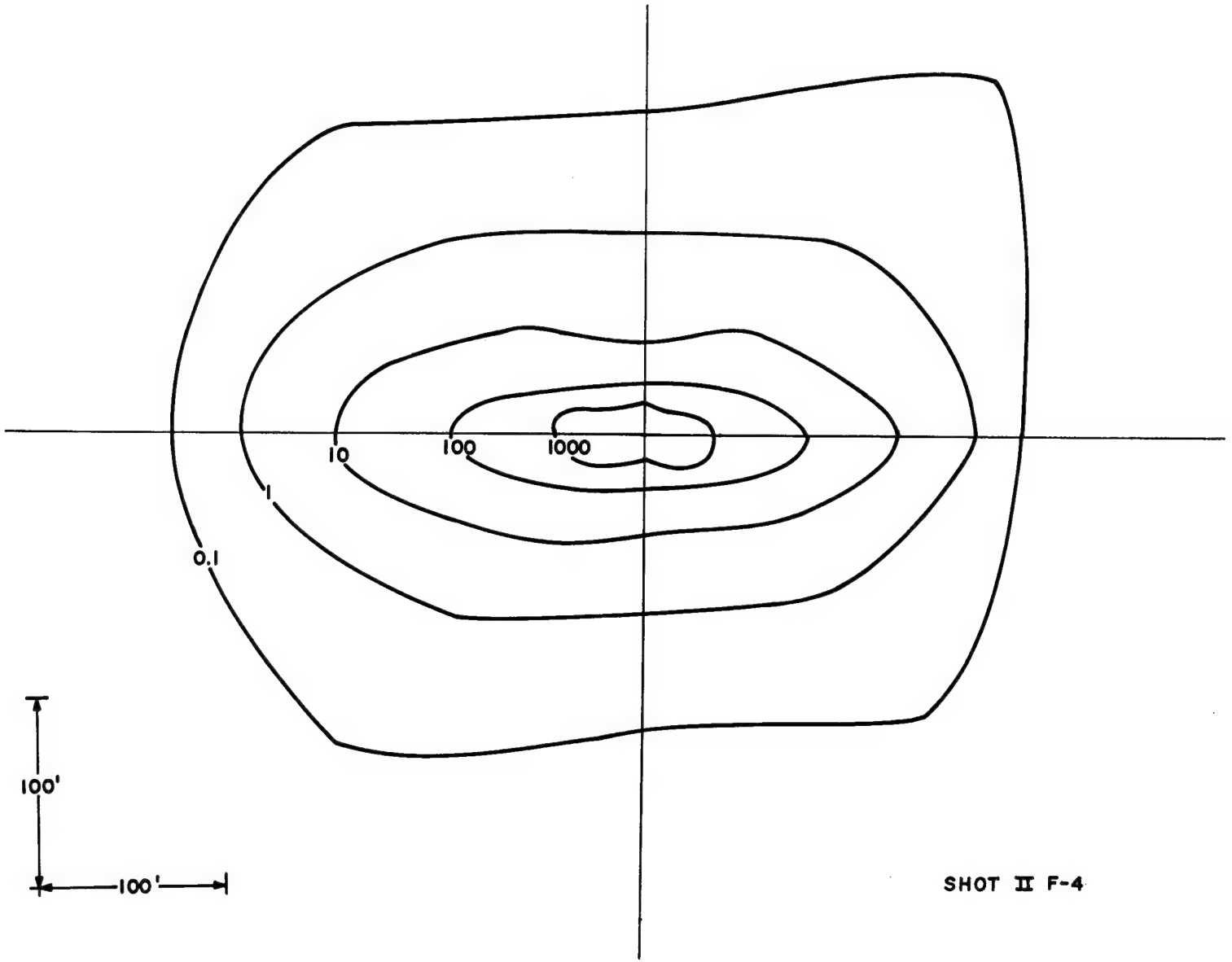

Figure D.30 Throwout deposition, 8-pound row charge, buried 2.5 feet, spaced 4 feet--contours are in gm/ft^2

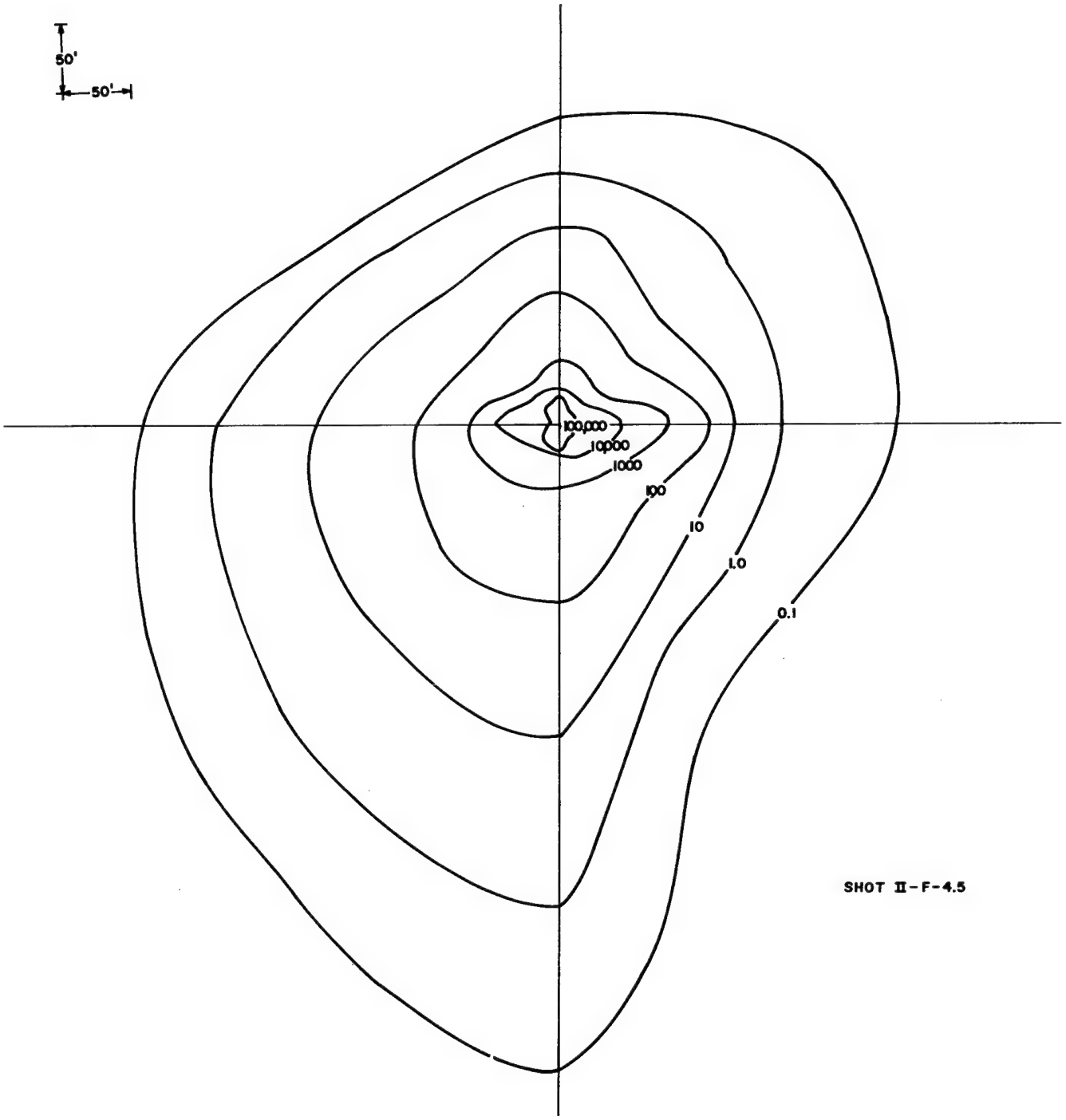

Figure D.31 Throwout deposition, 8-pound row charge, buried 2.5 feet, spaced 4.5 feet--contours are in gm/ft^2

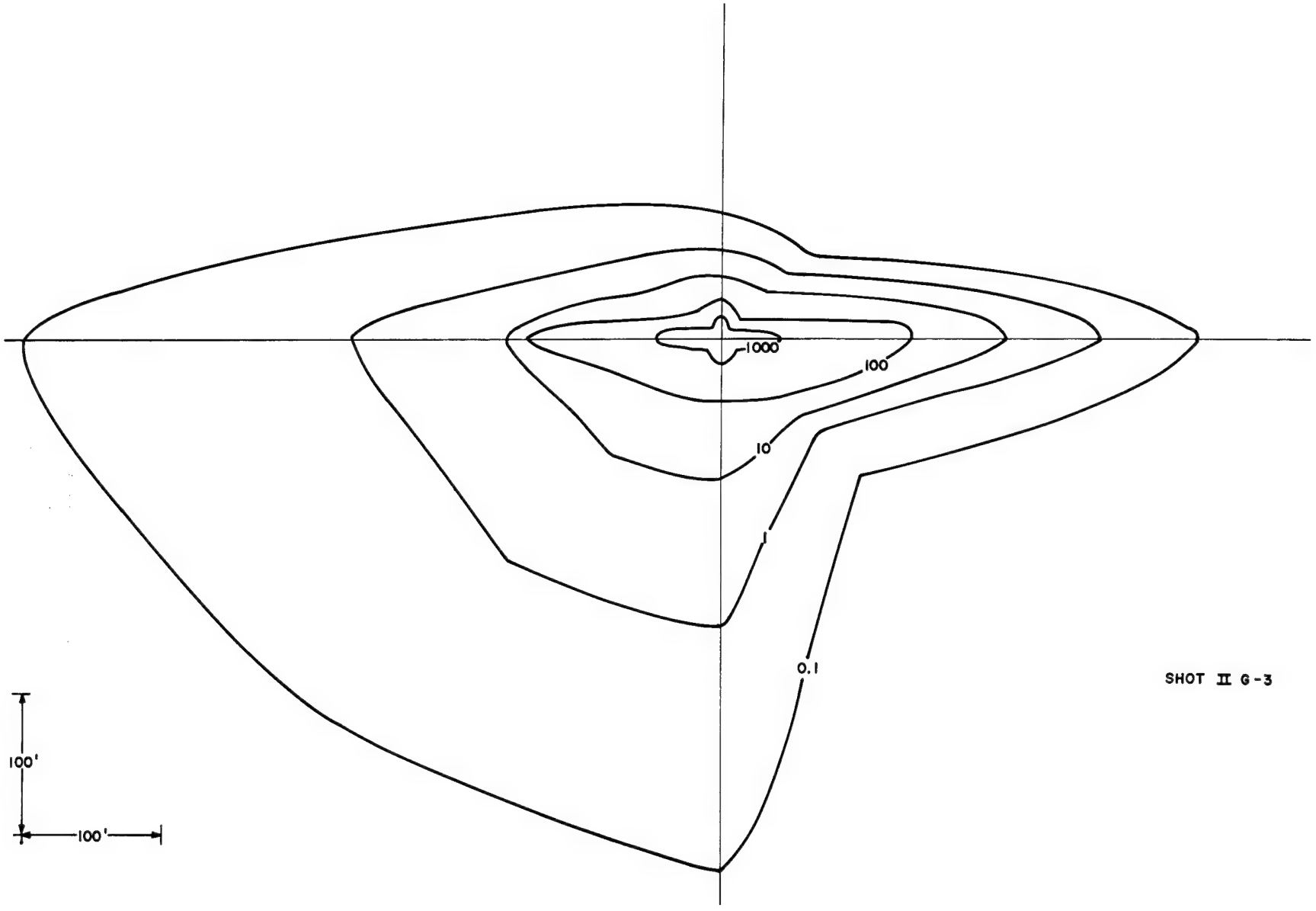

Figure D.32 Throwout deposition, 8-pound row charge, buried 3 feet, spaced 3 feet--contours are in gm/ft^2

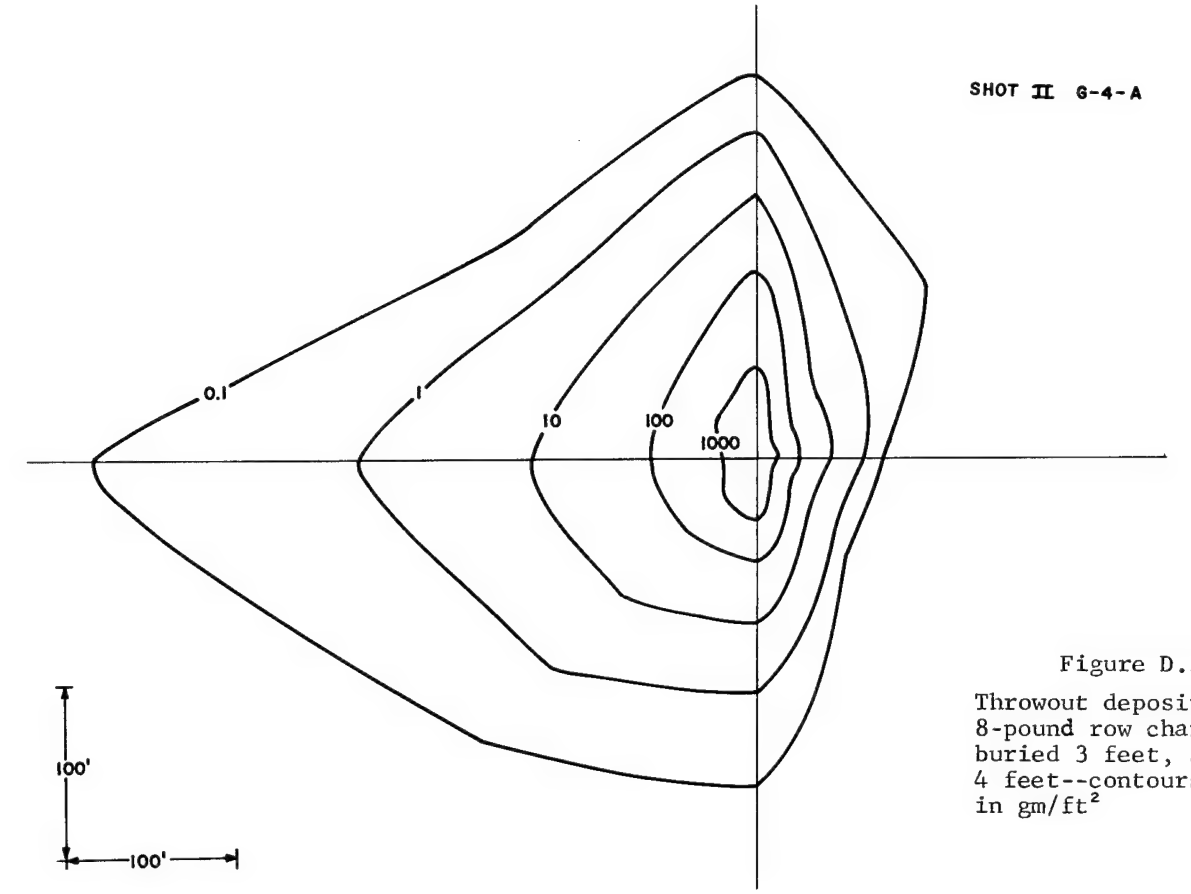

Figure D.33

Throwout deposition, 8-pound row charge, buried 3 feet, spaced 4 feet--contours are in gm/ft^2

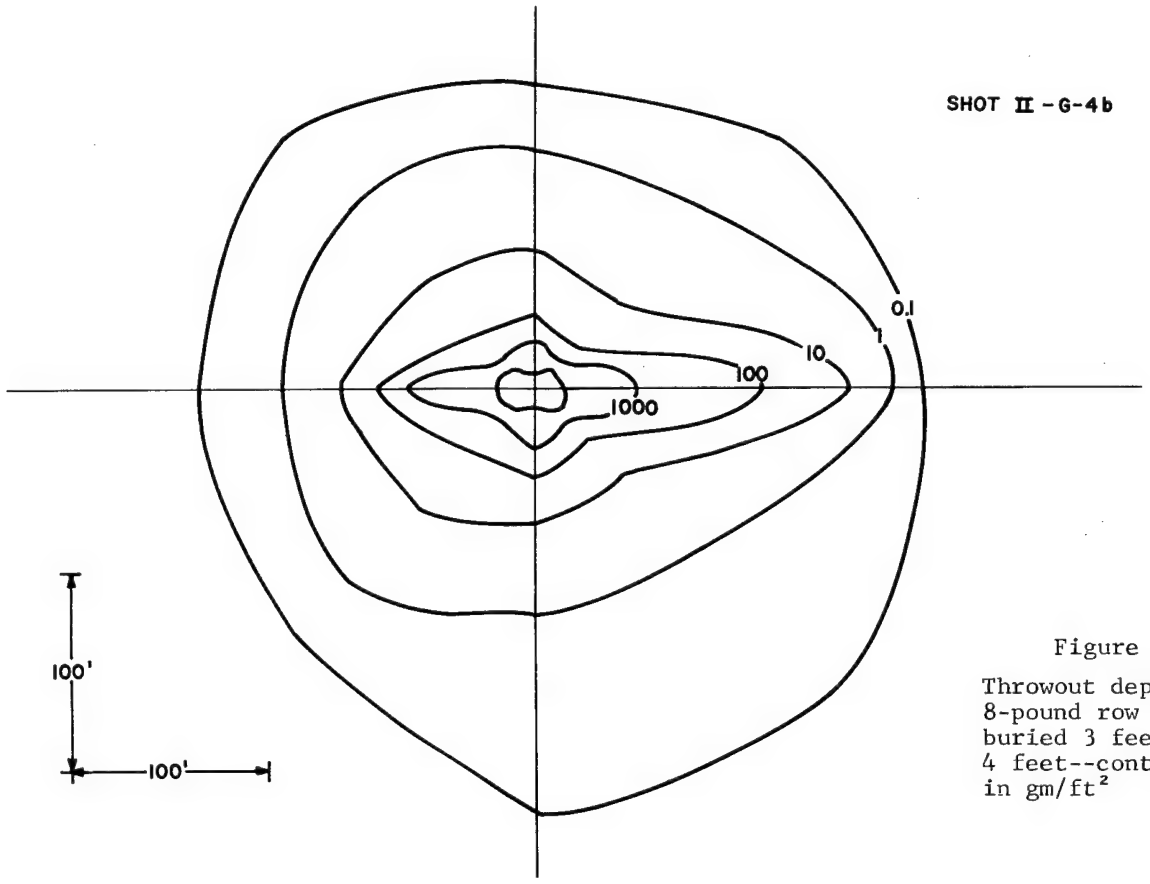

Figure D.34

Throwout deposition, 8-pound row charge, buried 3 feet, spaced 4 feet--contours are in gm/ft^2

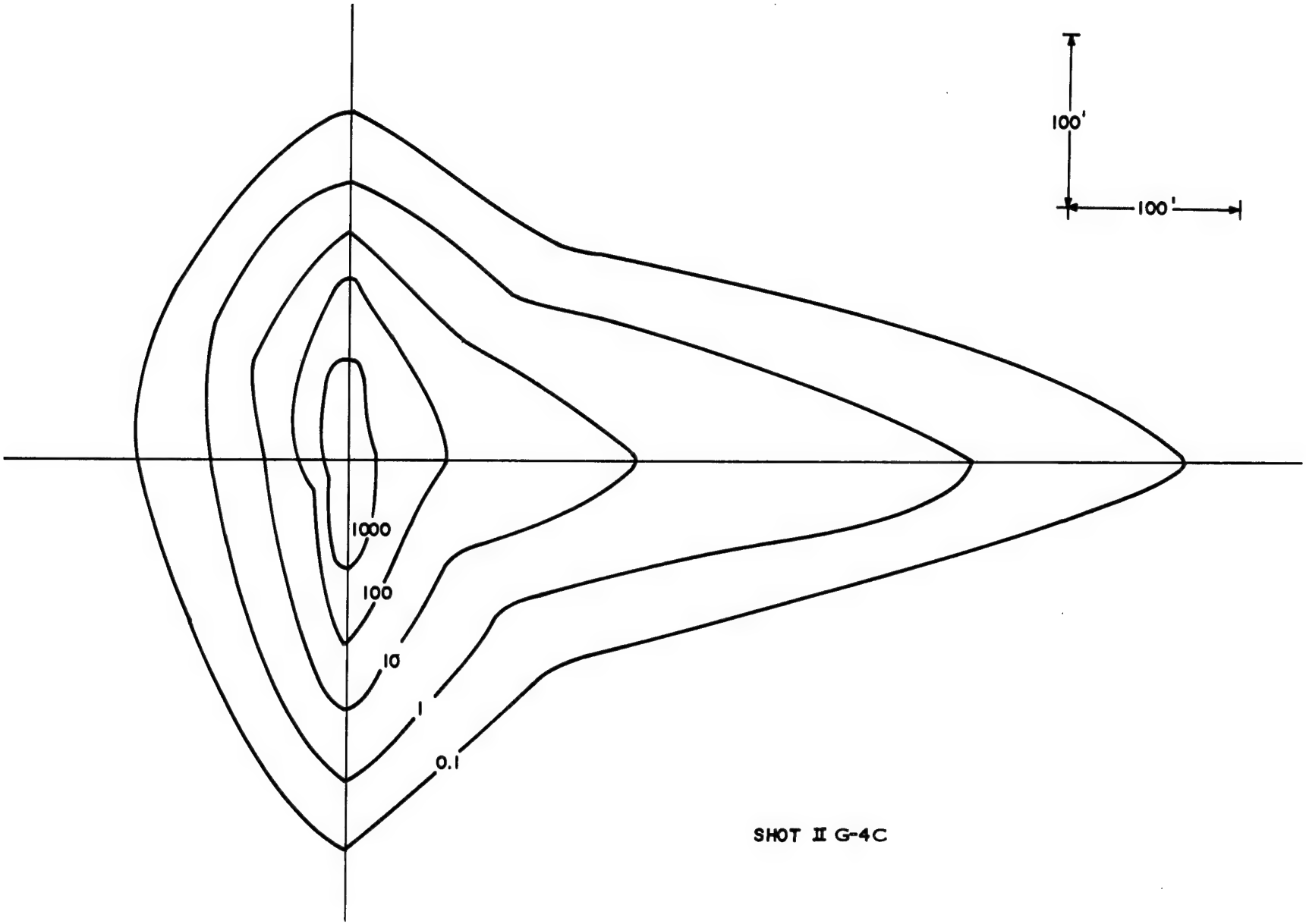

Figure D.35 Throwout deposition, 8-pound row charge, buried 3 feet, spaced 4 feet--contours are in gm/ft^2

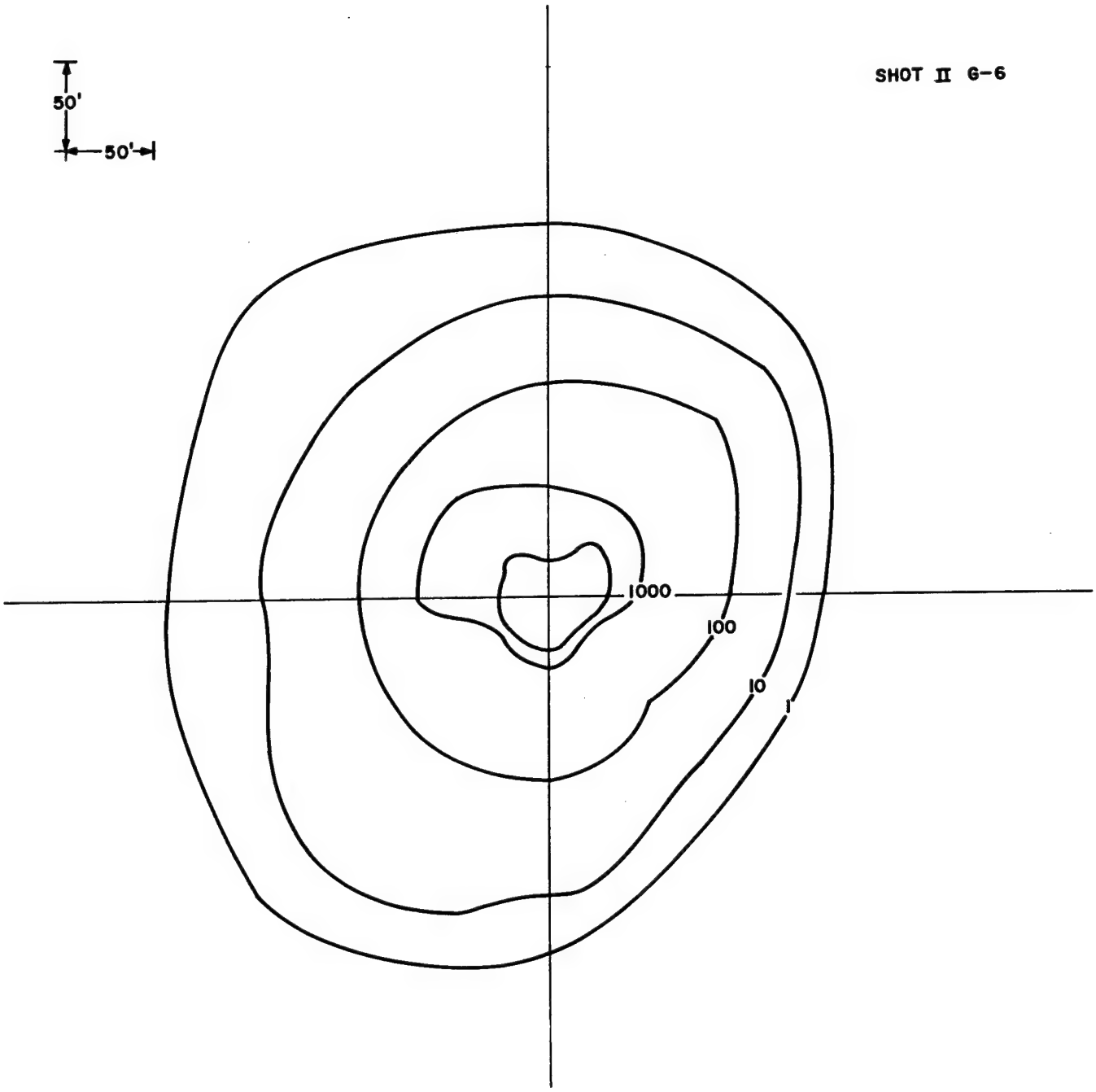

Figure D.36 Throwout deposition, 8-pound row charge, buried 3 feet, spaced 6 feet--contours are in gm/ft^2

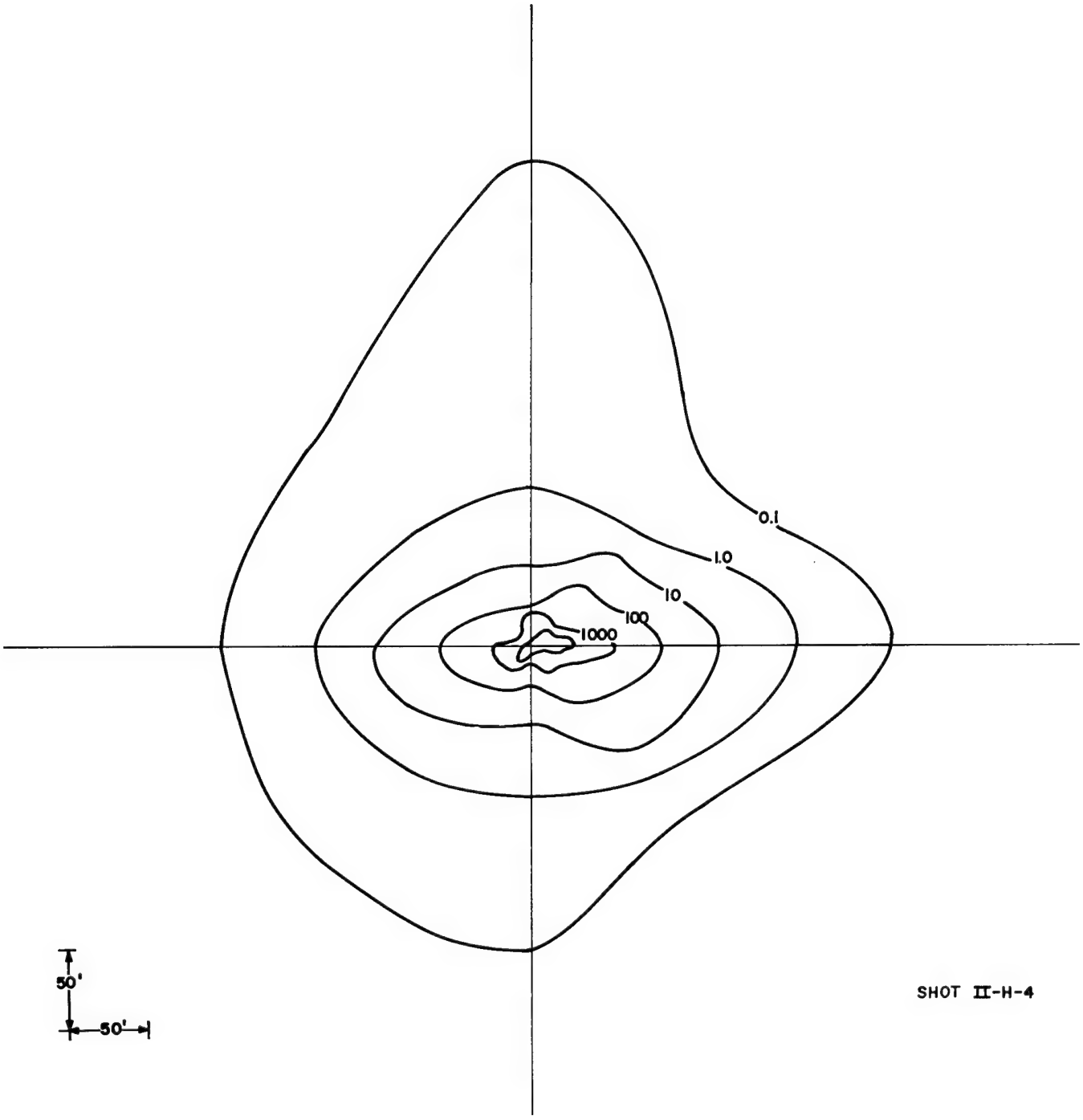

Figure D.37 Throwout deposition, 8-pound row charge, buried 3.5 feet, spaced 4 feet--contours are in gm/ft^2

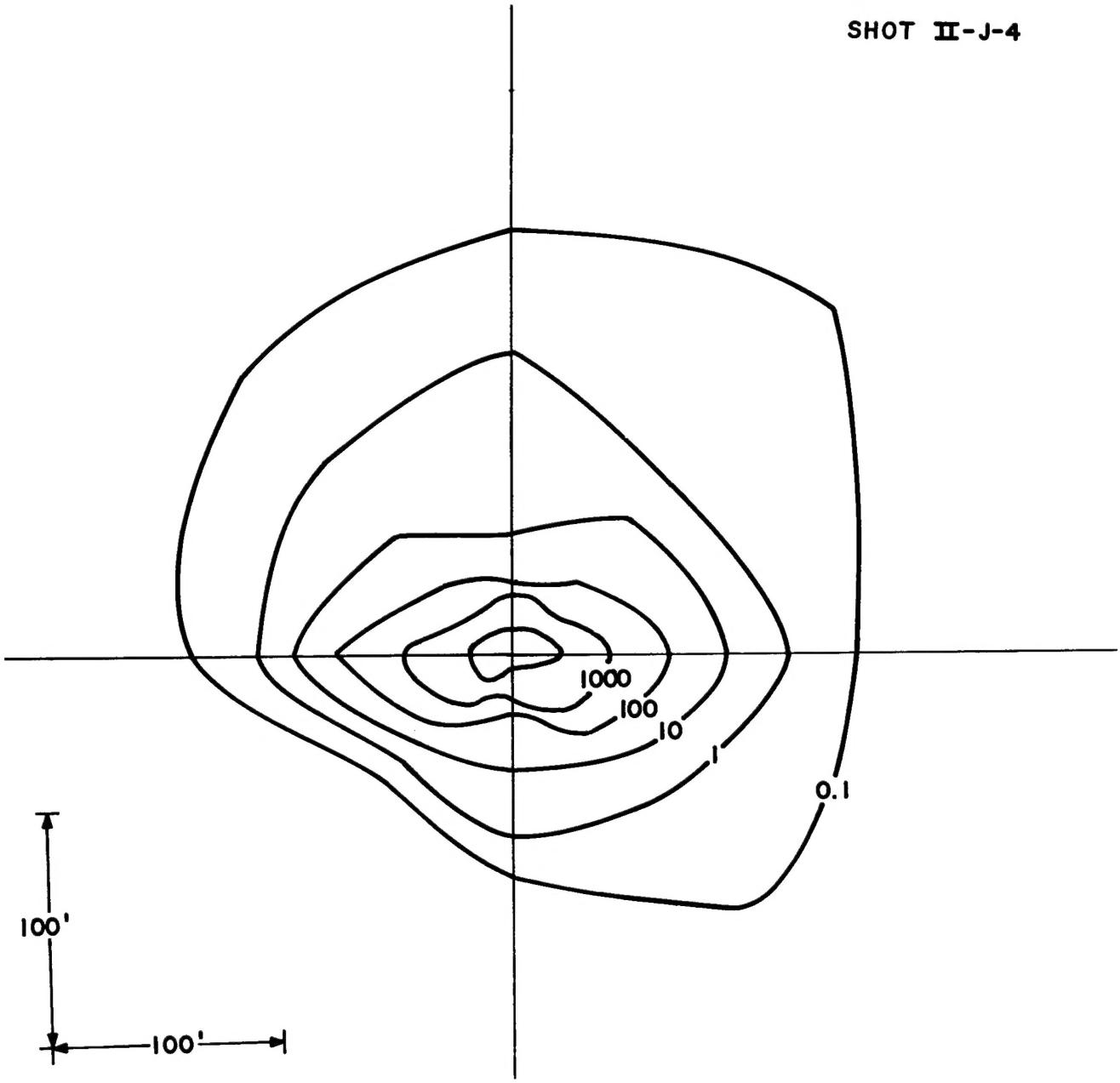

Figure D.38 Throwout deposition, 8-pound row charge, buried 4 feet, spaced 4 feet--contours are in gm/ft^2

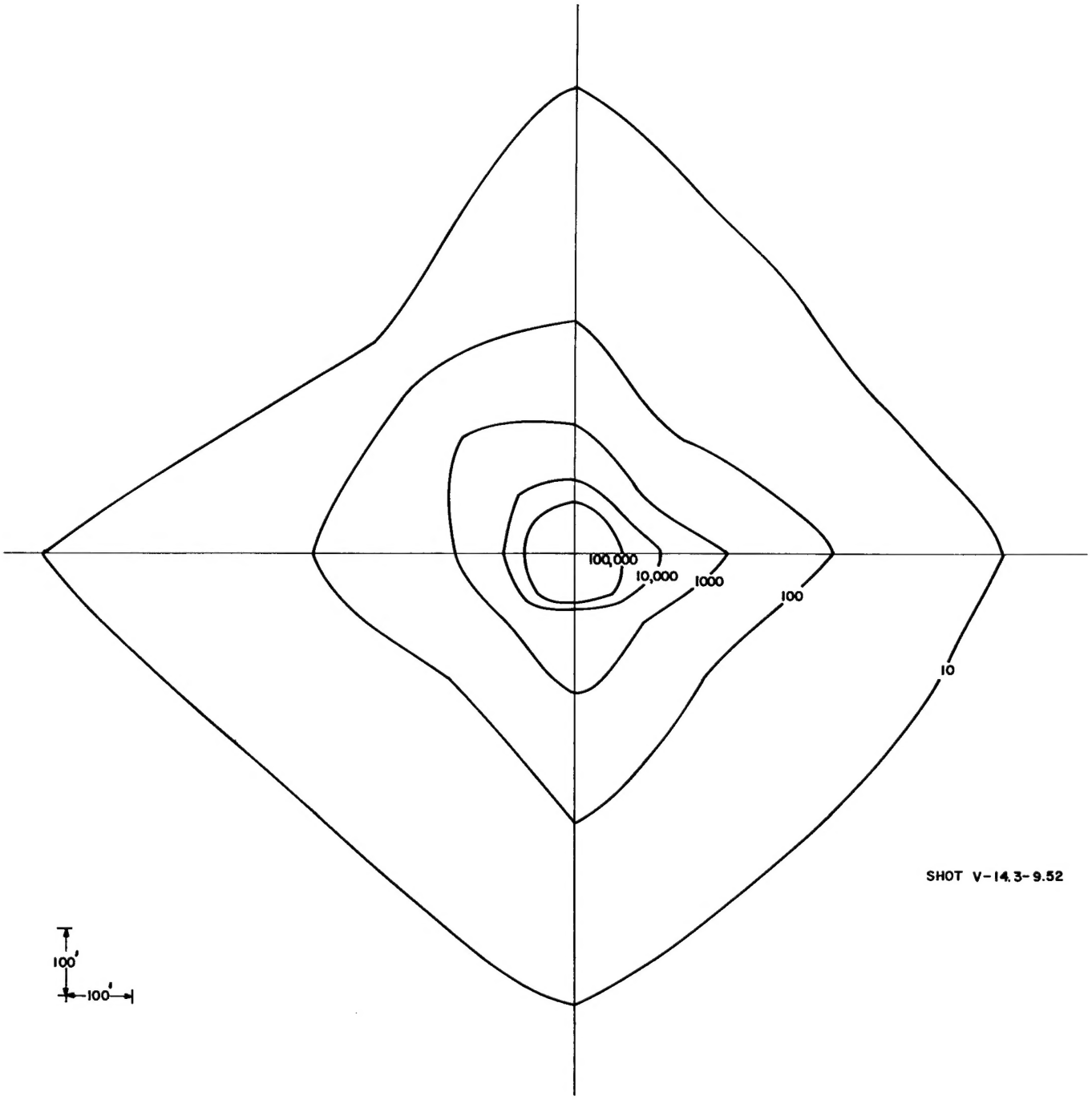

Figure D.39 Throwout deposition, 256-pound row charge, buried 9.52 feet, spaced 14.3 feet--contours are in gm/ft^2

DISTRIBUTION:
Maj. Gen. A. W. Betts, AEC/Division of Military Application
J. S. Kelly, AEC/DPNE (10)
Richard Hamburger, AEC/DPNE, Tech. Lib., Washington 25, D. C.
William Oakley, AEC/DPNE, Tech. Lib., Washington 25, D. C.
G. M. Dunning, AEC/Division Biol. and Medicine, Washington 25, D. C.
K. F. Hertford, Mgr., ALO
P. W. Ager, ALO
D. W. King, ALO (2)
J. E. Reeves, NVOO
R. E. Miller, NVOO
R. F. Beers, NVOO Consultant
P. Byerly, NVOO Consultant
G. B. Maxey, NVOO Consultant
T. F. Thompson, NVOO Consultant
E. C. Shute, USAEC, San Francisco Operations Office 2111 Bancroft Way, Berkeley 4, Calif. (SAN)
Russell Ball, SANOO, Berkeley, California
John Philip, SANOO, Berkeley, California (5)
Rodney Southwick, SANOO, Berkeley, California
John Rinehardt, Colorado School of Mines, Golden, Colo.
F. L. Smith, Colorado School of Mines, Golden, Colo.
E. M. Purcell, Harvard University, Cambridge, Mass.
Charles W. Martin, 201 T and AM Lab, Iowa State University, Ames, Iowa
Robert V. Whitman, MIT, Cambridge, Mass.
N. M. Newmark, University of Illinois, Urbana, Ill.
M. A. Cook, Explosives Research Group, Univ. of Utah
Ralph B. Baldwin, 1745 Alexander Rd., SE, East Grand Rapids, Mich.
J. J. Gilvarray, Research Laboratories, Allis-Chalmers Manufacturing Co., Milwaukee, Wis.
R. H. Carlson, Applied Physics Section, Mail Stop 21-31, Aerospace Division, Boeing Airplane Co., Seattle 24, Wash.
C. W. Lampson, BRL, Aberdeen Proving Gd., Maryland
J. G. Lewis/J. Kelso, HQ/DASA
P. Holdsworth, Commissioner, Dept. of Natural Resources, Box 1391, Juneau, Alaska
A. W. Patterson, Engineering Research and Development Laboratory, Nuclear Power Branch, Fort Belvoir, Va.
J. C. Mark, LASL
A. C. Graves, LASL
J. S. Foster/D. Sewell, LRL, Livermore
G. H. Higgins, LRL, Livermore (10)
M. D. Nordyke, LRL, Livermore
Ernest Graves, NCG/LRL, Livermore (3)
J. F. Moulton, NOL
R. W. McBride, OCE, Washington D. C., 20315
G. B. Olmsted, AFTAC, Washington 25, D. C.
W. H. Booth, OCE, Washington 25, D. C., 20315
M. D. Kirkpatrick, OCE, Gravelly Point, Va., 20315
W. E. Clark, Oak Ridge National Laboratory
D. T. Griggs, RAND Corp., 1700 Main Street, Santa Monica, Calif.
H. L. Brode, RAND Corp., 1700 Main Street, Santa Monica, Calif.
Davis S. Parker, Panama Canal Co., Canal Zone, Panama
Matthew C. Harrison, Panama Canal Co., Canal Zone, Panama
Roger M. Howe, Panama Canal Co., Canal Zone, Panama
John D. Hollen, Panama Canal Co., Canal Zone, Panama
R. B. Vaile, Jr., SRI, Menlo Park, Calif.
Chief, Superintendent, Suffield Experimental Station, Ralston, Alberta, Canada
G. H. S. Jones, P.O. Box 41, Ralston, Alberta, Canada
W. K. Cloud, U. S. Coast and Geodetic Survey, San Francisco Dist. Office, New Mint Bldg., San Francisco, Calif.
L. M. Murphy, U. S. Coast and Geodetic Survey, San Francisco Dist. Office, New Mint Bldg., San Francisco, Calif.
L. Obert/W. E. Duvall/T. C. Atchison, U. S. Bureau of Mines, Applied Physics Research Laboratory, College Park, Md.
L. R. Page/A. Brown, USGS, Room 1033, CSA Bldg., Washington 25, D. C.
E. M. Shoemaker, USGS, 4 Homewood Place, Menlo Park, California
F. Houser, USGS, Denver Federal Center, Denver, Colo.
C. F. Romney, HQ/USAF, Air Force Technical Applications Center, Washington 25, D. C.
F. R. Brown, Waterways Experiment Station, P. O. Box 631, Vicksburg, Miss. (WES)
John Strange, WES, Vicksburg, Miss.
A. R. W. Wilson, AEC, Beach Street, Coogee, New South Wales, Australia
T. D. J. Leech/H. E. Dann, Asst. Commissioner, Snowy Mountains Hydroelectric Authority, P. O. Box 332, Cosma North, New South Wales, Australia
TID-4500 (21st Ed.), UC-35 (548 copies)
S. P. Schwartz, 1
R. W. Henderson, 100
A. B. Machen, 2300
R. C. Prim, 5000
R. S. Claassen, 5100
F. W. Nielson, 5130
J. W. Easley, 5300
T. B. Cook, 5400
B. F. Murphey, 5410
C. R. Mehl, 5411
M. L. Merritt, 5412 (10)
L. J. Vortman, 5412
C. D. Broyles, 5413
J. D. Shreve, 5414
J. W. Weihe, 5420
R. M. Betz, 6010
G. A. Fowler, 7000
L. E. Hollingsworth, 7200
J. C. Eckhart, 7250
B. C. Benjamin, 7251
A. J. Max, 7254
D. G. Palmer, 7254
H. J. Plagge, 7254
W. J. Howard, 8100
W. A. Jamieson, 8233
Mrs. B. R. Allen, 3421-1
Mrs. M. G. Randle, 3421-3, Bldg. 836
Mrs. M. G. Randle, 3421-3, Bldg. 880
W. F. Carstens, 3423, Attn: J. M. Zanetti, 3423-1
C. E. Cockelreas, 3423-1
R. C. Smelich, 3427-3 (5)
L. D. Patterson, 3423-5, (for H. F. Carroll, USAEC)